On the Advantages of Nonlinear Continuum Scale Filtration Models

Philip Schroeder

Chair of Process Systems Engineering
TUM School of Life Sciences
Technical University of Munich

TUM School of Life Sciences
Technical University of Munich

On the Advantages of Nonlinear Continuum Scale Filtration Models

Philip Schroeder

Vollständiger Abdruck der von der TUM School of Life Sciences der Technischen Universität München zur Erlangung eines Doktors der Ingenieurwissenschaften (Dr.-Ing.) genehmigten Dissertation.

Vorsitz: Prof. Dr. Mirjana Minceva

Prüfer*innen der Dissertation: Prof. Dr.-Ing. Heiko Briesen
Prof. Alexander Mitsos, Ph.D.

Die Dissertation wurde am 30.03.2023 bei der Technischen Universität München eingereicht und durch die TUM School of Life Sciences am 26.05.2023 angenommen.

Abstract

In this publication-based dissertation, a series of research papers investigates the advantages of nonlinear modeling techniques in the analysis and optimization of cake filtration processes. To this end, two overall frameworks for mechanistic continuum scale modeling are examined:

1. the Conventional Filtration Theory, which provides an analytical approach to evaluate cake filtration data, but is limited in its ability to dynamically forecast the process
2. the Multiphase Flow Theory, which may describe the spatio-temporal development of the cake filtration process in detail, but can only be computed using numerical approximation schemes

The first part of this thesis evaluates the VDI 2762 guideline. While being built upon the conventional theory, this method is used to estimate the resistance of incompressible filter cakes from experimental data. Even though it is a widely applied standard procedure, systematic errors are induced to the procedure due to an underlying linearization approach. Therefore, a nonlinear model formulation is proposed to address this issue. In order to evaluate the novel method's validity, a large artificial data set is generated by employing Monte Carlo experiments. Examining the error performances for both, the linear, and the nonlinear technique, proves that the latter approach suppresses errors better, while the simplicity of the conventional theory is maintained.

In the second part, the scenario of filter aid cake filtration is examined in detail. Opposed to the previous case study, here the effects of cake compression, as well as cake-internal particle migration are described mathematically. Hence, the multiphase flow theory is used to develop a model, which in return allows to calculate the influence of time-dependent filter aid dosages on the cake growth process. Thereby, ideal dosage trajectories are obtained by employing an optimal control approach. The results suggest that varying the filter aid concentration as a control input can help to increase the process efficiency. For specific scenarios, both, the integral filter aid usage, as well as the area-specific energy consumption, are reduced simultaneously by up to $\approx 30\%$, and $\approx 5\%$ respectively.

Since the calculation of these optimization procedures is computationally intensive, a reduced order modeling method is employed to the filter aid cake filtration model. Hereby, the approach is based on the technique of proper orthogonal decomposition. Further, different adaptation techniques are examined to ensure that parameter variations can be captured accurately. In order to evaluate how the reduced order modeling architecture benefits the numerical efficiency, an optimization scenario is solved as a benchmark

problem. Using this method, the computational time can be reduced approximatively by a factor of 10, while producing only minor approximation errors.

A following discussion section elaborates on current developments, open questions, and possible future research in the domain of cake filtration modeling. Special focus lies on how both separate filtration theories may be combined to obtain new user-friendly procedures for the evaluation of experimental data from compressible cake filtration processes. After, the act of parametrizing the models is discussed by taking a closer look on novel process-analytical methods recently described in the literature. The last section analyses how the publications included in this thesis contribute toward the development of cyber-physical systems in the overall domain of solid-liquid separation. Hereby, the simulation model based on the multiphase flow theory, the optimal control algorithm, and the reduced order modeling architecture proposed throughout this work can be interpreted as newly available “puzzle pieces” needed to build a nonlinear model predictive control approach for cake filtration processes.

Kurzzusammenfassung

Diese publikationsbasierte Dissertation untersucht Vorteile, die nichtlineare mathematische Modelle bei der Analyse und Optimierung von Kuchenfiltrationsprozessen aufbringen können. Zu diesem Zweck werden zwei mechanistische Theorien zur Modellierung der Kuchenfiltration auf Kontinuumsebene betrachtet:

1. die konventionelle Filtrationstheorie, die einen analytischen Ansatz zur Auswertung von Experimentaldaten bietet, aber nur begrenzt dazu geeignet ist, den Prozess dynamisch vorherzusagen
2. die Mehrphasenströmungstheorie, die die dynamische zeit- und ortsabhängige Entwicklung des Kuchenfiltrationsprozesses detailliert beschreibt, aber nur numerisch gelöst werden kann

Der erste Teil dieser Arbeit widmet sich der VDI 2762 Richtlinie – eine auf der konventionellen Theorie aufbauende Methode, die zur Ermittlung des Widerstands von inkompressiblen Filterkuchen verwendet wird. Obwohl es sich hierbei um eine weit verbreitete Standardtechnik handelt, ist das Verfahren aufgrund eines Linearisierungsansatzes systematischen Fehlern unterworfen. Daher wird eine alternative nichtlineare Modellformulierung eingeführt, die dieses Problem löst. Um die Gültigkeit der neuen Methode zu bewerten, wird ein großer künstlicher Datensatz mit Hilfe von Monte Carlo Experimenten erzeugt. Bei der Untersuchung von sowohl der linearen als auch der nichtlinearen Technik wird deutlich, dass bei Letzterer die Fehler der Parameterermittlung vermindert werden, während gleichzeitig die Nutzerfreundlichkeit der konventionellen Theorie erhalten bleibt.

Im zweiten Teil der Dissertation wird das Szenario der Anschwemmfiltration – einem Spezialfall der Kuchenfiltration – im Detail untersucht. Im Gegensatz zur vorherigen Fallstudie werden nun die Effekte der Filterkuchenkompression sowie eines überlagerten Tiefenfiltrationsmechanismus mitberücksichtigt. Dazu wird mit Hilfe der Mehrphasenströmungstheorie ein Modell entwickelt, das auch den Einfluss einer zeitabhängigen Filterhilfsmitteldosage auf den Filtrationsprozess berechnen kann. Dabei werden mit Hilfe eines Optimalsteuerungsansatzes ideale Dosagetrajektorien ermittelt. Die Ergebnisse deuten darauf hin, dass die Variation der Filterhilfsmittelkonzentration zur Steigerung der Prozesseffizienz beitragen kann. Für bestimmte Szenarien werden gleichzeitig sowohl der integrale Filterhilfsmittelverbrauch als auch der flächenspezifische Energieverbrauch um bis zu $\approx 30\%$ bzw. $\approx 5\%$ reduziert.

Da die Optimierungsprozedur rechenintensiv ist, wird eine Modellreduktion für das Anschwemmfiltrationsmodell durchgeführt. Der Ansatz basiert auf der sogenannten „Proper Orthogonal Decomposition“. Darüber hinaus werden verschiedene Adaptionsmethoden

untersucht, die sicherstellen, dass das reduzierte Modell auch unter Parametervariationen genaue Ergebnisse liefert. Ein Optimierungsszenario wird als Testproblem gelöst, um zu prüfen, wie das reduzierte Modell die numerische Effizienz verbessert. Insgesamt kann mit dieser Methode die Rechenzeit um den Faktor 10 verringert werden, wobei nur geringe Approximationsfehler auftreten.

In einem abschließenden Diskussionsteil werden aktuelle Entwicklungen, offene Fragen und mögliche zukünftige Forschungsarbeiten zur Modellierung der Kuchenfiltration näher beleuchtet. Besonderes Augenmerk liegt dabei auf der Frage, wie die beiden verschiedenen Filtrationstheorien kombiniert werden können, um neue nutzerfreundliche Methoden zur Beschreibung kompressibler Kuchenfiltrationsprozesse zu erhalten. Anschließend wird diskutiert, wie die Modelle parametriert werden können. Hierbei werden die möglichen Einsatzzwecke neu entwickelter experimenteller Methoden betrachtet. Der letzte Abschnitt analysiert, wie die Publikationen dieser Arbeit zu der Entwicklung von cyber-physischen Systemen im Bereich der Fest-Flüssig-Trennung beitragen. Dabei können das auf der Theorie der Mehrphasenströmung basierende Modell, der Ansatz der optimalen Steuerung und die in dieser Arbeit vorgeschlagene Modellreduktionsarchitektur als neu verfügbare "Puzzleteile" interpretiert werden, die für die Entwicklung einer nichtlinearen modellprädiktiven Regelung von Kuchenfiltrationsprozessen erforderlich sind.

Contents

Abstract I

Kurzzusammenfassung III

List of Figures VII

Glossary VIII

1 Introduction

1.1 Motivation ... 1
1.2 Objectives ... 2
1.3 Thesis Outline ... 4

2 Theoretical Background

2.1 Physical Properties of Cake Filtration ... 6
2.1.1 Separation Mechanisms ... 7
2.1.2 Characteristic Quantities ... 8
2.1.3 Cake Compression ... 12
2.1.4 Filter Aid Utilization ... 14
2.2 Continuum Scale Cake Filtration Modeling ... 16
2.2.1 Conventional Theory ... 17
2.2.2 Multiphase Flow Theory ... 20
2.3 Remarks on Process Optimization ... 21
2.4 The Role of Computational Efficiency ... 24

3 Methodology

3.1 Model Simulations ... 26
3.1.1 Monte Carlo Experiments ... 26
3.1.2 Handling Partial Differential Equations ... 27
3.2 Employed Optimization Algorithms ... 27
3.3 Model Order Reduction ... 29

4 Full-Length Paper Summaries

4.1 Publication I – Monte Carlo Study ... 31
4.2 Publication II – Optimal Control Study ... 32
4.3 Publication III – Model Order Reduction Study ... 33

5 Overall Discussion
5.1 Synergies from Combining the Filtration Theories 35
5.2 Experimental Considerations 37
5.2.1 Model Parameterization 37
5.2.2 Further Experimental Phenomena 41
5.3 Transition to Cyber-Physical Systems 42
5.3.1 Analysis of Process Optimization 43
5.3.2 Real Time Computations 46
5.3.3 Model Predictive Control 48
5.3.4 System-Wide Integration 50

6 Conclusions and Outlook 52

Bibliography 54

Full-Length Paper I 78

Full-Length Paper II 88

Full-Length Paper III 103

List of Publications 116

List of Figures

Figure 1 *Schematic representation of an idealized cake filtration process.* 6

Figure 2 *Illustration of cake filtration, depth filtration, and pore blocking as separate particle separation mechanisms.* 8

Figure 3 *Illustration of an arbitrary filter cake's internal pore-structure.* 9

Figure 4 *Idealized qualitative behavior for constant-pressure, and constant flow cake filtration processes.* 11

Figure 5 *Qualitative behavior for the porosity ε, and the permeability k in an incompressible (left) and a compressible (right) cake filtration process. Spatial variations in the compressible case result due to compressive stress p_S acting on the solid phase. Only compression resulting from particle deformation is illustrated.* 12

Figure 6 *Illustration of the precoat stage (left), and the bodyfeed stage (right); the thickness of the precoat layer is illustrated by the horizontal green line.* 15

Figure 7 *Illustration of different scales in cake filtration modeling. Adapted from [27].* ... 16

Figure 8 *Ideal experimental cake filtration data in the case of a constant pressure filtration (left); linearized data according to Eq. (15) (right).* 19

Figure 9 *Scheme for an open loop optimal control of a cake filtration plant.* 44

Figure 10 *Scheme for a digital twin of a filtration plant.* 46

Figure 11 *Scheme for a model predictive control approach of a cake filtration plant.* 48

Glossary

Roman letters

A	$[\mathrm{m}^2]$	area covered by filter medium
b	$[-]$	empirical form factor
c	$[-]$	volumetric filter aid concentration
d	$[\mathrm{m}]$	particle size
e	$[\mathrm{J} \cdot \mathrm{m}^{-2}]$	area-specific energy consumption
f	$[unit]$	arbitrary function or constitutive relationship
i	$[-]$	iteration
k	$[\mathrm{m}^2]$	permeability
K	$[-]$	concentration constant
L	$[\mathrm{m}]$	filter cake height
L_{PC}	$[\mathrm{m}]$	height of precoat layer
m	$[-]$	dimension of independent variables
n	$[-]$	dimension of system states
o	$[-]$	dimension of control variables
p	$[\mathrm{Pa}]$	process pressure
p_l	$[\mathrm{Pa}]$	liquid pore pressure
p_s	$[\mathrm{Pa}]$	solid stress
P	$[unit]$	arbitrary parameter
q_l	$[\mathrm{m} \cdot \mathrm{s}^{-1}]$	superficial liquid velocity
q_s	$[\mathrm{m} \cdot \mathrm{s}^{-1}]$	superficial solid velocity
r	$[\mathrm{m}^{-2}]$	height-specific filter cake resistance (intensive quantity)
R	$[\mathrm{m}^{-1}]$	total filter resistance (extensive quantity)
R_m	$[\mathrm{m}^{-1}]$	filter medium resistance
t	$[\mathrm{s}]$	time
T	$[\mathrm{s}]$	overall temporal domain, i.e., process end time
u	$[unit]$	arbitrary control parameter or control function
v	$[\mathrm{m} \cdot \mathrm{s}^{-1}]$	pore-space liquid velocity
V	$[\mathrm{m}^3]$	process-cumulative filtrate volume; filter cake volume (Eq. (12) only)
V_c	$[\mathrm{m}^3]$	control volume
V_p	$[\mathrm{m}^3]$	pore-space volume
V_s	$[\mathrm{m}^3]$	volume occupied by solid phase
$\dot{V}$	$[\mathrm{m}^3 \cdot \mathrm{s}^{-1}]$	volumetric flow rate of the filtrate at the filter outlet

x	[m]	spatial dimension; arbitrary independent variable (Eq. (20) only)
x_0	[$unit$]	left-hand limit of arbitrary independent variable
x_f	[$unit$]	right-hand limit of arbitrary independent variable
y	[$unit$]	arbitrary system state, i.e., dependent variable
z	[–]	spatial dimension; treated by Front Fixing Method

Greek letters

Δ	[–]	difference
ε	[–]	porosity
ε_s	[–]	solidosity
ε_{s2}	[–]	volumetric fine particle content
λ	[m^{-1}]	filter coefficient
μ	[$\mathrm{Pa} \cdot \mathrm{s}$]	viscosity
τ	[–]	tortuosity

Accents & Symbols

$\dot{}$	time derivative
$\widehat{\ }$	measured data, i.e., data produced by Monte Carlo method
$\langle\ \rangle$	spatially averaged quantity
bold	vectors or matrices

Abbreviations

CPS	Cyber-Physical System
CRediT	Contributor Roles Taxonomy
MPC	Model Predictive Control
POD	Proper Orthogonal Decomposition
ROM	Reduced Order Model
SAIM	Subangle Interpolation Method
VDI	Verein Deutscher Ingenieure; engl.: Association of German Engineers

Notably, this glossary does not contain the symbols and abbreviations used in the respective research papers included in the Appendix of this dissertation. Each individual publication holds its own corresponding list of symbols.

Chapter 1

Introduction

1.1 Motivation

Based on the principle of liquid flow through porous media, filtration is an established unit operation in the overall domain of mechanical solid-liquid separation processes. Hereby, the underlying technique offers various possibilities for phase separation as can be perceived by the sheer amount of distinctive industrial applications. To name a few, it poses a crucial step in the treatment of wastewater [1], [2], ensuring certain food and beverage qualities [3], [4], or the production of pharmaceuticals [5].

This work specifically examines the instance of cake filtration. It can be classified as a simple yet effective method in which a suspension flows through some membrane. Since this filter medium is ideally only permeable to the liquid phase, the solutes accumulate on the surface of said porous septum as the so-called *filter cake.* The particle-free *filtrate,* on the other hand, can be collected at the filter apparatus' outlet [6]. However, the initial simplicity is swiftly affected by effects occurring in real processes, such as cake compressibility, cake-internal particle migration, and therewith resulting heterogenous cake structures [7], [8]. Due to these phenomena, the process complexity is highly increased, and precise model-based investigations are hard to conduct. Consequently, to this day the majority of scientific works from this research domain focuses on experimental set-ups while still often relying on simplified mathematical models for process evaluation.

Here is also the point at which the publications included in this publication-based thesis intend to enable the use of more sophisticated filtration models as improved investigation tools in the spirit of Process Systems Engineering. Thereby, the use of simulation models can be perceived as an interconnecting piece between experimental studies and purely theoretical analyses [9], [10]. Certainly, mathematical models only serve an additional value if they aid in gaining further knowledge about the examined process by, e.g., supporting data evaluations, or calculating optimization scenarios. Hence, the intended applications and the scientific objectives to be answered are further elaborated in the next section.

1.2 Objectives

The overall narrative pervading all following objectives is the use of nonlinear mathematical continuum scale models to help facilitate the assessment of experimental data, and to improve the performance of cake filtration processes. During the course of this work, the focus lies on two different applications.

First, attention is given to the cake filtration norm VDI[1] 2762 [11]. Said guideline states a model that particularly in the German-speaking filtration community is often used as a foundation to evaluate cake filtration data obtained from typical experiments. However, despite being last updated in 2010, the model stated in this norm still relies on a linearization technique, which is intended to be solved graphically to obtain the unknown process parameters. From nowadays perspective this linearization procedure is not only anachronistic but also induces systematic statistical errors to the experimental results. By the means of Monte Carlo simulations [12], Objective I aims at eliminating said statistical errors only by reformulating the mathematical model in a more favorable nonlinear expression without altering the underlying established theory. In return, a more concise insight into the process data is offered.

Objective I

Eliminate the systematic statistical errors induced by the VDI 2762 norm by introducing an alternative nonlinear model formulation

---

Second, mathematical models for the special case of *filter aid* cake filtration are studied. As the name suggests, filter aid materials are added to the initial suspension to improve the performance of the process [13], [14]. Hereby, particularly the behavior of fibrous filter aids such as cellulose and viscose are investigated. These alternatives offer health and environmental benefits over traditionally used materials like kieselguhr [15], [16]. Nevertheless, fibrous filter aids also pose their own unique utilization challenges due to an increased compressible behavior [17]. Therefore, it becomes necessary to obtain a new process understanding, as the established phenomenological knowledge from the previously mentioned incompressible material system is no longer valid. Moreover, it was found that the effect of depth filtration has a significant impact on the filter aid filtration process [18]–[21]. Hence, the complete system behavior can typically only be captured using complex nonlinear mathematical models. As described by Coote [22], this is a challenging task to fulfill, and, as such, mathematically describing the process of filter aid filtration by

[1] Verein Deutscher Ingenieure, engl. Association of German Engineers

mechanistic relationships was not a priority in research until some years ago. Considering these preliminaries, the second objective of this thesis reads as follows.

Objective II

Develop a mechanistic continuum scale model for filter aid cake filtration including the following effects known from real processes:

- Cake compressibility
- Variable shares of impurity separation by surface and depth filtration
- Cake-internal particle migration

A challenge in the context of filter aid filtration is to find the ideal filter aid dosage. Commonly, the filter aid concentration is sought to maintain a high process efficiency as well as a desired filtrate quality, while minimizing the actual filter aid consumption, since all these elements have a significant impact on the monetary process cost. Even though it is known from experimental studies that such process specific optimal filter aid concentrations exist [23]–[25], established techniques in finding these unknown dosages are typically based on heuristics and still entail a significant amount of laboratory time [26], [26]. Rigorous mathematical investigations, on the other hand, are only applied sparsely in the area of solid-liquid separation (e.g., [27], [28]), and are non-existent for compressible fibrous systems.

To reduce this required experimental workload, the developed filtration model from Objective II shall be used as a basis to computationally determine the ideal constant filter aid dosage while incorporating long-term effects of real filtration processes, such as cake compression, and particle migration. Moreover, recent studies indicate that time-dependent dosage strategies may further increase the overall process efficiency compared to an optimal, but constant filter aid supply to the suspension [22], [29]. To examine this hypothesis, the method of optimal control is applied [30], such that the next thesis objective can be formulated.

Objective III

Develop an optimal control procedure to find filter aid dosage strategies that improve the overall filtration efficiency for arbitrary process scenarios and optimization goals

---

The optimization procedure developed in Objective III can be classified as an *a priori*, or feedforward method. Hereby, process disturbances and uncertainties are not taken into consideration when using the presented technique. Hence, the dosage strategies discovered throughout this work are only transferrable to real-life filtration plants under the assumption of ideal surrounding conditions. Another limitation lies in the involved computational requirements needed to fulfill Objective III.

Thus, it is highly desirable to increase the computational efficiency of the continuum scale model from Objective II. Lowering the numerical cost does not only make it more attractive to use model-based strategies to find ideal filter aid dosages in a practical context. Doing so may also create the possibility of conducting real-time online model simulations (commonly referred to as *digital twin*), which can indeed be used to characterize occurring process uncertainties [31]. To this end, Objective IV aims at reducing the model complexity by employing the method of proper orthogonal decomposition [32].

Objective IV

Increase the computational efficiency of the model introduced in Objective II by employing the method of proper orthogonal decomposition

---

1.3 Thesis Outline

This work is a publication-based thesis. Therefore, the full-length research papers containing the academic findings which answer the previously introduced Objectives are included in the Appendix:

- *Objective I:* Full-Length Paper I (p. 78)
- *Objectives II & III:* Full-Length Paper II (p. 88)
- *Objective IV:* Full-Length Paper III (p. 103)

In order to help facilitate the understanding of the individual studies, Chapter 2 of the main text contains the fundamental theoretical background about the cake filtration topics covered in the respective works. In detail, Section 2.1 introduces the physical properties of the process, along with the characteristic filtration quantities, and process influencing phenomena, such as cake compression, and cake-internal particle migration. Moreover, the potential shortcomings of any termini that were introduced in the previous sections without further context, as well as the special case of filter aid filtration are further elaborated.

Next, Section 2.2 of the same Chapter covers the established continuum scale modeling theories in the domain of cake filtration. Thereby, Subsection 2.2.1 introduces the so-called *Conventional Filtration Theory*, which is the foundation for the VDI 2762 guideline's modeling approach (→ *Objective I*). The more elaborate *Multiphase Flow Theory* is explained in Subsection 2.2.2. This theoretical framework is used to fulfill → *Objectives II – IV*.

Subsequently, Section 2.3 elaborates further on established process optimization techniques for solid-liquid separation processes. Moreover, the theory of numerical optimization and optimal control is introduced. Notably, this section only gives a general introduction needed to contextualize the underlying concepts. Hence, it does not contain any mathematical definitions or actual employed optimization algorithms, since these are covered in the individual Methodology, and Methods sections of this thesis, as well as the respective research papers.

Along similar lines, Section 2.4 of the second Chapter introduces the numerical concept of model order reduction. The mathematical theory, however, is covered at a later stage. Instead, this part is intended to inform about the cruciality of the computational efficiency for the model simulations encountered in this work specifically, as well as in the domain of process systems engineering in general.

After, Chapter 3 gives an overview on the scientific methodology. This part includes more information on the mathematical concepts elaborated in the previously described Sections 2.2, 2.3, and 2.4, as well as on the algorithms employed in the research papers. However, as each full-length paper contains an individual and detailed Methods section, this Chapter in itself is kept rather brief. It should, therefore, be seen as an outline needed to categorize each study in the overall background of numerical techniques.

Chapter 4 includes summaries of the individual studies. These summaries are intended to deliver more information than the corresponding papers' abstracts. Hereby it is ensured that the publications' respective methods and main findings are explained in sufficient detail, such that the following sections can be followed without referring to the full-length manuscripts included in the Appendix.

After all studies are introduced, Chapter 5 discusses the scientific findings in the context of the established filtration literature. To this end, the debate does not only entail the specific methodic frameworks used to create the research papers but aims at interconnecting the results with other state-of-the-art approaches in the overall domains of solid-liquid separation, and process systems engineering.

Finally, Chapter 6 recapitulates the dissertation. After drawing overall conclusions, the thesis is closed by summarizing in which fields the theoretical findings may be applied to improve established filtration processes.

Chapter 2

Theoretical Background

2.1 Physical Properties of Cake Filtration

The overall goal of cake filtration is to either recover the solid phase from the suspending liquid, or to purify and collect the liquid phase as the filtrate. Hereby, a pressure difference Δp – typically generated by a hydraulic pump, a vacuum, or merely by gravitation acting on the suspension – causes the initial slurry to flow through a filter medium. Ideally, the suspended particles cannot pass this membrane such that only the pure filtrate exits the apparatus' outlet. Therefore, the solid phase is collected on the inlet's side of the filter medium and forms the so-called filter cake, i.e., a porous agglomerate, which further grows over time [33]. This fundamental principle of cake filtration is schematically illustrated in Figure 1 for two process times $t_1 < t_2$ with $L(t)$ denoting the respective cake heights.

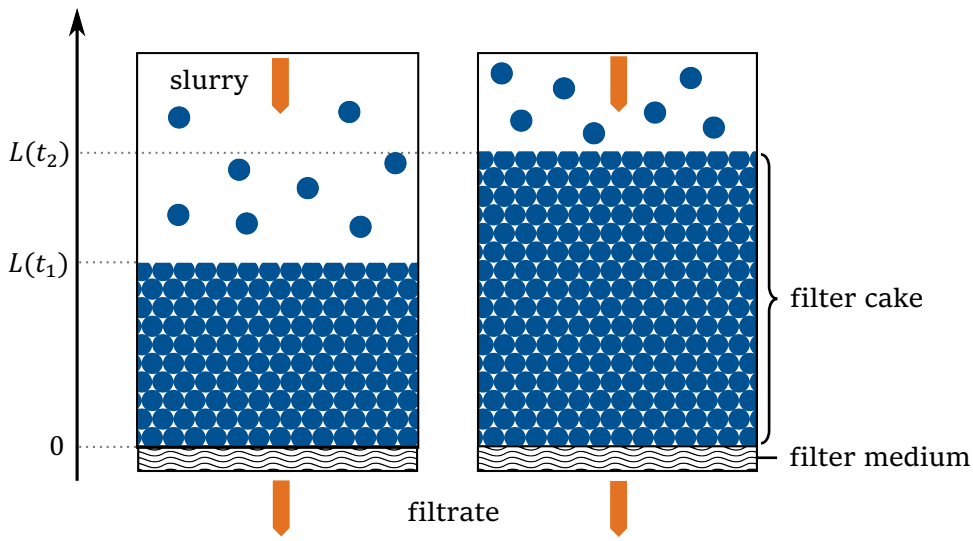

Figure 1 *Schematic representation of an idealized cake filtration process.*

Notably, different cake filtration set-ups are established in practice, such as tangential flow filters, or (semi-)continuous drum filters [34]. This thesis, however, focuses on the operation of dead-end cake filtration. In this case, the suspension's flow direction is perpendicular to the filter medium as demonstrated in Figure 1. Arguably, this type is the simplest form of cake filtration. Nevertheless, despite the physical simplicity it poses a

universal basis to the process, which can be used to draw overall conclusions. The proposed methods and findings from this work may then be adapted to more specific challenging case studies.

This subsection only covers those aspects of cake filtration that are relevant to the modeling focus of this thesis. These include, e.g., the characteristic process quantities and important filtration mechanisms to be captured, as well as the phenomenological aspects of filter aid utilization. For further information on the physical properties of cake filtration, it is referred to various textbooks, such as [6], [34], [35].

2.1.1 Separation Mechanisms

The solid phase is mainly separated from the suspending liquid via the mechanism of *surface filtration*. As previously described, the impurities are first deposited on top of the filter medium, after which subsequently incoming particles transit to the actual phase of cake filtration. At first glance, this is the only cause clearing the suspension on a macroscopic scale. However, this postulation is only valid if the dimension of the solids either exceeds the filter matrix' pore size, or if an agglomeration of particles builds bridges over said porous membrane [6]. Hence, especially in the beginning of the process it can be observed that particles may completely clog the septum if they are roughly the same size as the filter medium's pores. This second effect is described as *pore blocking*, and significantly lowers the transmissibility of the overall filter [36], [37]. Furthermore, a slurry's fine particle fraction may pass the surface pores unhindered and migrate through the filter cake. Hereby, the particles are only separated along their flow trajectory if they get caught by some stopping mechanism. Potential individual causes for this phenomenon can be, e.g., mechanical sieving or inter-particular interactions, such as electrostatic effects, or Van-der-Waals forces [38]–[41]. This act is commonly referred to as *depth filtration*[2]. The previously introduced particle separation mechanisms are schematically illustrated in Figure 2.

While a combination of all these effects is expected in cake filtration, especially the overlayed mechanism of depth filtration is an important aspect to be covered if filter aids are involved in the process as demonstrated in, e.g., [18]–[20], [43]. This is because particles separated by depth filtration occupy the cake-internal voids over the process time. Hence, just like the pore blocking mechanism, this hard-to-predict effect significantly influences the subsequent process and can be the cause for rapidly increasing pressure drops or collapsing filtrate flow rates.

[2] The mechanism of depth filtration should not be confused with *deep bed filtration*, which makes use of the same mechanism but denotes a different unit operation [42].

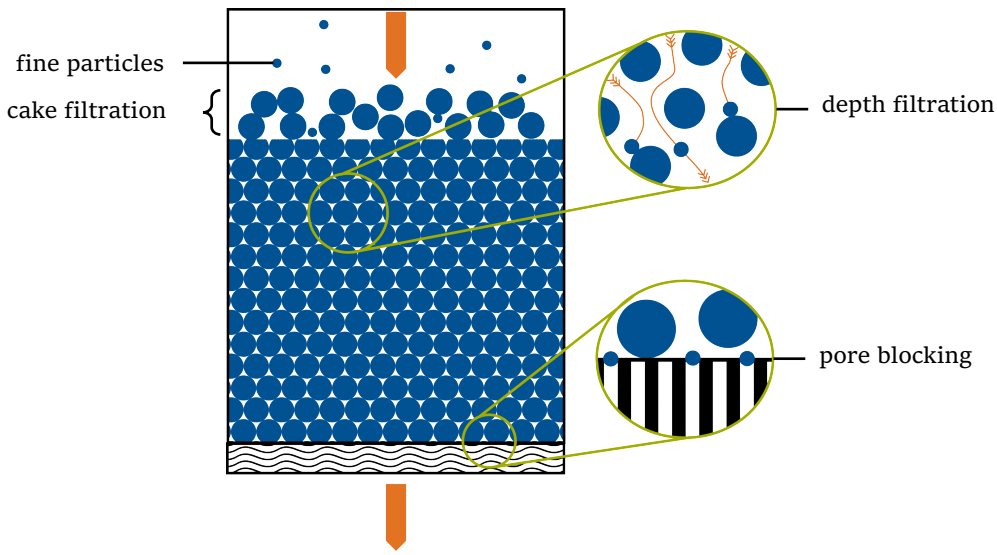

Figure 2 *Illustration of cake filtration, depth filtration, and pore blocking as separate particle separation mechanisms.*

Moreover, the suspended fine particles do not only migrate inside the filter cake but may also penetrate the filter medium and, thus, lower the final quality of the filtrate. The danger of such a potential particle breach happening lies particularly in the beginning of the filtration. Only during the course of the process, the filter cake increases in height, and, therefore, the fine particles inhibit longer individual flow trajectories, which raises their overall capture probability. In general, this is a desirable effect in cake filtration. However, once the capture capacity of a filter cake is reached, or if hydrodynamic forces cause the detachment of the fine particles from the porous filter matrix, the risk of impurities passing the filter medium may increase once again for longer filtration times [44]–[47].

As elaborated by Heertjes and Zuideveld [21], the action of depth filtration always takes place during the cake filtration processes examined in this work. Nevertheless, the extend of each separation mechanism strongly depends on the material systems in use. Therefore, a mathematical model should not only be able to distinguish between these mechanisms but also to quantify the actual share of impurities to be separated by depth filtration, and surface filtration respectively. Only then the calculations portray real-life processes precisely.

2.1.2 Characteristic Quantities

Figure 1 displays the growing filter cake as an idealized quasi-continuous medium. This representation is especially convenient for continuum scale modeling, which is further elaborated in Section 2.2. In general, however, a filter cake is a porous matrix which allows the liquid phase to pass through the network constructed by internal void. Therefore, Figure 3 presents a more accurate illustration of the microscopic physical structure for an arbitrary filter cake. In the following, the relevant physical quantities needed for the

mechanistic modeling of cake filtration processes will be introduced by the means of this illustration.

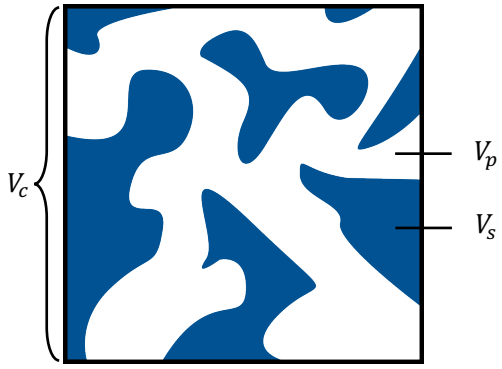

Figure 3 *Illustration of an arbitrary filter cake's internal pore-structure.*

The *porosity* ε is an intensive quantity crucial to describe filtration processes. It is calculated via the following relationship, where V_p denotes the pore-space volume, and V_c is the control volume, i.e., the overall cake volume [6].

$$\varepsilon = \frac{V_p}{V_c} \tag{1}$$

Notably, the quantification of voids may also be expressed in terms of *solidosity* ε_s by relating the volume occupied by the solid phase V_s to V_c. This quantity is more convenient to handle in some modeling approaches [8]. Nevertheless, the information content is equal, since it is the complementary to the porosity. Both quantities are linked via

$$\varepsilon_s = 1 - \varepsilon. \tag{2}$$

Especially for incompressible cakes the porosity depends on the characteristics of the examined material system such as particular shape [48], [49], and particle size distribution [50]–[52]. In general, the porosity of a filter cake can be anywhere from $\varepsilon = 0.1$ to $\varepsilon = 0.9$ [53], [54], with typical values ranging from $\varepsilon = 0.3$ to $\varepsilon = 0.7$ [6]. For instance, filter cakes built from monodisperse particles tend to be more porous than polydisperse systems. Especially for ideal bi-disperse spheres this effect is well-documented [55]–[57]. This is because additional fine particle fractions can populate the pores created by the coarser solids. Notably, this phenomenon is closely related to the previously introduced mechanism of depth filtration. Randomly orientated loose fibers packings are another material system causing high cake porosities [58], [59].

The *permeability* k is a quantity that was patronized by Darcy [60] to predict a liquid phase's flow rate through a porous medium resulting from an applied pressure difference (see also Section 2.2.1). Hence, the permeability can be understood as a material property that describes the extend of how the flow is impeded by the porous filter matrix. Therefore,

the permeability is strongly affected by porosity, as less pores also decrease the solid phase's ability to conduct the fluid flux. Several approaches exist that try to capture this relationship as a mechanistic mathematical formulation [61]. The most established is most likely the Kozeny-Carman equation, derived from the Hagen-Poiseuille relationship [62]:

$$k = \frac{4 \cdot d}{9 \cdot b \cdot \tau} \cdot \frac{\varepsilon^3}{(1-\varepsilon)^2} \tag{3}$$

As can be seen in Eq. (3), the permeability is not only directly related to the porosity ε, but also to the particle size d, the void network's tortuosity τ, as well as some material dependent empirical form factor b. However, while the Kozeny-Carman equation yields a high prediction accuracy for ideal cases, e.g., some uncompressed porous medium consisting of spherical particles, various authors questioned its actual use as an universal model to predict the permeability of filter cakes [54], [63], [64]. This is because real filter cakes are often inhomogeneous for which Eq. (3) is not valid. Consequently, a number of modifications, extensions, and alternative models to describe the permeability k is described in the literature promising a better data correlation to specific cases. Some works include, e.g., Happel [65] deducing relationships from the Navier-Stokes theory, Wakeman [66] incorporating particle size effects, and Nabovati et al. [67] describing fiber packings. Comprehensive collections and discussions of alternative approaches can also be found in, e.g., [68]–[70]. Thereby, it is often more convenient to exclude some hard-to-access quantities such as the tortuosity τ found in Eq. (3). Vague model assumptions may then be exchanged for purely empirical constitutive relationships. Especially exponential, and polynomial expressions that directly correlate the permeability k with the solidosity ε_s, as well as some possibly occurring fine particle deposition ε_{s2} have proven to be effective for the applications encountered in this thesis [23], [24], [44], [64], [71]. Using the additional empirical parameter(s) $\boldsymbol{P}$, the following equation can therefore be defined as:

$$k = f(\varepsilon_s, \varepsilon_{s2}, \boldsymbol{P}) \tag{4}$$

Often, the permeability k is reformulated as the quantity of *filter cake resistance* r, which is inversely related via the following equation [33].

$$k = \frac{1}{r} \tag{5}$$

Notably, r is an intensive quantity independent of the cake height. The extensive quantity, i.e., the total filter cake resistance R, can be calculated by linking r to the filter cake thickness L, and adding the filter medium resistance R_m [34] as described by Eq. (6).

$$R = L \cdot r + R_M \tag{6}$$

Since the filter cake height L can only grow over time, the filter resistance increases strictly monotonously during the process. Depending on the filter's operation mode, this can have different impacts on the *filtration pressure* p, and the *filtrate flow rate* $\dot{V}$ at the filter outlet. If the filtration is conducted by applying a constant pressure, the flow rate decreases continuously. *Vice versa*, in constant flow filtration, the resulting pressure drop rises over time to maintain the effluent's flow rate under the increasing filter resistance [33]. The typical qualitative time-dependent behaviors for $p(t)$, $\dot{V}(t)$, and $L(t)$ in ideal cake filtration processes are schematically depicted in Figure 4.

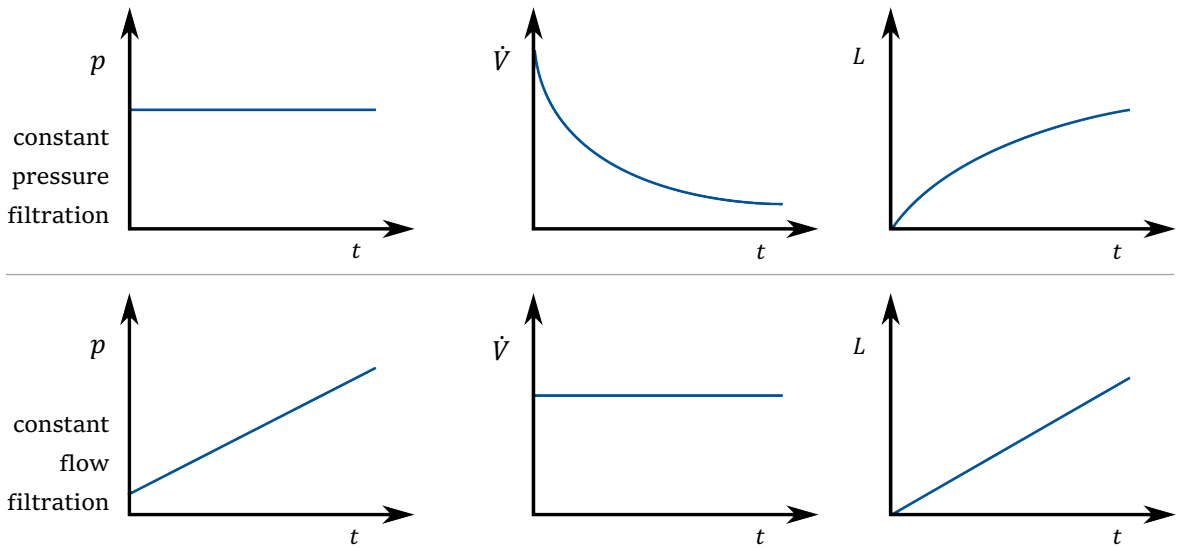

Figure 4 *Idealized qualitative behavior for constant-pressure, and constant flow cake filtration processes.*

Since cake-internal particle migration due to the mechanism of depth filtration has a significant impact on the process, it is further important to quantify the efficiency of fine particle retention. The plethora of capturing mechanisms introduced in the previous subsection is usually linked and summarized as the so-called *filter coefficient* λ as established by Iwasaki [72], and subsequently discussed by e.g., [38], [40], [41]. Considering the increase of the capture probability with ongoing process times, and a successive decrease once a critical fine particle deposition is reached, λ is traditionally expressed as an empirical relationship. Hereby, λ typically depends on the fine particle deposition ε_{s2} itself, further material properties like the solidosity ε_s, and some empirical system-dependent parameter(s) $\boldsymbol{P}$ as described by Eq. (7) [45].

$$\lambda = f(\varepsilon_s, \varepsilon_{s2}, \boldsymbol{P}) \tag{7}$$

Notably, the literature in the domain of solid-liquid separation suffers from a non-uniform nomenclature as priorly criticized by Chi Tien [73]. The nomenclature introduced throughout this thesis complies with the definitions established by his work. Many of his respective

studies had a significant impact to cake filtration modeling, which are built upon another very influential 13-part research paper series called *the role of porosity in filtration* by Tiller et al. ([58], [74]–[85]). Therefore, keeping consistent to these works contributes to the domain-wide effort of unifying the employed variable definitions. However, it is important to keep in mind that many references cited in this work may significantly deviate from this standard.

2.1.3 Cake Compression

So far, the previous subsections assumed ideal process conditions yielding incompressible filter cakes, i.e., the intensive main properties of cake filtration porosity ε, and permeability k are defined to be constant over the whole cake thickness. This assumption is approximatively valid for easy-to-handle solid phases with rigid material properties. However, as comprehensively described by Alles and Anlauf [7], the overall filtration pressure p yields a stress p_s on the solid phase, which causes microscopic effects such as particle rearrangement, particle deformation, or particle breakage. In return, the cake is often compressed. Hereby, this effect is especially pronounced for, e.g., solid phases from a biological origin [86]–[88], or fibrous materials [89], [90]. Figure 5 schematically compares an incompressible process with a compressible cake filtration.

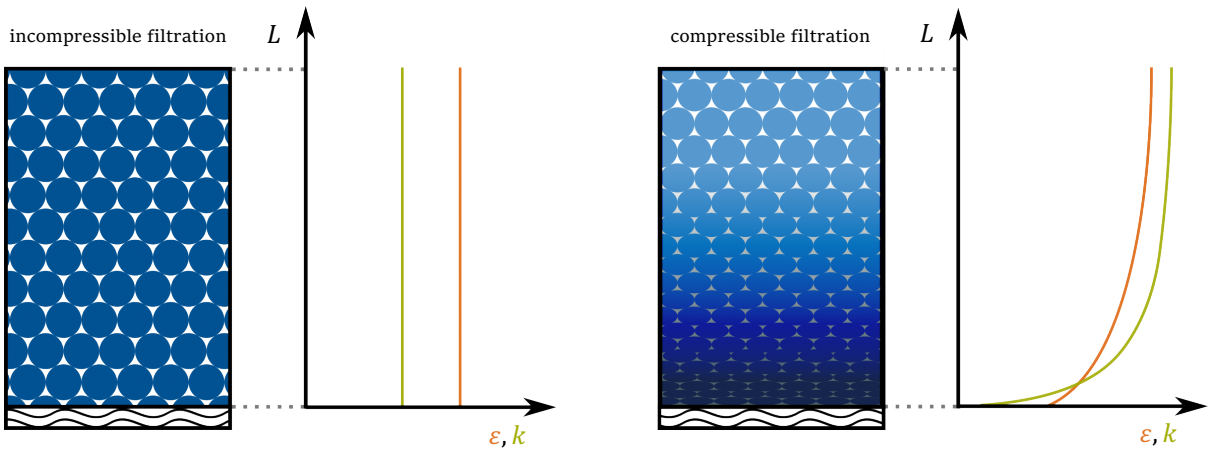

Figure 5 *Qualitative behavior for the porosity ε, and the permeability k in an incompressible (left) and a compressible (right) cake filtration process. Spatial variations in the compressible case result due to compressive stress p_s acting on the solid phase. Only compression resulting from particle deformation is illustrated.*

Qualitatively, the phenomenon of cake compression causes local variations in porosity and permeability, i.e., the quantities decrease exponentially over the filter cake height [17], [91], [92]. Hereby, the minimum of both quantities is located directly above the filter medium. This is often referred to as *skin effect* [81] which denotes a highly solid cake layer that strongly impedes the flow of the liquid phase. Now considering, e.g., a constant flow filtration, the overall filtration pressure drop p does not rise linearly as previously indicated

by Figure 4 but exponentially to maintain the flow rate of the filtrate. Therefore, compression is an undesirable effect lowering the process efficiency which may pose a limiting factor to the filtration.

In order to capture the compressive behavior of a material system in constitutive relationships, it becomes necessary to not only observe the overall macroscopic filtration pressure p, and the filtrate flow rate $\dot{V}$, but also the local pressure and flow variations inside the filter cake. Hereby, the pressure p can be assumed to transfer some of its potential as solid stress p_s onto the solid phase, while some share of liquid pore pressure p_l causes the interpore flow of the liquid phase, as first proposed by Ruth [93]. This can be described by a simple additive term, i.e., $p = p_l + p_s$. However, other authors proved that different relationships f – often additionally correlated with the solidosity ε_s – can be valid to link p_l with p_s depending on the material system in use [94], [95]. These relationships f result from varying definitions of the momentum balance over the filter cake, such that Eq. (8) can be formulated for an arbitrary cake filtration process.

$$\frac{\mathrm{d}p_s}{\mathrm{d}p_l} = f(\varepsilon_s) \tag{8}$$

Using the concepts introduced above, constitutive relationships[3] for local porosity (Eq. (9)), and permeability (Eq. (10)) variations can be constructed for the material system of interest. Various approaches were introduced in, e.g., [43], [96]–[98]. A comprehensive summary of many different material laws can also be found in [70], [99]. Hereby, these mostly empirical equations have in common that they correlate both, the porosity, and the permeability, with the stress acting on the solid phase p_s, and possibly some further parameters $\boldsymbol{P}$.

$$\varepsilon = f(p_s, \boldsymbol{P}) \tag{9}$$

$$k = f(p_s, \boldsymbol{P}) \tag{10}$$

The variable liquid pore pressure p_l resulting from cake compression also affects the internal flow rate v of the liquid phase in the pore space as established by Tiller and Cooper [77]. However, due to the heterogenous cake structure, it is inconvenient to directly quantify this velocity. Instead, the alternative superficial liquid flow rate q_l is often defined via the following relationship [27].

$$q_l = v \cdot \varepsilon \tag{11}$$

Hereby, the intra-particular voids are commonly not taken into consideration when determining the porosity [100], since they do not affect the flow rate of the liquid phase.

[3] In the domain of solid-liquid separation, these constitutive relationships capturing the compressive behavior are commonly referred to as material laws.

Further, the solid phase moves simultaneously towards the filter medium due to the compressive behavior of the filter cake [101]. Therefore, the superficial velocity for the solid phase must be introduced as q_s as well. However, neither q_l, nor q_s are described using constitutive relationships but are a direct result from mechanical models on continuum level. Thus, Section 2.2.2 elaborates further on this topic.

2.1.4 Filter Aid Utilization

Filter aids can be used to increase the efficiency of the cake filtration process. Hereby, these materials are added to the system if the initial suspension poses problems during the act of separation. This can be the case if, e.g., the slurry is very low concentrated, the impurities are hard to filter[4], the particles do not form a filter cake by themselves, or if simply no other solid-liquid separation technique is available [14]. Further, filter aids help in maintaining the flexibility of a plant, since various filtration problems can be addressed with the same set-up using the correct choice and dosage of different filter aids. However, since the filter aids are mixed with the initial solid phase, separating the final filter cake into both particle systems is costly. Therefore, this technique is often used for applications in which the filtrate is the target of recovery. Some applications include, but are not limited to, the beverage production [102], [103], the food industry [104], [105], water treatment [106]–[108], biotechnology [109], and the processing industry [13], [104].

The action of filter aids mainly originates from mechanical nature by creating a highly porous filter matrix [25], [100], [110]. Hereby, the impurity particles attach themselves into the created network of voids. Further, the cake permeability is significantly increased due to the lower solidosity [92], [109]. At the same time, filter aids also reinforce the filter cake, since a higher permeability also causes less stress to act on the solid phase which counters the effect of cake compression.

In the case of dead-end cake filtration, the process of dosing filter aids commonly consists of two separate stages referred to as *precoat* phase [13], and *bodyfeed* phase[5] [24]. Hereby, a layer of pure filter aid is first built upon the existing filter medium. This precoat ensures that during the initial time span of filtering the slurry no impurity particles cause fouling, i.e., pore blocking, of the filter medium, and that no fine particles migrate into the filtrate. Afterwards during the bodyfeed stage, a specific filter aid amount is continuously dosed to the suspension to be cleared which causes the actual filter cake to form [14], [43], [100]. This process is illustrated in Figure 6.

Just as in the general case of cake filtration, most of the impurities are directly separated along with the filter aid particles via the mechanism of surface filtration. Some fine particles, on the other hand, may migrate through the filter cake until they are

[4] Unscientifically speaking, for “jellylike”, or “sticky” particles
[5] Sometimes also called primary and secondary filtration phase [18], [111]

eventually immobilized by the mechanism of depth filtration [112]. Hence, the precoat incorporates these impurities successively during the process as can also be seen in the following figure. Various studies showed the importance in describing this phenomenon accurately [18]–[21], [111].

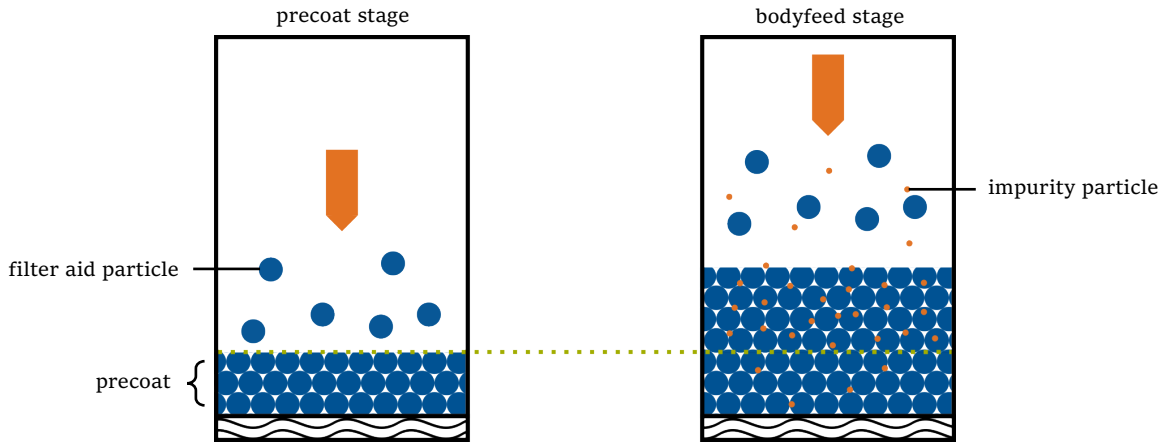

Figure 6 *Illustration of the precoat stage (left), and the bodyfeed stage (right); the thickness of the precoat layer is illustrated by the horizontal green line.*

There exists a variety of different materials that have been successfully identified for the use as filter aids. The longest established are those from mineral and fossil origins such as diatomaceous earth, commonly referred to as kieselguhr [15], [25], [110]. Hereby, kieselguhr is known as a very efficient filter aid, as it has been described to consist of up to 90% voids [13]. However, this traditional filter aid also goes along with several problems. First, due to its fossil origin it is not an endlessly available resource. Moreover, when exposed to aerosol dusts consisting of such filter aids people may become affected by Silicosis [113], which is a type of occupational lung disease and may further be the cause to lung cancer [114]. Hence, disposal does not only pose ecological issues [115], but is also considered a toxic waste [16].

Therefore, the use of alternative filter aids is researched on in recent years. Some of these alternatives include fibrous filter aids (e.g., cellulose [116], [117], viscose [118], wood fibers [104]), or materials from organic origin, such as rice hull ash [119]. Contrary to the classical filter aids, these materials are usually easier to recycle, and they tend to form less dust during handling. Moreover, due to their morphology and overall softer material properties, less wear and tear is caused on process equipment [104]. However, these characteristics often also yield substantial compressive behaviors, opposed to those filter aids from mineral origin, which can usually be approximated as incompressible [18], [90]. As established before, the effect of compression decreases the overall process efficiency significantly. Hence, it becomes important to find the ideal filter aid dosage (→ *Objective III*) to maintain a profitable process. This underlines the initial motivation to find accurate mathematical models (→ *Objective II*) that do not only represent the general process of cake filtration, but also cases involving filter aids in order to conduct rigorous mathematical optimizations.

2.2 Continuum Scale Cake Filtration Modeling

As mentioned in the introduction, the comparably new engineering discipline of *process systems engineering* emerged during the recent decades and aims at interconnecting the rapid development of computational capabilities with the more "traditional" domains of chemical engineering, and process engineering [120]. Especially complex mathematical model simulations benefit strongly from the ever-increasing computing power[6], since they can be used as a tool to gain new technical insights, and to improve the performance of established processes. One possible approach in process systems engineering is to examine the same process on various scales using different model formulations. Hereby, the area of solid-liquid separation and, thus, filtration is no exception. In their philosophical analysis, Kuhn et al. [121] classified the typical scales in cake filtration as the *microscopic scale,* and the *macroscopic scale,* which are intended to resolve the filtration process on the individual pore level, and on the continuum mechanical level, respectively. Additionally, the intermediate *mesoscopic scale* can be defined which intends to only resolve the relevant pore-network without the need for simulating the fully resolved filtration unit [122]. Figure 7 gives an overview over the respective scales.

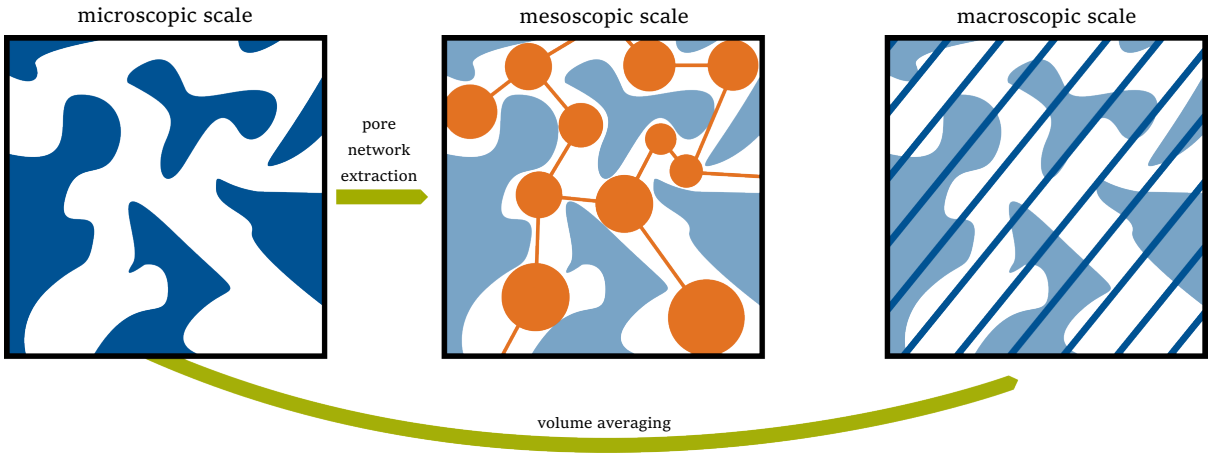

Figure 7 *Illustration of different scales in cake filtration modeling. Adapted from [27].*

This work especially addresses the use of continuum scale models. Hereby, continuum mechanical methods assume the filter cake structure as a whole instead of conducting a detailed characterization of the underlying porous media's heterogenous structures. In order to gather the information needed to employ the continuum scale, the method of volume averaging can be applied [123]. The functional relationship to calculate the volumetric averaged value $\langle f \rangle$ for an arbitrary physical quantity f depending on the spatial dimension $\boldsymbol{x}$, the control volume V_c, as well as the temporal dimension t is defined in Eq. (12). This technique is also illustrated in Figure 7. Further comprehensive information on the method's application to filtration models can be found in [27].

[6] Commonly referred to as Moore's law

$$\langle f(t,\boldsymbol{x})\rangle = \frac{1}{V_c}\int_{V_c} f(t,\boldsymbol{x})\,\mathrm{d}V \tag{12}$$

Notably, the technique of volume averaging can be employed over multiple dimensions, i.e., a three-dimensional structure can be reduced to a two-dimensional one. At this point once again, it may be spatially averaged to a one-dimensional quantity which is the dimension of interest in this work. Clearly, this process imposes a significant loss of detail especially in regard of heterogenous structures being present in the filter cake. At first glance, the method might therefore seem outdated considering that in the domain of solid-liquid separation the *micro-theoretic* and *micro-manipulative* paradigms are state-of-the-art according to Kuhn et al. [121]. However, despite the higher degree of accuracy that may be achieved from employing, e.g., pore scale methods, computational times of the corresponding simulations can take up to several hours for a single run. Continuum scale models, on the other hand, can typically be solved in a matter of seconds. Therefore, they are favorable for the objectives of this thesis; especially since the intended optimization procedures for the scenario of filter aid filtration require for fast and efficient processing.

In the following subsections, the two most established continuum scale modeling approaches for cake filtration processes are discussed. The first one is known as the *conventional filtration theory*, which advantage is its simplicity. Secondly, the *multiphase flow theory* allows for more detailed insights into the process but requires for numerical approximation schemes to be solved. Analyses and summaries of both theories can be found in [70], [91]. For the sake of completeness, some further mechanistic modeling techniques in the domain of cake filtration include, e.g.:

- [88], [124], [125] describing the process under consideration of individual particle dynamics
- [126]–[128] employing simulations based on computational fluid dynamics
- [129]–[131] applying pore-network extraction methods
- [132]–[134] investigating modeling approaches based on compressional rheology
- [135], [136] introducing a diffusion-type model architecture in Lagrangian coordinates

2.2.1 Conventional Theory

The foundation to the conventional theory of cake filtration modeling can be traced back to 1856, since it is built upon Darcy's law [60] as defined by the following equation.

$$\dot{V} = \frac{\Delta p \cdot k \cdot A}{\mu \cdot L} \tag{13}$$

In a historical context, this is one of the earliest mathematical relationships to predict the resulting fluid flow rate $\dot{V}$ through a porous medium depending on the pressure difference Δp applied to the system. Hereby, it is correlated with the solid phase's permeability k, the fluid's viscosity μ, as well as the height L, and cross-sectional area A of said porous medium. Initially, Darcy's law was assumed to be from empirical nature. However, in subsequent studies it was also derived mathematically by volumetric averaging of continuity equations [137]. Even though the derivation is only valid for the case of creeping Stokes flows, Bear [61] specifies that Darcy's law may produce accurate results for Reynold's numbers as high as 10. Therefore, Eq. (13) can be interpreted as a mechanistic physical model for ideal non-turbulent flows.

In order to apply this relationship to cake filtration set-ups, the flow rate of the filtrate is often assumed to be affected by two additive terms, namely, the height-specific filter cake resistance r, and the filter medium resistance R_m as described by Eq. (6). Hence, the differential form of Darcy's law suitable to describe the filtrate flow rate for cake filtration processes reads:

$$\frac{\mathrm{d}V}{\mathrm{d}t} = \frac{\Delta p \cdot A}{\mu} \cdot \frac{1}{(L \cdot r + R_m)} \tag{14}$$

This expression was similarly developed independently by both, Carman [138], and Hermans [139]. As elaborated by Buchwald[7] [140], Carman seems to be the first author to use this approach in the analysis of cake filtration. Nevertheless, Hermans' work had a lasting impact particularly in the German speaking filtration community. In any case, their respective works formed the foundation to what eventually was turned into the VDI 2762 norm [11], a three-part standard reference describing the best practices in laboratory cake filtration, and subsequent data analysis. Using Eq. (14) as a starting point and conducting a small number of steps described in said guideline yields Eq. (15).

$$\frac{t}{V} = \frac{K \cdot \mu \cdot r}{2 \cdot A^2 \cdot \Delta p} \cdot V + \frac{\mu \cdot R_M}{A \cdot \Delta p} \tag{15}$$

Hereby, K denotes the so-called concentration constant. It is defined by the area covered by the filter medium A, the cake height L, as well as the cumulative filtrate volume V.

$$K = \frac{A \cdot L}{V} \tag{16}$$

[7] Notably, the PhD thesis of Buchwald [140] contains many further comprehensive insights to the overall historical developments in cake filtration analysis along with detailed derivations of the respective mathematical models.

Notably, the derivation of Eq. (15) is only valid for the case of constant pressure filtration. However, this is the typical operation mode in laboratory environments to characterize the properties of the examined material system. Therefore, the formulation for constant flow applications is not further elaborated here but can, e.g., be found in [140].

The advantage of Eq. (15) lies in its linearized arrangement, i.e., the right-hand side can be interpreted as a linear function depending solely on the cumulative filtrate volume $V(t)$. Hence, the characteristic quantities r and R_m can be found by graphically plotting the experimental data as an (ideally) straight line in a $\frac{t}{V}$-over-V diagram as illustrated in Figure 8. Hereby, the intersection with the ordinate yields the value for R_m, while using the slope allows to directly solve for r.

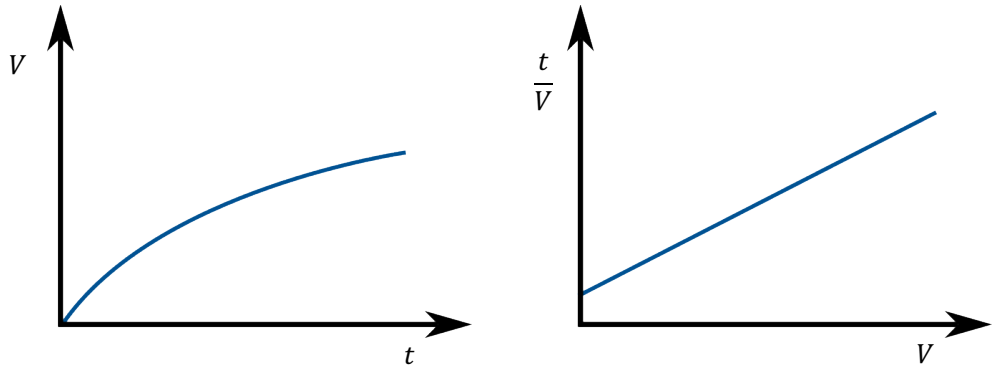

Figure 8 *Ideal experimental cake filtration data in the case of a constant pressure filtration (left); linearized data according to Eq. (15) (right).*

Undoubtedly, this model is easy to solve and often yields sufficient accuracy for the representation of incompressible cake filtration data. Moreover, due to the method's age established heuristics are available. For example, experienced filtration personal can quickly identify problems occurring in the filter cell if the process data deviates from the ideal linear function. As stated in the VDI guideline [11] an exponential data profile indicates towards pore blocking of the filter medium, and significant cake-internal fine particle migration happening. Therefore, even modern works still rely on this approach (e.g., [141]–[145]).

Nevertheless, the practical use of this initial form of the conventional theory is limited if the filter cake is compressible. As a result, systematic errors occur quickly even for moderate grades of cake compressibility using the previously introduced procedure. Therefore, many analytical extensions to the conventional theory have been derived in which compressibility is accounted for, e.g., [25], [74]–[76], [97], [146]. Hereby, particularly the works of Ruth [93], and Grace [147] laid the foundation to these formulations. Although those approaches may yield satisfying results for specific problems, the overall framework is critically assessed by various authors [88], [148], since compression is typically underestimated [149], and substantial relative errors of up to 15% [150] to 50% [151] are reported.

Some additional overall drawbacks remain despite the grade of cake compressibility: the resulting process quantities only contain or are reconstructed from global information,

i.e., mean values for the overall filter cake [91], [97]. Further, it is impractical to incorporate the phenomenon of cake-internal particle migration into the analytical framework of the conventional theory [151]. Although approaches exist to quantify the mechanism of depth filtration only, e.g., [21], [41], [72], works combining it with the mechanism of surface filtration show significant simplifications [43], [152], or require numerical solution procedures [112], [153] as they are based on complex systems of first principle partial differential equations.

2.2.2 Multiphase Flow Theory

The multiphase flow theory emerged due to the drawbacks, and the number of compromises imposed by the conventional filtration theory. As discussed by Tien [150], the progression into this new framework comprises less restrictive assumptions and, thus, promises to predict the process of cake filtration more accurately. Hereby, the transition from the conventional theory to the multiphase flow theory was significantly influenced by the paper series *the role of porosity in filtration* under the lead of Tiller, as introduced in Section 2.1.2. In 1960, Tiller and Cooper [77] published said series' part IV, in which the authors identified that the liquid phase's flow rate is not constant over the filter cake height. Ignoring this fact might produce significant errors, as demonstrated in Tiller's and Huang's successive work [154].

This is due to the relative movement occurring between the liquid and the solid phase resulting from the effect of cake compression. In order to account for this phenomenon, Darcy's law needs to be adjusted as discussed by, e.g., Shirato et al. [155], and Wakeman [156]. Using the definition in Eq. (11) for the superficial liquid velocity q_l, and superficial solid velocity q_s the generalized Darcy law including the slipping velocity reads as follows.

$$\frac{q_l}{\varepsilon} - \frac{q_s}{\varepsilon_s} = -\frac{1}{\varepsilon} \cdot \frac{k}{\mu} \cdot \frac{\partial p_l}{\partial x} \tag{17}$$

Further, the mechanistic relationships between the system states porosity ε, solidosity ε_s , as well as q_l, and q_s, are defined via the mass continuity equations given in Eq. (18) and Eq. (19), which are the governing model equations [157].

$$\frac{\partial \varepsilon}{\partial t} = \frac{\partial q_l}{\partial x} \tag{18}$$

$$\frac{\partial \varepsilon_s}{\partial t} = \frac{\partial q_s}{\partial x} \tag{19}$$

Using the obtained system states allows to derive an accurate mass balance which yields a Stefan Problem [158], [159]. Thereby, a moving boundary expression in the form of $\frac{\mathrm{d}L}{\mathrm{d}t}$ may be integrated to explicitly track the filter cake growth $L(t)$ over time including compressive effects.

To close the model equations, the constitutive relationships capturing the compressive behavior of the filter cake must be determined. These were previously defined in Eq. (9) and Eq. (10), and correlate the porous media's permeability k, as well as the porosity ε with the solid stress p_s. Hereby, p_s is directly coupled with the liquid pore pressure through a constitutive relationship defined in Eq. (8) which is derived from a momentum balance corresponding to the material system [94], [157].

Combining these parts of the multiphase flow theory leads to the final cake filtration models which significantly influenced this work: the model introduced by Stamatakis and Tien [160], and, further, the extended version presented by Tien et al. in [8]. This second formulation additionally allows to mechanistically describe the effect of superimposed depth filtration by incorporating the filter coefficient λ defined in Eq. (7). Thereby, conservation equations track the spatio-temporal development of the volumetric fine particle content ε_{s2} in both, the liquid, and the solid phase. The derivation of these models is also summarized in the textbook [91].

In conclusion, the multiphase flow theory offers two advantages over the conventional theory by describing the cake filtration process as a system of partial differential equations. Apart from the possibility to accurately describe the temporal and spatial developments of all introduced characteristic filtration quantities without the need for significant intermediate simplification steps, the mechanism of cake-internal particle migration can be seamlessly integrated (→ *Objective II*). However, this approach also marked the transition from an analytical framework to a numerical one, i.e., approximation schemes are needed to find solutions to the newly derived mathematical model equations which makes computations a lot more involved.

2.3 Remarks on Process Optimization

Industrially-scaled processes are intended to not only meet desired product criteria but also to be conducted economically. Hence, the ideal set of control parameters fulfilling these goals must be found. To this end, the technique of mathematical optimization has proven to be useful in numerous engineering applications [161], [162]. Naturally, this overall procedure has also been adopted in various solid-liquid separation processes. Optimization works have been described in the literature for, e.g., depth filters [39], [163], [164], and especially for membrane filtration processes [165]–[171].

However, this method is only sparsely applied in the domain of cake filtration processes. Rare examples include the investigation of ideal system pressures [17],

determining optimal filtration cycle times [34], [66], finding desired deposition profiles [153], or minimizing the process' energy expenditure [172]. Even rarer are applications to filter aid filtration, despite experimental works showing that it is crucial to find the ideal filter aid dosage which leads to an effective filtration [18], [25], [107]. Some historical approaches try to optimize the resistance of filter cakes made up from filter aids, and impurities using simple analytical models, e.g., in [23], [24], [64]. Further, Tittel [28] and Wegner [173] developed methods to find optimal filter aid dosages based on the filter aid filtration model developed by Berndt [43]. Notably, all the previously mentioned works originated between the 1960s and 1980s which restricted them by the limited computational capabilities of their time.

Latest studies indicate that the process efficiency can be further increased by adjusting the filter aid dosage during the process [22]. Typically, those variable control functions are obtained by conducting dynamic optimizations, or optimal control procedures. This technique has been applied by Kuhn and Briesen to filter aid filtration using an analytical approach using a strongly simplified model [29]. Subsequently, in his Ph.D. thesis Kuhn [27] implemented a numerical optimal control algorithm using a more elaborate model [112], which also includes the effect of depth filtration. Hereby it was demonstrated that dynamically varying the filter aid dosage only shows negligible impact for persistent suspension compositions. Nevertheless, once the slurry's impurity concentration varies, a time-varying filter aid supply can improve the process efficiency by up to ≈ 10 %. However, those works are only valid for classical filter aids, i.e., incompressible systems. Therefore, it remains unclear how the behavior of compressible filter aids might influence the optimal dosage, or if, e.g., negative impacts from cake compression can be counteracted by variable filter aid dosages. Hence, for alternative filter aid materials the process efficiency might be improved further (→ *Objective III)*.

Terminologically, this work differentiates between the techniques of *optimal control,* and *static optimization*. As indicated before, optimal control aims at finding arbitrary control *functions* $u(x)$ depending on an independent variable x[8]. Opposed to those dynamically varying inputs the static optimization is intended to find a control *parameter*, i.e., $u = \text{const}$. In the present context, the static optimization can therefore be assumed to be a special case of an optimal control problem. While these definitions seem trivial, a clear distinction is important. This is because the static optimization sets a benchmark which could similarly be obtained by systematic experimental investigations. Hence, employing an optimal control method offers the possibility to outperform such a baseline scenario exclusively through rigorous mathematical investigations.

According to Kirk [30], an optimal control problem requires three distinct parts. First, a dynamic model ($\boldsymbol{f}: \mathbb{R}^m \times \mathbb{R}^n \times \mathbb{R}^o \rightarrow \mathbb{R}^n$) describing the variable evolution of the system state(s) $\boldsymbol{y} \in \mathbb{R}^n$ depending on the independent variable(s) $\boldsymbol{x} \in \mathbb{R}^m$, and the vector of

[8] In most applications the independent variable x is the time t. However, the optimal control may also be calculated in dependence of other domains, e.g., space.

control functions ($\boldsymbol{u}$: $\mathbb{R}^m \to \mathbb{R}^o$). Second, pertinent inequality, and equality conditions, (g: $\mathbb{R}^m \times \mathbb{R}^n \times \mathbb{R}^o \to \mathbb{R}$), and ($h$: $\mathbb{R}^m \times \mathbb{R}^n \times \mathbb{R}^o \to \mathbb{R}$), e.g., constraints from physical, numerical, or technical nature. Third, some cost functional (J: $\mathbb{R}^m \times \mathbb{R}^n \times \mathbb{R}^o \to \mathbb{R}$) capturing the model's performance for the assessed control u. Hence, an arbitrary optimal control problem may be formally defined as follows.

$$\min_{\boldsymbol{u}} \; J\big(\boldsymbol{x}, \boldsymbol{y}(\boldsymbol{x}), \boldsymbol{u}(\boldsymbol{x})\big) \tag{20}$$

$$\left.\begin{aligned} s.t. \quad \frac{\mathrm{d}\boldsymbol{y}}{\mathrm{d}\boldsymbol{x}} &= \boldsymbol{f}\big(\boldsymbol{x}, \boldsymbol{y}(\boldsymbol{x}), \boldsymbol{u}(\boldsymbol{x})\big) \\ g\big(\boldsymbol{x}, \boldsymbol{y}(\boldsymbol{x}), \boldsymbol{u}(\boldsymbol{x})\big) &\leq 0 \\ h\big(\boldsymbol{x}, \boldsymbol{y}(\boldsymbol{x}), \boldsymbol{u}(\boldsymbol{x})\big) &= 0 \end{aligned}\right\} \forall\, \boldsymbol{x} \in [\boldsymbol{x_0}, \boldsymbol{x_f}]$$

Notably, optimization problems are usually denoted as minimization problems. However, these can be trivially transformed into maximization problems by multiplying the performance index J with -1. Hereby, several types of cost functionals exist which map the model's quantitative behavior to an easily assessable scalar. The most common types are called Mayer, and Lagrange functionals which, respectively, either only assess the cost at the model's final state or integrate the cost over the whole domain of interest. The combination of both types is referred to as Bolza functional.

Naturally, optimal control approaches are mathematically challenging since Eq. (20) results in an infinite dimensional optimization problem. Therefore, only some simple optimal control applications may be solved analytically by fulfilling the necessary conditions of optimality [161], [174], [175]. Due to the strong nonlinearities and complex process interactions imposed by the multiphase flow theory, those analytical approaches are ruled out as infeasible for this work. Nevertheless, numerical approaches can be used to iteratively construct an optimal control solution. These are broadly categorized as direct and indirect methods [176], [177]. Hereby, indirect methods rely on deriving a boundary value problem that satisfies the previously mentioned optimality conditions. Since, both, indirect methods, and analytical approaches, are not investigated throughout this work, they are not further discussed here. For a review of the corresponding theory it is referred to [178]. Applications of the previously mentioned techniques for cake filtration can be found in [27], [29], and [153].

Instead, the focus lies on direct approaches. These overall techniques rely on a straight-forward transformation of the initial optimal control problem stated in Eq. (20) into a regular finite-dimensional nonlinear program. One possibility is to discretize the domain of the control u for which arbitrary functions are then parameterized using a numerical optimization algorithm [179], [180]. In general, direct methods are especially well-suited for handling optimal control problems that include models consisting of partial differential equations, as well as difficult problem constraints [176], [181]. However, typically these iterative procedures only approximate the solution, since – from a computational perspective – the discretization cannot become infinitely small. The intention

of achieving a better accuracy of the control trajectory u by either increasing the underlying function's order (*p-method*) or decreasing the discretization size (*h-method*) often leads to a significantly higher computation time. Therefore, numerically efficient and precise model calculations are crucial for this type of optimal control approach – an issue that is closely related to → *Objective IV* and is covered in the next section of this thesis. More information and deeper insights on direct methods, the theory of optimal control, as well as numerical optimization in general can be found in various textbooks, e.g., [182]–[186].

2.4 The Role of Computational Efficiency

If partial differential equations are used to resolve physical quantities on both, the spatial, and the temporal dimension, usually numerical techniques are employed that rely on discretization schemes producing large systems of ordinary differential equations [187]. In return, the corresponding simulations can take up significant computational time spans to be solved. As stated in Section 2.2, employing continuum scale models is already in favor of low numerical cost compared to alternative methods. Therefore, simple forward simulations often do not encounter any temporal computing constraints by themselves. However, advanced methods using these models as a foundation to solve further problems – such as the optimization procedures encountered in this work – do. This is because the simulations must be repeatedly evaluated under parameter variation. Depending on the desired accuracy, and the complexity of the algorithm hundreds or thousands of single processing runs may add up consequently rendering the intended techniques uneconomic or even practically infeasible.

Thus, particularly the simulation procedures for those models based on the multiphase flow theory shall be sped-up in the scope of this thesis. This matter was previously addressed in [188]. Hereby, the cake filtration model based on the system of partial differential equations introduced in [8] was transformed into a cake thickness-averaged formulation which yields a simpler model consisting of ordinary differential equations only. This does not only make the model easier to implement but also decreases the numerical cost significantly. However, due to the averaging approach any transient spatial information is lost which limits the model's applicability in further analyses of the cake formation process, and, thus, conducting detailed optimizations.

Nevertheless, in recent years other numerical techniques were developed to raise the computational efficiency of mathematical model simulations independently of the ever-increasing hardware performance. These approaches can be broadly summarized as reduced order modeling (ROM) methods [189]–[191], for which a main property is to explicitly retain the underlying full order model's quantitative solution features. This work focuses on so-called projection-based model order reduction [192]. Hereby, the most established method is probably the technique of proper orthogonal decomposition (POD) [193], [194]. To this day, the method has been applied in many engineering disciplines – including some

employments of the POD in the domain of fluid flow through porous media, e.g., [195]–[197]. However, only one ROM study is known for incompressible cake filtration processes [198], and no works exist incorporating either the influence of cake compressibility or examining filter aid filtration. Therefore, the POD method is applied to the modeling framework introduced in Section 2.2 (→ *Objective IV*).

Notably, many further extensions to the POD method exist such as several ROM adaptation approaches [199], [200] enabling the ROM to represent the underlying full-order dynamics under parameter variations which is required for optimization procedures. Moreover, some techniques are established to efficiently handle nonlinear terms occurring in the reduced model equations, e.g., the discrete empirical interpolation method [201], [202], or the gappy POD [203], [204]. However, to explain those features would go beyond the scope of this introduction to the POD method. The overall theory on the application of projection-based ROM to systems of partial differential equations is summarized in, e.g., the following textbooks [187], [205]–[207].

Chapter 3

Methodology

This thesis is set exclusively in the methodological domain of computer-aided techniques and numerical procedures applied to the process of cake filtration. Hereby, no process data from real-world filtration experiments is investigated. Instead, new knowledge is generated via means of model-based investigations. This chapter gives a brief outline on the methods used to solve the modeling architectures encountered in Section 2.2. Further, those techniques employed to address the objectives explained throughout the introduction are introduced while referring to the theoretical foundations elaborated in Sections 2.3 and 2.4. As the actual methods are explained in detail during the respective studies, the following overview is kept short and concise with the intention to avoid unnecessary repetitions. Notably, all involved numerical procedures were implemented in MATLAB (The MathWorks, Inc., Natick, Massachusetts, US), versions 2018a, 2021b, and 2022b, and can be solved using regular consumer-grade computers.

3.1 Model Simulations

3.1.1 Monte Carlo Experiments

Full-Length Paper I (p. 78) examines the occurrence of systematic errors when the model stated in the VDI 2762 norm (see Section 2.2.1) is used to evaluate cake filtration data. To this end, employing a so-called Monte Carlo method [12] allows to cost-effectively generate a vast set of artificial experimental data by repeatedly simulating the incompressible cake filtration model with known parameter values. During this process, noise is imposed to the ideal computed effluent's volumetric flow rate $\dot{V}$, as well as the specific cake resistance r. These disturbance modes account for two different effects frequently observed in laboratory environments. While the scattering flow rate of the filtrate describes small variations that may occur during the experiments, a variable filter resistance results due to a possible bias in taking samples from the solid phase during the preparation of the experiment. For both disturbance modes, the noise level was varied from 0% to 20% of the respective nominal variable values. Hereby, the noise is generated from normally distributed (pseudo-)random

numbers using MATLAB's `randn` algorithm [208]. In total, 3000 *in silico* filtration experiments were computed; each for an assumed total process time of $t = 100$ s.

3.1.2 Handling Partial Differential Equations

Full-Length Paper II (p. 88), as well as Full-Length Paper III (p. 103) employ the multiphase flow theory as introduced in Section 2.2.2 to represent the process of filter aid cake filtration. Due to the chosen framework these models comprise partial differential equations which can only be solved numerically by approximation techniques.

The models are classified as a Stefan problem due to the filter cake's height growth over time $L(t)$. Therefore, the Front Fixing Method[9] [210] is applied to transform the time-dependent system boundaries $x = [0, L(t)]$ to the fixed interval $z = [0, 1]$. This procedure allows to employ the Method of Lines as a numerical solution technique in both aforementioned Studies [211]. Hereby, the spatial dimension is discretized which converts the system of partial differential equations into a set of ordinary differential equations. After transformation, each resulting ordinary differential equation describes the temporal development of a system state at one distinct coordinate of the filter cake over time. Occurring spatial derivatives are approximated using three-point central, and five-point upwind finite differencing schemes [187]. The remaining temporal dimension is integrated using MATLAB's `ode15s` method [212]. As this algorithm is an implicit integration approach, it is especially well-suited for stiff systems of ordinary differential equations which usually arise when the Method of Lines is applied [187].

Typically, numerical algorithms contain floating point variables which only fulfill a limited machine precision [213]. Therefore, round-of errors might accumulate when basic mathematical operations between variables of highly different magnitudes are performed. Hence, all model equations are non-dimensionalized through process-inherent scaling of variables in order to improve the numerical stability of the solution technique described above.

3.2 Employed Optimization Algorithms

Full-Length Paper II (p. 88) aims at finding optimal operation strategies to increase the overall process efficiency for different filter aid cake filtration processes. To this end, Eq. (21) states the examined minimization problem subject to the cake filtration models[10] based on the multiphase flow theory as introduced in Section 2.2.2.

[9] Sometimes also referred to as Landau transformation [187], [209]
[10] Notably, the formal optimization problem is not stated in its entirety, as the complete formulation would be rather involved containing numerous model equations.

$$\min_{c,\, L_{PC}} e \tag{21}$$

Hereby, a Lagrange-type cost functional is incorporated by mapping the time-dependent pressure drop $\Delta p \in \mathbb{R}$, and the volumetric flow rate of the effluent $\dot{V} \in \mathbb{R}$ to the scalar value of the area-specific energy consumption (e: $\mathbb{R} \times \mathbb{R} \times \mathbb{R} \rightarrow \mathbb{R}$) over the process time $t \in \mathbb{R}$:

$$e\left(t, \Delta p, \dot{V}\right) = \int_T \Delta p(t)\dot{V}(t)\, \mathrm{d}t \tag{22}$$

Moreover, the model's performance is influenced by two controls to be optimized, i.e., $c \in \mathbb{R}$ as the filter aid concentration dosed to the suspension, and $L_{PC} \in \mathbb{R}$ as the height of the initial precoat layer.

Study II encompasses two optimization approaches. First, the static optimization is examined, where the filter aid concentration is defined as a constant control parameter, i.e.,

$$c = \text{const.} \tag{23}$$

Moreover, physically-motivated inequality constraints are imposed on the controls as the height of the precoat layer L_{PC} cannot be negative. Similarly, the filter aid concentration is prevented from taking negative values, and, at the same time, is restricted from exceeding the solidosity ε_s of the filter cake's top layer.

$$0 \leq L_{PC} \tag{24}$$

$$0 \leq c(t) \leq \varepsilon_s\left(x = L(t)\right)$$

The resulting static optimization problem is solved by processing the default gradient-based interior-point algorithm provided by MATLAB's `fmincon` method [214].

In the same study, the technique of optimal control is subsequently employed to determine the ideal time-varying filter aid concentration $c(t)$. Hereby, (c: $\mathbb{R} \rightarrow \mathbb{R}$) is defined as a solution to the optimal control problem stated in Eq. (21) if the corresponding cost functional outperforms the benchmark set by the previously described static optimization scenario. To this end, the optimal control trajectory c is approximated by a direct h-method. In this approach, piecewise linear functions are parameterized over the whole temporal domain T. Hereby, the discretization size of these function segments is repeatedly bisected, while for each new iteration the optimization procedure is initialized with the obtained optimal parameter values from the previous iteration. This algorithm ensures that the newly emerging linear functions converge robustly towards a well-defined optimum. Study II gives further detailed explanations on the iterative procedure to derive c. The observant reader might also have noticed that the overall procedure is illustrated on this thesis' cover page.

As the previously described method transforms the infinite dimensional optimization problem stated in Eq. (21) into a finite-dimensional nonlinear program, it is solved by Matlab's `fmincon` method, too. For this case, the sequential quadratic programming algorithm [214] was chosen while using central finite differencing to obtain the required gradient and Hessian. Hereby, the central scheme achieves a higher order of accuracy compared to MATLAB's default forward step scheme [187]. Further, the sequential quadratic programming procedure can mimic Newton's method of optimization for constrained problems as described by the corresponding documentation [214]. Since Newton's method of optimization features quadratic convergence characteristics in a local region around the optimal solution, it is well-suited for employing the procedure. This is because for each new iteration i the optimization algorithm's initial guess for the control parameters describing the trajectory c already lies in a local region around the sought-for trajectory refinement. Hence, the SQP procedure operates significantly faster than the default interior-point algorithm.

Study III incorporates the same static optimization problem defined in Eq. (21). In this paper, the iterative procedure provides a benchmark, too. However, contrary to Study II, the optimization task itself is not the main subject of investigation. Instead, the optimization scenario merely provides a sample problem to be solved using the model order reduction approach.

Notably, Paper I involves an optimization procedure as well, since the parameter estimation problem can be expressed in the following form as an unconstrained least squares problem:

$$\min_{\boldsymbol{P}} \quad J(\hat{x}, \hat{y}, \boldsymbol{P}) \tag{25}$$

$$J = \sum_{i=1}^{N} \left(\hat{y}_i - f(\hat{x}_i, \boldsymbol{P})\right)^2$$

Here, x is the independent, and y the dependent variable, whereas the $\widehat{\ }$-accent denotes data obtained from the Monte Carlo method. Further, f is the examined model function, N the total number of data points, and $\boldsymbol{P}$ the parameter set to be determined. However, the implementation and processing of the parameter estimation procedure is trivial. In this work, MATLAB's `fminsearch` method was employed using standard options which results in the computation of the well-known Nelder-Mead Simplex technique [215], a gradient-free optimization algorithm.

3.3 Model Order Reduction

Full-Length Paper III (p. 103) incorporates a study to increase the computational efficiency of the cake filtration model simulation based on the multiphase flow theory described in

Section 2.2.2. To this end, a ROM is built using the POD method as introduced in Section 2.4 by roughly following the main steps outlined in [205]. Hereby, first a representative sample data base capturing the system's dynamics is obtained through simulating the full order model. After, performing a singular value decomposition to the data matrix using MATLAB's `svd` routine yields a collection of corresponding $L2$-optimal basis functions. This is commonly referred to as direct approach in the POD literature. The found set of orthogonal POD modes is subsequently truncated, such that the reduced basis captures most of the system's dynamics. In a next step, employing the Galerkin Method [187] allows to project the full order model equations onto the diminished POD basis. The resulting system of ordinary differential equations is significantly smaller compared to the underlying full order model. Finally, after numerical integration the obtained solution features are transformed from the reduced order space back to the high dimensional model space.

During the study, the previously described technique is referred to as *local POD*, since the POD basis is constructed from only one full order model simulation using a single representative parameter set. However, poor results are expected for different control parameter configurations as required in the benchmark optimization procedure. Therefore, two additional extensions to this initial POD method are evaluated. First, the *global* POD approach involves enriching the data matrix used for the singular value decomposition with results from multiple full order model simulations under parameter variation. Moreover, the Subangle Interpolation Method (SAIM)[11] is introduced as a ROM adaptation technique [199]. As the name suggests, this approach interpolates one set of basis functions into the other while maintaining the required orthogonality properties.

[11] The SAIM is a special case of the Grassman manifold technique [216].

Chapter 4

Full-Length Paper Summaries

This chapter presents the summaries of the research papers investigating the use of nonlinear continuum scale models in cake filtration. The corresponding full-length articles along with their meta data, copyright information, as well as contributor roles taxonomy (CrediT) are contained in the Appendix on pages 78, 88, and 103, respectively.

4.1 Publication I – Monte Carlo Study

The first paper addresses → *Objective I* of this thesis by proposing an evolution to the widely applied VDI 2762 guideline [11] which is intended to evaluate experimental cake filtration data. As elaborated in Section 2.2.1, the technique is based on a filtration model (see Eq. (15)) in the framework provided by the conventional theory. However, the precision in estimating the filter resistance as the parameter of interest is limited due to several drawbacks imposed by the linearization procedure described in VDI 2762. First, a linearization of the model leads to the distortion of experimental error distributions. Second, meaningful linear model graphs can only be obtained, if the full data set is cropped by the first few measured values. Since the choice of the number of data points to be dropped lies in the individual assessment of the experimenter, a subjective bias is imposed to the overall data set, and, therefore, some process information is always lost.

Hence, the simple premise of this study's alternative approach lies in resolving Eq. (14) as a root function which is then used as the model in the parameter optimization problem Eq. (25) stated in Section 3.2. This nonlinear fitting method indeed offers the possibility to get a clearer overall picture about the conducted process, as all available process data points can be utilized. Further, error distributions remain normally distributed under the use of the root-shaped mathematical model. Thus, the method of least squares is ideally suited to determine the characteristic process quantities.

In order to investigate these claims for obtainable practical benefits a big set of filtration data is needed. Only then, the so-called *law of large numbers* [217] can be fulfilled to make statistically significant statements. However, it is not feasible to generate this data in a real-life laboratory environment – not only due to the sheer number of experiments needed, but especially due to the limited replicability of each experimental run. It is most

likely impossible to produce multiple real data sets that inhibit the same "true" unknown value for the filter resistance. Therefore, the required data was created by employing Monte Carlo experiments, as described in Section 3.1.1.

Using this artificial data base, the filter resistance is estimated using both, the original VDI 2762 procedure, as well as the proposed nonlinear fitting method. After, the relative errors of the obtained specific filter resistances are calculated under consideration of the true parameter value known from the model input to the Monte Carlo runs.

Upon closer inspection of the error performances for both parameter estimation procedures, the advantages of the proposed modified fitting method become clear. Even though both techniques achieve comparable accuracies for low noise levels, the nonlinear parameter estimation approach manages to stay accurate under the influence of high disturbances: for the representative noise level of 10% to the nominal value of the filtrate flow rate $\dot{V}$, the nonlinear parameter estimation strategy performs roughly 2 magnitudes more precisely. Moreover, it was shown that the VDI 2762 strategy inhibits the tendency to underestimate the parameter values which is most likely due to the shifted error distribution. In a practical context, this might lead to further problems in process design.

Arguably, linear models are much easier to solve analytically, or – as a matter of fact – graphically as proposed by the VDI 2762 norm. However, the reasoning for simplicity does not hold in regard of nowadays repertoire of computational tools[12] being available to process engineers. Hereby, employing the proposed nonlinear parameter estimation method increases the accuracy while still being based on the very same theory. Regarding the previous argumentation, the study concludes by challenging the original VDI 2762 guideline as best practice. Instead, it is advised to use the modified fitting method in the evaluation of incompressible cake filtration data.

4.2 Publication II – Optimal Control Study

The overall goal of the second study aims at → *Objective III* of this thesis, i.e., finding optimal strategies for the dosage of filter aids in cake filtration processes. Hereby, especially fibrous filter aids are the focus of investigation, since they offer several benefits over the traditionally used kieselguhr as elaborated in Section 2.1.4 of this thesis. However, only few detailed process models exist that can derive dynamically optimized dosage profiles, none of which are suitable to describe filter cakes made up from compressible fibers.

Therefore, the first half of this study addresses → *Objective II*, i.e., developing a mathematical continuum scale model that is able to accurately describe those filtration phenomena known from real processes. Apart from cake compression, effects to be modeled include an additional precoat phase, as well as variable shares of interfering depth filtration.

[12] In fact, even Microsoft Excel offers the possibility to easily calculate the proposed nonlinear fitting method.

Hereby, the framework provided by the multiphase flow theory as introduced in Section 2.2.2 is adapted to the stated problem. Since the resulting system of partial differential equations does not inhibit an analytical solution, the model is solved numerically using the approximation techniques described in Section 3.1.2 of this thesis.

The second part of the study is dedicated to solving the actual challenge of finding the optimal process conditions. By employing the techniques described in Section 3.2, the optimization problem stated in Eq. (21) is solved for two different scenarios. The first run considers a simplified model formulation in which cake-internal fine particle migration is neglected, i.e., impurities are only separated via the effect of surface filtration. Subsequently, the full model including the mechanism of depth filtration is examined for various shares of fine particles that are initially immobilized by surface filtration. Moreover, both scenarios are evaluated for two different parameter sets in order to represent varying extends of cake compressibility.

Following general conclusions can be drawn from examining the results of all scenarios: First, the positive impact time-dependent filter aid dosages offer rises for stronger degrees of filter cake compressibility. Further, the more impurities are separated by the mechanism of depth filtration, the higher the benefit of an optimal control becomes. Hence, the most profit from employing an optimal control procedure can be obtained by assuming the edge case of a highly compressible material system with the absence of fine particle surface filtration. Hereby, the area-specific energy expenditure is cut by approximatively 5% compared to an already optimized process under ideal, but constant filter aid dosage. Moreover, using the Lagrangian cost functional of energy minimization the time-integral filter aid consumption can be simultaneously reduced by up to 30% for this scenario. However, if surface filtration is the lone mechanism of impurity separation employing an optimal control procedure shows only negligible impact.

In conclusion, real filtration processes must be examined for their qualitative separation mechanisms in order to assess whether employing an optimal control yields a significant impact on the process cost. Nevertheless, it is important to keep in mind that all optimal control scenarios are compared to an ideal benchmark. Therefore, only implementing the static optimization strategy to a real-world filtration set-up might already increase the process performance. Moreover, the proposed optimization approach can be used as a tool to decrease the experimental effort needed to find appropriate filter aid dosages to specific filtration problems.

4.3 Publication III – Model Order Reduction Study

The optimal control scenarios employed during the previous study involve a significant computational load to be solved. Therefore, this third research paper is an extension to Publication II by addressing → *Objective IV* of this thesis, i.e., increasing the numerical efficiency of the underlying compressible cake filtration model simulation. To this end, a

ROM is built by employing the POD method using data provided through full order model simulations[13] under sparse parameter variation. Hereby, the local POD, global POD, and SAIM are examined on their performance in solving a test problem which calculates the ROM for varying control inputs. All the previously described techniques are briefly introduced in Section 3.3 of this thesis.

In this study, the static optimization problem of energy minimization (see Eq. (21)) is set as the benchmark, since the qualitative behavior is known from the preceding study. The optimization procedure is solved for the initial full order model, as well as the derived ROMs. However, the interest does not lie in finding the optimal solution *per se*. Instead, the key performance indicators for the different POD approaches are defined as the numerical accuracy, as well as the computational speed. Due to the lack of an analytical solution to the full order model, the numerical accuracy is examined by calculating the relative error of the ROM simulations compared to those from the full order model. Moreover, the computational efficiency is assessed by evaluating the elapsed computational time the ROM needs to solve the benchmark problem compared to the full order model.

By applying the POD method, the dimensionality of the resulting ROM can be diminished to $\approx 2\,\%$ compared to the underlying full order dimension. Due to the significantly smaller system of ordinary differential equations to be integrated the computational efficiency is increased approximatively 10-fold when processing the benchmark problem using the local POD. Thereby, a low relative error of $\approx 1.4\,\%$ can be maintained on average over the whole parameter range of interest. Higher numerical accuracies are achievable by applying the global POD, or the SAIM, which yield average relative errors of $\approx 0.18\,\%$, and $\approx 0.06\,\%$, respectively, compared to the full order model simulations. However, using either method also increases the computational load slightly, since more full order model simulations are required to generate the necessary data to build the ROM.

In conclusion, each POD method should be chosen in regard of the intended application. Employing the local POD, for example, would offer benefits in real-time critical environments due to the higher computational efficiency. On the other hand, especially in regard of more complex ROM applications such as the optimal control approach introduced in Publication II, the SAIM should be preferred over the local POD. This is because for a given computational load relative errors of the resulting ROM computations are up to two magnitudes lower compared to the other techniques examined.

[13] The numerical techniques used to simulate the full order model are mostly identical to those introduced in Publication II. To avoid repetitiveness, no further information on the full order model is included in this section.

Chapter 5

Overall Discussion

This chapter elaborates further on the findings of the individual papers. However, as the initially stated Objectives of this thesis were already addressed in the respective summaries of the previous Chapter, the following discussion does not focus on the individual scope of the distinct studies. Instead, they are collectively revisited in the context of advantages, challenges, as well as remaining open questions that are offered by employing nonlinear mathematical models to the unit operation of cake filtration.

5.1 Synergies from Combining the Filtration Theories

Both modeling frameworks investigated in this study, i.e., the VDI 2762 guideline based on the conventional theory, as well as the multiphase flow theory, offer their own separate set of use cases and drawbacks. The procedures described in Publication I are especially well-suited to gain a quick overview on the underlying filtration data. Hereby, the modified nonlinear fitting method proposed in Publication I increases the accuracy in process evaluation.

Recently, Buchwald [140] investigated similar parameter estimation techniques based on nonlinear continuum scale models independently from this study. Apart from demonstrating how non-ideal starting phases of cake filtration processes can be accounted for by using adapted model formulations, Buchwald also supports the findings from Publication I by proving that the nonlinear fitting procedure is less sensitive towards experimental errors. However, even though these works address some of the downsides of the original linearized VDI 2762 strategy, the limitations elaborated in Section 2.2.1 remain: the possibilities of conducting mathematical optimizations are limited, and the applicability of the overall method is restricted to incompressible material systems with negligible shares of depth filtration.

Models based on the multiphase flow theory, on the other hand, do not inhibit these flaws due to their ability to provide additional dynamic information. As demonstrated in Publication II, this enables to indeed take the mechanisms of cake compressibility, as well as impurity separation by depth filtration into account in the respective simulations. Moreover, the framework may support real filtration set ups by conducting theoretical

investigations which help to find ideal operation conditions that increase the overall process efficiency significantly. However, the presented nonlinear model equations must be approximated by employing numerical algorithms which are not trivial to implement, and might involve significant computational times to process.

This high discrepancy between the complexity of those modeling techniques has been discussed before by, e.g., Tien [73]. As also elaborated in Section 2.2.1, extensions to the conventional theory exist which promise to capture the mechanism of compressibility reliably. However, following Tien's argumentation, these formulations quickly increase in complexity as well, while still producing comparably high relative errors. Thus, especially the phenomenon of cake compression remains difficult to assess mathematically. This is particularly critical, since, so far, this thesis clearly distinguished between incompressible and compressible filtration processes. However, as extensively discussed by Alles [17] most material systems occurring in filtration are – at least to a certain degree – compressible. Hence, assuming ideally incompressible filter cakes, such as in the VDI 2762 norm, potentially induces additional errors from this layer of model abstraction. Considering these preliminaries, the domain of cake filtration suffers from the lack of reliable but simple evaluation strategies for only minorly compressible cake filtration processes.

In order to find better methods, the multiphase flow theory can be taken advantage of due to its ability to accurately represent such slight cake compressibility by adjusting the according parameters. Hereby, employing the corresponding model simulations as Monte Carlo experiments could serve as a basis to generated large data sets with precisely defined process properties and known parameter values similarly to the conducted procedure in Publication I. Using this approach would allow to first evaluate the quantitative compressibility range for which the conventional filtration theory still provides accurate predictions. Doing so offers the further possibility to evolve the VDI 2762 strategy in terms of defining best practices when to refrain from the incompressible cake filtration model stated in said guideline. In return, adapted models that are able to represent the effect of (slight) cake compressibility can be developed with the overall goal of user friendliness, as well as maintaining simple parametrization procedures.

Notably, a similar approach has been conducted by Tien and Bai [150]. However, this study addressed the validity of the modification to the conventional theory proposed by Tiller et al. [218] in comparison to the multiphase flow framework. While the study demonstrated that using Tiller's approach indeed a high accuracy can be achieved even for strongly non-ideal filter cakes, the adjustment model is highly complex and, thus, not comparable to the simplicity of the VDI 2762 technique. Moreover, the work is based on real experimental data which naturally contains uncertainties that potentially distort the obtained model statistics.

Further regarding the VDI 2762 procedure, experienced filtration personnel may also assess which qualitative filtration phenomena occur during the process by "reading" deviations from the ideal linearized $\frac{t}{V}$-over-V diagrams, as discussed in Section 2.2.1 (see

Figure 8, right). For the current moment, this heuristic information is lost when the novel nonlinear fitting method proposed in Publication I is employed. Nevertheless, such patterns in the qualitative change of the nonlinear model function $V(t)$ can be identified by conducting further studies. To this end, Monte Carlo experiments may be calculated from models based on the multiphase flow theory not only for varying levels of cake compressibility, but also under consideration of additional cake filtration phenomena. This allows to investigate the VDI 2762 strategy further in regard of, e.g., varying shares of depth filtration.

5.2 Experimental Considerations

Regarding this section's discussion, it is important to keep in mind that this thesis focuses on numerical investigations only. Experimental filtration data is not included in this work, and, therefore, results from the respective publications included throughout Chapter 4 should rather be interpreted as from qualitative nature. These theoretical findings provide general insights to the cake filtration process, which are intended to be transferred to more specific problems. Nevertheless, all employed models can be considered as fundamentally validated. Concerning the conventional theory, many applications from the last decades show good agreement of the VDI 2762 strategy in comparison to experimental filtration data from approximatively incompressible cake filtration experiments [11], [33]. Further, models based on the multiphase flow theory have been used to evaluate various material systems in laboratory environments [150]. Recently, the modeling framework was also experimentally validated for further materials, e.g., microcrystalline cellulose [219] which is similar to the intended application of fibrous filter aids in Publication II.

Hence, this subsection discusses the combination of the respective models with real-world experimental methods. Hereby, the first part elaborates how to accurately parameterize the models in order to enable quantitative predictions. Second, it is discussed how further phenomena that may be observed in cake filtration experiments can be incorporated mathematically.

5.2.1 Model Parameterization

Mechanistic mathematical models can only predict the physical process reliably if the corresponding model parameters are determined accurately enough. Hereby, cake filtration models pose no exception, for which the characteristic quantities and parameters involved in the various constitutive relationships must be estimated. Notably, it is important to distinguish between fixed structural model parameters, and control parameters. The latter act as model inputs which may be adjusted freely for previously defined ranges. Even though this thesis investigates physically motivated mechanistic continuum scale models, an increased number of involved structural empirical parameters also amplifies the risk of

model overfitting[14] [221], [222]. Therefore, each estimated structural parameter must be valid for the overall intended control parameter range.

Some model parameters, e.g., the viscosity μ of the suspending liquid, can be obtained by measurements through dedicated laboratory equipment. Often, however, model parameters can only be estimated indirectly by involving proxy data originating from the experiment of interest. As elaborated throughout this thesis, the main purpose of the strategy presented in the VDI 2762 norm is, in fact, to relate the measured system state of cumulative filtrate volume V to the independent variable time t. Employing a linear regression (see Eq. (15)) can then be used to determine the rather abstract material properties of specific filter resistance r, and filter medium resistance R_M. All further remaining model parameters, i.e., the area covered by the filter medium A, and the final filter cake height L, can be directly found by trivial measurements. Since this procedure is a well-documented standard practice, it is, therefore, not further elaborated during this subsection.

However, once further mechanisms, such as cake compression, and particle migration, are incorporated into the model architecture, the process of obtaining the model parameters becomes a lot more involved. Considering the multiphase flow theory, the parameters of specific filter resistance r – or permeability k (see Eq. (4) and Eq. (10)) –, and filter coefficient λ (see Eq. (7)) are exchanged for constitutive relationships. Therefore, depending on the employed model complexity, 5 to 9 empirical parameters must be estimated. Historically, the compressive behavior of a material system is hereby examined using dedicated material experiments. As discussed by Tien [91] these methods can be broadly categorized into destructive, and non-destructive procedures. In a naïve approach, the works of Meeten [223], as well as Smiles and Rosenthal [224] propose to dissect compressed porous materials into segments, from which the solidosity can be obtained using the known density, weight, and volume properties. Even though such destructive methods only allow to inspect the filter cake's characteristic process quantities for one specific time span, additional measurements, such as particle size distributions, can be readily implemented. Another established non-destructive method makes use of a so-called compression-permeability cell [147]. Hereby, a piston applies a series of pre-defined forces to a filter cake sample. After each compression step, the liquid phase flows through the compacted material. Under the assumption that the whole compressed cake reaches an equilibrium, the pressure data can then be correlated to permeability, and porosity which is sufficient to parameterize the constitutive relationships given in Eq. (9) and Eq. (10). Often these material laws are simple enough to be solved analytically by linear regression. Nevertheless, the method is frequently criticized. As described in, e.g., [79], [80], [101], additional effects, such as friction and structural support given by the walls, and piston of the compression-permeability cell, can distort the true quantitative compression behavior of the examined filter cake samples.

[14] A famous intuitive example is Von Neumann's elephant [220].

Alternatively, a least squares parameter estimation problem similar to the one stated in Eq. (25) can be defined by using the previously mentioned macroscopic pressure and flow data from laboratory cake filtration experiments. Nevertheless, as discussed by Tien [73] the full-order system of partial differential equations must be integrated for each iteration of the underlying parameter optimization procedure. To this end, Stamatakis and Tien [160] employed a simplified parameter estimation approach by using a strongly constrained parameter space. However, this technique only yielded inconsistent parameter values. Notably, a full-fledged parameter optimization problem is comparable to those problems investigated in Publication II. Therefore, it was – most likely due to missing computational capabilities – simply not possible to process the method until recently which explains the unreliable outcome.

Hence, the authors simulating the multiphase flow theory typically relied on obtaining the required parameter values through compression-permeability measurements, as explained in [95]. However, even though the same material systems were examined repeatedly, significant deviations in the stated parameter sets can be observed in the studies throughout the time, e.g., in [8], [95], [148], [150], [160]. This matter indicates towards multiple local minima being present in the high-dimensional parameter search space. Moreover, it proves the difficulties in conducting experiments using compressibility-permeability cells. Further, it remains critical that parameters impacting the fine particle migrations were not investigated in the original paper series. For example, in [8] the authors waived completely on estimating the filter coefficient λ in favor of merely conducting qualitative parameter studies using the model's simulation results. This is because established parameter estimation methods known from the unit operation of deep bed filtration, such as described in [38], and [225], are not applicable due to the cake's moving boundary in combination with cake compressibility being present.

Naturally, experimental research in solid-liquid separation made progress during the last decades. Therefore, novel process analytical methods became available, which provide deeper insights to the process development. Apart from modifications to the established methods like compression-permeability cells [7], [226], [227], significant advancements in experimental non-invasive *in situ* techniques can be found in the literature. Hereby, some authors investigated techniques based on including probes to the filter chamber that enable to quantify the spatial distribution of the liquid pore pressure [91], [228]. Moreover, in an early work Shirato et al. [229] tried to support the determination of a filter cake's local porosity by measuring the electric conductivity. Since then, this approach has been researched on in the overall area of saturated porous media as discussed in the review by Cai et al. [230]. Therefore, working on the development of incorporating such probes to the filter cake would help to directly resolve the cake compression inside the filtration unit. Thus, the drawback of the dedicated compressibility-permeability cells could be further reduced. Moreover, it has been stated that tracking the development of the cake height $L(t)$ is a cumbersome task [73]. Therefore, usually only the final cake height is included in parameter estimation procedures. However, since the location of the previously mentioned

probes at the filter apparatus is known, a sudden change in the measurement values could help to additionally quantify the filter cake's growth rate indirectly. Some groups also researched on dedicated sensor set ups which can track the filter cake thickness dynamically over time, e.g., by employing optic [231], [232], or acoustic approaches [233]. However, these methods require extensive calibration to the specific experiment [91].

Particularly promising novel approaches are based on imaging techniques. Early adopters employed nuclear magnetic resonance measurements [234], [235] which was later proven to allow for both, tracking the dynamic development of solidosity, as well as the filter cake thickness [236]. Further, the use of x- and γ-rays was investigated in a similar way [237], [238] [239]. Hereby, a big potential lies in the characterization of cake filtration processes using micro-computed tomography. While one of the first reported uses by Tiller et al. [84] was still limited, the technique became not only more capable but also more accessible. Latest studies employing this imaging method manage to directly estimate the permeability, as well as solidosity of the porous material from these measurements [240], [241]. Moreover, this method allows to parameterize the filter coefficient in order to describe the mechanism of depth filtration, since the spatial distribution of fine particles can be directly identified in the solid phase. The viability of resolving particle migration has been demonstrated in, e.g., [242]. An overview on the technique of micro-computed tomography in porous media can be found in [243].

Notably, unparameterized models can also help in optimizing the experimental investigations. Since the multiphase flow theory provides insights to the spatial and the temporal domain, sensitivities for the unknown parameters can be calculated. In return, this sensitivity information may be used to employ the method of model based experimental design [244], [245]. This approach allows to find ideal experimental conditions under which measured data yields a maximum of information content for the determination of specific process parameters. Therefore, the technique can help to significantly reduce the required experimental workload which is beneficial for measurements that consume a substantial time span to conduct, such as micro-computed tomography imaging. Coincidentally, model based experimental design is also closely related to optimal control problems. Particularly indirect methods rely on processing sensitivity information [246], such that the implementation of one approach also benefits the development of the respective other method.

Concluding this section, experimental data from different origins should be used to parameterize the cake filtration models reliably. Due to the increased computational capabilities it is now possible to numerically solve the parameter estimation problem presented in Eq. (25) using models based on the multiphase flow theory, as well as the dynamic data of pressure, volumetric flow rate, and filter cake height. However, only relying on such macroscopic process data does not guarantee to produce accurate and consistent parameter estimations, since the high-dimensional parameter space may contain multiple local minima, all of which satisfy the optimization problem. Therefore, dedicated material experiments should be conducted to find a reliable initial guess for the parameter set. Even

though no experimental data is presented throughout this thesis, the respective publications included in this work originated as part of the research project „Prozessverständnis und optimale Steuerung von realen Anschwemmfiltrationsprozessen mit kompressibler Filterschicht"[15]. The interested reader can find more information on the parameterization process, and choice of well-suited constitutive relationships for the proposed nonlinear cake filtration models in the final report of said research project [247]. Hereby, various of the previously described techniques were used to estimate the model parameters. Notably, the resulting simulations describe the underlying filtration data accurately which further validates the framework of the multiphase flow theory in regard of filter aid cake filtration processes and adds support to the findings of → *Objective II* of this thesis.

5.2.2 Further Experimental Phenomena

Models are always an abstraction of reality by employing several assumptions. These assumptions are chosen to simplify the underlying mathematical structure, while maintaining the necessary qualitative behavior to represent relevant process phenomena. Simplifications are essential, since otherwise the numerical complexity of the systems of equations, as well as the number of model parameters to be determined would increase significantly.

Hence, one noticeable assumption concerns the impact of the filter medium on the cake filtration process. Despite being an obvious and important part to filtration experiments, especially in filter aid filtration the filter medium resistance R_M is magnitudes smaller compared to the overall cake resistance R [20] – even more so, if the resulting filter cake is compressible. Therefore, it is common practice in the modeling of cake filtration to express the filter medium resistance as a fraction of the cake resistance itself [91], [139] which eliminates this quantity completely. In the literature, the filter medium resistance is described to only affect the filtration pressure significantly, if the solid particles clog the pores of the filter medium [37]. Due to the absence of particle migration in the VDI 2762 strategy, pore clogging is not intended to be determined using this method. Moreover, for the optimization technique introduced in Publication II an inequality constraint was employed that prevented fine particles to penetrate the filter medium altogether. Thus, no detailed mathematical descriptions for the filter medium were included in this thesis. Nevertheless, more studies explored this scenario for other problems that are limited by the filter medium's performance. Hereby, approaches range from simple exponential-type empirical relationships [248], [249] to rate-based methods defined by differential equations [250]. Employing such models offers the possibility to investigate the optimization and

[15] IGF project nr. 19947 BG; supported by the German Federal Ministry for Economic Affairs and Energy via AiF and DECHEMA.

control of further scenarios, e.g., ideal membrane cleaning conditions via backwashing or chemical treatment [251], [252].

Notably, the cake compression described during this work is a purely plastic deformation, i.e., the model equations do not cover any occurring re-expansion of the porous structure after releasing the applied system pressure. This assumption was chosen due to the common filtration mode of conducting the solid-liquid separation in uninterrupted batches. Hence, the focus lies especially on optimizing the filtration in itself without taking following processing steps into consideration. However, once the batch-wise cake filtration is connected to extra unit operations in an overall plant, elastic deformation might become an important effect to model. At the time of writing this thesis, another research group extended the framework of the multiphase flow theory for such elastic cake compression [253], [254].

The previous subsection elaborated that during compressibility-permeability cell experiments walls act as a supporting structure to the filter cake which affects the resulting cake compression. As discussed in [255] the wall effect is a general phenomenon in porous media which is not accounted for in the presented continuum scale model formulations from Publications II and III. Nevertheless, this influence can be assessed by extending the existing cake filtration model architectures. To this end, Kuhn [27] presented one possible approach which may be seamlessly integrated into his 1D continuum scale cake filtration model [112]. Hereby, the technique of optimal control is considered to search for ideal variable filter cell dimensions which in return support the cake structure. Another work employing both, experimental, and model-based investigations taking advantage of the reinforcing wall effect is presented by Bandelt [256] who examines adding packing structures to the filtration vessel.

In cake filtration processes the suspended particles may also be affected by sedimentation occurring at the same time [257]. Nevertheless, the volumetric flow rates caused by the applied pressure differences outreach naturally occurring sedimentation speeds in most cases [258]. If, however, sedimentation cannot be neglected during the solid-liquid separation process, the determined specific cake resistances are reported to deviate by up to a factor of 3.75 when using regular cake filtration models [84]. Notably, some authors also described the sedimentation process in a similar approach to the multiphase flow theory [259] which makes the effect readily applicable to the presented modeling architecture.

5.3 Transition to Cyber-Physical Systems

In an industrial context, Cyber-Physical Systems (CPS) denote the combination of digital components with their respective physical counterparts [260]. For the case of cake filtration this could refer to, e.g., a mathematical model and a filtration plant acting in unison. Hereby, particularly the multiphase flow theory can provide the foundation for cake filtration CPS

due to the detailed process insights offered from the numerical model simulations. However, even though the theoretical foundation of the multiphase flow theory is well-researched in the literature since the 1990s, only few recorded uses in academia can be found as elaborated by Olivier et al. [70]. Moreover, this framework has most likely not been applied to industrially scaled problems yet. One reason is probably the extensive parameterization process. Nevertheless, many novel methods became available during the recent years as discussed in Section 5.2.1. According to Civan [261] another reason might be the lack of computational capabilities allowing for both, conducting numerical optimization procedures, as well as real-time simulations. These issues have been addressed by Publications II and III throughout Chapter 4 of this thesis.

Thus, this subsection examines some thoughts regarding the contribution of these studies towards the creation of CPS in the domain of cake filtration. Hereby, various scenarios are discussed which particularly differ in the requirements for sensor equipment, as well as communication and data exchange between the digital and physical components. Notably, the focus remains on filter aid filtration processes in order to stay consistent with the findings from Publications II and III. Nevertheless, all overall principles can be applied with minor adjustments to the generalized case of cake filtration.

5.3.1 Analysis of Process Optimization

Publication II determined optimal time-varying filter aid dosage trajectories through employing the technique of optimal control. Hereby, → *Objective III* of this thesis has been addressed by providing strategies that minimize the energy consumption by up to 5 % while also reducing the filter aid consumption by up to 30 %. Nevertheless, these overall theoretical findings must be transferred to physical plants in order to realize the potential savings.

In the proposed implementation, the optimal control procedure acts as an open loop control, as illustrated in Figure 9. As can be seen in the scheme, the procedure is contextualized as an open loop control since no feedback signals including possibly occurring process disturbances, i.e., resulting deviations of the system states from the ideal calculated model states, are incorporated into the control technique. Therefore, efforts should be undertaken to make the control strategy as robust as possible [262]. Hereby, the feedforward control can most likely only show its full potential if the surrounding parameters, such as the inlet concentration of the fine particles, are determined *a priori* by, e.g., conducting batch-wise laboratory experiments. Likewise, the filter cell's PID controller must precisely maintain the chosen operation mode, i.e., constant flow or constant pressure, in order to conduct the control strategy successfully [263].

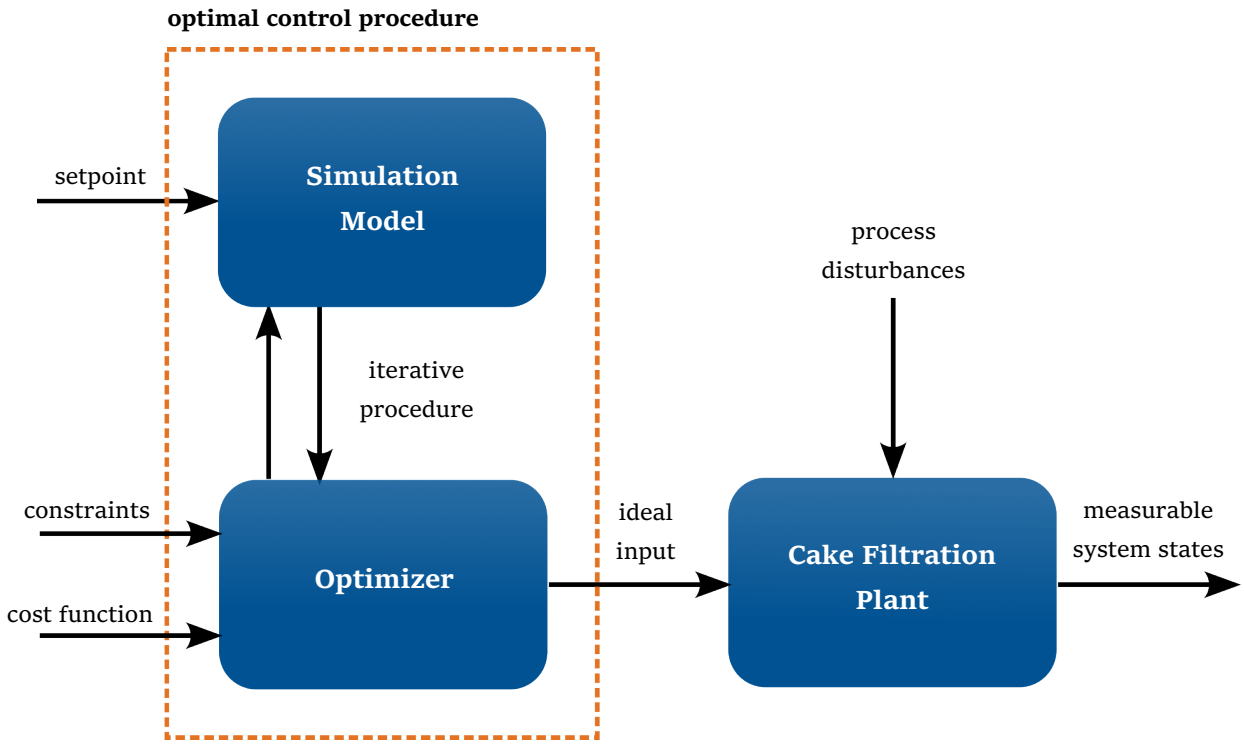

Figure 9 *Scheme for an open loop optimal control of a cake filtration plant.*

During the investigations conducted in Publication II the optimization scenario of energy minimization was investigated as it seems to be the established standard approach in the domain of solid-liquid separation [27], [169], [170], [172]. Thus, comparability is maintained with previous studies. Nevertheless, the proposed procedure can be adapted to many further use cases as long as the resulting optimization problems consist of well-posed cost functionals that can be calculated from the available quantities and inhibit clearly defined extrema. Hereby, alternative performance measures could prove to be economically more feasible. Some plausible alternative scenarios could be, e.g., the minimization of the overall filter resistance R in the form of a Mayer cost functional, or the maximization of the filtration time t until a critical pressure difference Δp is reached. Although the latter approach transforms the procedure into a free-end time optimization problem, which is harder to solve due to the variable temporal domain, it could prove to be beneficial in generalized cake filtration problems. At the same time, the system can be extended by additional inputs, such as controllable filtrate flow rates $\dot{V}(t)$. Hereby, Blankert et al. [169] demonstrated that varying the flux over time in order to achieve a constant power filtration is optimal for membrane filtration processes.

From a numerical perspective, the optimization procedure proposed in Publication II obtains the ideal control functions by employing systematic gradient-based search algorithms. However, even though quasi-continuous optimal trajectories can be found reliably, some minor numerical artifacts[16] in the solution trajectories can be observed upon

[16] Often referred to as „wiggles“ in the optimal control literature

closer inspection of, e.g., Figure 11 (b) from said study. Despite making sure to use high integration tolerances, as well as a central finite differencing scheme these artifacts are a direct result of numerical inaccuracies. Moreover, due to the bisectional grid refinement approach the optimal control algorithm is subject to an $O(2^i)$ complexity, i.e., unknown optimization parameters double with each iteration i. This does not only cause an exponentially increasing computational time but also affects the technique's robustness.

In order to achieve a smoother approximation, and to increase the efficiency of the numerical procedures, the algorithm should be adjusted by more sophisticated methods which yield a better numerical stability. For example, employing an internal numerical differentiation technique could help in reducing the errors in the estimation of the gradients by using the same points for finite differencing that were used to integrate the system of differential equations. Further, the optimal control algorithm could benefit from employing an adaptive mesh refinement based on a combined *hp*-method, or a wavelet-based approach. Particularly wavelet-based optimal control [264]–[266] proved to be superior to classical *h*-methods by only selectively refining the discretization grid where a high impact to the cost function is expected. In return, the degrees of freedom are limited. Additionally, this approach would maintain best practice in computer science to avoid exponential time complexities where possible. For the sake of completeness, particularly genetic optimization algorithms should be mentioned as alternative methods to numerically solve the minimization problem stated in Eq. (21). Hereby, the advantages of genetic algorithms have been demonstrated in recent years, as they prove to be efficient in iterating towards global minima along high-dimensional parameter search spaces frequently occurring in, e.g., machine learning models [267], [268].

Regarding the resulting CPS from employing an optimal control procedure, the benefits lie especially in automatically determining mathematically optimal set-points for the respective inputs instead of purely relying on heuristic knowledge from the operators. Further, the required experimental work in finding ideal controls is reduced. Concerning the actual achievable impact from applying the optimal control procedure, it is important to keep in mind that the initially stated benefits are compared to an already ideal but constant reference dosage scenario. Typically, established filter aid dosing strategies are conducted by supplying a constant filter aid concentration which includes a significant safety margin to ensure particle-free filtrates. Hence, simply employing the filter aid dosage derived from the static optimization approach might yield savings compared to the established conservative dosing strategies, since the control's set point can be shifted closer toward the mathematical optimum. Moreover, no additional investments to existing plant infrastructure are required to employ this application to real-world filtration set ups.

Despite obtaining optimal set points through the open loop control, the idea should not be confused with an *expert system* from a terminological perspective. Although both techniques show similarities, the latter approach derives control recommendations from data-based models rather than mechanistic models. Such data-based decision support systems have been investigated for cake filtration processes by, e.g., data mining and setting

up decision trees [269], employing fuzzy logic [26], [270], or setting up discrete control rules based on human knowledge [271]. Nevertheless, compared to these techniques mechanistic models offer deeper insights and allow for rigorous mathematical optimization procedures. The optimal time-varying dosage strategies from Publication II, for example, cannot be found easily using a data-based model. This is because in typical filter aid cake filtration processes the precoat dimension is chosen from established standards, and time-varying filter aid dosages are not state-of the art. Hence, the required information is simply not available in the underlying data sets.

5.3.2 Real Time Computations

Achieving a high computational efficiency in the simulation of mathematical models is not only important for time-economic reasons. Once a mathematical model fulfills real-time requirements, it can serve as a *digital twin* [272]. This further level in CPS acts as a state observer, i.e., system states that cannot be determined directly are reconstructed from measurements of other physical quantities [31]. As shown in Figure 10, the simulation model does not pose a preceding input stage to the filtration plant as it was the case for the open-loop control approach from the previous subsection. Instead, both building blocks are interconnected in parallel, such that the digital twin can mirror the current states of the physical plant [273].

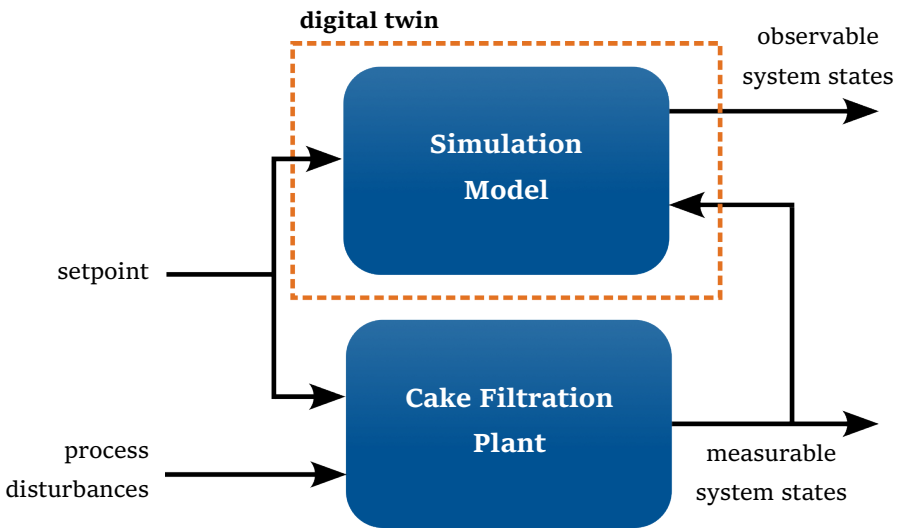

Figure 10 *Scheme for a digital twin of a filtration plant.*

Hereby, the models based on the multiphase flow theory proposed in Publication II can be adopted as digital twins for filter aid cake filtration processes. This approach allows plant operators to gain tailed insights into the process, which otherwise would not be possible. This is because no online sensors to determine the system states of solidosity ε_s, local impurity deposition ε_{s2}, and, as discussed in Section 5.2.1, even the temporal development

of the cake height $L(t)$ are readily available. The biggest advantage offered by interconnecting the filtration model with the plant is that random process disturbances, such as fluctuating volumetric flow rates, or shifting impurity characteristics, can be monitored in real-time. Hence, possibly forming blocking layers due to, e.g., a varying impurity concentration [20], or compression [81] can be easily detected.

In order to fulfill the required computational efficiency, a naïve approach could be to rely on Moore's law, i.e., solving the problem using more potent computing hardware in the future. Nevertheless, this would only help to a certain degree. This is because the integrator of the system of differential equations is an iterative procedure. Hence, Publication III proposed to apply the POD technique to significantly simplify the model structure while maintaining most of the simulation's quantitative accuracy. Since the ROM diminished the simulation time by a factor of 10 compared to the full-order model (→ *Objective IV*), the architecture is well-suited to be used as a real-time digital twin model for cake filtration processes.

Nevertheless, projection-based model order reduction is not the only surrogate modeling technique appropriate to fulfill this task. Apart from linearization approaches [274], [275] traditionally encountered in system's engineering and engineering cybernetics, particularly various data-based modeling contributions can be found in the literature for the domain of solid-liquid separation. For example, cake filtration predictions based on artificial neural networks are described in [269]. Similarly, Fan et al. [276] employed a wavelet neural network to a membrane-based ultrafiltration process, and Banerjee et al. [277] explored the possibilities of using different machine learning applications to deep bed filtration-type set ups. Notably, the determination of problem-appropriate artificial neural network architectures involves a high computational load for hyperparameter tuning and the corresponding network parameter estimation[17]. Nevertheless, the resulting machine learning models are computationally efficient to solve as, e.g., demonstrated in [278], and [279] where the data based models are used to employ optimization calculations.

Hence, the potential building blocks for the creation of a digital twin in filter aid filtration are available, not only due to the insights provided by Publication II and III. However, the challenging task of acquiring accurate online process data as a model input remains. The process analytical methods, and material experiments used during the model parameterization stage (see Section 5.2.1) are not feasible to engage in the actual filtration environment. Future research must investigate the usability of novel sensors, such as those introduced for the dynamic tracking of the cake growth rate. Further, studies should also focus on which combination of more traditional sensors, e.g., to measure the turbidity, particle size, and -distribution, yields enough information to employ a robust digital twin. To this end, it may additionally be beneficial to combine the mechanistic models with data-based techniques, e.g., either as physical informed neural networks [280], or by employing machine learning based soft sensors. This is because despite many fundamental theoretical

[17] In the discipline of machine learning commonly referred to as *training*

investigations on fibrous media (e.g., [281]–[283]) its mechanistic behavior is still poorly understood [284].

5.3.3 Model Predictive Control

In a broad context, model predictive control (MPC) is an advanced process control technique which provides a higher level of sophistication to the CPS. Hereby, the digital twin architecture introduced in the previous section is extended by an additional optimal control procedure. Therefore, the digital twin is not only used as a state observer for the current time step. Instead, it can be used to simulate the future process outcome under consideration of immediate process disturbances [285]. Hence, the determined control strategy offers advantages over traditional approaches based on, e.g., PID controllers. While feedback controllers only *react* to deviations from the reference variable, MPC can *detect* occurring process variations as early as possible. The control algorithm may then supply appropriate signals to the plant's actors such that an ideal process trajectory is always maintained [286]. Thus, MPC acts proactively to prevent critical deviations from the optimal conditions. The MPC architecture is illustrated in Figure 11. Compared to the optimal control scheme depicted in Figure 9, the MPC can be defined as a closed loop control, since a feedback signal of the measurable process outcome is connected to the controller.

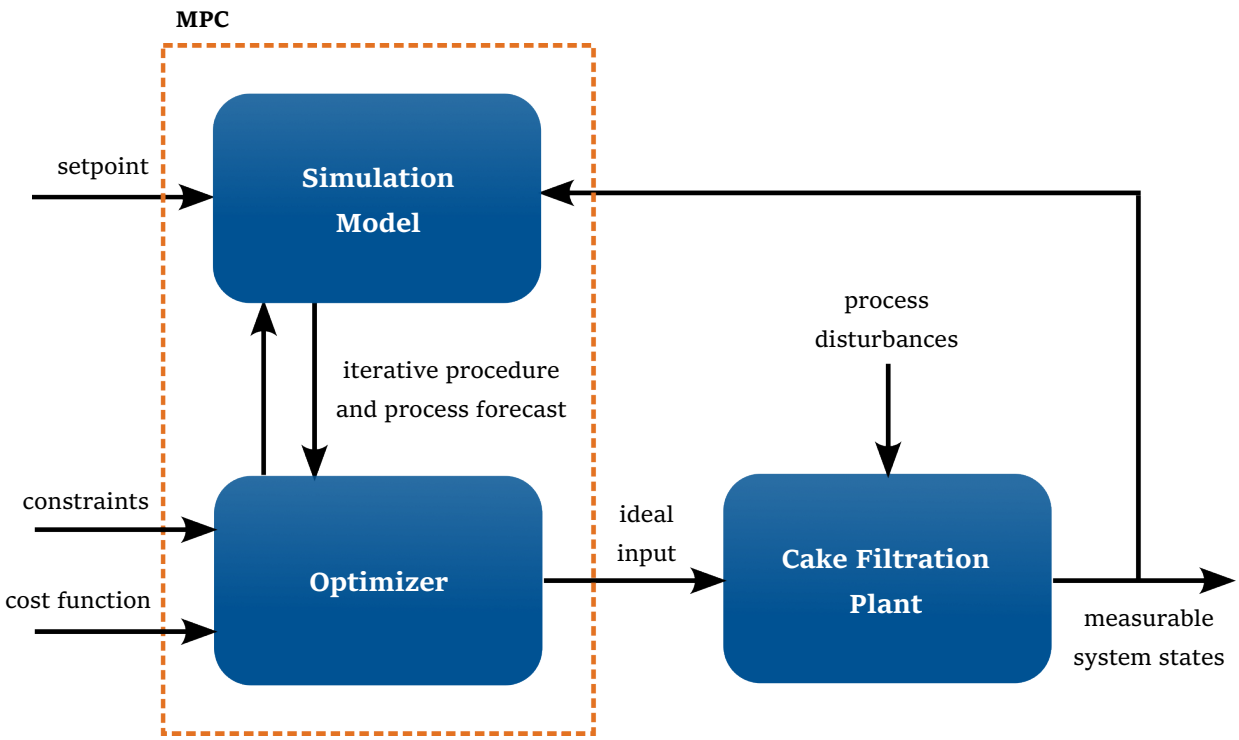

Figure 11 *Scheme for a model predictive control approach of a cake filtration plant.*

Since both, the real-time simulations using the digital twin, as well as the corresponding optimization procedure are computationally expensive, MPC is especially well-suited for

comparably slow applications as they appear in, e.g., processes engineering. Despite MPC being an established technique since the 1980s in various areas [287], only few model based control approaches are described in the domain of solid-liquid separation such as for membrane-based processes [288]–[290]. Notably, for these applications the specific process performance was increased significantly compared to the respective baseline scenarios. The sparsity of the implementation for cake filtration processes is most likely due to the complex mathematical models needed to accurately describe the involved material systems, a challenging numerical optimization thereof, and a lack of adequate online sensors to characterize the occurring process disturbances [273], [287].

To this end, Publication II provides a detailed optimization procedure that can be employed to determine the ideal reference trajectories. In combination with the discussed possible digital twin architecture, these open questions can be readily addressed. Due to the underlying modeling framework being based on a system of partial differential equations, the resulting control loop can be classified as a nonlinear MPC [176]. Opposed to linear MPC which uses, e.g., linearized state-space approximations around desired set-points, employing a nonlinear MPC offers the possibility to describe the whole system dynamics. Particularly for cake-filtration processes this behavior is necessary as, typically, no controllable steady-state can be obtained due to the ever-increasing process pressure in the case of a constant rate filtration (compare Figure 4). Hereby, the growing filter cake can also be interpreted as the system's memory, i.e., occurring blocking layers due to a suboptimal impurity deposition, or cake compression remain in the apparatus until the filtration is restarted. In order to prevent these situations traditional control systems for filter aid filtration processes include high safety margins in the filter aid supply. However, by employing a MPC these safety margins can be significantly decreased as process disturbances may be detected in real time. In return, tweaking the control strategy accordingly ultimately leads to decreased cost functionals.

The remaining challenge is to implement actors to the cake filtration plants that can be adjusted by the signals provided from the MPC. For the presented case of filter aid cake filtration variable filter aid dosages can be supplied via, e.g., valve control, or mixing different types of filter aids using distinctive storage tanks. Hereby, inspiration can also be taken from wastewater treatment plants [291], where dynamic dosages of coagulants, and reagents are common practice. Moreover, for the generalized case of cake filtration the filtrate flow rate can be set as a control variable. For making use of this input only minor adjustments to existing plant infrastructure are necessary, since most filtration set-ups already incorporate a feedback control to maintain a constant flow rate. Further, variable pressure filtrations from simple modifications are described in the literature [91]. Therefore, compared to the challenging online data acquisition problem needed to create the digital twin, employing the MPC strategies to the real plant is a much simpler task to resolve.

5.3.4 System-Wide Integration

So far, this section solely investigated model-based methods to optimize the cake filtration process in itself. However, the relationships illustrated in Figure 4 imply a discontinuity of the real-world dead-end cake filtration. Reaching a stopping criterium, i.e., a minimal flow rate, or a maximum pressure drop, ends the filtration, and the filter cake undergoes further processing by connected unit-operations. Therefore, it is important to also incorporate the apparatus' preceding and proceeding stages. For example, additional mechanical, thermical, or chemical steps may be used to further enhance the purity of the filtrate, or the quality of the solid phase. Some steps include, but are not limited to, filter cake consolidation, drying, washing, or a combination of those [259], [292]–[296]. Hereby, the interconnection of the different unit operations is often affected by non-ideal surrounding circumstances, such as variable pump efficiency curves as examined by, e.g., Blankert et al. [170] for membrane filtration processes, or necessary off-times for cleaning cycles and maintenance of the filter chamber, and filter medium [6].

Therefore, it only becomes possible to make reliable statements about the overall plant efficiency and, thus, process economy, if the whole system is taken into consideration. Regarding, for example, applications in pharmaceutical engineering, the overall downstream processing phase takes a significant share of the overall production cost [297]. Undoubtedly, a notable portion of these cost is occupied by other unit operations such as chromatography [298]. However, filtration remains a crucial part in the separation of solutes as especially the preparation of sterile water, buffers, and sanitizing agents is costly [297]. Hence, the determination of ideal control strategies is a decisive factor for economic operations. Staying in the area of pharmaceutical engineering for consistency, Mesbah et al. [299] described a MPC application, which encompasses a complete pharmaceutical manufacturing plant including the downstream processing phase in one global model. However, this approach is based on a linear state-space representation, which only allows for a rudimental description of the filtration step. Thus, no detailed optimization of the solid-liquid separation stage is possible. No further plantwide nonlinear model-based control applications for cake filtration processes are described in the literature. This statement is supported by the work of Bähner et al. [300], which examines an optimal scheduling problem of parallelized dead-end filtration systems using simplified models as well. Hereby, the authors identified the absence of precise simulation models as a missing link to employ a nonlinear MPC – an issue that was, in fact, addressed by this thesis. Therefore, a high positive impact on the process efficiency can be expected when integrating the proposed MPC architecture to plantwide models.

Notably, this thesis only examined the one-dimensional continuum scale in filtration modeling. However, as described in Section 2.2, solid-liquid separation is a complex process where mechanisms can be described in various levels of detail from the microscale examining individual particles up to the macroscale for the entire process. This subsection's headline could, therefore, not only be interpreted in terms of integrating the overall

processing plant, but also as the integration[18] of filtration models on various dimensions and scales. Staying in the continuum scale regime, the modeling architecture can be extended to two- or three-dimensional formulations which offer the possibility of describing, e.g., the wall effect explained in Section 5.3.1 in more detail. Hereby, the proposed ROM architecture from Publication III can be readily adapted. Moreover, multiscale modeling approaches may help to bridge the gap between the micro- and the continuum scale [301]. Modeling the particle-particle interactions helps in accurately predicting the behavior of the overall separation process – especially in regard of the hard-to-assess characteristics of fibrous media. In return, understanding the occurring mechanisms' interactions on the pore scale offers the chance to further optimize the process. The potential of employing such multiscale techniques has been demonstrated by Geerling et al. [164] who managed to improve the design of depth filters. Subsequent research on extending those multiscale optimizations to the problem of (filter aid) cake filtration seems like a logical consequence.

[18] No pun intended.

Chapter 6

Conclusions and Outlook

Contrary to the dominating experimental research in the domain of filtration, this thesis covered mathematical modeling approaches on continuum scale. Employing such theoretical techniques offers deeper insights to the process and facilitates the optimization of real filtration set-ups. In detail, two distinctive applications were investigated:

1. Evolving the widely applied VDI 2762 model into a more favorable formulation (**Publication I**)
2. Optimizing compressible (filter aid) cake filtration models in terms of ideal control inputs (**Publication II**) and computational efficiency (**Publication III**)

Despite being based on different theoretical frameworks, both applications share the overall narrative of introducing nonlinear equations. Concerning the initial VDI 2762 guideline, exchanging the linear model for a nonlinear formulation has proven to eliminate subjective errors, and avoids shifted error distributions. Hereby, the established conventional filtration theory is maintained, while the nonlinear model can still be solved using standard methods. Therefore, it is recommended to introduce the proposed modified fitting method in all applications, where the original VDI 2762 guideline is established as the evaluation method of choice.

Further, applying the nonlinear multiphase flow theory to compressible filter aid cake filtration offers a better understanding of the process dynamics, since the spatio-temporal development of the separation process' characteristic quantities can be described in detail. These more precise insights allow for rigorous mathematical optimizations. Depending on the exact interplay of occurring filtration mechanisms, the process efficiency can be increased significantly, which, ultimately, may also lead to reduce the involved monetary process cost. Nevertheless, the corresponding simulation requires for an advanced numerical knowledge to be deployed, and a higher experimental effort to be parameterized.

Thus, one should refrain from classifying either theoretical framework as *better*, or *worse*. Besides, a mathematical model always remains merely an approximation of reality, regardless of the desired degree of detail. Therefore, it is necessary to identify the relevant phenomena in specific applications to determine which technique is best suited for the individual problem.

Considering future research on continuum scale modeling in cake filtration, the multiphase flow theory is yet to be applied to industrially-scaled processes. Especially in

hindsight of filter aid filtration, the numerical techniques that were proposed during this work should be connected in the overall domain of CPS and advanced process control, i.e., for real-time process monitoring, and model predictive control. Notably, filtration models based on the multiphase flow theory can be parameterized more accurately in recent years. This is because many novel experimental methods became available, which offer further process insights opposed to only examining the classical macroscopic data of the filtrate flow rate, and the filtration pressure. Furthermore, by adapting the proposed ROM architecture, multidimensional, and multiscale modeling techniques can be incorporated in forthcoming studies considering the ever-increasing computational capabilities.

Apart from the rather pragmatic engineering point of view that focuses on processing filtrate which complies with set requirements, continuing future research in this direction follows the tradition of dedicating the unit operation to sustainability. After all contemplations, optimizing the control parameters reduces the generation of unnecessary waste, and minimizes the overall energy consumption. Both effects are, therefore, not only beneficial on the economical, but also on the ecological impact.

Bibliography

[1] K.-M. Yao, M. T. Habibian, and C. R. O'Melia, "Water and waste water filtration. Concepts and applications," Environ. Sci. Technol., vol. 5, no. 11, pp. 1105–1112, Nov. 1971, doi: 10.1021/es60058a005.

[2] C. R. O'Melia and W. Stumm, "Theory of Water Filtration," Journal - American Water Works Association, vol. 59, no. 11, pp. 1393–1412, Nov. 1967, doi: 10.1002/j.1551-8833.1967.tb03469.x.

[3] K. Sutherland, "Food and beverage: Filtration in the food and beverage industries," Filtration & Separation, vol. 47, no. 2, pp. 28–31, Mar. 2010, doi: 10.1016/S0015-1882(10)70078-1.

[4] R. Heusslein and U. Brendel-Thimmel, "Food and beverage: Linking filter performance and product safety," Filtration & Separation, vol. 47, no. 6, pp. 26–31, Nov. 2010, doi: 10.1016/S0015-1882(10)70262-7.

[5] T. H. Meltzer, Filtration in the pharmaceutical industry. in Advances in parenteral sciences, no. 3. New York: M. Dekker, 1987.

[6] H. Anlauf, Wet cake filtration: fundamentals, equipment, and strategies. Weinheim, Germany: Wiley-VCH, 2019.

[7] C. M. Alles and H. Anlauf, "Filtration mit kompressiblen Kuchen: Effiziente Konzepte für eine anspruchsvolle Trennaufgabe," Chemie Ingenieur Technik, vol. 75, no. 9, pp. 1221–1230, Sep. 2003, doi: 10.1002/cite.200303268.

[8] C. Tien, R. Bai, and B. V. Ramarao, "Analysis of cake growth in cake filtration: Effect of fine particle retention," AIChE J., vol. 43, no. 1, pp. 33–44, Jan. 1997, doi: 10.1002/aic.690430106.

[9] "Systemverfahrenstechnik: About us." https://www.svt.wzw.tum.de/en/about-us/ (accessed Mar. 17, 2023).

[10] M. Kuhn and H. Briesen, "Systemverfahrenstechnik – Eine philosophische Begriffsanalyse," Chemie Ingenieur Technik, vol. 91, no. 9, pp. 1229–1237, Sep. 2019, doi: 10.1002/cite.201800220.

[11] Verein Deutscher Ingenieure, "VDI-Norm 2762: Mechanical solid-liquid-separation by cake filtration, Part 2: Determination of filter cake resistance." Beuth Verlag GmbH, Berlin, 2010.

[12] J. M. Hammersley and D. C. Handscomb, Monte Carlo Methods. Dordrecht: Springer Netherlands, 1964. doi: 10.1007/978-94-009-5819-7.

[13] K. Bennett, "Precoat Filtration," Filtration & Separation, vol. 37, no. 3, pp. 32–33, Apr. 2000.

[14] H. Gasper, D. Oechsle, and E. Pongratz, Eds., Handbuch der industriellen Fest-/Flüssig-Filtration, 1st ed. Wiley, 2000. doi: 10.1002/352760300X.

[15] P. Buttrick, “Filtration - The Facts,” Brewer & Distiller International, vol. 3, no. 12, pp. 12–19, 2007.

[16] G. Blümelhuber, “Kieselgurfilter-Schlämme? Entsorgungsprobleme?,” Brauwelt, vol. 147, no. 28, pp. 757–760, 2007.

[17] C. M. Alles, “Prozeßstrategien für die Filtration mit kompressiblen Kuchen,” Ph.D. thesis, Universität Fridericiana Karlsruhe (TH), Fakultät für Chemieingenieurwesen und Verfahrenstechnik, 2000.

[18] F. Hebmüller, “Einflussfaktoren auf die Kieselgurfiltration von Bier,” Ph.D. thesis, Technische Universität Bergakademie Freiberg, Fakultät für Maschinenbau, Verfahrens- und Energietechnik, 2003.

[19] K. Husemann, F. Hebmüller, and M. Esslinger, “Bedeutung der Tiefenfiltration bei der Kieselgurfiltration von Bier,” Monatsschrift für Brauwissenschaft, vol. 55, no. 3–4, pp. 44–50, 2002.

[20] P. M. Heertjes and P. L. Zuideveld, “Clarification of liquids using filter aids Part I. Mechanisms of filtration,” Powder Technology, vol. 19, no. 1, pp. 17–30, Jan. 1978, doi: 10.1016/0032-5910(78)80070-9.

[21] P. M. Heertjes and P. L. Zuideveld, “Clarification of liquids using filter aids Part II. Depth filtration,” Powder Technology, vol. 19, no. 1, pp. 31–43, Jan. 1978, doi: 10.1016/0032-5910(78)80071-0.

[22] N. Coote, “Turning the art of filter-aid filtration into a science,” in International Symposium: Filtration and Separation of Fine Particle Suspensions, Proceedings, W. Höflinger, Ed., Vienna: Austrian Chemical Society, 1999.

[23] J. Haba and R. Koch, “Analyse des Filtrationsprozesses unter Einsatz von Filterhilfsmitteln,” Chemische Technik, vol. 30, no. 2, pp. 91–94, 1978.

[24] D. H. Sutherland and P. Hidi, “An investigation of filter-aid behaviour,” Transactions of the Institution of Chemical Engineers, vol. 44, no. 4, pp. T122–T127, 1966.

[25] P. C. Carman, “The Action of Filter Aids,” Ind. Eng. Chem., vol. 30, no. 10, pp. 1163–1167, Oct. 1938, doi: 10.1021/ie50346a016.

[26] M. Fellner, T. Lauer, U. Lübken, and P. Neyses, “Manager mit situativer Führung,” Brauindustrie, vol. 10, pp. 50–53, 2012.

[27] M. Kuhn, “New Paths in Filtration – Optimal Control Approaches Based on Continuum Models,” Ph.D. thesis, Technische Universität München, Wissenschaftszentrum Weihenstephan für Ernährung, Landnutzung und Umwelt, Lehrstuhl für Systemverfahrenstechnik, 2018.

[28] R. Tittel, “Die Anschwemmfiltration als ein Prozess zur Klärung von Flüssigkeiten,” Ph.D. thesis, Technische Universität Dresden, Sektion Verarbeitungs- und Verfahrenstechnik, 1987.

[29] M. Kuhn and H. Briesen, “Dosage of Filter Aids in the Case of Pure Surface Filtration – An Optimal Control Approach,” Computer Aided Chemical Engineering, vol. 37, pp. 1655–1660, 2015, doi: 10.1016/B978-0-444-63577-8.50121-2.

[30] D. E. Kirk, Optimal control theory: an introduction. Mineola, N.Y: Dover Publications, 2004.

[31] A. Rasheed, O. San, and T. Kvamsdal, “Digital Twin: Values, Challenges and Enablers From a Modeling Perspective,” IEEE Access, vol. 8, pp. 21980–22012, 2020, doi: 10.1109/ACCESS.2020.2970143.

[32] J. Weiss, “A Tutorial on the Proper Orthogonal Decomposition,” in AIAA Aviation 2019 Forum, Dallas, Texas: American Institute of Aeronautics and Astronautics, Jun. 2019. doi: 10.2514/6.2019-3333.

[33] S. Ripperger, W. Gösele, C. Alt, and T. Loewe, “Filtration, 1. Fundamentals,” in Ullmann’s Encyclopedia of Industrial Chemistry, Wiley-VCH Verlag GmbH & Co. KGaA, Ed., Weinheim, Germany: Wiley-VCH, 2013, pp. 1–38. doi: 10.1002/14356007.b02_10.pub3.

[34] Z. Berk, “Filtration and Expression,” in Food Process Engineering and Technology, Elsevier, 2013, pp. 217–240. doi: 10.1016/B978-0-12-415923-5.00008-3.

[35] C. Tien, Principles of filtration. Amsterdam, Boston, Paris: Elsevier, 2012.

[36] M. Hlavacek and F. Bouchet, “Constant flowrate blocking laws and an example of their application to dead-end microfiltration of protein solutions,” Journal of Membrane Science, vol. 82, no. 3, pp. 285–295, Jul. 1993, doi: 10.1016/0376-7388(93)85193-Z.

[37] P. M. Heertjes, “Studies in filtration,” Chemical Engineering Science, vol. 6, no. 4–5, pp. 190–203, Apr. 1957, doi: 10.1016/0009-2509(57)85018-0.

[38] A. Zamani and B. Maini, “Flow of dispersed particles through porous media — Deep bed filtration,” Journal of Petroleum Science and Engineering, vol. 69, no. 1–2, pp. 71–88, Nov. 2009, doi: 10.1016/j.petrol.2009.06.016.

[39] K. J. Ives, The scientific basis of filtration. Dordrecht: Springer Netherlands, 1975.

[40] K. J. Ives, “Rapid filtration,” Water Research, vol. 4, no. 3, pp. 201–223, Mar. 1970, doi: 10.1016/0043-1354(70)90068-0.

[41] J. P. Herzig, D. M. Leclerc, and P. Le. Goff, “Flow of Suspensions through Porous Media—Application to Deep Filtration,” Ind. Eng. Chem., vol. 62, no. 5, pp. 8–35, May 1970, doi: 10.1021/ie50725a003.

[42] V. Jegatheesan and S. Vigneswaran, “Deep Bed Filtration: Mathematical Models and Observations,” Critical Reviews in Environmental Science and Technology, vol. 35, no. 6, pp. 515–569, Nov. 2005, doi: 10.1080/10643380500326432.

[43] R. Berndt, “Zur Prozessmodellierung der Filtration von Suspensionen unter besonderer Berücksichtigung der Anschwemmfiltration,” Ph.D. thesis, Technische Universität Dresden, 1981.

[44] R. Bai and C. Tien, “Particle Detachment in Deep Bed Filtration,” Journal of Colloid and Interface Science, vol. 186, no. 2, pp. 307–317, Feb. 1997, doi: 10.1006/jcis.1996.4663.

[45] C. Tien and B. V. Ramarao, Granular filtration of aerosols and hydrosols, 2nd ed. Amsterdam, Boston: Elsevier, 2007.

[46] I. M. Leichkis, “Breakdown of particles into flow during filtration on precoat filters,” Chemical Engineering and Processing: Process Intensification, vol. 32, no. 4, pp. 209–216, Aug. 1993, doi: 10.1016/0255-2701(93)80002-X.

[47] I. M. Leichkis, “Filtration on precoat filters as a Markov process,” Chemical Engineering and Processing: Process Intensification, vol. 32, no. 5, pp. 301–310, Oct. 1993, doi: 10.1016/0255-2701(93)85014-7.

[48] A.-B. Yu, R.-P. Zou, and N. Standish, “Packing of Ternary Mixtures of Nonspherical Particles,” J American Ceramic Society, vol. 75, no. 10, pp. 2765–2772, Oct. 1992, doi: 10.1111/j.1151-2916.1992.tb05502.x.

[49] K. Vollmari, T. Oschmann, S. Wirtz, and H. Kruggel-Emden, “Pressure drop investigations in packings of arbitrary shaped particles,” Powder Technology, vol. 271, pp. 109–124, Feb. 2015, doi: 10.1016/j.powtec.2014.11.001.

[50] R. P. Dias, M. Mota, J. Teixeira, and A. Yelshin, “Study of ternary glass spherical particle beds: porosity, tortuosity, and permeability,” Filtration, vol. 5, no. 1, pp. 68–75, 2005.

[51] M. J. MacDonald, C.-F. Chu, P. P. Guilloit, and K. M. Ng, “A generalized Blake-Kozeny equation for multisized spherical particles,” AIChE J., vol. 37, no. 10, pp. 1583–1588, Oct. 1991, doi: 10.1002/aic.690371016.

[52] H. J. H. Brouwers, “Packing fraction of particles with lognormal size distribution,” Phys. Rev. E, vol. 89, no. 5, p. 052211, May 2014, doi: 10.1103/PhysRevE.89.052211.

[53] I. F. Macdonald, M. S. El-Sayed, K. Mow, and F. A. L. Dullien, “Flow through Porous Media-the Ergun Equation Revisited,” Ind. Eng. Chem. Fund., vol. 18, no. 3, pp. 199–208, Aug. 1979, doi: 10.1021/i160071a001.

[54] C. Tien and B. V. Ramarao, “Can filter cake porosity be estimated based on the Kozeny–Carman equation?,” Powder Technology, vol. 237, pp. 233–240, Mar. 2013, doi: 10.1016/j.powtec.2012.09.031.

[55] R. P. Dias, J. A. Teixeira, M. G. Mota, and A. I. Yelshin, “Particulate Binary Mixtures: Dependence of Packing Porosity on Particle Size Ratio,” Ind. Eng. Chem. Res., vol. 43, no. 24, pp. 7912–7919, Nov. 2004, doi: 10.1021/ie040048b.

[56] A. P. Shapiro and R. F. Probstein, “Random packings of spheres and fluidity limits of monodisperse and bidisperse suspensions,” Phys. Rev. Lett., vol. 68, no. 9, pp. 1422–1425, Mar. 1992, doi: 10.1103/PhysRevLett.68.1422.

[57] H. J. H. Brouwers, “Random packing fraction of bimodal spheres: An analytical expression,” Phys. Rev. E, vol. 87, no. 3, p. 032202, Mar. 2013, doi: 10.1103/PhysRevE.87.032202.

[58] F. M. Tiller and H. Cooper, “The role of porosity in filtration: Part V. Porosity variation in filter cakes,” AIChE J., vol. 8, no. 4, pp. 445–449, Sep. 1962, doi: 10.1002/aic.690080405.

[59] C. P. Kyan, D. T. Wasan, and R. C. Kintner, “Flow of Single-Phase Fluids through Fibrous Beds,” Ind. Eng. Chem. Fund., vol. 9, no. 4, pp. 596–603, Nov. 1970, doi: 10.1021/i160036a012.

[60] H. Darcy, Les fontaines publiques de la ville de Dijon. Paris: Dalmont, 1856.

[61] J. Bear, Modeling Phenomena of Flow and Transport in Porous Media, vol. 31. in Theory and Applications of Transport in Porous Media, vol. 31. Cham: Springer International Publishing, 2018. doi: 10.1007/978-3-319-72826-1.

[62] N. Epstein, “On tortuosity and the tortuosity factor in flow and diffusion through porous media,” Chemical Engineering Science, vol. 44, no. 3, pp. 777–779, 1989, doi: 10.1016/0009-2509(89)85053-5.

[63] F. J. Valdes-Parada, J. A. Ochoa-Tapia, and J. Alvarez-Ramirez, “Validity of the permeability Carman–Kozeny equation: A volume averaging approach,” Physica A: Statistical Mechanics and its Applications, vol. 388, no. 6, pp. 789–798, Mar. 2009, doi: 10.1016/j.physa.2008.11.024.

[64] P. M. Heertjes and P. L. Zuideveld, “Clarification of liquids using filter aids Part III. Cake Resistance in surface filtration,” Powder Technology, vol. 19, no. 1, pp. 45–64, Jan. 1978, doi: 10.1016/0032-5910(78)80072-2.

[65] J. Happel, “Viscous flow in multiparticle systems: Slow motion of fluids relative to beds of spherical particles,” AIChE J., vol. 4, no. 2, pp. 197–201, Jun. 1958, doi: 10.1002/aic.690040214.

[66] R. Wakeman, “The influence of particle properties on filtration,” Separation and Purification Technology, vol. 58, no. 2, pp. 234–241, Dec. 2007, doi: 10.1016/j.seppur.2007.03.018.

[67] A. Nabovati, E. W. Llewellin, and A. C. M. Sousa, “A general model for the permeability of fibrous porous media based on fluid flow simulations using the lattice Boltzmann method,” Composites Part A: Applied Science and Manufacturing, vol. 40, no. 6–7, pp. 860–869, Jul. 2009, doi: 10.1016/j.compositesa.2009.04.009.

[68] P. Xu and B. Yu, “Developing a new form of permeability and Kozeny–Carman constant for homogeneous porous media by means of fractal geometry,” Advances in Water Resources, vol. 31, no. 1, pp. 74–81, Jan. 2008, doi: 10.1016/j.advwatres.2007.06.003.

[69] R. Schulz, N. Ray, S. Zech, A. Rupp, and P. Knabner, “Beyond Kozeny–Carman: Predicting the Permeability in Porous Media,” Transp Porous Med, vol. 130, no. 2, pp. 487–512, Nov. 2019, doi: 10.1007/s11242-019-01321-y.

[70] J. Olivier, J. Vaxelaire, and E. Vorobiev, “Modelling of Cake Filtration: An Overview,” Separation Science and Technology, vol. 42, no. 8, pp. 1667–1700, Jun. 2007, doi: 10.1080/01496390701242186.

[71] A. Hackl, E. Heidenreich, W. Höflinger, and R. Tittel, Eds., Filterhilfsmittelfiltration. in Fortschritt-Berichte VDI Reihe 3, Verfahrenstechnik, no. 348. Düsseldorf: VDI-Verlag, 1993.

[72] T. Iwasaki, “Some Notes on Sand Filtration,” JAWWA, vol. 29, pp. 1591–1602, 1937.

[73] C. Tien, “Cake filtration research—a personal view,” Powder Technology, vol. 127, no. 1, pp. 1–8, Sep. 2002, doi: 10.1016/S0032-5910(02)00063-3.

[74] F. M. Tiller, “The role of porosity in filtration. I. Numerical methods.,” AIChE J., vol. 46, pp. 467–479, 1953.

[75] F. M. Tiller, “The role of porosity in filtration. II. Analytical equations for constant rate filtration,” AIChE J., vol. 51, pp. 282–290, 1955.

[76] F. M. Tiller, “The role of porosity in filtration. III. Variable pressure-variable rate filtration,” AIChE J., vol. 4, pp. 170–174, 1958.

[77] F. M. Tiller and H. R. Cooper, “The role of porosity in filtration: IV. Constant pressure filtration,” AIChE J., vol. 6, no. 4, pp. 595–601, Dec. 1960, doi: 10.1002/aic.690060418.

[78] F. M. Tiller and M. Shirato, “The role of porosity in filtration: VI. New definition of filtration resistance,” AIChE J., vol. 10, no. 1, pp. 61–67, Jan. 1964, doi: 10.1002/aic.690100121.

[79] F. M. Tiller, S. Haynes, and W.-M. Lu, “The role of porosity in filtration VII effect of side-wall friction in compression-permeability cells,” AIChE J., vol. 18, no. 1, pp. 13–20, Jan. 1972, doi: 10.1002/aic.690180104.

[80] F. M. Tiller and W.-M. Lu, “The role of porosity in filtration VIII: Cake nonuniformity in compression–permeability cells,” AIChE J., vol. 18, no. 3, pp. 569–572, May 1972, doi: 10.1002/aic.690180317.

[81] F. M. Tiller and T. C. Green, “Role of porosity in filtration IX skin effect with highly compressible materials,” AIChE J., vol. 19, no. 6, pp. 1266–1269, Nov. 1973, doi: 10.1002/aic.690190633.

[82] F. M. Tiller and C. S. Yeh, “The role of porosity in filtration. Part X: Deposition of compressible cakes on external radial surfaces,” AIChE J., vol. 31, no. 8, pp. 1241–1248, Aug. 1985, doi: 10.1002/aic.690310803.

[83] F. M. Tiller and C. S. Yeh, “The role of porosity in filtration. Part XI: Filtration followed by expression,” AIChE J., vol. 33, no. 8, pp. 1241–1256, Aug. 1987, doi: 10.1002/aic.690330803.

[84] F. M. Tiller, N. B. Hsyung, and D. Z. Cong, “Role of porosity in filtration: XII. Filtration with sedimentation,” AIChE J., vol. 41, no. 5, pp. 1153–1164, May 1995, doi: 10.1002/aic.690410511.

[85] F. M. Tiller and J. H. Kwon, “Role of porosity in filtration: XIII. Behavior of highly compactible cakes,” AIChE J., vol. 44, no. 10, pp. 2159–2167, Oct. 1998, doi: 10.1002/aic.690441005.

[86] K.-J. Hwang, P.-Y. Su, E. Iritani, and N. Katagiri, “Compression and filtration characteristics of yeast-immobilized beads prepared using different calcium concentrations,” Separation Science and Technology, vol. 51, no. 11, pp. 1947–1953, Jul. 2016, doi: 10.1080/01496395.2016.1187629.

[87] S. J. Skinner et al., “Quantification of wastewater sludge dewatering,” Water Research, vol. 82, pp. 2–13, Oct. 2015, doi: 10.1016/j.watres.2015.04.045.

[88] D. J. Lee and C. H. Wang, “Theories of cake filtration and consolidation and implications to sludge dewatering,” Water Research, vol. 34, no. 1, pp. 1–20, Jan. 2000, doi: 10.1016/S0043-1354(99)00096-2.

[89] T. Mattsson, M. Sedin, and H. Theliander, “Filtration properties and skin formation of micro-crystalline cellulose,” Separation and Purification Technology, vol. 96, pp. 139–146, Aug. 2012, doi: 10.1016/j.seppur.2012.05.029.

[90] F. H. Braun, “Auswirkungen des Einsatzes von Zellulose als Filterhilfsmittel in der Bierfiltration,” Ph.D. thesis, Technische Universität München, Fakultät Wissenschaftszentrum Weihenstephan für Ernährung, Landnutzung und Umwelt, 2012.

[91] C. Tien, Introduction to cake filtration: analyses, experiments and applications, 1st ed. Amsterdam, Boston: Elsevier, 2006.

[92] A. Rushton, Ed., Mathematical Models and Design Methods in Solid-Liquid Separation. Dordrecht: Springer Netherlands, 1985. doi: 10.1007/978-94-009-5091-7.

[93] B. F. Ruth, “Studies in Filtration III. Derivation of General Filtration Equations,” Ind. Eng. Chem., vol. 27, no. 6, pp. 708–723, Jun. 1935, doi: 10.1021/ie50306a024.

[94] C. Tien, S. K. Teoh, and R. B. H. Tan, “Cake filtration analysis—the effect of the relationship between the pore liquid pressure and the cake compressive stress,” Chemical Engineering Science, vol. 56, no. 18, pp. 5361–5369, Sep. 2001, doi: 10.1016/S0009-2509(01)00263-9.

[95] R. Bai and C. Tien, “Further work on cake filtration analysis,” Chemical Engineering Science, vol. 60, no. 2, pp. 301–313, Jan. 2005, doi: 10.1016/j.ces.2004.08.008.

[96] B. F. Ruth, “Correlating Filtration Theory with Industrial Practice.,” Ind. Eng. Chem., vol. 38, no. 6, pp. 564–571, Jun. 1946, doi: 10.1021/ie50438a010.

[97] F. M. Tiller and C.-D. Tsai, “Theory of Filtration of Ceramics: I, Slip Casting,” J American Ceramic Society, vol. 69, no. 12, pp. 882–887, Dec. 1986, doi: 10.1111/j.1151-2916.1986.tb07388.x.

[98] C. van Wyk, “A study of the compressibility of wool, with special reference to South African merino wool,” The Onderstepoort journal of veterinary science and animal industry, vol. 21, no. 1, pp. 99–127, 1946.

[99] Q. Liu and J. C. Santamarina, “Mudcake growth: Model and implications,” Journal of Petroleum Science and Engineering, vol. 162, pp. 251–259, Mar. 2018, doi: 10.1016/j.petrol.2017.12.044.

[100] K. Luckert, Ed., Handbuch der mechanischen Fest-Flüssig-Trennung. Essen: Vulkan-Verlag, 2004.

[101] M. Shirato, T. Aragaki, R. Mori, and K. Sawamoto, “Predictions of constant pressure and constant rate filtrations based upon an approximate correction for side wall friction in compression permeability cell data,” J. Chem. Eng. Japan, vol. 1, no. 1, pp. 86–90, 1968, doi: 10.1252/jcej.1.86.

[102] P. Buttrick, “Choices, choices,” Brewer & Distiller International, vol. 6, no. 2, pp. 10–16, 2010.

[103] B. Gehring, D. Oechsle, and V. Kottke, “Parameterisation of horizontal leaf filters and optimisation for the filtration of beer,” Filtration & Separation, vol. 34, no. 1, pp. 67–72, Jan. 1997, doi: 10.1016/S0015-1882(97)84824-0.

[104] E. Geerdes, “Precoat Filtration with Organic Filter Aids,” Filtration & Separation, vol. 34, no. 10, pp. 1040–1043, 1997.

[105] A. S. Elsenbast and D. C. Morris, “Diatomaceous Silica Filter-Aid Clarification,” Ind. Eng. Chem., vol. 34, no. 4, pp. 412–418, Apr. 1942, doi: 10.1021/ie50388a006.

[106] D. Guo et al., “Diatomite precoat filtration for wastewater treatment: Filtration performance and pollution mechanisms,” Chemical Engineering Research and Design, vol. 137, pp. 403–411, Sep. 2018, doi: 10.1016/j.cherd.2018.06.036.

[107] H. E. Babbit and E. R. Bauman, “Effect of body feed on the filtration of water through diatomite,” University of Illinois at Urbana Champaign, College of Engineering, Engineering Experiment Station, Bulletin; no. 425, 1954.

[108] V. Bhardwaj and M. J. Mirliss, “Diatomaceous Earth Filtration for Drinking Water,” in Water Encyclopedia, J. H. Lehr and J. Keeley, Eds., 1st ed.Wiley, 2004, pp. 174–177. doi: 10.1002/047147844X.mw1818.

[109] T. Hunt, “Filter Aids,” in Encyclopedia of industrial biotechnology, M. C. Flickinger, Ed., John Wiley & Sons, 2009, pp. 1190–1197.

[110] P. C. Carman, “The Action of Filter Aids,” Ind. Eng. Chem., vol. 31, no. 8, pp. 1047–1050, Aug. 1939, doi: 10.1021/ie50356a025.

[111] A. Hackl and W. Höflinger, “Precoat-Filtration am Vakuumtrommelfilter, Prozeßmodelle fur die Tiefenfiltration,” Chemie Ingenieur Technik, vol. 57, no. 8, pp. 706–707, 1985.

[112] M. Kuhn and H. Briesen, “Dynamic Modeling of Filter-Aid Filtration Including Surface- and Depth-Filtration Effects,” Chem. Eng. Technol., vol. 39, no. 3, pp. 425–434, Mar. 2016, doi: 10.1002/ceat.201500347.

[113] “Wissenschaftliche Begründung für die Berufskrankheit Nummer 4112. Lungenkrebs durch die Einwirkung von kristallinem Siliziumdioxid (SiO2) bei nachgewiesener Quarzstaublungenerkrankung (Silikose oder Siliko-Tuberkulose),” BArbBl, S.-. Bek. des BMA vom 1. August 2001 - IVa 4-45222-2106/4112, 2001.

[114] Centre international de recherche sur le cancer, Ed., Silica, some silicates, coal dust and para-aramid fibrils. in IARC monographs on the evaluation of carcinogenic risks to humans, no. 68. Lyon: IARC, 1997.

[115] W. Höflinger and J. Graf, “Wirtschaftlichkeit der kieselgurfreien Bierfiltration,” Brauwelt, vol. 145, no. 15, pp. 466–471, 2005.

[116] A. Zeller, “Substitution der Kieselgur durch regenerierbare Zellulosefasern auf einem neuartigen Filtrationssystem für Brauereien,” Ph.D. thesis, Fakultät für Mechanische Verfahrenstechnik, Technische Universität Bergakademie Freiberg, 2011.

[117] F. Braun, T. Becker, W. Back, and M. Krottenthaler, “Investigation of Beer Filtration Using Cellulose Fibers in a Pilot-Scale Filter Plant,” Journal of the American Society of Brewing Chemists, vol. 68, no. 3, pp. 139–147, Jun. 2010, doi: 10.1094/ASBCJ-2010-0523-01.

[118] J. Zacharias and R. Schneid, “Bierfiltration mit Viskose-fasern – Verfahren für kompressible Filterhilfsmittel,” Brauwelt, vol. 35, pp. 1012–1015, 2017.

[119] F. Braun, N. Hildebrand, S. Wilkinson, W. Back, M. Krottenthaler, and T. Becker, “Large-Scale Study on Beer Filtration with Combined Filter Aid Additions to Cellulose Fibres,” Journal of the Institute of Brewing, vol. 117, no. 3, pp. 314–328, 2011, doi: 10.1002/j.2050-0416.2011.tb00475.x.

[120] E. N. Pistikopoulos et al., “Process systems engineering – The generation next?,” Computers & Chemical Engineering, vol. 147, p. 107252, Apr. 2021, doi: 10.1016/j.compchemeng.2021.107252.

[121] M. Kuhn, W. Pietsch, and H. Briesen, “Clarifying Thoughts About the Clarification of Liquids - Filtration and the Philosophy of Science,” Chemie Ingenieur Technik, vol. 89, no. 9, pp. 1126–1132, Sep. 2017, doi: 10.1002/cite.201700025.

[122] Q. Xiong, T. G. Baychev, and A. P. Jivkov, “Review of pore network modelling of porous media: Experimental characterisations, network constructions and applications to reactive transport,” Journal of Contaminant Hydrology, vol. 192, pp. 101–117, Sep. 2016, doi: 10.1016/j.jconhyd.2016.07.002.

[123] S. Whitaker, The Method of Volume Averaging, vol. 13. in Theory and Applications of Transport in Porous Media, vol. 13. Dordrecht: Springer Netherlands, 1999. doi: 10.1007/978-94-017-3389-2.

[124] K. J. Dong, R. P. Zou, R. Y. Yang, A. B. Yu, and G. Roach, "DEM simulation of cake formation in sedimentation and filtration," Minerals Engineering, vol. 22, no. 11, pp. 921–930, Oct. 2009, doi: 10.1016/j.mineng.2009.03.018.

[125] J. Dueck, E. Djatschenko, and T. Neesse, "Computersimulation von Filterkuchenstrukturen," Chemie Ingenieur Technik, vol. 79, no. 11, pp. 1913–1919, Nov. 2007, doi: 10.1002/cite.200700131.

[126] R. Deshpande, S. Antonyuk, and O. Iliev, "DEM-CFD study of the filter cake formation process due to non-spherical particles," Particuology, vol. 53, pp. 48–57, Dec. 2020, doi: 10.1016/j.partic.2020.01.003.

[127] V. Puderbach, K. Schmidt, and S. Antonyuk, "A Coupled CFD-DEM Model for Resolved Simulation of Filter Cake Formation during Solid-Liquid Separation," Processes, vol. 9, no. 5, p. 826, May 2021, doi: 10.3390/pr9050826.

[128] B. Li, K. M. Dobosz, H. Zhang, J. D. Schiffman, K. Saranteas, and M. A. Henson, "Predicting the performance of pressure filtration processes by coupling computational fluid dynamics and discrete element methods," Chemical Engineering Science, vol. 208, p. 115162, Nov. 2019, doi: 10.1016/j.ces.2019.115162.

[129] I. M. Griffiths, I. Mitevski, I. Vujkovac, M. R. Illingworth, and P. S. Stewart, "The role of tortuosity in filtration efficiency: A general network model for filtration," Journal of Membrane Science, vol. 598, p. 117664, Mar. 2020, doi: 10.1016/j.memsci.2019.117664.

[130] F. Wang and U. D. Schiller, "Computational characterization of nonwoven fibrous media: I. Pore-network extraction and morphological analysis," Phys. Rev. Materials, vol. 4, no. 8, p. 083803, Aug. 2020, doi: 10.1103/PhysRevMaterials.4.083803.

[131] J. Tansey and M. T. Balhoff, "Pore Network Modeling of Reactive Transport and Dissolution in Porous Media," Transp Porous Med, vol. 113, no. 2, pp. 303–327, Jun. 2016, doi: 10.1007/s11242-016-0695-x.

[132] E. Höfgen, S. Kühne, U. A. Peuker, and A. D. Stickland, "A comparison of filtration characterisation devices for compressible suspensions using conventional filtration theory and compressional rheology," Powder Technology, vol. 346, pp. 49–56, Mar. 2019, doi: 10.1016/j.powtec.2019.01.056.

[133] K. A. Landman, L. R. White, and M. Eberl, "Pressure filtration of flocculated suspensions," AIChE J., vol. 41, no. 7, pp. 1687–1700, Jul. 1995, doi: 10.1002/aic.690410709.

[134] R. Buscall and L. R. White, "The consolidation of concentrated suspensions. Part 1.—The theory of sedimentation," J. Chem. Soc., Faraday Trans. 1, vol. 83, no. 3, p. 873, 1987, doi: 10.1039/f19878300873.

[135] D. E. Smiles, “A theory of constant pressure filtration,” Chemical Engineering Science, vol. 25, no. 6, pp. 985–996, 1970, doi: 10.1016/0009-2509(70)85043-6.

[136] B. V. Ramarao and C. Tien, “Approximate Analysis of Fine-Particle Retention in the Cake Filtration of Suspensions,” Ind. Eng. Chem. Res., vol. 44, no. 5, pp. 1424–1432, Mar. 2005, doi: 10.1021/ie049469j.

[137] S. Whitaker, “Flow in porous media I: A theoretical derivation of Darcy’s law,” Transp Porous Med, vol. 1, no. 1, pp. 3–25, 1986, doi: 10.1007/BF01036523.

[138] P. C. Carman, “A study of the mechanism of filtration,” Journal of the Society of Chemical Industry, vol. 52, no. 36, pp. T280–T286, 1933.

[139] P. H. Hermans and H. L. Bredée, “Zur Kenntnis der Filtrationsgesetze,” Recl. Trav. Chim. Pays-Bas, vol. 54, no. 9, pp. 680–700, 1935, doi: 10.1002/recl.19350540902.

[140] T. Buchwald, “Nonlinear parameter estimation of experimental cake filtration data,” Ph.D. thesis, Fakultät für Maschinenbau, Verfahrens- und Energietechnik, Technische Universität Bergakademie Freiberg, 2021.

[141] S. Ottoboni et al., “Development of a Novel Continuous Filtration Unit for Pharmaceutical Process Development and Manufacturing,” Journal of Pharmaceutical Sciences, vol. 108, no. 1, pp. 372–381, Jan. 2019, doi: 10.1016/j.xphs.2018.07.005.

[142] S. Kühne and U. A. Peuker, “Cake Filtration of Multicomponent Suspensions,” Chem. Eng. Technol., vol. 41, no. 1, pp. 96–101, Jan. 2018, doi: 10.1002/ceat.201700164.

[143] P. M. Bandelt Riess, J. Engstle, M. Kuhn, H. Briesen, and P. Först, “Decreasing Filter Cake Resistance by Using Packing Structures,” Chem. Eng. Technol., vol. 41, no. 10, pp. 1956–1964, Oct. 2018, doi: 10.1002/ceat.201800254.

[144] F. M. Mahdi and R. G. Holdich, “Laboratory cake filtration testing using constant rate,” Chemical Engineering Research and Design, vol. 91, no. 6, pp. 1145–1154, Jun. 2013, doi: 10.1016/j.cherd.2012.11.012.

[145] J. W. Tichy, “Zum Einfluss des Filtermittels und der auftretenden Interferenzen zwischen Filterkuchen und Filtermittel bei der Kuchenfiltration,” Ph.D. thesis, Technische Universität Kaiserslautern, Fachbereich Maschinenbau und Verfahrenstechnik, 2007.

[146] R. G. Holdich, “Prediction of solid concentration and height in a compressible filter cake,” International Journal of Mineral Processing, vol. 39, no. 3–4, pp. 157–171, Oct. 1993, doi: 10.1016/0301-7516(93)90013-Z.

[147] H. P. Grace, “Resistance and compressibility of filter cakes,” Chemical Engineering Progress, vol. 49, pp. 303–318, 1953.

[148] S.-K. Teoh, R. B. H. Tan, and C. Tien, “Analysis of cake filtration data—A critical assessment of conventional filtration theory,” AIChE J., vol. 52, no. 10, pp. 3427–3442, Oct. 2006, doi: 10.1002/aic.10952.

[149] S.-K. Teoh, R. B. H. Tan, and C. Tien, “A new procedure for determining specific filter cake resistance from filtration data,” Chemical Engineering Science, vol. 61, no. 15, pp. 4957–4965, Aug. 2006, doi: 10.1016/j.ces.2006.03.048.

[150] C. Tien and R. Bai, “An assessment of the conventional cake filtration theory,” Chemical Engineering Science, vol. 58, no. 7, pp. 1323–1336, Apr. 2003, doi: 10.1016/S0009-2509(02)00655-3.

[151] D. J. Lee, S. P. Ju, J. H. Kwon, and F. M. Tiller, “Filtration of highly compactible filter cake: Variable internal flow rate,” AIChE J., vol. 46, no. 1, pp. 110–118, Jan. 2000, doi: 10.1002/aic.690460114.

[152] C. Tien, “Retention of fine particles within filter cakes in cake filtration,” J. Chin. Inst. Chem. Eng., vol. 22, no. 6, pp. 385–390, 1991.

[153] S. Osterroth, “Mathematical models for the simulation of combined depth and cake filtration processes,” Ph.D. thesis, Fachbereich Mathematik, Technische Universität Kaiserslautern, 2018.

[154] F. M. Tiller and C. J. Huang, “Filtration Equipment - Theory,” Ind. Eng. Chem., vol. 53, no. 7, pp. 529–537, Jul. 1961, doi: 10.1021/ie50619a021.

[155] M. Shirato, M. Sambuichi, H. Kato, and T. Aragaki, “Internal flow mechanism in filter cakes,” AIChE J., vol. 15, no. 3, pp. 405–409, May 1969, doi: 10.1002/aic.690150320.

[156] R. J. Wakeman, “A numerical integration of the differential equation describing the formation of and flow in compressible filter cakes,” Trans. Inst. of Chem. Eng., vol. 56, pp. 258–265, 1978.

[157] K. Rietema, “Science and technology of dispersed two-phase systems—I and II,” Chemical Engineering Science, vol. 37, no. 8, pp. 1125–1150, 1982, doi: 10.1016/0009-2509(82)85058-6.

[158] K. Atsumi and T. Akiyama, “A Study of Cake Filtration: Formulation as a Stefan Problem,” J. Chem. Eng. Japan, vol. 8, no. 6, pp. 487–492, 1975, doi: 10.1252/jcej.8.487.

[159] Max. S. Willis and I. Tosun, “A rigorous cake filtration theory,” Chemical Engineering Science, vol. 35, no. 12, pp. 2427–2438, 1980, doi: 10.1016/0009-2509(80)85055-X.

[160] K. Stamatakis and C. Tien, “Cake formation and growth in cake filtration,” Chemical Engineering Science, vol. 46, no. 8, pp. 1917–1933, 1991, doi: 10.1016/0009-2509(91)80153-P.

[161] S. R. Upreti, Optimal Control for Chemical Engineers, 1st ed. Boca Raton: CRC Press, Taylor & Francis Group, 2013. doi: 10.1201/b13045.

[162] H. P. Geering, Optimal control with engineering applications. Berlin, New York: Springer, 2007.

[163] M. Kuhn, C. Kirse, and H. Briesen, “Improving the design of depth filters: A model-based method using optimal control theory,” AIChE J., vol. 64, no. 1, pp. 68–76, Jan. 2018, doi: 10.1002/aic.15866.

[164] C. Geerling, M. Azimian, A. Wiegmann, H. Briesen, and M. Kuhn, “Designing optimally-graded depth filter media using a novel multiscale method,” AIChE J, vol. 66, no. 2, Feb. 2020, doi: 10.1002/aic.16808.

[165] R. Paulen and M. Fikar, Optimal Operation of Batch Membrane Processes. in Advances in Industrial Control. Cham: Springer International Publishing, 2016. doi: 10.1007/978-3-319-20475-8.

[166] M. Kuhn and H. Briesen, “Optimizing the Axial Resistance Profile of Submerged Hollow Fiber Membranes,” Processes, vol. 9, no. 1, p. 20, Dec. 2020, doi: 10.3390/pr9010020.

[167] S. Gergely, E. Bekassy-Molnar, and Gy. Vatai, “The use of multiobjective optimization to improve wine filtration,” Journal of Food Engineering, vol. 58, no. 4, pp. 311–316, Aug. 2003, doi: 10.1016/S0260-8774(02)00376-X.

[168] N. Kalboussi, A. Rapaport, T. Bayen, N. B. Amar, F. Ellouze, and J. Harmand, “Optimal Control of Membrane-Filtration Systems,” IEEE Trans. Automat. Contr., vol. 64, no. 5, pp. 2128–2134, May 2019, doi: 10.1109/TAC.2018.2866638.

[169] B. Blankert, B. H. L. Betlem, and B. Roffel, “Dynamic optimization of a dead-end filtration trajectory: Blocking filtration laws,” Journal of Membrane Science, vol. 285, no. 1–2, pp. 90–95, Nov. 2006, doi: 10.1016/j.memsci.2006.07.044.

[170] B. Blankert, C. Kattenbelt, B. H. L. Betlem, and B. Roffel, “Dynamic optimization of a dead-end filtration trajectory: Non-ideal cake filtration,” Journal of Membrane Science, vol. 290, no. 1–2, pp. 114–124, Mar. 2007, doi: 10.1016/j.memsci.2006.12.024.

[171] A. J. B. van Boxtel, Z. E. H. Otten, and H. J. L. J. van der Linden, “Dynamic optimization of a one-stage reverse-osmosis installation with respect to membrane fouling,” Journal of Membrane Science, vol. 65, no. 3, pp. 277–293, Jan. 1992, doi: 10.1016/0376-7388(92)87029-W.

[172] J. Köry, A. Krupp, C. Please, and I. Griffiths, “Optimising Dead-End Cake Filtration Using Poroelasticity Theory,” Modelling, vol. 2, no. 1, pp. 18–42, Jan. 2021, doi: 10.3390/modelling2010002.

[173] K. Wegner, “Hydrodynamische Modellierung der Klärfiltration mit körnigen Stoffen unter besonderer Berücksichtigung der Anschwemmfiltration mit Schichtzunahme,” Ph.D. thesis, Technische Universität Dresden, Fakultät für Maschinenwesen, 1985.

[174] R. W. H. Sargent, “Optimal control,” Journal of Computational and Applied Mathematics, vol. 124, no. 1–2, pp. 361–371, Dec. 2000, doi: 10.1016/S0377-0427(00)00418-0.

[175] R. F. Hartl, S. P. Sethi, and R. G. Vickson, “A Survey of the Maximum Principles for Optimal Control Problems with State Constraints,” SIAM Rev., vol. 37, no. 2, pp. 181–218, Jun. 1995, doi: 10.1137/1037043.

[176] M. Diehl, H. G. Bock, H. Diedam, and P.-B. Wieber, “Fast Direct Multiple Shooting Algorithms for Optimal Robot Control,” in Fast Motions in Biomechanics and Robotics. Lecture Notes in Control and Information Science, vol 340., M. Diehl and K. Mombaur, Eds., in Lecture Notes in Control and Information Sciences, vol. 340. Berlin, Heidelberg: Springer, 2006, pp. 65–93. doi: 10.1007/978-3-540-36119-0_4.

[177] A. Nzali, “Zur Lösung optimaler Steuerungsprobleme,” Ph.D. thesis, Mathematisch-Naturwissenschaftliche Fakultät II, Humboldt-Universität zu Berlin, 2002.

[178] A. E. Bryson and Y.-C. Ho, Applied optimal control: optimization, estimation, and control, Rev. printing. Washington, New York: Hemisphere Pub. Corp., 1975.

[179] C. J. Goh and K. L. Teo, “Control parametrization: A unified approach to optimal control problems with general constraints,” Automatica, vol. 24, no. 1, pp. 3–18, Jan. 1988, doi: 10.1016/0005-1098(88)90003-9.

[180] D. Kraft, “On Converting Optimal Control Problems into Nonlinear Programming Problems,” in Computational Mathematical Programming. NATO ASI Series, vol 15., K. Schittkowski, Ed., Berlin, Heidelberg: Springer, 1985, pp. 261–280. doi: 10.1007/978-3-642-82450-0_9.

[181] R. W. H. Sargent and G. R. Sullivan, “The development of an efficient optimal control package. Lecture Notes in Control and Information Sciences.,” in Optimization Techniques. Lecture Notes in Control and Information Sciences, vol 7., J. Stoer, Ed., in Lecture Notes in Control and Information Sciences, vol. 7. Berlin, Heidelberg: Springer, 1978, pp. 158–168. doi: 10.1007/BFb0006520.

[182] M. Papageorgiou, M. Leibold, and M. Buss, Optimierung: Statische, dynamische, stochastische Verfahren für die Anwendung. Berlin, Heidelberg: Springer, 2012. doi: 10.1007/978-3-540-34013-3.

[183] D. Liberzon, Calculus of Variations and Optimal Control Theory: A Concise Introduction. Princeton University Press, 2012. doi: 10.1515/9781400842643.

[184] G. Leugering et al., Eds., Constrained Optimization and Optimal Control for Partial Differential Equations, vol. 160. in International Series of Numerical Mathematics, vol. 160. Basel: Springer, 2012. doi: 10.1007/978-3-0348-0133-1.

[185] M. Ulbrich and S. Ulbrich, Nichtlineare Optimierung. Basel: Springer, 2012. doi: 10.1007/978-3-0346-0654-7.

[186] L. T. Biegler, Nonlinear programming: concepts, algorithms, and applications to chemical processes. in MOS-SIAM series on optimization. Philadelphia: Society for Industrial and Applied Mathematics : Mathematical Programming Society, 2010.

[187] A. Vande Wouwer, P. Saucez, and C. Vilas, Simulation of ODE/PDE Models with MATLAB®, OCTAVE and SCILAB: Scientific and Engineering Applications. Cham: Springer International Publishing, 2014. doi: 10.1007/978-3-319-06790-2.

[188] F. Civan, "Practical model for compressive cake filtration including fine particle invasion," AIChE J., vol. 44, no. 11, pp. 2388–2398, Nov. 1998, doi: 10.1002/aic.690441107.

[189] U. Baur, P. Benner, and L. Feng, "Model Order Reduction for Linear and Nonlinear Systems: A System-Theoretic Perspective," Arch Computat Methods Eng, vol. 21, no. 4, pp. 331–358, Dec. 2014, doi: 10.1007/s11831-014-9111-2.

[190] D. J. Lucia, P. S. Beran, and W. A. Silva, "Reduced-order modeling: new approaches for computational physics," Progress in Aerospace Sciences, vol. 40, no. 1–2, pp. 51–117, Feb. 2004, doi: 10.1016/j.paerosci.2003.12.001.

[191] W. H. A. Schilders, H. A. van der Vorst, and J. Rommes, Eds., Model Order Reduction: Theory, Research Aspects and Applications, vol. 13. in Mathematics in Industry, vol. 13. Berlin, Heidelberg: Springer, 2008. doi: 10.1007/978-3-540-78841-6.

[192] P. Benner, S. Gugercin, and K. Willcox, "A Survey of Projection-Based Model Reduction Methods for Parametric Dynamical Systems," SIAM Rev., vol. 57, no. 4, pp. 483–531, Jan. 2015, doi: 10.1137/130932715.

[193] A. Chatterjee, "An introduction to the proper orthogonal decomposition," Current Science, vol. 78, no. 7, pp. 808–817, 2000.

[194] Y. C. Liang, H. P. Lee, S. P. Lim, W. Z. Lin, K. H. Lee, and C. G. Wu, "Proper Orthogonal Decomposition and its Applications - Part I: Theory," Journal of Sound and Vibration, vol. 252, no. 3, pp. 527–544, May 2002, doi: 10.1006/jsvi.2001.4041.

[195] E. Gildin, M. Ghasemi, A. Romanovskay, and Y. Efendiev, "Nonlinear Complexity Reduction for Fast Simulation of Flow in Heterogeneous Porous Media," in SPE Reservoir Simulation Symposium, The Woodlands, Texas, USA: SPE, Feb. 2013, p. SPE-163618-MS. doi: 10.2118/163618-MS.

[196] M. Ghasemi and E. Gildin, "Localized model order reduction in porous media flow simulation," Journal of Petroleum Science and Engineering, vol. 145, pp. 689–703, Sep. 2016, doi: 10.1016/j.petrol.2016.06.030.

[197] M. Alotaibi, V. M. Calo, Y. Efendiev, J. Galvis, and M. Ghommem, "Global–local nonlinear model reduction for flows in heterogeneous porous media," Computer Methods in Applied Mechanics and Engineering, vol. 292, pp. 122–137, Aug. 2015, doi: 10.1016/j.cma.2014.10.034.

[198] S. Osterroth, O. Iliev, and R. Pinnau, "On Efficient Approaches for Solving a Cake Filtration Model Under Parameter Variation," in Model Reduction of Parametrized Systems, P. Benner, M. Ohlberger, A. Patera, G. Rozza, and K. Urban, Eds., in MS&A, vol. 17. Cham: Springer International Publishing, 2017, pp. 455–470. doi: 10.1007/978-3-319-58786-8_28.

[199] F. Vetrano, C. Le Garrec, and G. Mortchelewicz, “Assessment of Strategies for Interpolating POD Based Reduced Order Model and Application to Aeroelasticity,” Journal of Aeroelasticity and Structural Dynamics, no. 2, pp. 85–104, 2012, doi: 10.3293/asdj.2011.13.

[200] T. Lieu and M. Lesoinne, “Parameter Adaptation of Reduced Order Models for Three-Dimensional Flutter Analysis,” in 42nd AIAA Aerospace Sciences Meeting and Exhibit, Reno, Nevada: American Institute of Aeronautics and Astronautics, Jan. 2004. doi: 10.2514/6.2004-888.

[201] S. Chaturantabut and D. C. Sorensen, “Discrete Empirical Interpolation for nonlinear model reduction,” in Proceedings of the 48h IEEE Conference on Decision and Control (CDC) held jointly with 2009 28th Chinese Control Conference, Shanghai, China: IEEE, Dec. 2009, pp. 4316–4321. doi: 10.1109/CDC.2009.5400045.

[202] S. Chaturantabut and D. C. Sorensen, “Nonlinear Model Reduction via Discrete Empirical Interpolation,” SIAM J. Sci. Comput., vol. 32, no. 5, pp. 2737–2764, Jan. 2010, doi: 10.1137/090766498.

[203] R. Everson and L. Sirovich, “Karhunen–Loève procedure for gappy data,” J. Opt. Soc. Am. A, vol. 12, no. 8, p. 1657, Aug. 1995, doi: 10.1364/JOSAA.12.001657.

[204] K. Willcox, “Unsteady flow sensing and estimation via the gappy proper orthogonal decomposition,” Computers & Fluids, vol. 35, no. 2, pp. 208–226, Feb. 2006, doi: 10.1016/j.compfluid.2004.11.006.

[205] S. L. Brunton and J. N. Kutz, Data-Driven Science and Engineering: Machine Learning, Dynamical Systems, and Control, 1st ed. Cambridge University Press, 2019. doi: 10.1017/9781108380690.

[206] A. Quarteroni and G. Rozza, Eds., Reduced Order Methods for Modeling and Computational Reduction. Cham: Springer International Publishing, 2014. doi: 10.1007/978-3-319-02090-7.

[207] A. Quarteroni, A. Manzoni, and F. Negri, Reduced Basis Methods for Partial Differential Equations, vol. 92. in UNITEXT, vol. 92. Cham: Springer International Publishing, 2016. doi: 10.1007/978-3-319-15431-2.

[208] C. B. Moler, Numerical Computing with Matlab. Society for Industrial and Applied Mathematics, 2004. doi: 10.1137/1.9780898717952.

[209] H. G. Landau, “Heat conduction in a melting solid,” Quart. Appl. Math., vol. 8, no. 1, pp. 81–94, 1950, doi: 10.1090/qam/33441.

[210] J. Crank, Free and moving boundary problems. in Oxford science publications. Oxford, New York: Clarendon Press; Oxford University Press, 1987.

[211] W. E. Schiesser and G. W. Griffiths, A compendium of partial differential equation models: method of lines analysis with Matlab. Cambridge, New York: Cambridge University Press, 2009.

[212] L. F. Shampine and M. W. Reichelt, “The MATLAB ODE Suite,” SIAM J. Sci. Comput., vol. 18, no. 1, pp. 1–22, Jan. 1997, doi: 10.1137/S1064827594276424.

[213] The MathWorks, Inc., “Floating-point relative accuracy.” https://de.mathworks.com/help/matlab/ref/eps.html (accessed Mar. 19, 2023).

[214] The MathWorks, Inc., “Constrained Nonlinear Optimization Algorithms.” https://de.mathworks.com/help/optim/ug/constrained-nonlinear-optimization-algorithms.html#brnpd5f (accessed Mar. 19, 2023).

[215] J. A. Nelder and R. Mead, “A Simplex Method for Function Minimization,” The Computer Journal, vol. 7, no. 4, pp. 308–313, Jan. 1965, doi: 10.1093/comjnl/7.4.308.

[216] D. Amsallem and C. Farhat, “Interpolation Method for Adapting Reduced-Order Models and Application to Aeroelasticity,” AIAA Journal, vol. 46, no. 7, pp. 1803–1813, Jul. 2008, doi: 10.2514/1.35374.

[217] F. M. Dekking, C. Kraaikamp, H. P. Lopuhaä, and L. E. Meester, “The law of large numbers,” in A Modern Introduction to Probability and Statistics, in Springer Texts in Statistics. London: Springer, 2005, pp. 181–194. doi: 10.1007/1-84628-168-7_13.

[218] F. M. Tiller, R. Lu, J. H. Kwon, and D. J. Lee, “Variable flow rate in compactable filter cakes,” Water Research, vol. 33, pp. 15–22, 1999.

[219] J. Wetterling, T. Mattsson, and H. Theliander, “Modelling filtration processes from local filtration properties: The effect of surface properties on microcrystalline cellulose,” Chemical Engineering Science, vol. 165, pp. 14–24, Jun. 2017, doi: 10.1016/j.ces.2017.02.017.

[220] F. Dyson, “A meeting with Enrico Fermi,” Nature, vol. 427, no. 6972, pp. 297–297, Jan. 2004, doi: 10.1038/427297a.

[221] K. P. Burnham, D. R. Anderson, and K. P. Burnham, Model selection and multimodel inference: a practical information-theoretic approach, 2nd ed. New York: Springer, 2002.

[222] H. Akaike, “A new look at the statistical model identification,” IEEE Trans. Automat. Contr., vol. 19, no. 6, pp. 716–723, Dec. 1974, doi: 10.1109/TAC.1974.1100705.

[223] G. H. Meeten, “A dissection method for analysing filter cakes,” Chemical Engineering Science, vol. 48, no. 13, pp. 2391–2398, Jul. 1993, doi: 10.1016/0009-2509(93)81060-9.

[224] D. Smiles and M. Rosenthal, “The movement of water in swelling materials,” Soil Res., vol. 6, no. 2, p. 237, 1968, doi: 10.1071/SR9680237.

[225] R. Bai and C. Tien, “Effect of Deposition in Deep-Bed Filtration: Determination and Search of Rate Parameters,” Journal of Colloid and Interface Science, vol. 231, no. 2, pp. 299–311, Nov. 2000, doi: 10.1006/jcis.2000.7130.

[226] T. Lutz, L. Wilen, and J. Wettlaufer, “A method for measuring fluid pressure and solid deformation profiles in uniaxial porous media flows,” Review of Scientific Instruments, vol. 92, no. 2, p. 025101, Feb. 2021, doi: 10.1063/5.0019519.

[227] J. Tomas and B. Reichmann, “Compression, Permeation and Flow Behavior of Wet Nanoparticle Cakes, in situ Tested with a Press-Shear Cell,” Chem. Eng. Technol., vol. 25, no. 11, pp. 1053–1060, Nov. 2002, doi: 10.1002/1521-4125(20021105)25:11<1053::AID-CEAT1053>3.0.CO;2-S.

[228] M. Fathi-Najafi and H. Theliander, “Determination of local filtration properties at constant pressure,” Separations Technology, vol. 5, no. 3, pp. 165–178, Aug. 1995, doi: 10.1016/0956-9618(94)00115-9.

[229] M. Shirato, T. Aragaki, K. Ichimura, and N. Ootsuji, “Porosiy Variation in Filter Cake under Constant-Pressure Filtration,” J. Chem. Eng. Japan, vol. 4, no. 2, pp. 172–177, 1971, doi: 10.1252/jcej.4.172.

[230] J. Cai, W. Wei, X. Hu, and D. A. Wood, “Electrical conductivity models in saturated porous media: A review,” Earth-Science Reviews, vol. 171, pp. 419–433, Aug. 2017, doi: 10.1016/j.earscirev.2017.06.013.

[231] M. Hamachi and M. Mietton-Peuchot, “Cake Thickness Measurement with an Optical Laser Sensor,” Chemical Engineering Research and Design, vol. 79, no. 2, pp. 151–155, Mar. 2001, doi: 10.1205/02638760151095962.

[232] M. Saleem and G. Krammer, “Optical in-situ measurement of filter cake height during bag filter plant operation,” Powder Technology, vol. 173, no. 2, pp. 93–106, Apr. 2007, doi: 10.1016/j.powtec.2006.12.008.

[233] K. Takahashi, Y. Kobayashi, T. Yokota, and K. Koyama, “Measurement of cake thickness on membrane for microfiltration of yeast using ultrasonic polymer concave transducer.,” J. Chem. Eng. Japan, vol. 24, no. 5, pp. 599–603, 1991, doi: 10.1252/jcej.24.599.

[234] M. A. Horsfield, E. J. Fordham, C. Hall, and L. D. Hall, “1H NMR imaging studies of filtration in colloidal suspensions,” Journal of Magnetic Resonance (1969), vol. 81, no. 3, pp. 593–596, Feb. 1989, doi: 10.1016/0022-2364(89)90098-X.

[235] E. J. La Heij, P. J. A. M. Kerkhof, K. Kopinga, and L. Pel, “Determining porosity profiles during filtration and expression of sewage sludge by NMR imaging,” AIChE J., vol. 42, no. 4, pp. 953–959, Apr. 1996, doi: 10.1002/aic.690420408.

[236] S. Buetehorn et al., “NMR imaging of local cumulative permeate flux and local cake growth in submerged microfiltration processes,” Journal of Membrane Science, vol. 371, no. 1–2, pp. 52–64, Apr. 2011, doi: 10.1016/j.memsci.2011.01.018.

[237] P. Sedin, C. Johansson, and H. Theliander, “On the Measurement and Evaluation of Pressure and Solidosity in Filtration,” Chemical Engineering Research and Design, vol. 81, no. 10, pp. 1393–1405, Nov. 2003, doi: 10.1205/026387603771339618.

[238] B. Bierck, S. Wells, and R. Dick, “Compressible cake filtration: monitoring cake formation and shrinkage using synchrotron X-rays,” Journal of Water Pollution Control Federation, vol. 60, no. 5, pp. 645–650, 1988.

[239] L. Bergstrom, C. H. Schilling, and I. A. Aksay, “Consolidation Behavior of Flocculated Alumina Suspensions,” J American Ceramic Society, vol. 75, no. 12, pp. 3305–3314, Dec. 1992, doi: 10.1111/j.1151-2916.1992.tb04426.x.

[240] Z. Feng, Y. Fan, X. Dong, X. Ma, and R. Chen, “Permeability estimation in filter cake based on X-ray microtomography and Lattice Boltzmann method,” Separation and Purification Technology, vol. 275, p. 119114, Nov. 2021, doi: 10.1016/j.seppur.2021.119114.

[241] Z. Zhao, X.-P. Zhou, and Q.-H. Qian, “Fracture characterization and permeability prediction by pore scale variables extracted from X-ray CT images of porous geomaterials,” Sci. China Technol. Sci., vol. 63, no. 5, pp. 755–767, May 2020, doi: 10.1007/s11431-019-1449-4.

[242] J. R. A. Godinho, K. Chellappah, I. Collins, P. Ng, M. Smith, and P. J. Withers, “Time-lapse imaging of particle invasion and deposition in porous media using in situ X-ray radiography,” Journal of Petroleum Science and Engineering, vol. 177, pp. 384–391, Jun. 2019, doi: 10.1016/j.petrol.2019.02.061.

[243] T. Leißner et al., “3D ex-situ and in-situ X-ray CT process studies in particle technology – A perspective,” Advanced Powder Technology, vol. 31, no. 1, pp. 78–86, Jan. 2020, doi: 10.1016/j.apt.2019.09.038.

[244] G. Franceschini and S. Macchietto, “Model-based design of experiments for parameter precision: State of the art,” Chemical Engineering Science, vol. 63, no. 19, pp. 4846–4872, Oct. 2008, doi: 10.1016/j.ces.2007.11.034.

[245] L. Pronzato and A. Pázman, Design of Experiments in Nonlinear Models: Asymptotic Normality, Optimality Criteria and Small-Sample Properties, vol. 212. in Lecture Notes in Statistics, vol. 212. New York: Springer, 2013. doi: 10.1007/978-1-4614-6363-4.

[246] L. Grüne, M. Schaller, and A. Schiela, “Sensitivity Analysis of Optimal Control for a Class of Parabolic PDEs Motivated by Model Predictive Control,” SIAM J. Control Optim., vol. 57, no. 4, pp. 2753–2774, Jan. 2019, doi: 10.1137/18M1223083.

[247] U. A. Peuker and H. Briesen, “Prozessverständnis und optimale Steuerung von realen Anschwemmtiltrationsprozessen mit kompressibler Filterschicht,” Freiberg, Freising, Schlussbericht zum IGF-Vorhaben Nr. 19947 BG, Apr. 2022.

[248] F. M. Tiller, “Clogging phenomena in the filtration of liquefied coal,” Chem. Eng. Prog., vol. 77, pp. 61–68, 1981.

[249] D. J. Lee, “Filter medium clogging during cake filtration,” AIChE J., vol. 43, no. 1, pp. 273–276, Jan. 1997, doi: 10.1002/aic.690430132.

[250] A. Broeckmann, J. Busch, T. Wintgens, and W. Marquardt, “Modeling of pore blocking and cake layer formation in membrane filtration for wastewater treatment,” Desalination, vol. 189, no. 1–3, pp. 97–109, Mar. 2006, doi: 10.1016/j.desal.2005.06.018.

[251] K. L. Jepsen, M. V. Bram, L. Hansen, Z. Yang, and S. M. Ø. Lauridsen, “Online Backwash Optimization of Membrane Filtration for Produced Water Treatment,” Membranes, vol. 9, no. 6, p. 68, Jun. 2019, doi: 10.3390/membranes9060068.

[252] E. Zondervan and B. Roffel, “Dynamic optimization of chemical cleaning in dead-end ultra filtration,” Journal of Membrane Science, vol. 307, no. 2, pp. 309–313, Jan. 2008, doi: 10.1016/j.memsci.2007.09.067.

[253] B. Kh. Khuzhayorov, G. Ibragimov, U. Saydullaev, I. Shadmanov, and F. M. Ali, “Filtration of suspensions with forming of an elasto-plastic cake,” Waves in Random and Complex Media, pp. 1–24, Oct. 2022, doi: 10.1080/17455030.2022.2136417.

[254] B. Kh. Khuzhayorov, U. Saydullaev, G. Ibragimov, and N. Wahi, “An Axisymmetric Problem of Suspension Filtering with Formation of Elastic–Plastic Cake Layer,” Symmetry, vol. 14, no. 6, p. 1202, Jun. 2022, doi: 10.3390/sym14061202.

[255] T. Neumann, K. Boettcher, and P. Ehrhard, “Strömungen durch monodisperse Kugelschüttungen bei Berücksichtigung des Wandeffekts,” Chemie Ingenieur Technik, vol. 91, no. 9, pp. 1251–1259, Sep. 2019, doi: 10.1002/cite.201800103.

[256] P. M. Bandelt Riess, “Using Packed Beds as a Strategy to Enhance Filtration Processes,” Ph.D. thesis, TUM School of Life Sciences, Technische Universität München, 2022.

[257] S. Berres, R. Bürger, and W. L. Wendland, “Mathematical Models for the Sedimentation of Suspensions,” in Multifield Problems in Solid and Fluid Mechanics, R. Helmig, A. Mielke, and B. I. Wohlmuth, Eds., in Lecture Notes in Applied and Computational Mechanics, vol. 28. Springer Berlin Heidelberg, 2006, pp. 7–44. doi: 10.1007/978-3-540-34961-7_1.

[258] G. Annemüller and H.-J. Manger, Klärung und Stabilisierung des Bieres: Grundlagen - Technologie - Anlagentechnik - Qualitätsmanagement, 1. Auflage. in VLB-Fachbücher. Berlin: Verlag der VLB Berlin, 2011.

[259] R. Bürger, F. Concha, and K. H. Karlsen, “Phenomenological model of filtration processes: 1. Cake formation and expression,” Chemical Engineering Science, vol. 56, no. 15, pp. 4537–4553, Aug. 2001, doi: 10.1016/S0009-2509(01)00115-4.

[260] M. Hoffmann et al., “Developing Industrial CPS: A Multi-Disciplinary Challenge,” Sensors, vol. 21, no. 6, p. 1991, Mar. 2021, doi: 10.3390/s21061991.

[261] F. Civan, “Chapter 12 - Cake Filtration: Mechanism, Parameters and Modeling,” in Reservoir Formation Damage, Elsevier, 2016, pp. 295–341. doi: 10.1016/B978-0-12-801898-9.00012-6.

[262] Z. K. Nagy and R. D. Braatz, “Open-loop and closed-loop robust optimal control of batch processes using distributional and worst-case analysis,” Journal of Process Control, vol. 14, no. 4, pp. 411–422, Jun. 2004, doi: 10.1016/j.jprocont.2003.07.004.

[263] E. S. Tarleton, “A new approach to variable pressure cake filtration,” Minerals Engineering, vol. 11, no. 1, pp. 53–69, Jan. 1998, doi: 10.1016/S0892-6875(97)00138-6.

[264] T. Binder, A. Cruse, C. A. Cruz Villar, and W. Marquardt, “Dynamic optimization using a wavelet based adaptive control vector parameterization strategy,” Computers & Chemical Engineering, vol. 24, no. 2–7, pp. 1201–1207, Jul. 2000, doi: 10.1016/S0098-1354(00)00357-4.

[265] M. Schlegel, K. Stockmann, T. Binder, and W. Marquardt, “Dynamic optimization using adaptive control vector parameterization,” Computers & Chemical Engineering, vol. 29, no. 8, pp. 1731–1751, Jul. 2005, doi: 10.1016/j.compchemeng.2005.02.036.

[266] F. Assassa and W. Marquardt, “Dynamic optimization using adaptive direct multiple shooting,” Computers & Chemical Engineering, vol. 60, pp. 242–259, Jan. 2014, doi: 10.1016/j.compchemeng.2013.09.017.

[267] F. H. F. Leung, H. K. Lam, S. H. Ling, and P. K. S. Tam, “Tuning of the structure and parameters of a neural network using an improved genetic algorithm,” IEEE Trans. Neural Netw., vol. 14, no. 1, pp. 79–88, Jan. 2003, doi: 10.1109/TNN.2002.804317.

[268] J. D. Schaffer, D. Whitley, and L. J. Eshelman, “Combinations of genetic algorithms and neural networks: a survey of the state of the art,” in COGANN-92: International Workshop on Combinations of Genetic Algorithms and Neural Networks, Baltimore, MD, USA: IEEE Comput. Soc. Press, 1992, pp. 1–37. doi: 10.1109/COGANN.1992.273950.

[269] M. Eberhard, “Optimisation of Filtration by Application of Data Mining Methods,” Ph.D. thesis, Fakultät Wissenschaftszentrum Weihenstephan für Ernährung, Landnutzung und Umwelt, Technische Universität München, 2006.

[270] D. Campbell, M. Lees, P. Rogers, R. Glastonbury, and M. Pecar, “Process Optimisation of Beer Filtration using Fuzzy Control,” in Proceedings of the 6th IASTED International Conference, H. Leung, Ed., Anaheim, USA: ACTA Press, 2002, pp. 636–640.

[271] M. Fellner, J. Lehmann, H. Wening, and T. Becker, “Expertensysteme in der Brauerei,” Brauwelt, vol. 33, pp. 952–955, 2008.

[272] E. Negri, L. Fumagalli, and M. Macchi, “A Review of the Roles of Digital Twin in CPS-based Production Systems,” Procedia Manufacturing, vol. 11, pp. 939–948, 2017, doi: 10.1016/j.promfg.2017.07.198.

[273] P. Verboven, T. Defraeye, A. K. Datta, and B. Nicolai, “Digital twins of food process operations: the next step for food process models?,” Current Opinion in Food Science, vol. 35, pp. 79–87, Oct. 2020, doi: 10.1016/j.cofs.2020.03.002.

[274] S. L. Brunton, M. Budišić, E. Kaiser, and J. N. Kutz, "Modern Koopman Theory for Dynamical Systems," SIAM Rev., vol. 64, no. 2, pp. 229–340, May 2022, doi: 10.1137/21M1401243.

[275] A. Narasingam and J. S.-I. Kwon, "Application of Koopman operator for model-based control of fracture propagation and proppant transport in hydraulic fracturing operation," Journal of Process Control, vol. 91, pp. 25–36, Jul. 2020, doi: 10.1016/j.jprocont.2020.05.003.

[276] Z. Fan, P. Ji, J. Zhang, D. Segets, D.-R. Chen, and S.-C. Chen, "Wavelet neural network modeling for the retention efficiency of sub-15 nm nanoparticles in ultrafiltration under small particle to pore diameter ratio," Journal of Membrane Science, vol. 635, p. 119503, Oct. 2021, doi: 10.1016/j.memsci.2021.119503.

[277] A. Banerjee, S. Pasupuleti, K. Mondal, and M. M. Nezhad, "Application of data driven machine learning approach for modelling of non-linear filtration through granular porous media," International Journal of Heat and Mass Transfer, vol. 179, p. 121650, Nov. 2021, doi: 10.1016/j.ijheatmasstransfer.2021.121650.

[278] K. A. Griffiths and R. C. Andrews, "Application of Artificial Neural Networks for Filtration Optimization," J. Environ. Eng., vol. 137, no. 11, pp. 1040–1047, Nov. 2011, doi: 10.1061/(ASCE)EE.1943-7870.0000439.

[279] E. Salehi, M. Askari, M. H. Aliee, M. Goodarzi, and M. Mohammadi, "Data-based modeling and optimization of a hybrid column-adsorption/depth-filtration process using a combined intelligent approach," Journal of Cleaner Production, vol. 236, p. 117664, Nov. 2019, doi: 10.1016/j.jclepro.2019.117664.

[280] S. Cai, Z. Mao, Z. Wang, M. Yin, and G. E. Karniadakis, "Physics-informed neural networks (PINNs) for fluid mechanics: a review," Acta Mech. Sin., vol. 37, no. 12, pp. 1727–1738, Dec. 2021, doi: 10.1007/s10409-021-01148-1.

[281] B. Xiao et al., "A novel fractal solution for permeability and Kozeny-Carman constant of fibrous porous media made up of solid particles and porous fibers," Powder Technology, vol. 349, pp. 92–98, May 2019, doi: 10.1016/j.powtec.2019.03.028.

[282] D. Shou, J. Fan, and F. Ding, "Hydraulic permeability of fibrous porous media," International Journal of Heat and Mass Transfer, vol. 54, no. 17–18, pp. 4009–4018, Aug. 2011, doi: 10.1016/j.ijheatmasstransfer.2011.04.022.

[283] S. Zhu, R. H. Pelton, and K. Collver, "Mechanistic modelling of fluid permeation through compressible fiber beds," Chemical Engineering Science, vol. 50, no. 22, pp. 3557–3572, Nov. 1995, doi: 10.1016/0009-2509(95)00205-J.

[284] D. T. Paterson, T. S. Eaves, D. R. Hewitt, N. J. Balmforth, and D. M. Martinez, "Flow-driven compaction of a fibrous porous medium," Phys. Rev. Fluids, vol. 4, no. 7, p. 074306, Jul. 2019, doi: 10.1103/PhysRevFluids.4.074306.

[285] L. Grüne and J. Pannek, Nonlinear Model Predictive Control. in Communications and Control Engineering. Cham: Springer International Publishing, 2017. doi: 10.1007/978-3-319-46024-6.

[286] S. J. Qin and T. A. Badgwell, "A survey of industrial model predictive control technology," Control Engineering Practice, vol. 11, no. 7, pp. 733–764, Jul. 2003, doi: 10.1016/S0967-0661(02)00186-7.

[287] F. Allgöver, R. Findeisen, and Z. K. Nagy, "Nonlinear Model Predictive Control: From Theory to Application," Journal of the Chinese Institute of Chemical Engineers, vol. 35, no. 3, pp. 299–315, 2004, doi: 10.6967/JCICE.200405.0299.

[288] E. González, O. Díaz, L. Vera, L. E. Rodríguez-Gómez, and J. Rodríguez-Sevilla, "Feedback control system for filtration optimisation based on a simple fouling model dynamically applied to membrane bioreactors," Journal of Membrane Science, vol. 552, pp. 243–252, Apr. 2018, doi: 10.1016/j.memsci.2018.02.007.

[289] L. L. T. Chan, C.-P. Chou, and J. Chen, "Hybrid model based control for membrane filtration process," IFAC-PapersOnLine, vol. 49, no. 7, pp. 1085–1090, 2016, doi: 10.1016/j.ifacol.2016.07.347.

[290] A. Robles, M. V. Ruano, J. Ribes, A. Seco, and J. Ferrer, "Model-based automatic tuning of a filtration control system for submerged anaerobic membrane bioreactors (AnMBR)," Journal of Membrane Science, vol. 465, pp. 14–26, Sep. 2014, doi: 10.1016/j.memsci.2014.04.012.

[291] O. Bello, Y. Hamam, and K. Djouani, "Coagulation process control in water treatment plants using multiple model predictive control," Alexandria Engineering Journal, vol. 53, no. 4, pp. 939–948, Dec. 2014, doi: 10.1016/j.aej.2014.08.002.

[292] M. Shirato, T. Murase, M. Iwata, and N. .Hayash, "Deliquoring by Expression - Part 1 Constant Pressure Expression," Drying Technology, vol. 4, no. 3, pp. 363–386, Aug. 1986, doi: 10.1080/07373938608916335.

[293] E. Vorobiev, "Unified model for the prediction of consecutive solid–liquid filtration and expression at the constant pressure," AIChE Journal, vol. 68, no. 3, Mar. 2022, doi: 10.1002/aic.17547.

[294] R. J. Wakeman and A. Rushton, "A structural model for filter cake washing," Chemical Engineering Science, vol. 29, no. 9, pp. 1857–1865, Sep. 1974, doi: 10.1016/0009-2509(74)85002-5.

[295] S. Noerpel, V. Siauw, and H. Nirschl, "Filter Cake Washing of Mesoporous Particles," Chem. Eng. Technol., vol. 35, no. 4, pp. 661–667, Apr. 2012, doi: 10.1002/ceat.201100467.

[296] F. Destro et al., "Mathematical modeling and digital design of an intensified filtration-washing-drying unit for pharmaceutical continuous manufacturing," Chemical Engineering Science, vol. 244, p. 116803, Nov. 2021, doi: 10.1016/j.ces.2021.116803.

[297] Northeast Biomanufacturing Center & Collaborative, “Chapter 11: Downstream Processing,” in Introduction to Biomanufacturing, Montgomery County Community College, 2016.

[298] O. Coskun, “Separation Techniques: Chromatography,” North Clin Istanbul, vol. 3, no. 2, pp. 156–160, 2016, doi: 10.14744/nci.2016.32757.

[299] A. Mesbah, J. A. Paulson, R. Lakerveld, and R. D. Braatz, “Model Predictive Control of an Integrated Continuous Pharmaceutical Manufacturing Pilot Plant,” Org. Process Res. Dev., vol. 21, no. 6, pp. 844–854, Jun. 2017, doi: 10.1021/acs.oprd.7b00058.

[300] F. D. Bähner, P. A. Santacoloma, and J. K. Huusom, “Optimal operation of parallel dead-end filters in a continuous bio-based process,” Food and Bioproducts Processing, vol. 114, pp. 263–275, Mar. 2019, doi: 10.1016/j.fbp.2019.02.001.

[301] H. Li and J. Sansalone, “Multi-scale physical model simulation of particle filtration using computational fluid dynamics,” Journal of Environmental Management, vol. 271, p. 111021, Oct. 2020, doi: 10.1016/j.jenvman.2020.111021.

Full-Length Paper I

Parameter Estimation for Incompressible Cake Filtration: Advantages of a Modified Fitting Method

Kuhn, Michael; **Pergam, Philip**; Briesen, Heiko

Chemical Engineering & Technology, Volume 43, 2020, 493-501

DOI: 10.1002/ceat.201900511

Copyright

© 2020 The Authors. Published by WILEY-VCH Verlag GmbH & Co. KGaA, Weinheim

Reprinted by permission of John Wiley and Sons; License Number 5491871122572 issued on February 18, 2023 via Copyright Clearance Center:
https://www.copyright.com/

CRediT

- Michael Kuhn: Conceptualization, Methodology, Writing - Original Draft
- Philip Pergam: Methodology, Software, Writing - Review & Editing
- Heiko Briesen: Writing - Review & Editing, Supervision, Funding acquisition

Michael Kuhn
Philip Pergam
Heiko Briesen*

Parameter Estimation for Incompressible Cake Filtration: Advantages of a Modified Fitting Method

There is a widely used linear strategy to determine the parameters specific cake resistance and filter medium resistance in incompressible cake filtration. In this article, it is intended to demonstrate that this strategy has some disadvantages and should be replaced by an alternative nonlinear approach which yields more exact results. Even though the gains in precision are small for most cases, the nonlinear strategy is favored because it involves no extra effort and is grounded in the same physical theory as the original approach. This claim is based on a broad simulation study using noisy data with known parameter values to compare both fitting strategies and judge their accuracies.

This is an open access article under the terms of the Creative Commons Attribution-NonCommercial License, which permits use, distribution and reproduction in any medium, provided the original work is properly cited and is not used for commercial purposes.

Keywords: Cake filtration, Filter cake resistance, Filter medium resistance, Mathematical modeling, Parameter estimation

Received: September 19, 2019; *revised:* October 28, 2019; *accepted:* December 17, 2019

DOI: 10.1002/ceat.201900511

1 Introduction

In cake filtration, important parameters are filter cake resistance and filter medium resistance. Resistance of cake and medium cause pressure drop in the fluid phase and, therefore, influence the filtration setup, such as choice of filter apparatus and suitable pumps as well as integration of filtration into the larger process. As long as filter cakes can be considered incompressible, these two parameters are indeed decisive and are the only descriptors to be determined by parameter fitting as all others are known from the experimental conditions [1, 2]. Filter cakes can be considered incompressible depending on their material properties and the operation conditions. Material properties are, e.g., compressibility of the primary particles and friction between the particles [3].

Important operation conditions are flow rate or overall differential pressure, respectively, and maximal cake height. Compressibility effects become more pronounced when these variables increase. In case of compressible filter cakes, further parameters need to be determined that characterize the compression behavior [4, 5]. Even though many substances can exhibit compressible behavior during filtration, also the assumption of incompressibility is often valid, especially for incompressible primary particles and moderate operation conditions. For this reason, we focus only on incompressible cake filtration in this article and, therefore, on the parameters filter cake resistance and filter medium resistance.

Additionally, it must be assured that the substance system considered exhibits pure cake filtration behavior, i.e., that all newly separated particles are captured on the cake surface only. If, on the contrary, also depth filtration occurs, i.e., small particles are separated within the already existing filter cake, the phenomenological behavior changes and other analysis tools have to be used [6, 7]. Depth filtration effects can be expected especially when very broad and possibly multimodal particle size distributions of the dispersed phase are encountered because in that case small particles can pass through the pores created by the larger particles and internally block the previously built-up cake. However, just as compression, this effect is neglected and only ideal cake filtration is considered here.

There is a relatively simple and widely used procedure to determine the parameters filter cake resistance and filter medium resistance, which is reported classically in the guideline VDI 2762, Part 2 [1]. The approach is also described in overview articles and established textbooks [1, 8], used as a reference for validating alternative strategies [9], and is still employed in very recent publications [10–12]. It is also standard in industrial research. For this reason, the classical procedure must be seen as state-of-the-art.

Before more details are given on the general approach, a comment on the two characteristic parameters is in order. In most cases, the sought-for filter cake resistance is used as specific resistance. In some cases, it refers to filter cake mass, i.e., resistance per filter cake mass; sometimes it is expressed in relation to filter cake height, i.e., resistance per cake height. In the latter case, specific cake resistance is the inverse of the filter cake permeability. In the remaining article, we will rely on height-specific cake resistances; this does, however, not restrict the generality of the found results because both height- and

Dr. Michael Kuhn, Philip Pergam, Prof. Heiko Briesen
heiko.briesen@tum.de
Technical University of Munich, Chair of Process Systems Engineering, Gregor-Mendel-Strasse 4, 85354 Freising, Germany.

 © 2020 The Authors. Published by WILEY-VCH Verlag GmbH & Co. KGaA.

mass-specific resistances can easily be converted into each other, as will be shown later on.

Additionally, it is important to note that the so-called medium resistance does not characterize the used filter medium or septum alone, but is characteristic for the used medium together with the first layers of separated substances. Additional resistance effects resulting from these first layers are, therefore, also called "interference resistance", referring to the interference between medium and the separated dispersed phase [13]. The interaction of the filter medium with the particles to be separated is, e.g., discussed by Hund et al. [14]. In case of precoat filtration, the interaction was investigated by Rainer et al. [15, 16]. Due to the fact that in classical experiments specific cake resistance is the decisive parameter because it is usually much larger than the medium resistance, including the interference effect [1], we will focus in the remaining article mainly on this variable.

Considering the experimental strategy to determine the sought-for parameters, a suspension is created with known mass concentration of the substance to be separated. This suspension is filtered in a laboratory filter cell, either in the mode of constant flow or constant pressure, where the latter is the dominant mode of operation because no process control system is needed to assure a constant flow rate while the overall flow resistance increases due to cake growth. For this reason, also constant pressure filtration is focused upon in this article. During the whole separation process, the accumulated liquid mass at the filter outlet is measured by an automatic scale. Using either the filter cake height at the end of filtration or the mass of separated matter together with the collected liquid volume, converted from the mass using the density, as a function of time, the parameters cake resistance and medium resistance can be calculated [1, 2].

In the next section, the mathematics behind this calculation procedure is described. So far, it is only noted that the already mentioned standard method is based on a linear representation of the measured data and a corresponding linear model formulation that is fitted to these data points [1, 2, 17]. In our opinion, such strategies were very helpful to evaluate experimental data manually on paper sheets; however, current computer tools make them obsolete. The aim of this article is to show that the said linear representation leads to a decreased accuracy in the parameter fitting procedure. Therefore, an alternative procedure is proposed. It is based on the same basic model equations, i.e., the same physical theory, only the data are not represented linearly and instead a root function is fitted to the raw data. It is shown that this latter fitting procedure, even though it does not cause any extra effort and is, as mentioned, based on the same established theory, leads to more accurate results.

It is worth mentioning that an analogous development took place in a completely different field of research, namely enzyme kinetics based on the Michaelis-Menten equation [18–20]. In this area, also first linear representations were used to determine the characteristic parameters. Afterwards, nonlinear fitting of algebraic equations was applied and still later the development shifted to the direct use of differential equations [21]. Whereas working with differential equations directly is not required in case of incompressible cake filtration as all equations can be solved analytically, the analogy between enzyme kinetics and filtration holds for the decision between linear and nonlinear fits. As will be seen in Sect. 3, the quality of fits crucially depends on the distribution of errors. Accordingly, it was found in enzyme kinetics research that linear plots result in "error bars which are asymmetrical" [18] and "suffer from a highly biased weighting of points and should never be used." [19].

2 Model Equations

Modeling of incompressible cake filtration is briefly recapitulated now. For deriving the general model equation, from which specific cake and medium resistance are derived, one starts by decomposing the overall pressure drop across the filter Δp[1)] into the pressure drop across the cake Δp_c and across the medium Δp_M, i.e.:

$$\Delta p = \Delta p_C + \Delta p_M \tag{1}$$

For the cake, Darcy's law is used in the following form:

$$\Delta p_C = \frac{Q\,\mu H}{A\,k} = \frac{Q\,\mu H\,r}{A} \tag{2}$$

where Q is the volumetric flow rate, i.e., dV/dt, μ is the dynamic viscosity, A is the filter's cross-sectional area, k denotes the permeability, and r the height-specific resistance. Cake height H can be substituted and expressed by:

$$H = \frac{V\,K}{A} \tag{3}$$

with the factor K, often referred to as concentration constant [1], being defined as:

$$K = \frac{c}{(1-\varepsilon)} = \frac{H\,A}{V} \tag{4}$$

and c being the volumetric concentration of impurities in the suspension; ε is the cake's porosity. Also, for the filter medium Darcy's law is applied. However, as the medium height does not play a role here, specific resistance and height are combined into the total resistance of the medium R_M, yielding:

$$\Delta p_M = \frac{Q\,\mu R_M}{A} \tag{5}$$

Putting these components together and writing dV/dt for Q yields:

$$\Delta p = \frac{r\,\mu\,K}{A^2}\,V\,\frac{dV}{dt} + \frac{R_M\,\mu}{A}\,\frac{dV}{dt} \tag{6}$$

Solving this differential equation by separation of variables and using the initial condition $V(t{=}0) = 0$ leads to:

$$t = \frac{r\,\mu K}{2\,\Delta p\,A^2}\,V^2 + \frac{R_M\,\mu}{\Delta p\,A}\,V = P_2\,V^2 + P_1\,V \tag{7}$$

1) List of symbols at the end of the paper.

 © 2020 The Authors. Published by WILEY-VCH Verlag GmbH & Co. KGaA.

which can be rearranged to

$$\frac{t}{V} = \frac{r\,\mu K}{2\,\Delta p\,A^2}\,V + \frac{R_M\,\mu}{\Delta p\,A} = P_2\,V + P_1 \tag{8}$$

as traditionally used for determining the parameters r and R_M. As can be easily seen, in both equations, the parameters P_1 and P_2 have the same meaning, namely $P_1 = R_M\,\mu(\Delta p\,A)^{-1}$ and $P_2 = r\,\mu K\,(2\,\Delta p\,A^2)^{-1}$. As μ, Δp, and A are known from the experimental conditions as well as the used setup, and the final cake height H, contained in K, can be determined after the experiment, R_M can be directly computed from P_1 and r from P_2. However, the quadratic Eq. (7) can also be resolved for V, yielding the root function:

$$V = \frac{-P_1 + \sqrt{P_1^2 + 4\,P_2 t}}{2\,P_2} \tag{9}$$

The claim of the present article is that it makes a difference whether Eq. (8) or (9) is used for fitting it to the experimental data and determining R_M and r. Before moving on to the parameter fitting strategy, a remark is made on the specific resistance r. As mentioned, here r is considered as height-specific; therefore, also the final cake height H is included in the factor K. However, substituting $K_m = m/V$ for K in Eq. (4), where m is the filter cake mass at the end of filtration, the equation stays the same, only r takes the meaning of r_m, i.e., the mass-specific resistance [1, 2]. This was meant when we mentioned earlier that the height- and mass-specific form are equivalent and that we do not limit the generality of our approach due to the primary focus on height-specific filter cake resistances.

3 Parameter Estimation

In this section, the fitting strategy is described and some theoretical background on parameter estimation is provided. Regarding notation, the independent variable is denoted by x, the dependent variable by y. Measured data are marked using a hat sign, i.e., $\hat{x}$ and $\hat{y}$, and data from the model f depend on the parameter vector $\boldsymbol{P}$. In case of the usual least-squares strategy for N experimentally determined points, the cost function is formulated as:

$$J = \sum_{i=1}^{N} \left[\hat{y}_i - f(\hat{x}_i, P)\right]^2 \tag{10}$$

and the corresponding optimization problem is:

$$\min_{P} J\left(\hat{x}_i, \hat{y}_i, P\right) \tag{11}$$

Now, different strategies for parameter estimation are formulated; the first is based on the linear model of Eq. (8), the second on the nonlinear form of Eq. (9). In the remaining article, the two cases are referred to as Strategy 1 and 2, respectively. Strategy 1 is the classical approach known from the literature [1, 2]. Strategy 2 is the alternative method proposed in this paper. For Strategy 1, the cost function becomes:

$$J_1 = \sum_{i=1}^{N} \left[\left(\frac{\hat{t}_i}{\hat{V}_i}\right) - \left(P_2\hat{V}_i + P_1\right)\right]^2 \tag{12}$$

i.e., a linear parameter fitting problem is encountered. Correspondingly, Strategy 2 yields the following nonlinear cost function

$$J_2 = \sum_{i=1}^{N} \left[\hat{V}_i - \left(\frac{-P_1 + \sqrt{P_1^2 + 4\,P_2\,\hat{t}_i}}{2\,P_2}\right)\right]^2 \tag{13}$$

To assess the adequacy of the two fitting strategies proposed so far, some theoretical background is required. As mentioned, both Strategy 1 and 2 rely on a least-squares approach. Due to the fact that both fitting equations, Eqs. (8) and (9), can be analytically recast into each other, fitting results are expected to be identical for perfect experimental data, which is, however, not realistic in an actual experimental setting. So, the main question is how both approaches deal with real data that are inevitably noisy.

Least-squares methods can be shown to be reliable for linear as well as nonlinear cost functions as long as all errors are normally or at least approximately normally distributed [22]. At this point, the crucial question is how the errors occurring in filtration experiments behave. t/V, i.e., the decisive quantity in case of Strategy 1, is intuitively not expected to scatter in a normally distributed way. However, if this were the case, Strategy 1 would be reliable to determine the parameters. On the contrary, Strategy 2 is reliable as long as the errors of V are normally distributed. The actual distribution of errors for both strategies is discussed in the next sections when we turn to our simulation study.

Please note that an increasing error magnitude with larger values of the independent variable, i.e., liquid volume in case of Strategy 1 and time for Strategy 2, is not a problem with respect to the quality of the found parameter values. As the mentioned heteroscedasticity, i.e., the increasing spread or dispersion of the observed variables, does not affect the accuracy but only the efficiency with which the parameters are determined, it is not further accounted for in this work. Should computational efficiency be an issue, different strategies to handle heteroscedasticity are known in the literature, e.g., by scaling of variables [22, 23]. To substantiate our claim further, i.e., that the applied fitting strategy makes a difference, a numerical study is presented in the following article.

4 Computational Methods and Simulation Strategy

Strategy 1 and 2 are tested for determining the decisive parameters P_1 and P_2, respectively, R_M and r. In this respect, as mentioned, the focus is laid on the more important parameter of specific filter cake resistance r. To truly test a fitting strategy, the actual parameter values must be known. For that reason, forward simulations are conducted in which Eq. (9) is solved with known values of P_1 and P_2 for 100 s with one data point per second. These ideal solutions are perturbed with different levels of noise, and the obtained noisy data are in turn used as

 © 2020 The Authors. Published by WILEY-VCH Verlag GmbH & Co. KGaA.

fictitious experiments to determine the parameter values. In each case, it is checked how well the true parameter values are found again as is a common strategy when testing parameter fitting procedures [24].

Forward simulations as well as parameter fitting are conducted in MATLAB (version 2018a; Mathworks, Natick, MA). Noise is generated using the function *randn* which yields normally distributed random numbers; the optimization problem is solved with *fminsearch* in which the maximal number of iterations and of function evaluations are both set to 1 000 000 while the other options remained at their default settings.

Next, the exact generation of noisy data is explained in more detail. In all cases, noise is assumed to be normally distributed with previously defined standard deviations. Flow rate $dV/dt = Q$ and specific filter cake resistance r are supplied with noise. In both cases, the level of noise, i.e., its standard deviation, is given in % of the nominal variable value. Please note that this also implies that the standard deviation changes over time for the flow rate as dV/dt decreases with time in the mode of constant pressure filtration. Noise is added to dV/dt because the flow rate was observed to show some scattering in published studies [9] as well as in our own experiments [11].

It is important to mention that normally distributed noise on dV/dt causes also scattered values of the cumulated volume V as schematically shown in some publications [1, 2]. As the noise on dV/dt simply adds up, scattering on V is also normally distributed because any linear combination of independent randomly distributed variables is also randomly distributed [9]. Due to this summing up, the error bands on V can become larger over time which is also in agreement with published experimental findings [11]. For the reasons discussed, we believe that our noise model simulates the true flow behavior in constant-pressure filtration quite well, a point we will also elaborate more in the discussion of the results.

However, there is also another possible source of experimental errors. It can be imagined that r itself is prone to uncertainties, e.g., due to biases when taking samples of the powder or particle system used for the experiments. To account for this effect, also normally distributed noise is added to specific cake resistance r. Noise on dV/dt and r, therefore, accounts for two different effects: the first covers non-idealities when conducting the experiment, the second includes uncertainties when preparing the experiment.

Our two noise modes are illustrated in Fig. 1 where it is shown how a noisy flow rate (a) influences cumulated volume V (b); the effect of variations in specific filter cake resistance on the resulting trajectory of V is also displayed (c). The figure reveals that a noisy flow rate results in jagged curves whereas variations in r still give smooth, but diverging curves. This behavior is due to the fact that noise on r mimics variations when preparing the experiment as explained, and, therefore, only affects the model parameter r in a time-invariant way. A noisy flow rate, on the other hand, is intended to model transient effects. As in reality both phenomena often occur together, their combined effects will be studied later on.

The filter medium resistance R_M has not been subjected to noise because, as justified above, it is not studied in detail here. Please note that data on experimentally occurring noise are scarce in the literature; raw data and error bands are often not shown or only single experimental runs are discussed. Therefore, we also had to rely on our own lab experiences to choose realistic noise intensities. However, it is claimed that all noise levels analyzed in the remaining article are within the range commonly encountered when conducting filtration experiments.

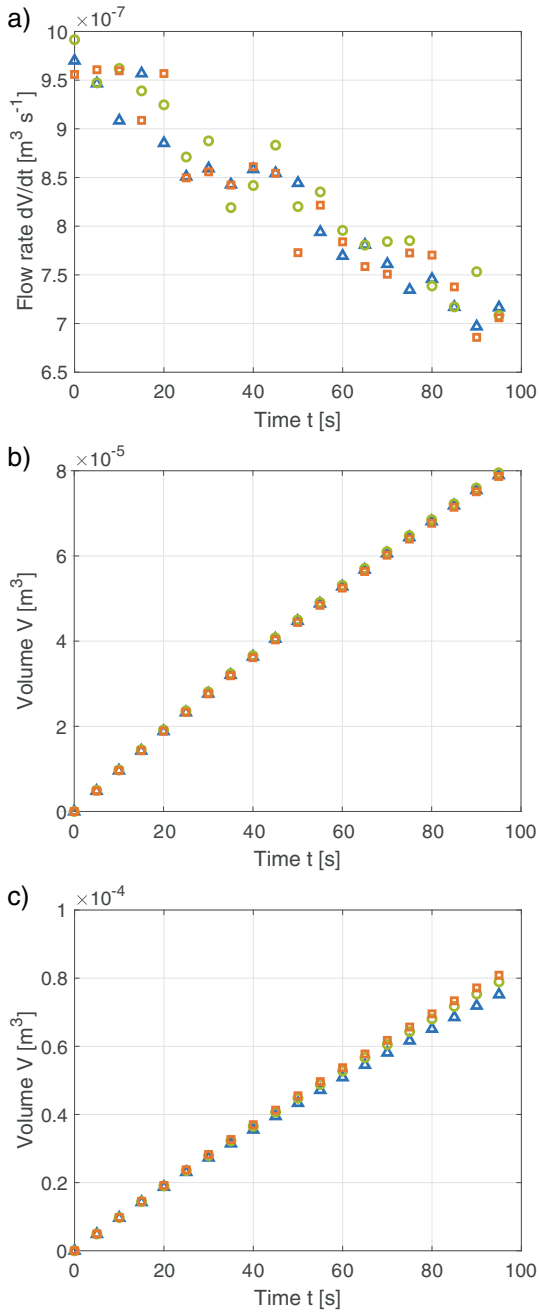

Figure 1. Illustration of the noise generation procedure. A noisy flow rate (a) leads to noise on the cumulative volume (b); variations in specific filter cake resistance also affect the cumulative volume (c); three randomly generated data sets are shown (marked by different symbols) as used in each inner iteration of the Monte-Carlo method; the noise level on the flow rate is 2.5 % and 20 % on specific filter cake resistance.

 © 2020 The Authors. Published by WILEY-VCH Verlag GmbH & Co. KGaA.

To evaluate the model fits, a two-stage strategy is employed which is divided into an inner and an outer iteration. In the inner iteration, three-fold experiments are mimicked by generating three different sets of noisy data, i.e., noise is generated with three different random number seeds, as displayed in Fig. 1. These three-fold datasets are used together for one model fit. In an outer iteration, 1000 repetitions of such triple experiments are performed, again each run with different random number seeds. By the outer iteration, statistical information is obtained on the determined parameters, i.e., mainly error bars on *r*. Therefore, conclusions can be drawn about which fitting strategy performs better "in the long run". As computational methods where repeated use is made of random numbers are often referred to as Monte-Carlo methods, also the described procedure can be classified as a Monte-Carlo approach.

5 Results

Using the simulation strategy described in the last section, various data sets were generated to test and compare parameter fitting Strategy 1 and 2. For didactic reasons, first some single selected cases are shown and subsequently turned to overview representations. The first are more tangible but contain less information, the second are denser information-wise but, therefore, also more difficult to interpret.

As expected, no detectable differences between Strategy 1 und 2 are found in case of non-noisy data, i.e., the true parameter values can be reliably identified with both approaches. Thus, this case is not further discussed. Before both strategies are compared in detail, a problem is considered that can occur with Strategy 1, i.e., the linear fit. Linear representation of the data can cause highly nonlinear segments at the beginning of the experiments. Therefore, no meaningful fits can be conducted without cropping the data for small times. A comparison of a full, non-cropped data set and an adapted data set is shown in Fig. 2 together with the corresponding linear fit; a 10 % noise level on flow rate is used.

In case of the non-cropped data, the fitting error of specific cake resistance r is 9.66 %; after cropping the data, it can be reduced to 5.65 %. Error, here and in the remaining article, is defined as the difference between the parameter value determined by fitting r_f and the true value r_t relative to r_t, i.e.:

$$\text{Error} = \frac{r_f - r_t}{r_t} \times 100\% \tag{14}$$

For the results of Fig. 2, the first 15 data points, i.e., 15 s, were cropped. It is important to note that this behavior is no artefact of the simulation strategy or noise generation method, as the same behavior was also observed with our own experimental data. The necessity to crop data sets is also mentioned in the literature [1]. As cropping of data is not required in case of Strategy 2, here already is the first advantage of the proposed method because it avoids the decision of how many data points to drop, which is always to some degree arbitrary. In the remaining, article only cropped data are used in case of Strategy 1 to allow a meaningful comparison of the two approaches; the same cut-off of 15 s is used throughout this work as this proved a good threshold.

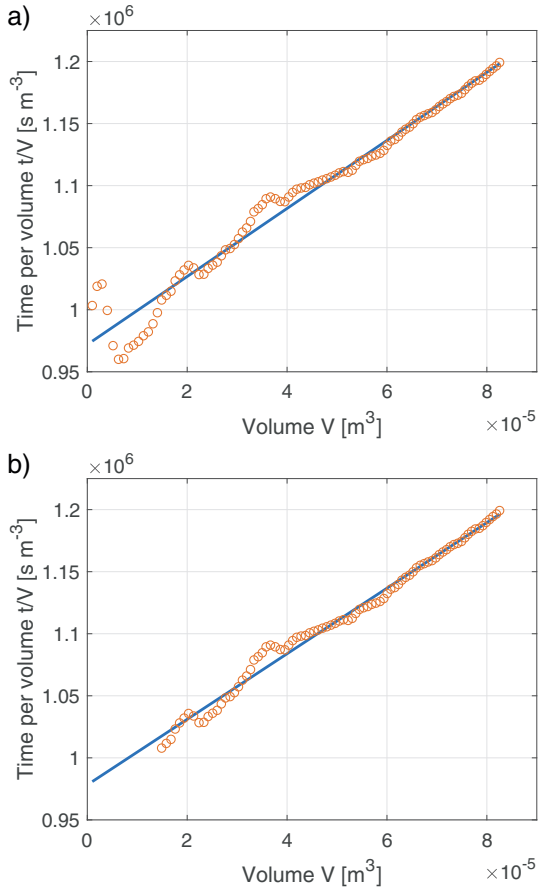

Figure 2. Exemplary comparison of Strategy 1 for the non-cropped data set (a) and cropped data (b); raw data are displayed as circles; continuous lines are the linear fits.

For uncropped data, Strategy 1 would yield a significantly worse performance than the results shown in the following. Also, whereas in Fig. 2 only a single experimental run is shown to illustrate the problem, all subsequent results will be given for a triple determination, which was described in Sect. 4 as the internal iteration of our Monto-Carlo method. Please note that in the following figures the raw data (displayed by circles in Fig. 2) are omitted and only the fitted lines are presented together with the confidence intervals of the raw data (given for every fifth data point) in order to keep the plots clear and understandable.

Fig. 3 presents curve fits with both strategies for a case with a low level of noise, i.e., a standard deviation of 1 % on the nominal value of the flow rate. Already in this case it can be observed that the fitting with Strategy 2 leads to more exact results: The fitting error of the specific filter cake resistance is 1.944 % as determined by Strategy 1, compared to a value of 1.75 % when using Strategy 2. Insignificant as this difference may be for all practical purposes, it proves already that the two methods deviate. Also, the shown fictitious experiments are quite close to ideal data that are hardly found in real experiments.

Turning from this singular example with only the threefold inner iteration to the full data set obtained by the additional

 © 2020 The Authors. Published by WILEY-VCH Verlag GmbH & Co. KGaA.

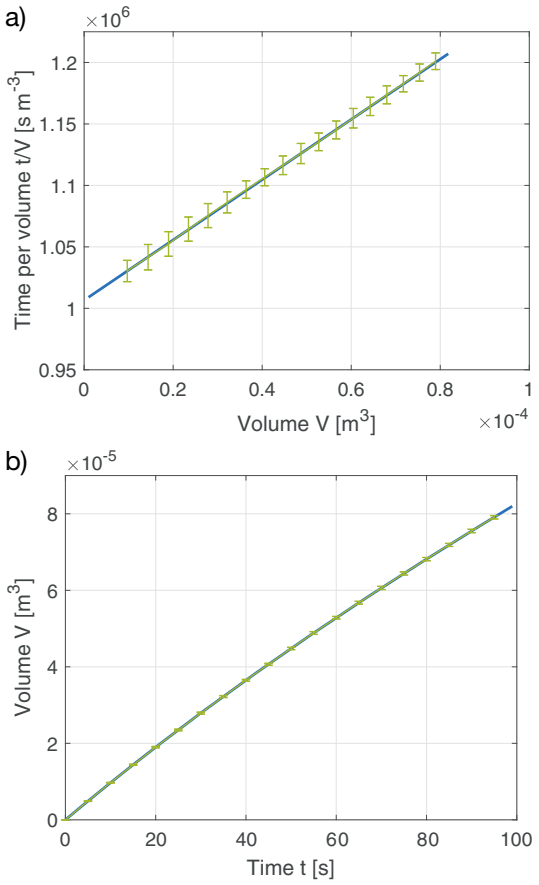

Figure 3. Fits of data with low noise level on the flow rate and a true specific filter cake resistance of $10^{12}\,m^{-2}$ using the classical Strategy 1 (a) and the new, nonlinear Strategy 2 (b); confidence intervals of the raw data are displayed for every fifth value (green).

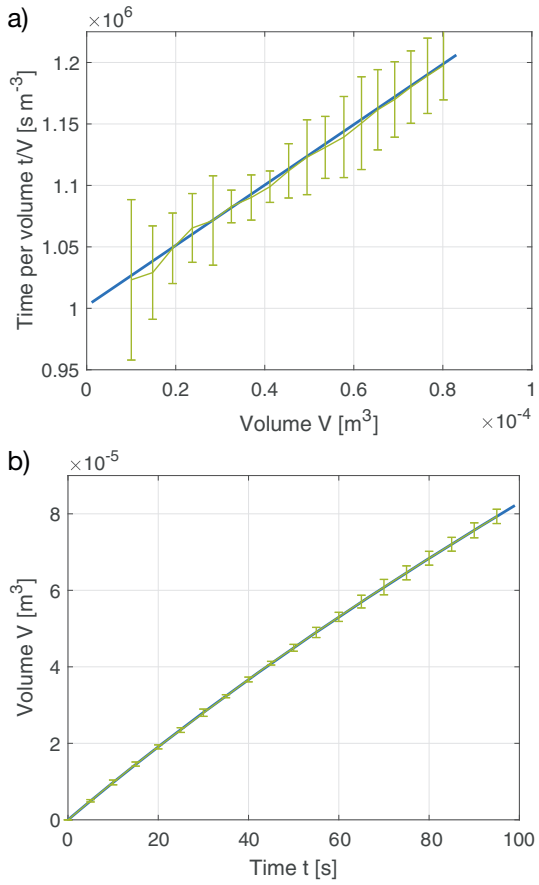

Figure 4. Fits of data with high noise level on the flow rate and a true specific filter cake resistance of $10^{12}\,m^{-2}$ using the classical Strategy 1 (a) and the new, nonlinear Strategy 2 (b); confidence intervals of the raw data are displayed for every fifth value (green).

1000 outer iterations, Strategy 1 yields an average error of −0.0128 % (± 0.060 %) compared to the value of −0.001 % (± 0.053 %) in case of Strategy 2. Here and in the following, the percentage values within brackets are the confidence intervals of the fitting errors based on a confidence level of 99 %. The same confidence level is also used in all plots where confidence intervals are shown. As the reported confidence intervals refer to the errors, smaller values are not per se an advantage. If, e.g., the average error is large but the obtained confidence interval for that error is small, this only means that the wrong parameter value is identified with a low variation.

All results shown so far also underline the trivial truth that repetition of experiments is important for a reliable determination of parameters. Single experimental runs, as, e.g., displayed in Fig. 2, can exhibit large variations and, therefore, lead to inexact parameter values. Three-fold repetitions, as used in Fig. 3 and all remaining fits of this article, already lead to an increased accuracy. If many such three-fold experimental runs are considered, as modeled by our outer iteration (see Sect. 4), the accuracy can still be improved remarkably.

Next, data with a higher level of noise but the same true specific filter cake resistance are considered. In Fig. 4, an analogous comparison is shown for a flow rate-specific noise of 10 %. Here, the fitting errors become 1.69 % and −0.31 % for Strategy 1 und 2, respectively. When turning to the full data set including the 1000 outer iterations, Strategy 1 yields an average error of −1.024 % (± 0.6 %) compared to the value of 0.0499 % (± 0.525 %) from Strategy 2. Thus, it can be observed that the new Strategy 2 becomes more effective, the higher the noise level on the experimental data is. It also becomes apparent what was already conjectured in Sect. 3, namely that the distribution of errors matters for the fitting procedure. Whereas Strategy 2 relies on data with normally distributed errors, a distorted scaling of errors is encountered in Strategy 1 which is the reason for the worse quality of the determined parameters.

As a third example, noise is added to the specific filter cake resistance r along with a flow rate-specific noise of 5 %; the standard deviation of r is 1 % of its nominal value. For this case, scattered data and fitting results are presented in Fig. 5. Based on this noisy r, the errors are −4.35 % and −2.95 % for Strategy 1 und 2, respectively. Including again the outer iterations, average errors of −0.271 % (± 0.29 %) and 0.076 % (± 0.26 %) are obtained from Strategy 1 and 2, respectively. First of all, this example demonstrates how important the outer

 © 2020 The Authors. Published by WILEY-VCH Verlag GmbH & Co. KGaA.

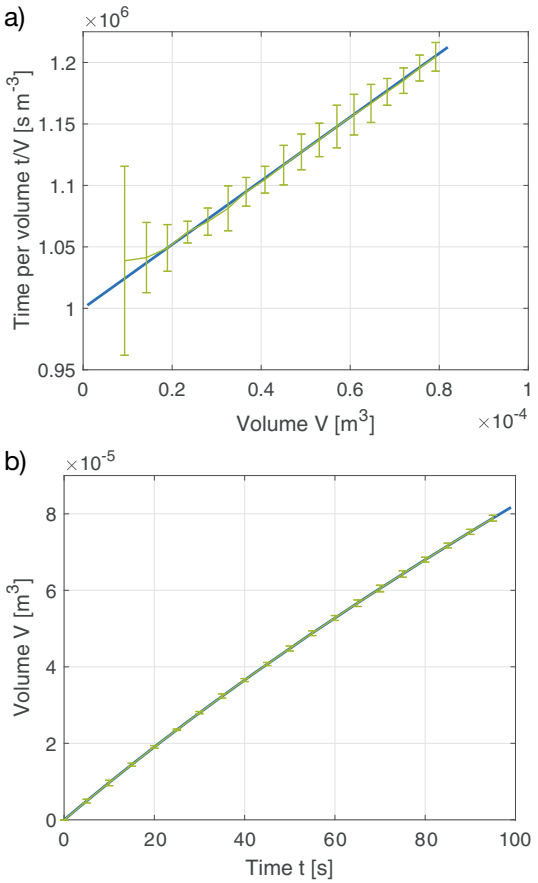

Figure 5. Fits of data with noise both on flow rate and specific filter cake resistance; the mean true specific filter cake resistance is 10^{12} m^{-2}; comparison of Strategy 1 (a) and the new, nonlinear Strategy 2 (b); confidence intervals of the raw data are displayed for every fifth value (green).

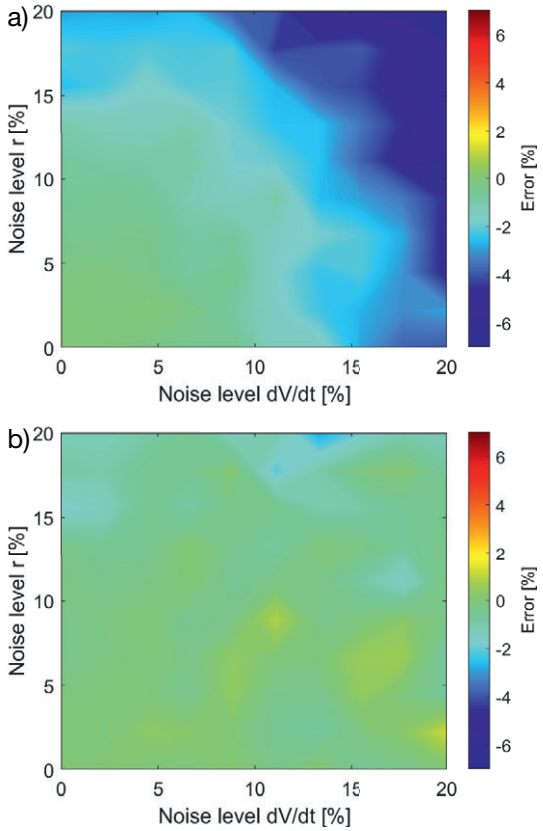

Figure 6. Heat maps showing the average fitting errors obtained by Strategy 1 (a) and the new, nonlinear Strategy 2 (b) for different levels of noise added to the flow rate dV/dt and specific filter cake resistance r; the mean true specific resistance is 10^{12} m^{-2}. Dark blue and dark red on the color scale denote the found parameter values that are too low or too high, respectively.

iteration is. Whereas the single example shown in Fig. 5 led to relatively high fitting errors for both approaches, on the average Strategy 1 and 2 perform better than in this example. This shows again that repetition of experiments cannot be overestimated. However, also here Strategy 2 is superior to Strategy 1.

Now the more complex display of results is considered. The heat maps displayed in Fig. 6 comprise the results of many singular fits as they were discussed so far; all are shown again for 1000 outer iterations. Various different levels of noise on the flow rate dV/dt and on specific filter cake resistance r as well as combinations of both are displayed. The color scale denotes the resulting fitting errors; areas of green color indicate that the correct parameter values were identified, blue and red colors symbolize found parameter values that are too low or too high, respectively.

In general, Fig. 6 confirms what the single examples discussed so far already indicated: Strategy 2 consistently performs better than Strategy 1, i.e., it allows to determine the specific filter cake resistance with a higher accuracy. Additionally, it can be seen that, on the average, fitting error increases both with ascending noise levels on dV/dt and r. For small levels of noise, e.g., less than 10 % and certainly less than 5 %, both strategies seem to yield acceptable results. However, it must be taken into account, that Fig. 6 only shows the long-term behavior. Both types of noise can still result in considerable fitting errors when only few experimental runs are considered, as usually done in experimental practice and as indicated in Fig. 5. An additional disadvantage of Strategy 1 is that it has a clear tendency to underestimate the true specific filter cake resistance (mostly the blue color range is present in Fig. 6a); compare Eq. (14) for our definition of fitting error. This underestimation might be a problem for process design because, as a consequence, equipment such as pumps might be chosen undersized.

Before providing some overall conclusions, a few additional clarifications are required. It is important to note that the qualitative behavior displayed in Fig. 6 is the same also for different nominal values of specific filter cake resistance r. Even though the nominal value $r = 10^{12}$ m^{-2} was used throughout the article, the findings are unaffected if the decimal power is varied in the realistic range from 10^{11} to 10^{16}. Furthermore, the overall time span and discretization of time points could affect the fitting results, i.e., the whole experimental time considered and the intervals at which data points are saved. However, it was found that, excluding unrealistically short experimental times, this

 © 2020 The Authors. Published by WILEY-VCH Verlag GmbH & Co. KGaA.

effect is negligible. Also, it might be objected that only the new Strategy 2 was compared with the traditional t/V-V plot (Strategy 1) whereas also some sources suggest to use a $\mathrm{d}V/\mathrm{d}t$-V plot [1]. In answer to this, it must be said that t/V is much more common in the literature, and, even more importantly, the uneven scaling of errors does equally occur in the $\mathrm{d}V/\mathrm{d}t$-V approach as in Strategy 1. Also, some conducted simulation studies confirmed the hypothesis and demonstrated that the latter strategy performs even worse than Strategy 1. A last remark about the parameter fitting itself: Both investigated fitting strategies result in well-posed optimization problems with pronounced minima regarding the sought-for parameter r; the obtained solutions are insensitive to the provided initial values. Fitting errors in case of Strategy 1, therefore, result from a systematic bias rather than from multiple minima.

6 Conclusions

The present article had a very simple aim, namely, to show that a nonlinear fit, based on a root function, is superior to the classical linear strategy when it comes to determining the parameters for incompressible cake filtration, mainly specific filter cake resistance. There are different advantages of the nonlinear approach. First of all, a cropping of data, as is often necessary for small times when using the linear strategy, is not required. This eliminates a subjective factor in the fitting process and prevents that useful data points are discarded. However, the main advantage is that the nonlinear strategy consistently leads to more exact results.

In order to warrant this claim, a broad Monte-Carlo simulation study with two different noise models was presented. Firstly, noise was added to the flow rate which mimics variations in conducting the filtration experiments; secondly, the nominal values of specific filter cake resistance were supplied with noise in order to model variations when preparing the experiment. For both modes of noise, it was checked how well the two different fitting approaches were able to identify the true parameter values. In this respect, it must be stressed that such an evaluation is only possible by a simulation study because only then the true parameter values are known and, therefore, the fitting quality can be assessed adequately.

In conclusion, all filtration experimentalists who deal with incompressible substances, or substances that can be considered approximately as such under the given process conditions, are advised to evaluate their data by the nonlinear method proposed in this article. Even though the gain in precision is in the order of some percent, there is no reason to refrain from using the nonlinear fit. It is more exact and involves no extra effort because practically all available software tools nowadays allow fitting nonlinear functions with a comparable computational efficiency as linear models. Also, the nonlinear fitting strategy removes arbitrariness in data point selection. Finally, it requires no shift to a new theoretical framework as this new approach is based on the familiar and well-tested theory of incompressible cake filtration.

Acknowledgment

This research was supported by the German Federal Ministry for Economic Affairs and Energy (via AiF and DECHEMA), IGF-Project No. 19947 BG. We thank Peter Bandelt of our group (Chair of Process Systems Engineering, Technical University of Munich) for beneficial discussions on the experimental side of determining parameters in cake filtration and Verena Hargarten, also a member of the group, for valuable input on parameter estimation in enzyme kinetics.

The authors have declared no conflict of interest.

Symbols used

A	[m^2]	cross-sectional area of filter
c	[–]	volumetric concentration or volume fraction of impurities
H	[m]	filter cake height
J	[variable]	value of cost function
k	[m^2]	permeability
K	[–]	concentration constant, reference to filter cake height
K_m	[kg m^{-3}]	concentration constant, reference to solid mass
m	[kg]	filter cake mass
N	[–]	maximal index of measured points
Δp	[kg m^{-1}s^{-2}]	differential pressure
P	[variable]	fit parameters
Q	[m^{3}s^{-1}]	volumetric flow rate
r	[m^{-2}]	specific or relative resistance
R_M	[m^{-1}]	resistance of filter medium
t	[s]	time
V	[m^3]	liquid volume
x	[–]	independent variable
y	[–]	dependent variable

Greek letters

ε	[–]	porosity or void fraction
μ	[kg m^{-1}s^{-1}]	dynamic viscosity

Sub- and superscripts

C	cake
f	parameter value determined by fitting
i	index
m	mass
M	medium
t	true parameter value

References

[1] VDI 2762 – Part 2, *Mechanical solid-liquid separation by cake filtration – Determination of filter cake resistance*, VDI guideline, Verein Deutscher Ingenieure, Düsseldorf **2010**.

 © 2020 The Authors. Published by WILEY-VCH Verlag GmbH & Co. KGaA.

[2] S. Ripperger, W. Gösele, C. Alt, *Filtration, 1. Fundamentals*, in Ullmann's Encyclopedia of Industrial Chemistry, Wiley-VCH, Weinheim **2012**. DOI: https://doi.org/10.1002/14356007.b02_10.pub2

[3] C. M. Alles, H. Anlauf, *Chem. Ing. Tech.* **2003**, *75 (9)*, 1221–1230. DOI: https://doi.org/10.1002/cite.200303268

[4] F. M. Tiller, H. Cooper, *AIChE J.* **1962**, *4 (4)*, 445–449. DOI: https://doi.org/10.1002/aic.690080405

[5] K. Stamatakis, C. Tien, *Chem. Eng. Sci.* **1991**, *46 (8)*, 1917–1933. DOI: https://doi.org/10.1016/0009-2509(91)80153-P

[6] C. Tien, R. Bai, B. V. Ramarao, *AIChE J.* **1997**, *43 (1)*, 33–44. DOI: https://doi.org/10.1002/aic.690430106

[7] M. Kuhn, H. Briesen, *Chem. Eng. Technol.* **2006**, *39 (3)*, 425–434. DOI: https://doi.org/10.1002/ceat.201500347

[8] C. Tien, *Introduction to Cake Filtration*, 1st ed., Elsevier, Amsterdam **2006**.

[9] S.-K. Teoh, R. B. H. Tan, C. Tien, *Chem. Ing. Tech.* **2006**, *61 (15)*, 4957–4965. DOI: https://doi.org/10.1016/j.ces.2006.03.048

[10] S. Kühne, U. A. Peuker, *Chem. Eng. Technol.* **2018**, *41 (1)*, 96–101. DOI: https://doi.org/10.1002/ceat.201700164

[11] P. M. Bandelt Riess, J. Engstle, M. Kuhn, H. Briesen, P. Först, *Chem. Eng. Technol.* **2018**, *41 (10)*, 1956–1964. DOI: https://doi.org/10.1002/ceat.201800254

[12] M. Azimian, A. Wiegmann, in *Proc. of FILTECH 2018*, Filtech Exhibitions Germany, Meerbusch, **2018**.

[13] J. W. Tichy, *Zum Einfluss des Filtermittels und der auftretenden Interferenzen zwischen Filterkuchen und Filtermittel bei der Kuchenfiltration*, Ph.D. Thesis, Technische Universität Kaiserslautern **2007**.

[14] D. Hund, S. Antonyuk, S. Ripperger, *EPJ Web Conf.* **2017**, *140*, 09033. DOI: https://doi.org/10.1051/epjconf/201714009033

[15] M. Rainer, W. Höflinger, *Chem. Ing. Tech.* **2003**, *75 (7)*, 883–888. DOI: https://doi.org/10.1002/cite.200303215

[16] M. Rainer, *Aufbau und Eigenschaften von Precoatschichten auf Filtermedien für die Anschwemmfiltration*, Ph.D. Thesis, Technische Universität Wien **2003**.

[17] E. S. Tarleton, S. A. Willmer, *Chem. Eng. Res. Des.* **1997**, *75 (5)*, 497–507. DOI: https://doi.org/10.1205/026387697524001

[18] R. J. Ritchie, T. Prvan, *Biochem. Educ.* **1996**, *24 (4)*, 196–206. DOI: https://doi.org/10.1016/S0307-4412(96)00089-1

[19] R. B. Martin, *J. Chem. Educ.* **1997**, *74 (10)*, 1238–1240. DOI: https://doi.org/10.1021/ed074p1238

[20] F. Ranaldi, P. Vanni, E. Giachetti, *Biochem. Educ.* **1999**, *27 (2)*, 87–91. DOI: https://doi.org/10.1016/S0307-4412(98)00301-X

[21] A. Cornish-Bowden, *Fundamentals of Enzyme Kinetics*, 4th ed., Wiley-VCH, Weinheim **2012**.

[22] J. M. Wooldridge, *Introductory Econometrics*, 5th ed., South-Western, Mason, OH **2013**.

[23] D. Asteriou, S. G. Hall, *Applied Econometrics*, Palgrave Macmillan, New York **2007**.

[24] E. Walter, L. Pronzato, *Identification of Parametric Models*, 1st ed., Springer, London **1997**.

 © 2020 The Authors. Published by WILEY-VCH Verlag GmbH & Co. KGaA.

Full-Length Paper II

Optimal dosage strategies for filter aid filtration processes with compressible cakes

Pergam, Philip; Kuhn, Michael; Briesen, Heiko

Chemical Engineering Science, Volume 262, 2022, 117989

DOI: 10.1016/j.ces.2022.117989

Copyright

© 2022 Chemical Engineering Science, published by Elsevier Ltd. All rights reserved.

Reprinted by permission of Elsevier for use in the author's dissertation. Individual licensing is not required.
https://www.elsevier.com/about/policies/copyright#Author-rights

CRediT

- Philip Pergam: Methodology, Software, Writing - Original Draft
- Michael Kuhn: Conceptualization, Methodology, Writing - Review & Editing
- Heiko Briesen: Conceptualization, Writing - Review & Editing, Supervision, Funding acquisition

Chemical Engineering Science 262 (2022) 117989

Contents lists available at ScienceDirect

Chemical Engineering Science

journal homepage: www.elsevier.com/locate/ces

Optimal dosage strategies for filter aid filtration processes with compressible cakes

Philip Pergam, Michael Kuhn, Heiko Briesen *

Process Systems Engineering, Technical University of Munich, Gregor-Mendel-Str. 4, 85354 Freising, Germany

HIGHLIGHTS

- Time-varying filter aid dosage is superior to optimal but constant filter aid supply.
- The cost function of energy minimization also reduces overall filter aid usage.
- Constant filter aid supply is approximatively optimal for pure surface filtration.
- Filter aid usage can be reduced by up to $\approx 30\%$ if mainly depth filtration takes place.
- Benefit of employing optimal control rises the more compressible the process is.

ARTICLE INFO

Article history:
Received 3 May 2022
Received in revised form 2 August 2022
Accepted 4 August 2022
Available online 9 August 2022

Keywords:
Cake filtration
Filter aid filtration
Precoat filtration
Simulation
Optimal control
Optimization

ABSTRACT

We establish optimal time-dependent dosage strategies for compressible filter aid materials, focusing on dead-end filter aid filtration processes operated in constant flow mode. To this end, we apply a direct optimal control approach by repeatedly evaluating a mathematical filtration model with filter aid concentration as the unknown time-dependent control function. Our algorithm iteratively constructs the sought-for trajectory to minimize a cost functional representing previously defined performance goals. We evaluate our optimal control approach for two different model formulations. In the first one, all impurity particles are separated by pure surface filtration on top of the existing filter cake, whereas in the second one, the model is extended toward depth filtration in the filter cake. Particularly for the latter, optimally controlled dosage strategies yield a significant performance improvement of up to 30% reduced filter aid consumption compared with the already optimized but constant filter aid dosage.

© 2022 Elsevier Ltd. All rights reserved.

1. Introduction

Adding filter aids to filtration processes is a well-established technique for separating suspensions that are difficult to handle (Bennet, 2000; Gasper et al., 2000). Filter aids deliver mechanical reinforcement to the filter cake structure (Hunt and Flickinger, 2010; Luckert, 2004) and therefore increase the cake's permeability (Rushton, 1985). Newly developed, commercially available filter aid materials, such as cellulose, are believed to offer environmental and health benefits (Rettenmaier Söhne, 2022). Consequently, these filter aids are investigated to potentially replace traditionally used materials (e.g., kieselgur or perlite) (Braun et al., 2010; Braun, 2012), which are suspected to give rise to waste disposal issues and pose a health hazard (Buttrick, 2007; Bluemelhuber, 2007; World Health Organization International Agency for Research on Cancer, 1997). Nevertheless, contrary to the rigid filter aids, the aforementioned additives suffer from increased compressibility due to their softer material structure and fibrous morphology (Alles, 2000). Thus, their dosage is more challenging to handle in practice. Unsuitable concentrations will exert a significant impact on the filtration performance since filter cake compression usually takes place near the filter medium, and the resulting lower-layer blocking (often referred to as *skin effect*) leads to a rapid increase in the overall differential pressure (Alles, 2000; Tiller and Green, 1973).

Various authors identified superimposed fine particle migration inside the filter cake as an additional factor affecting filtration performance (Berndt, 1981; Tittel, 1987; Hebmüller, 2003; Husemann et al., 2003; Heertjes and Zuideveld, 1978). Thus, it is common for the filter aid filtration processes to be accompanied by a so-called *precoat* stage (Bennet, 2000). A precoat denotes a layer of pure filter aid that is deposited on top of the filter medium. The actual *bodyfeed* filtration of an impure suspension with ongoing filter

* Corresponding author.
E-mail address: heiko.briesen@tum.de (H. Briesen).

https://doi.org/10.1016/j.ces.2022.117989
0009-2509/© 2022 Elsevier Ltd. All rights reserved.

aid dosage only follows after precoat deposition (Sutherland and Hidi, 1966). Hereby, the precoat layer helps prevent the migration of impurities into the filtrate at the beginning of the process. Nevertheless, an unnecessarily large precoat raises the filter resistance, whereas an insufficiently small initial layer has too little potential for separating fine particles. Thus, choosing the precoat height as an additional control variable imposes further difficulties in the search for optimal operation strategies.

Although the importance of finding a suitable constant filter aid dosage during the bodyfeed stage has been acknowledged for decades (e.g., (Sutherland and Hidi, 1966; Carman, 1938; Haba and Koch, 1978), theoretical investigations to reduce experimental work required to find suitable filter aid concentrations are uncommon. This is most likely due to the complex mathematical models required to portray previously explained effects of real filter aid filtration processes (compare to Section 2.1 Mathematical Models). Rare examples are the studies of Heertjes and Zuideveld (Heertjes and Zuideveld, 1978), as well as Berndt (Berndt, 1981), Wegner (Wegner, 1985), and Tittel (Tittel, 1987), which examined analytical optimizations using strongly simplified models. Heidenreich et al. (Heidenreich et al., 1985) implemented results from these optimizations into the computational control engine of a specific filtration plant to ensure optimal dosage. In a recent study, Iliev et al. derived a detailed mathematical model for incompressible filter cakes influenced by simultaneous depth filtration inside the cake (Iliev et al., 2018). This research is also summarized in the thesis of Osterroth (Osterroth, 2018). Although the focus of Osterroth's work lies on in-depth mathematical analysis and model reduction, an additional optimization study to obtain desired deposition profiles is included as well. Nonetheless, his work does not examine filter aid filtration but cake filtration in general.

Even less common are studies examining possible advantages of time-varying filter aid concentrations. Practical attempts toward finding those time-dependent dosage strategies are sparse and mostly based on heuristics rather than systematic investigations (e.g., (Braun, 2012; Hebmüller, 2003; Coote and Höflinger, 1999). Only Kuhn and Briesen conducted rigorous mathematical optimizations for incompressible filter aid filtration processes with and without superimposed effects of depth filtration. Although the latter follows a numerical optimal control approach (Kuhn, 2018) based on a mathematical continuum-scale model (Kuhn and Briesen, 2016), the former derives an analytical control solution using a simplified model (Kuhn and Briesen, 2015). Assuming the absence of impurity particle migration, they found the optimal time-dependent filter aid concentration trajectory to be proportional to the time-varying impurities contained in the suspension. To the best of our knowledge, there were no other theoretical studies conducted on increasing process performance using time-dependent filter aid dosage strategies. For related research areas, Blankert et al. applied dynamic optimization calculations for dead-end membrane filtration processes (Blankert et al., 2006; Blankert et al., 2007). Moreover, Kuhn et al. solved an optimal control problem for deep bed filters (Kuhn et al., 2017), and subsequently, Kuhn and Briesen developed an optimal control method for hollow-fiber membrane filtrations (Kuhn and Briesen, 2021). All of these examples yielded cost benefits, which supports the motivation for our work.

To expand Kuhn's findings, we first apply an optimal control approach for compressible dead-end filter aid filtration processes operated in a constant flow mode with surface filtration being the only mechanism of impurity separation. As a challenging case study, we consider a constant share of impurities contained in the suspension and examine the goal of energy minimization. According to Kuhn et al., the optimal solution would be a constant dosage of filter aids for incompressible cakes (Kuhn and Briesen, 2015), which we hypothesize to be different when cake compressibility is considered.

Subsequently, we conduct our optimal control algorithm for an extended model formulation. Here, operation conditions remain the same, but now, we focus on simultaneous depth filtration taking place in the filter cake fundamentally altering filter aid filtration. As previously explained, fine particle migration has a significant influence on filtration performance. Kuhn found optimal time-dependent filter aid dosage trajectories that qualitatively differ from those obtained with his incompressible, pure surface filtration model (Kuhn, 2018). Consequently, we hypothesized the same to happen when solving the optimal control problem for compressible models, including fine particle migration.

2. Methods

2.1. Mathematical models

For our purposes, we require one-dimensional continuum-scale models comprising systems of partial differential equations. In this manner, we are able to compute detailed transient simulations with spatial dependencies. At first glance, this modeling technique might seem outdated in terms of methods for pore-scale calculations being available (Kuhn et al., 2017). However, for the chosen optimization approach, the model must be evaluated repeatedly, which requires a fast and efficient simulation procedure. Typically, continuum-scale models can be solved in a few seconds compared with pore-scale models, whose calculation time can take up to several hours, currently rendering optimization infeasible.

2.1.1. Surface filtration with compressible filter cakes ("Surface Filtration Model")

Stamatakis and Tien introduced the following mathematical model in 1991 (Stamatakis and Tien, 1991), in which the effect of cake compression is mathematically described by the liquid phase's relative movement to the solid phase. A comprehensive derivation of all equations can also be found in (Tien, 2006). Our derivations mainly follow this model. In cases where we deviate further explanation will be given throughout the paper. For better readability, we omit the variable's dependencies on time and space (t, x) in the equations. These dependencies will only be explicitly denoted upon their first appearance in the text. Furthermore, a schematic of the process is given in Fig. 1. All physical quantities used by the mathematical model are marked in the graphic.

Continuity Eq. (1) is the governing equation of the model. That partial differential equation describes the filter cake's time-dependent spatial development of solidosity $\varepsilon_s(t, x)$, i.e., the volumetric share of solids within the porous structure.

$$\frac{\partial \varepsilon_s}{\partial t} = \frac{\partial}{\partial x}\left(-\varepsilon_s \frac{k}{\mu}\frac{\partial p_s}{\partial x}\right) - q_{lm}\frac{\partial \varepsilon_s}{\partial x} \tag{1}$$

Here, $k(t, x)$ denotes the filter cake's permeability and $p_s(t, x)$ denotes the compressive stress acting on the solid phase. The constant values μ and q_{lm} are the dynamic viscosity and superficial flow rate at the filter medium outlet, respectively. Notably, the numeric values for q_{lm} are negative, as the direction of flow is opposed to the origin of the coordinate system. In filtration literature, porosity $\varepsilon(t, x)$ may often be used instead of solidosity ε_s. Its information content is interchangeable ($\varepsilon = 1 - \varepsilon_s$).

To describe time-dependent filter cake height $L(t)$, we replaced the original differential equation describing the growth rate $\frac{dL}{dt}$ in Ref. [Tien, 2006, p. 57] by Eq. (2) derived from a mass balance. Using this relationship yields highly similar results, but it proves to be faster and numerically more stable during our optimization procedures.

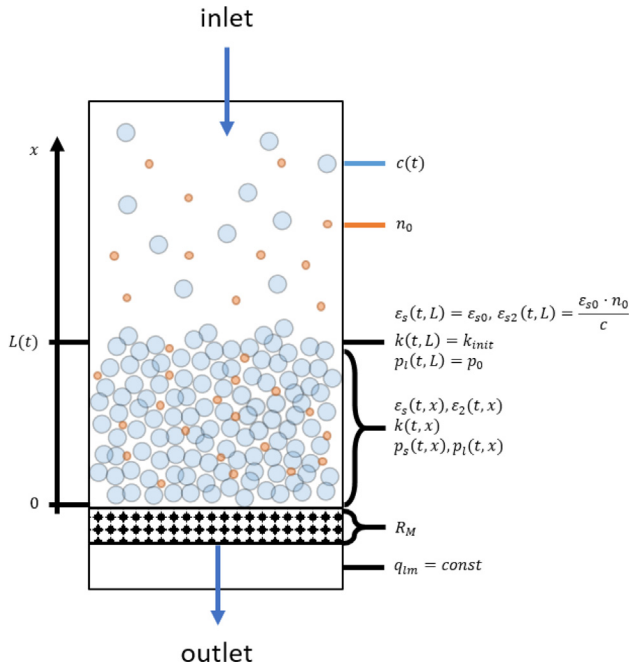

Fig. 1. Schematic representation of the Surface Filtration Model.

$$\frac{dL}{dt} = \frac{c}{\frac{1}{L}\int_0^L \varepsilon_s \, dx - c} \cdot |q_{lm}| \tag{2}$$

In the previous equation, $c(t)$ denotes the filter aid concentration contained in the suspension. Notably, impurities are not considered in Eq. (2). However, we assume that this equation is valid because in filter aid filtration impurities are often expected to attach themselves into the voids of the pore network. Thus, these particles do not significantly contribute to cake growth unless the filter aid concentration is very small (Berndt, 1981; Tittel, 1987; Hebmüller, 2003; Kuhn, 2018). Ordinary differential equations, as encountered in Eq. (2), require initial conditions to have a clearly defined solution. At the first glance, one could argue that the trivial initial condition $L(t = 0\text{s}) = 0\text{m}$ is suitable for our problem, as prior to the filtration no particles were present in the system. Nevertheless, this is not possible due to numerical restrictions implemented by Eq. (1). Thus, further details on the procedure for finding the necessary initial conditions will be given in Section 2.2.1 Simulation Algorithm.

The original model by Stamatakis and Tien does not consider dynamic changes of filter aid concentration c in the feed suspension. Thus, we introduce a new relationship to keep track of the actual filter aid concentration over time. In Eq. (3), $u(t)$ is an arbitrary control function that must be parameterized to solve our optimization problem (compare Sections 2.2.2 Optimization Algorithm and 2.2.3 Optimal Control Algorithm).

$$c(t) = u(t) \tag{3}$$

Now, the dynamic impurity deposition $\varepsilon_{s2}(t, x)$ can be modeled. Because depth filtration is neglected, we assumed fine particle deposition at a given spatial location to not change significantly during the course of the process. Mathematically, this results in a trivial partial differential equation

$$\frac{\partial \varepsilon_{s2}}{\partial t} = 0, \tag{4}$$

along with an extra boundary condition

$$\varepsilon_{s2}(t, x = L) = \frac{\varepsilon_{s0} \cdot n_0}{c}, \tag{5}$$

with which time- and space-dependent deposition of impurities can be calculated. Here, n_0 is the impurity concentration in the suspension. Furthermore, index 0 applied on ε_s defines the solidosity at the top layer of the filter cake in its uncompressed state. Kuhn and Briesen derived boundary condition Eq. (5) in Ref. (Kuhn and Briesen, 2016). Notably, in this work, n_0 is constant. If an optimal control is required for the case of time-varying impurity concentrations, an additional time-dependent function for n_0 in the form of Eq. (3) must be introduced.

The remaining necessary boundary conditions needed to solve Eq. (1) are given according to the study of Tien [Tien, 2006, p. 58]:

$$\text{at } (t, x = L): \ \varepsilon_s = \varepsilon_{s0} \tag{6}$$

$$\text{at } (t, x = 0): \ \frac{k}{\mu}\frac{\partial p_l}{\partial x} = |q_{lm}| = \frac{p_l}{\mu R_M} \tag{7}$$

Here, R_m denotes the filter medium resistance and $p_l(t, x)$ is the pore liquid pressure. In its most simple form, p_l relates to p_s as

$$\frac{dp_l}{dp_s} = -1. \tag{8}$$

By combining the value for p_l known from the boundary condition in Eq. (7)[1] with the pressure relationship in Eq. (8), we can calculate the overall process pressure $p_0(t)$, which will be used to minimize our cost functional during the subsequent optimization stage.

$$p_0 = p_l + p_s \tag{9}$$

There are various relationships between the pore liquid pressure p_l and the compressive stress p_s that have been previously investigated by Tien et al. (Tien et al., 2001). In this study, since our focus lies on finding optimal dosage strategies, we only consider Eq. (8). The implementation of alternatives to Eq. (8) is straightforward, as described in (Tien, 2006). Our proposed optimization procedures are not affected by altering this model refinement option.

Eq. (10) and (11) are two constitutive relationships needed to close the model. In these equations, p_a, δ, and β denote empirically adjustable parameters.

$$k = k_{init} \cdot \left(1 + \frac{p_s}{p_a}\right)^{-\delta} \tag{10}$$

$$p_s = p_a\left(\left(\frac{\varepsilon_s}{\varepsilon_{s0}}\right)^{\frac{1}{\beta}} - 1\right) \tag{11}$$

The so-called material laws correlate compressive stress with permeability and porosity, respectively. Because of their simplicity, such exponential relationships are commonly used in the cake filtration literature to capture the compressive behavior for a wide range of materials (e.g., (Alles, 2000; Carman, 1938; Tien et al., 2001; Sørensen et al., 1996). However, the determined empirical coefficients are only valid for a constant material composition. Since we handle time-dependent filter aid concentrations in our calculations, the cake composition changes, and therefore also the filter cake's specific characteristics. To account for these dependencies, we introduce an additional constitutive relationship. Eq. (12) calculates $k_{init}(t, x)$ as the local initial permeability at an uncompressed state depending on impurity deposition ε_{s2}, as well as the uncompressed permeability k_0 and solidosity ε_{s0} of the pure filter aid material.

$$k_{init} = k_0 \cdot e^{-s\frac{\varepsilon_{s2}}{\varepsilon_{s0}}} \tag{12}$$

[1] The left-hand side is the well-known Darcy's law implying movement of the cake's solid phase to be 0 at the filter medium.

As this approach follows Sutherland (Sutherland and Hidi, 1966), the empirical parameter s is known as the Sutherland-constant in the literature. We deem the introduction of the previous equation as valid, as specifically the Sutherland equation has proven to be accurate for filter aid materials (Berndt, 1981; Heertjes and Zuideveld, 1978).

2.1.2. Combined surface and depth filtration with compressible filter cakes ("Combined Model")

In 1997, Tien et al. extended their model toward depth filtration (Tien et al., 1997), which serves as the foundation for our second model formulation in this study. Fig. 2 contains a schematic of this model. Here, impurity particles are no longer instantly immobilized at the filter cake surface as it was the case in the previous section. Instead, impurities migrate through the filter cake, where the fine particles are eventually separated by the mechanism of depth filtration, as indicated by the green arrow.

The governing relationship is once more a continuity Eq. (13).

$$\frac{\partial \varepsilon_s}{\partial t} = \frac{\partial}{\partial x}\left(-\varepsilon_s \frac{k}{\mu}\frac{\partial p_s}{\partial x}\right) - \left(q_{lm} + \int_0^x N dx\right)\frac{\partial \varepsilon_s}{\partial x} + (1-\varepsilon_s)N \tag{13}$$

Notably, Eq. (13) is closely related to Eq. (1), except for the rate of impurity deposition $N(t,x)$, which is an additional factor influencing dynamic development of cake solidosity ε_s. This quantity can be calculated by Eq. (14) and is composed of the product of the filter coefficient $\lambda(t,x)$, the local impurity concentration left in the suspension $n(t,x)$, and a velocity component.

$$N = \left| q_l - q_s \frac{1-\varepsilon_s}{\varepsilon_s} \right| \cdot \lambda \cdot n \tag{14}$$

As we are examining compressible cakes, the solid and the liquid phase move simultaneously. Hence, a relative velocity term results inside the absolute value parenthesis consisting of $q_l(t,x)$ as the liquid phase superficial velocity and $q_s(t,x)$ as the solid phase superficial velocity. Both quantities are given by the following two equations[2]:

$$q_l = -\varepsilon_s \frac{k}{\mu}\frac{\partial p_s}{\partial x} + (1-\varepsilon_s)q_{lm} + (1-\varepsilon_s)\int_0^x N dx \tag{15}$$

$$q_s = \varepsilon_s \frac{k}{\mu}\frac{\partial p_s}{\partial x} + \varepsilon_s q_{lm} + \varepsilon_s \int_0^x N dx \tag{16}$$

Moreover, the filter coefficient λ can be expressed by Eq. (17). The constitutive relationship has been simplified compared with the original model's equation. This is because for filter aid filtration, it is expected for the filtration efficiency to be amplified when additional impurities are deposited as the capture probability of impurities increases (Kuhn, 2018; Zamani and Maini, 2009).

$$\lambda = \lambda_0\left(1 + \frac{\lambda_c \cdot \varepsilon_{s2}}{1-\varepsilon_s}\right) \tag{17}$$

Although we still examine an initial constant share of impurities n_0 in the suspension, we need an additional conservation equation for said fine particles, as impurities are not separated instantly by surface filtration, as was the case in the first model. Thus, the partial differential Eq. (18) accounts for depth filtration by tracking the dynamic spatial fine particle content left in the suspension.

$$\frac{\partial(\varepsilon n)}{\partial t} = -\frac{\partial(q_l n)}{\partial x} - N \tag{18}$$

[2] Differentiating Eq. (15) with respect to x results in the right hand side of Eq. (13), which leads back to the basic continuity equation $\frac{\partial \varepsilon_s}{\partial x} = \frac{\partial q_l}{\partial x}$ for flow through porous media. The same relationship applies to Eq. (1).

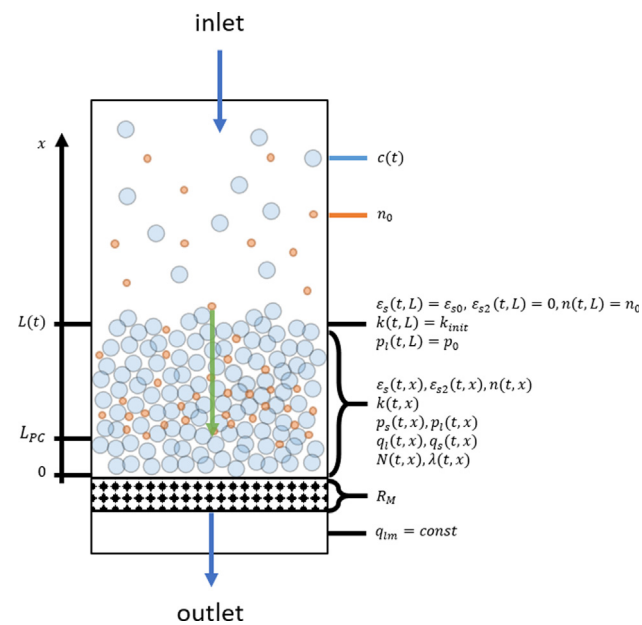

Fig. 2. Schematic representation of the Combined Model.

Similarly, the conservation Eq. (19) describes the dynamic development of separated impurities ε_{s2}.

$$\frac{\partial \varepsilon_{s2}}{\partial t} = -\frac{\partial}{\partial x}\left(q_s \frac{\varepsilon_{s2}}{\varepsilon_s}\right) + N \tag{19}$$

The boundary conditions needed to solve this system of partial differential equations are provided by Tien et al. (Tien et al., 1997):

$$\text{at}\,(t, x = L): \ \varepsilon_s = \varepsilon_{s0} \tag{20}$$

$$\varepsilon_{s2} = 0 \tag{21}$$

$$n = n_0 \tag{22}$$

$$\text{at}\,(t, x = 0): \ \frac{k}{\mu}\frac{\partial p_l}{\partial x} = |q_{lm}| = \frac{p_l}{\mu R_M} \tag{23}$$

Thus far, Eq. (21) and (22) indicate that impurities are only separated by depth filtration inside the filter cake. However, in filter aid filtration, it is more realistic that some share of impurities is separated at the top of the filter cake, and only the remaining fine particle fraction will be exposed to depth filtration (Tittel, 1987; Hebmüller, 2003). This can be modeled by the following boundary conditions, where γ denotes the share of impurities immobilized at the filter cake's uppermost layer.

$$\text{at}\,(t, x = L): \ \varepsilon_{s2}(t, x = L) = \frac{\varepsilon_s \cdot \gamma \cdot n_0}{c} \tag{24}$$

$$n = (1-\gamma)\cdot n_0 \tag{25}$$

For the filter cake's growth rate $\frac{dL}{dt}$, we reuse Eq. (2). Here, the same argumentation of impurities not significantly contributing to the filter cake height applies. Details on the implementation of the required initial conditions are provided in Section 2.2.1 Simulation Algorithm.

All following model calculations were carried out using model parameters provided by Tien [Tien, 2006, p. 70; 87]. The parameter sets represent high cake compressibility (*parameter set HC*) and low cake compressibility (*parameter set LC*). Values for k_0 and s had to be adjusted because Eq. (12) is not part of the original

model. Thus, we freely selected the parameter values with a focus on keeping the model simulations in realistic ranges of filtration pressure and solidosity. Moreover, we handled the additional parameter γ in two ways. First, γ was set to 0 to reproduce the original boundary conditions. Subsequently, we varied the value of γ to examine how a changing share of depth filtration will affect the optimal operating conditions. Appendix A contains the parameter values used for the simulations.

Neither of the models was directly developed for filter aid filtration but for the cake filtration process in general. Nevertheless, we are confident that combined with our assumptions, the model is valid for representing different filter aid filtration processes using the original parameters. This can be further justified by the following two reasons:

a) Filter aid filtration can be defined as a specific case of cake filtration. Here, the initial suspension contains a bidisperse particle size distribution. The fine particle fraction represents the impurity particles, and the coarse particle fraction is the filter aid material. For our application, the share of the coarse particle fraction can be actively manipulated by our optimal control approach.
b) The values of the mostly incompressible *parameter set LC* were estimated on the basis of experiments with calcium carbonate filter cakes. Calcium carbonate is – although rarely – used as a filter aid material in itself (Carman, 1938).

Despite all evidence justifying our adaptations, we emphasize that the following simulations do not represent any specific experimental set-ups and must rather be regarded as qualitative parameter studies.

2.2. Numerical procedures

2.2.1. Simulation algorithm

Because of the dynamic filter cake growth described by Eq. (2), the system's upper boundary $x = L(t)$ is time-dependent. Thus, both models can be mathematically defined as moving boundary problems. To numerically solve this class of problems, Tien et al. applied the following transformation:

$$z = \frac{x}{L} \tag{26}$$

This approach is known as the front fixing method (Crank, 1984) and ensures that every height coordinate is defined in the range of $z = 0$ to $z = 1$ for all times.

Apart from applying the front fixing method, the models were scaled by process-inherent nondimensionalization of the variables. Even when using double precision variables, machine precision only reaches a maximum of $2.2 \cdot 10^{-16}$ (The MathWorks, Inc.), which can lead to loss of significance if mathematical operations between variables of highly different magnitudes are performed. Albeit the studies of Tien et al. demonstrate that solutions for single forward simulations are possible without treating the model equations, we experienced significant convergence problems during numerical optimization without proper scaling. This is most likely due to the imprecisely estimated gradients required for the optimization algorithms. Appendix B contains the necessary relationships for applying both, the front fixing method, and nondimensionalization, along with the resulting model equations.

All final equations are solved using the method of lines as a numerical solution technique, which has been successfully applied previously by Tien et al. (Tien et al., 1997) as well as Kuhn and Briesen (Kuhn and Briesen, 2016). The method of lines transforms an initial partial differential equation into a system of ordinary differential equations, where each ordinary differential equation represents one coordinate in space. Local dependencies are then coupled via spatial derivatives approximated by finite differences. Here, we chose an equidistant discretization grid with 150 mesh points. First-order spatial derivatives are approximated by a five-point upwind finite difference scheme, and second-order spatial derivatives are calculated using a five-point central finite difference scheme. More information on the theory as well as practical hints on the numerical implementation is provided in Ref. (Schiesser and Griffiths, 2009; Wouwer et al., 2014).

However, solving both models by applying the previously explained numerical techniques renders direct implementation of initial conditions impossible, as explained in Section 2.1 Mathematical Models. If $L(0\text{s})$ were set to 0m, the upper and lower boundary would be located on the same point, such that the spatial dimension could not be discretized as required by the method of lines. Thus, we implemented an extended initialization procedure. For the *Surface Filtration Model*, a simplified cake filtration model based on an incompressible mass balance (Eq. (27)) was solved analytically for a simulation time span of $t = 1\text{s}$.

$$L(t) = \frac{c}{\varepsilon_{s0}} |q_{lm}| t \tag{27}$$

For such short durations, almost no pressure drop occurs over the system. Hence, it is justified to assume an incompressible filter cake development for the said time span. Consequently, Darcy's law for laminar flow through porous media can be used to calculate the pore liquid pressure profile along the filter cake height for each grid point $x = 0\text{m} \ldots x = L(1\text{s})$.

$$p_l = \frac{\mu}{k} x |q_{lm}| \tag{28}$$

By setting $p_0(1\text{s}) = p_l(1\text{s}, L(1\text{s}))$, the solid stress $p_s(1\text{s}, x)$ is obtained for each discretized coordinate using Eq. (9). Subsequently, Eq. (11) can be used to calculate the solidosity profile $\varepsilon_s(1\text{s}, x)$. Moreover, the initialized impurity deposition profile $\varepsilon_{s2}(1\text{s}, x)$ is assumed to be constant and can be calculated by Eq. (5). The resulting values $L(1\text{s})$, $\varepsilon_s(1\text{s}, x)$, and $\varepsilon_{s2}(1\text{s}, x)$ are supplied as initial conditions to the corresponding full model equations. Finally, the simulation is computed for the user-defined simulation time span T minus 1s, which is the time span covered by the initialization procedure.

For the *Surface Filtration Model*, the impurity deposition will influence the pressure drop, but fine particles will not migrate into the filtrate by definition. Hence, the precoat stage is negligible. This is not the case for the *Combined Model*. Therefore, the simulation must be expanded into a three-stage procedure in the case of simultaneous depth filtration taking place. First, the initialization phase follows the procedure explained above, except that the required initial values for n (Eq.(18)) and ϵ_{s2} (Eq. (19)) are now set to 0 due to the nature of the precoat stage with no impurities being present in the system. Second, the full model is calculated for an infinite simulation time span with the parameter n_0 being set to 0; the integration of the corresponding system of ordinary differential equations only stops with the help of an event function after reaching the desired precoat height L_{PC}. Third, the parameter n_0 is set to the user-defined impurity concentration and the body-feed stage is calculated for the simulation time span using the end values of the precoat stage as initial values.

With these preparations, the resulting time-dependent system of ordinary differential equations can be solved by standard methods. We implemented all numerical procedures in Matlab 2021b (supplier: The MathWorks, Inc., Natick, Massachusetts, USA). For time integration, we used Matlab's ode15s as an implicit ordinary differential equation solver. Implicit solvers are computationally expensive but superior in handling stiff systems of differential equations, which usually arise when solving partial differential

equations by employing the method of lines. Moreover, ode15s can handle mass matrices, which is useful for treating the boundary conditions as a system of differential–algebraic equations. More information is provided in Ref. (Wouwer et al., 2014). For the integrator's options, absolute and relative error tolerances 'AbsTol' and 'RelTol' were set to the low value of 1e-8. These options ensure accurate model simulations to numerically compute the gradients required for the optimization procedures as precisely as possible.

All calculations were performed on a regular desktop computer (processor: Intel® Core™ i5-8400, performance: 2.80 GHz, memory: 16 GB RAM). Computation times were approximately 0.5 s for one simulation of the *Surface Filtration Model* and 7 s for a single simulation of the *Combined Model*.

2.2.2. Optimization algorithm

First, we apply static optimizations for both models, which provide reference scenarios to evaluate the possible benefits of optimally controlled solutions. In this study, all optimizations were executed with the performance goal of minimizing the overall energy expenditure. Mathematically, this can be represented by the following nonlinear optimization problem:

$$\min_{\boldsymbol{u_p}} \; e. \tag{29}$$

Here, the cost functional e denoting area-specific energy consumption can be calculated by the time integral in Eq. (30), comprising the superficial filtrate flow q_{lm} and the pore liquid pressure difference along the filter cake height.

$$e = \int_0^T |q_{lm}|(p_l(t,L) - p_l(t,0))dt \tag{30}$$

Herein, $\boldsymbol{u_p}$ denotes the respective control variables solving the optimization problem Eq. (29). As per definition, the goal of static optimization is to find a mathematically optimal constant filter aid dosage. Thus, the only unknown optimization parameter u_p for the *Surface Filtration Model* is a scalar parametrizing the control function $u(t)$ contained in Eq. (3) as a constant value, as described by Eq. (31).

$$\begin{aligned} c(t) &= u_p = const \\ 0 &< u_p < \varepsilon_{s0} \end{aligned} \tag{31}$$

Since the precoat height is an additional control variable for the *Combined Model*, $\boldsymbol{u_p}$ becomes a vector containing the following two optimization parameters.

$$\begin{aligned} c(t) &= u_{p1} = \text{const} \\ L_{PC} &= u_{p2} \\ 0 &< u_{p1} < \varepsilon_{s0} \\ 0 &< u_{p2} \end{aligned} \tag{32}$$

Moreover, optimizations for the *Combined Model* are feasible if the inequality condition Eq. (33) is satisfied.

$$\frac{\int_0^T |q_{lm}| n(t,0)dt}{\int_0^T |q_{lm}|dt} < \frac{n_0}{n_{frac}} \tag{33}$$

Introducing n_{frac} ensures that the final impurity concentration in the filtrate cannot exceed a previously defined fraction of the initial impurity concentration contained in the suspension. Notably, due to the nature of transport equations, Eq. (33) cannot be defined as an equality condition where the right-hand side is set to 0. For all following optimizations of the *Combined Model*, n_{frac} was set to 100, i.e., the impurity concentration in the filtrate must be more than 100 times smaller than the concentration initially contained in the suspension.

All nonlinear optimizations were performed by Matlab's fmincon function using the default interior-point algorithm. The optimizer's options were set to use central finite differences to calculate the necessary gradients. Doing so requires double the model evaluations and therefore has a large impact on the computational cost. However, central schemes can calculate the required gradients with higher precision. Hence, robustness and speed of convergence are significantly improved. Matlab's Parallel Computing Toolbox was enabled for finite differencing to counteract the additional computation time.

2.2.3. Optimal control algorithm

Optimal control is distinguished from static optimization by allowing the respective controls to be time- and/or space-dependent functions. Since optimal control theory is a large field of research in itself, only some important aspects needed to contextualize our optimal control approach are revisited here. More fundamental information and theoretical investigations on this topic can e.g. be found in Refs. (Betts, 2010; Lewis et al., 2012). Some basic terminology and strategies are briefly introduced in the following.

Numerical methods for solving optimal control problems can be broadly categorized into indirect and direct approaches. Indirect methods are usually more accurate as they solve the necessary conditions for optimality through the transformation of the optimal control problem into a boundary value problem. However, direct methods are typically easier to implement for complex systems, such as the one in this study. This is because, for direct methods, the optimal control problem can be expressed as a finite-dimensional nonlinear optimization problem, as already introduced in the Subsection 2.2.2 Optimization Algorithm. A well-established technique is to discretize the control function's domain into a mesh of η subintervals. Thereafter, an arbitrary control function is parametrized for each respective subinterval. Theoretically, with $\eta \to \infty$, the solution of the nonlinear program converges toward the true solution of the optimal control problem within machine precision. A reasonable choice of subintervals η secures a good approximation to the solution of the optimal control problem. Consequently, the accuracy of the transformed optimal control problem can be increased by either decreasing the discretization size of the underlying mesh (*h-method*) or by raising the degree of the arbitrary control function (*p-method*).

We based our optimal control algorithm on a first-order *h-method* with iterative bisectional mesh refinement, as it proved to be successful in our previous studies (Kuhn, 2018; Kuhn and Briesen, 2021). The following figure depicts the method schematically.

As shown in Fig. 3, the filter aid concentration $c(t)$ is the sought-for trajectory in our specific application. To find this function, the simulation time span is split into a number of η_i subintervals, where the amount of subintervals doubles with each iteration i. Thus, the arbitrary control function $u(t)$ introduced in Eq. (3) can be defined for each subinterval as a piecewise-linear function:

$$\begin{aligned} c_{\eta_i}(t) &= u_{\eta_i,p1} \cdot t + u_{\eta_i,p2} \\ 0 &< c_{\eta_i}(t) < \varepsilon_{s0} \end{aligned} \tag{34}$$

Herein, the index η_i applied on $c(t)$ denotes the iteration-dependent subinterval discretization set of the filter aid concentration, and $\boldsymbol{u_{\eta_i,p}}$ is the associated vector of control parameters. Hence, the nonlinear program parametrizes the unknown control parameters $u_{\eta_i,p1}$ and $u_{\eta_i,p2}$ to solve the optimization problem introduced in Eq. (29).

The optimal control procedure is initialized with the optimal constant filter aid dosage obtained from the static optimization approach. Subsequently, all following refinement steps are initial-

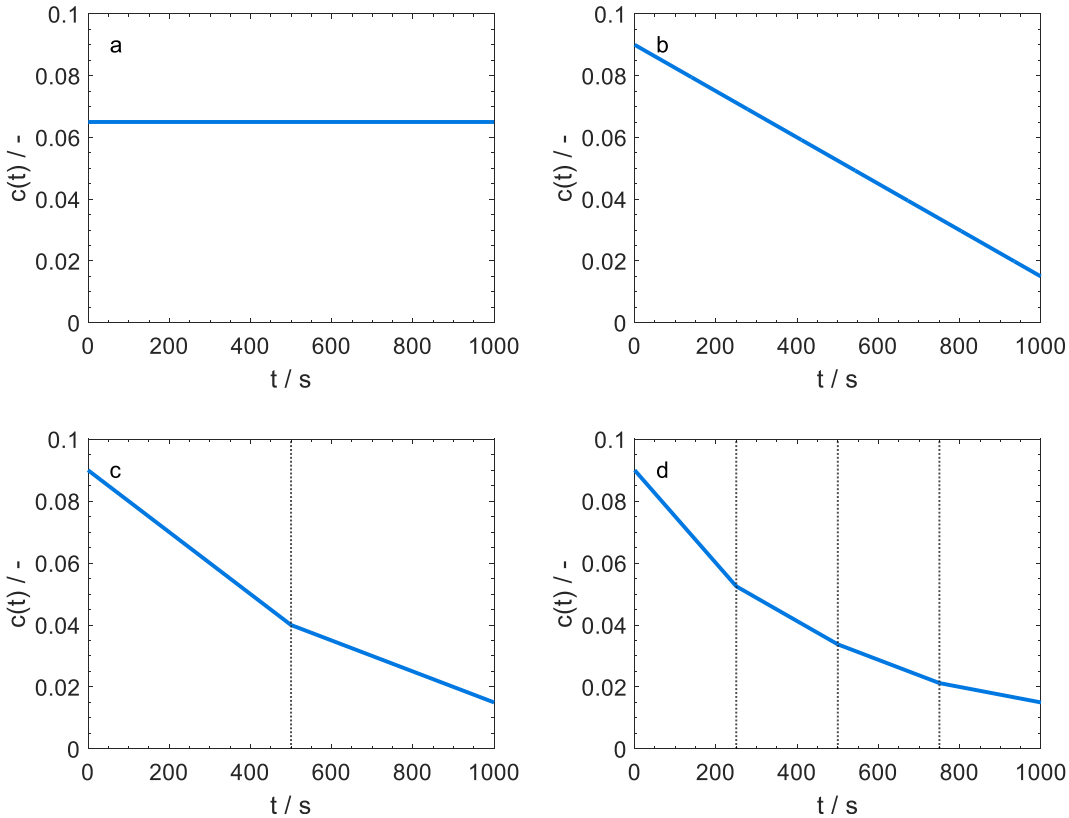

Fig. 3. Schematic representation of the iterative optimal control procedure. a: initialization with a statically optimized solution; b: first iteration with one interval; c: second iteration with two subintervals; d: third iteration with four subintervals.

ized with the optimal parameter values known from the respective previous iterations. Notably, the control procedure is identical for both model formulations, except that the inequality condition Eq. (33) must be met for the *Combined Model*. The precoat height L_{PC} was not handled as an additional optimal control parameter, as was the case for the static optimization procedure. We noticed that including L_{PC} in the optimal control algorithm has a negligible effect on the cost function but primarily increases computation time. Hence, L_{PC} was fixed to the value obtained in the preceding static optimization. In this study, optimal control solutions were obtained by setting the number of iterations to five for the *Surface Filtration Model* and four for the *Combined Model*.

All nonlinear optimizations were carried out by Matlab's fmincon function using the sequential quadratic programming algorithm. The optimizer's options were set to use central finite differences to calculate high precision gradients while using the Parallel Computing Toolbox for accelerating computing times.

3. Results and discussion

3.1. Optimization of the surface filtration model

First, results for the *Surface Filtration Model* are examined. Static optimizations were calculated for both parameter sets to determine the optimal constant filter aid concentrations c while minimizing the area-specific energy expenditures. Unless stated otherwise, the impurity concentration n_0 for the *parameter set HC* is 0.01, and for the *parameter set LC* 0.005 for all following scenarios. Fig. 4 shows how varying c for different simulation runs results in a parabola-shaped cost functional. The respective global minima are marked as orange circles and can be determined easily by the optimization algorithm. For the cost comparison, absolute values

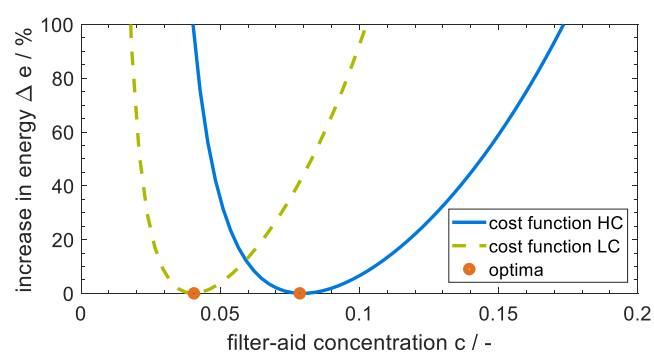

Fig. 4. Globally optimal constant filter aid dosage c for the Surface Filtration Model. blue: cost function for parameter set HC; green: cost function for parameter set LC.

were transformed into a relative scale representing percentual increases in the area-specific energy consumption if the process is not executed at the optimum.

The parabola shape results due to two reasons affecting the pressure drop, and thus, having a negative impact on energy expenditure. On the one hand, low filter aid dosage leads to a low cake height which in itself would be beneficial for the overall cake resistance. However, due to the lack of filter aid particles, local impurity depositions are more pronounced, and the filter cake's pores will clog more easily. In return, the local permeability decreases rapidly. On the other hand, a high supply of filter aid lowers the impurity deposition. In this case, local permeability would be more beneficial compared to the previous example. Nevertheless, the filter cake's growth rate will rise drastically, which consequently increases the total filter resistance. Both phenomena hinder the flow of the liquid phase through the porous filter cake.

Hence, the global optima displayed in Fig. 4 can be interpreted as a trade-off between both effects to prevent the pressure drop from increasing exponentially, while maintaining the specified constant flow filtration.

Furthermore, the existence of single global minima enables us to find unique optimal operation curves along the domain of possible impurity concentrations for each parameter set. As an example, Fig. 5 shows these operation curves for both parameter sets. If depth filtration is negligible, the optimal constant filter aid dosage can be directly obtained for varying impurity concentrations and otherwise identical operation conditions. Such optimal curves might yield benefits in real process set-ups, e.g., if batches of the same type of suspension with a varying share of impurities must be filtered.

3.2. Optimal control of the surface filtration model

Time-varying optimal filter aid dosage strategies $c(t)$ for the *Surface Filtration Model* are constructed according to our optimal control algorithm. The calculated trajectories are displayed in Fig. 6 for both parameter sets. Previously obtained optimized but constant solutions for the filter aid concentrations are plotted alongside, as they represent the benchmarks for the optimal control solutions. The qualitative shapes of the resulting dosage functions are similar for both parameter sets: optimally controlled filter aid concentration trajectories begin at higher concentrations compared to the reference cases but subsequently decrease. Toward the end of the process, a small ascent in the filter aid concentration can be observed.

Supplying a higher share of filter aids at the beginning of the process results in a greater filter cake growth rate compared with the reference scenario (Fig. 7(a)) but according to Eq. (5) also lowers the impurity deposition near the filter medium where compression affects permeability the most. Thus, the dosage strategy helps in counteracting the so-called skin effect. By contrast, a larger number of impurity particles are accepted in the top layers of the filter cake, as no further filtration potential is needed toward the end of the process.

However, the obtained performance benefits by time-varying filer-aid dosages are hardly recognizable. Fig. 7(b) displays the filtration pressure over time. Calculating the area-specific energy consumption from the liquid pressure drop yields $\approx 0.31\%$ relative energy savings for *parameter set HC* and $\approx 0.003\%$ relative energy savings for *parameter set LC* compared with the respective benchmark scenarios. By applying the optimal solution for the minimization of area-specific energy expenditure, area-specific filter aid consumption, calculated by

$$V_c = \int_0^T |q_{lm}| \cdot c(t)dt \tag{35}$$

is also decreased. Therefore, relative filter aid consumption is reduced by $\approx 0.49\%$ for *parameter set HC* and $\approx 0.098\%$ for *parameter set LC* compared with the optimized constant dosage.

Recall, that this work only investigates filtration processes operated in constant flow mode. Therefore, the diagram for the filtrate flow $q(t) = \text{const}$ of a simulation with optimal filter aid dosage will be equal to those of sub-optimal simulations. Since the cumulative filtrate volume is merely the integral of the filtrate flow,

$$V = \int_0^T |q_{lm}|dt \tag{36}$$

the resulting linear functions are identical as well. Due to the lack of information content relevant to our work, these graphs are omitted here.

For the *parameter set HC*, the existence of a time-varying optimal control solution to our minimization problem verifies our initial hypothesis of cake compression affecting the qualitative solution known from Kuhn and Briesen (Kuhn and Briesen, 2015). Furthermore, the optimal control solution for *parameter set LC* shows much lower variations compared with the trajectory of *parameter set HC*. Here, variations only appear in the fourth decimal. This behavior is in accordance with the findings of Kuhn and Briesen as well, and, therefore our optimization calculations are further validated by their work. According to them, in the case of an incompressible cake filtration with a constant share of impurities the optimal filter aid dosage profile depending on time is constant. Indeed, for a real use case the minor variations shown in the trajectory of Fig. 4(b) can be interpreted as constant.

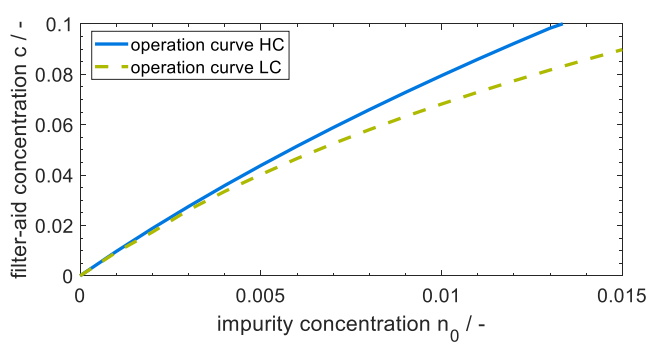

Fig. 5. Optimal operation curves for the Surface Filtration Model. blue: operation curve for parameter set HC; green: operation curve for parameter set LC.

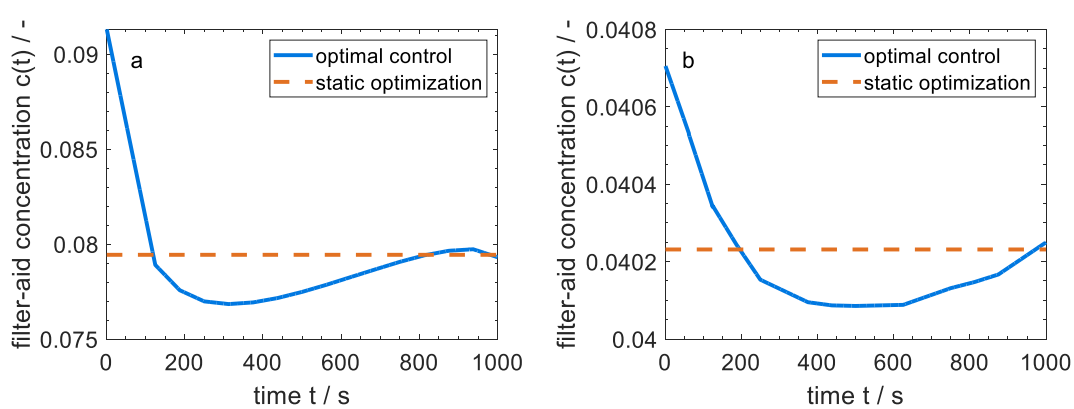

Fig. 6. Time-dependent filter aid dosage for the Surface Filtration Model obtained by the optimal control method (blue) and optimal constant benchmark (orange). a: parameter set HC; b: parameter set LC.

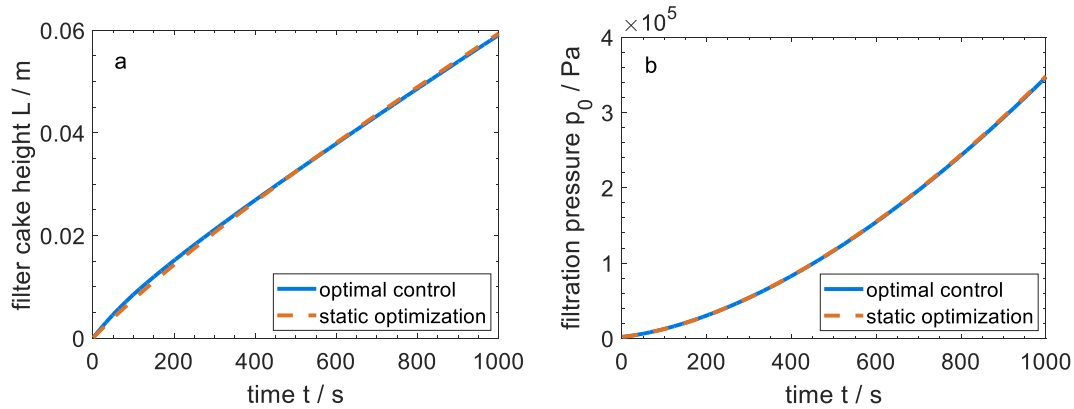

Fig. 7. Quantities for the Surface Filtration Model resulting from the optimal control method (blue) and the optimal constant benchmark (orange) for parameter set HC. a: time-dependent filter cake growth; b: time-dependent filtration pressure.

Nevertheless, savings in energy as well as in filter aid consumption compared with the static optimal conditions are moderate at best, if depth filtration is neglected. Especially in hindsight of unavoidable experimental noise in a real-world environment, obtained performance gains $< 1\%$ may be irrelevant. However, note that these are only the additional savings obtained by introducing time-varying operation strategies compared with an already optimized but constant dosage. Such optimal static filter aid supply marks a hard theoretical benchmark, which we assume to be rarely realized in practice purely by intuition. Thus, merely obtaining the benchmark might already be beneficial for real processes. Moreover, it was neither guaranteed that a time-varying optimal control solution exists, nor that it would yield a significant performance benefit. In fact, there is no *a priori* method available to assess how an optimal control approach affects the cost functional. Therefore, it was necessary to evaluate the influence of a dynamic filter aid dosage using the full-scale optimal control algorithm.

3.3. Optimization of the combined model

Next, we examine static optimizations for the *Combined Model*. The calculated optima are also single global minima, comprising the optimal combination of filter aid concentration c and the precoat height L_{PC}. Fig. 8(a) displays the area-specific energy consumption depending on the bodyfeed filter aid concentration with an optimal precoat height. Once again absolute values were transformed onto a relative scale. The qualitative solution behavior is similar to the results known from the *Surface Filtration Model*, and the outcome can be explained with the same argumentation as before. Fig. 8(b) shows the opposite case, namely, area-specific energy consumption depending on precoat height with an optimal bodyfeed filter aid concentration. The energy consumption is observed to increase monotonically for higher precoats with the unbounded minimum being located at $L_{PC} = 0$m. This trivial operation point describes no filtration taking place initially, and thus, no energy is spent on the process. To maintain the desired filtration performance, the true feasible minimum is defined by the inequality condition Eq. (33), which is plotted as a black vertical line. The nonlinear program finds the smallest possible optimal precoat height, such that the overall filter resistance is minimized and impurities are prevented from migrating into the filtrate.

3.4. Optimal control of the combined model

Subsequently, the calculated constant optima are compared with the results obtained via the optimal control procedure. The solutions for scenario $\gamma = 0$, i.e., where no impurities are separated by surface filtration, are displayed in Fig. 9. Fine particle migration is observed to affect the qualitative shape of the filer-aid dosage trajectory. Function $c(t)$ starts near 0, from where it will quickly rise to a maximum higher than the concentration known from the statically optimized case. A phase of the monotonous decrease can be observed from here. In the last time intervals, the filter aid supply approaches 0 again.

With the optimal control approach, the time-dependent filter aid dosage leads to a redistribution of separated impurities ε_{s2}, as shown in Figure 10(a). Using these strategies, an accumulation of fine particles at the lower filter cake layers is prevented. In this spatial region, a greater impurity deposition is the cause of filter cake blocking due to a higher compression taking place. Instead, the optimized filter aid trajectories cause a more uniform distribution of impurity deposition for wide time spans of the process.

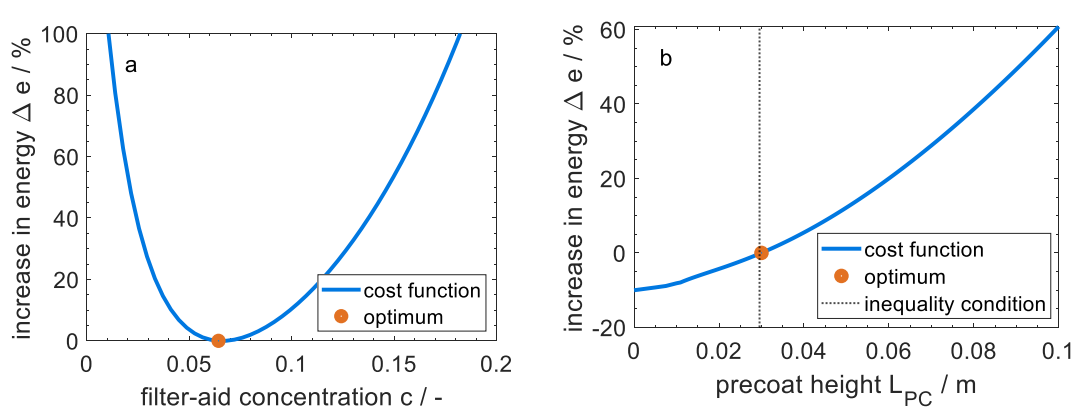

Fig. 8. Globally optimal constant control variables for the Combined Model using parameter set HC. a: filter aid dosage c; b: precoat height L_{PC}

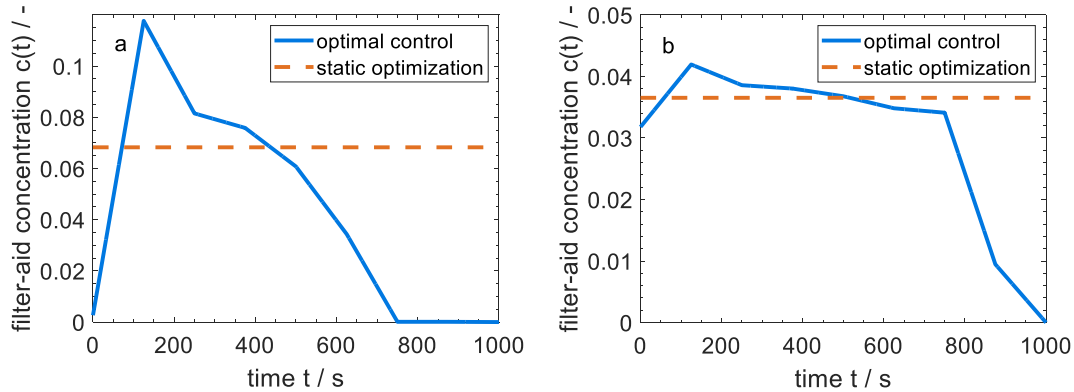

Fig. 9. Time-dependent filter aid dosage for the Combined Model ($\gamma = 0$) obtained by the optimal control method (blue) and optimal constant benchmark (orange). a: parameter set HC; b: parameter set LC.

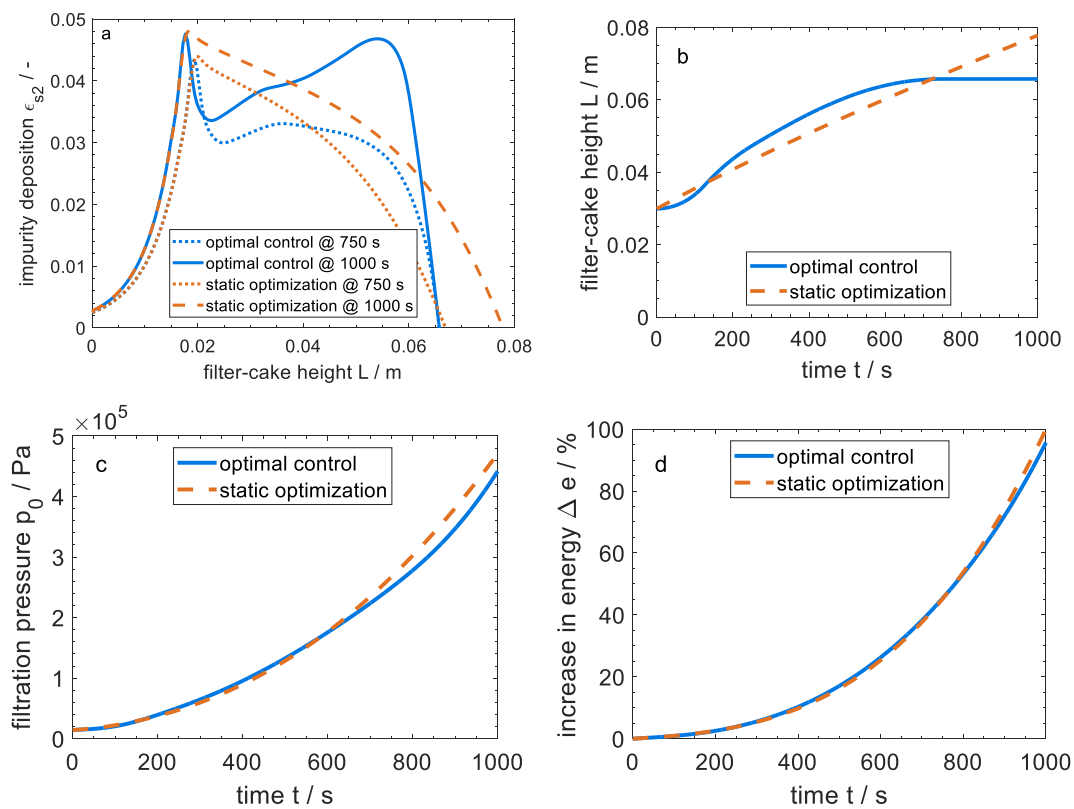

Fig. 10. Quantities for the Combined Model resulting from the optimal control method (blue) and optimal constant benchmark (orange) for parameter set HC. a: impurity deposition at t = 750 s (dotted lines) and t = 1000 s (solid line/dashed line); b: filter cake height; c: filtration pressure; d: area-specific energy consumption.

Only toward the end of the filtration, the impurities are accumulated at the top of the filter cake, where permeability is not strongly affected by compression. Avoiding impurity deposition in the lower filter cake regions along with the overall lower filter cake height (Figure 10(b)) yields a lower total filter resistance and therefore a lower pressure drop (Figure 10(c)). Initially, the pressure drop rises quicker compared with the reference case due to a faster cake growth rate resulting from a higher filter aid supply. However, the area-specific energy consumption is smaller at the end of the process, as the lower cake layers are "prepared" for long-term effects (Figure 10(d)). Notably, in Figure 10(d) values were converted into a relative scale, with 100 % representing the end value obtained by static optimization.

Applying this strategy, compared with the constant reference scenario, the following performance benefits can be achieved for the *Combined Model*. The area-specific energy consumption was lowered by $\approx 4.5\%$ for *parameter set HC* and by $\approx 0.9\%$ for *parameter set LC*. Moreover, according to Eq. (35), the relative filter aid consumption is reduced by $\approx 29.1\%$ for *parameter set HC* and by $\approx 14.9\%$ for *parameter set LC* compared with the already optimized constant dosage. While savings in energy consumption may still seem moderate – reaching 5 % only under certain conditions – the filter aid consumption was drastically reduced.

The same optimal control approach was applied for an assumed $\gamma = 0.5$, i.e., where 50 % of impurities are initially separated by surface filtration. In total, the qualitative solutions are similar to the previous results of scenario $\gamma = 0$. However, variations of the filter aid dosage over the simulation time span are not as pronounced (Fig. 11). This causes a smaller gain of the performance index compared with the previous example. Relative savings are $\approx 0.35\%$ (*parameter set HC*) / 0.15% (*parameter set LC*) for area-specific energy expenditure and $\approx 4.7\%$ (*parameter set HC*) / $\approx 4.5\%$ (*pa-*

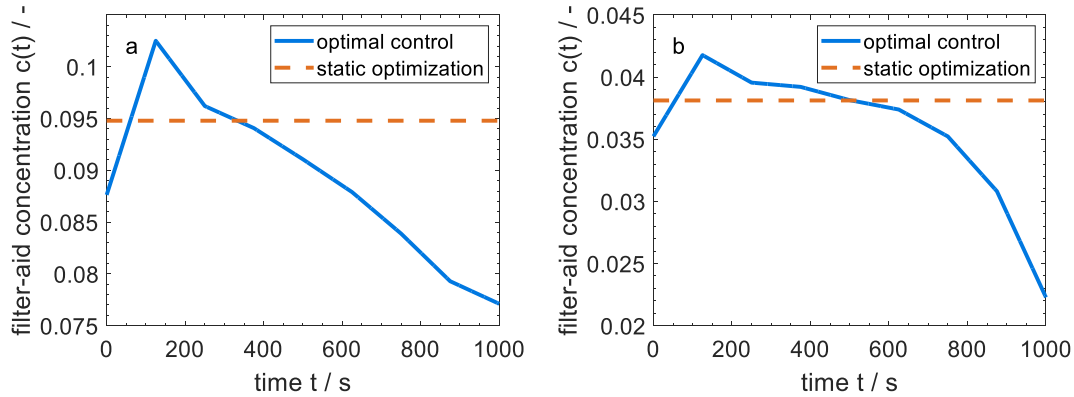

Fig. 11. Time-dependent filter aid dosage for the Combined Model ($\gamma = 0.5$) obtained by the optimal control method (blue) and optimal constant benchmark (orange). a: parameter set HC; b: parameter set LC.

rameter set LC) for filter aid consumption compared with the optimized constant dosage benchmark case. Obtaining a lower benefit was expected, as this scenario approaches the first optimal control example of the *Surface Filtration Model*, where no depth filtration is taking place.

Our findings are backed by the work of Heertjes and Zuideveld (Heertjes and Zuideveld, 1978), who observed an accumulation of impurities near the precoat/bodyfeed interface for different experimental set-ups. In case of such a blocking event happening, the pressure drop is significantly increased. To avoid this effect, the authors proposed to apply strategies to form a homogenous impurity deposition profile along the filter cake height. They prevented the formation of blocking regions by varying the filter aid type. With the currently available enhanced theoretical models and computational capabilities, we achieved this goal by only varying filter aid concentration over time.

Notably, our calculated optimal dosage profiles are compared with already optimized reference cases. We assume that in real-life scenarios, filter aid bodyfeed concentrations are still often obtained by intuition, heuristics, and "trial and error," rather than by rigorous mathematical optimizations. Thus, the static optimization approach alone might outperform currently established filter aid dosage strategies in industrial practice without requiring additional investments in plant instrumentation. Moreover, we did not examine time-varying impurities contained in the suspension to evaluate the effect of cake compression on the optimization. Naturally, practical benefits of optimal control will be even larger, if the dynamic impurity supply can be quantified. Lastly, the performance index of area-specific energy minimization might not be the economically most feasible. Nevertheless, the optimal control approach can easily be extended for combined cost functions or multivariable controls, such as $q_{lm}(t)$, i.e., a time-varying filtrate flow.

4. Conclusions

We applied optimization algorithms on compressible filter aid filtration models based on the multiphase cake filtration theory. Albeit this theory has been derived in the 1980s and 1990s, it did – to the best of our knowledge – not find a practical use for industrially scaled processes. By applying these models, we close a gap in the theoretical investigations on optimal operation conditions, and, therefore, contribute to reduce the experimental work required to determine the optimal process control.

The obtainable performance benefits from time-varying filter aid dosages for a constant supply of impurities strongly depend on specific process conditions. In conclusion, the more impurities are separated by depth filtration in the filter cake, the higher the positive effect of optimal control becomes. In the extreme case of 100 % depth filtration, time-dependent filter aid trajectories will lead to the reduction of up to $\approx 29.1\%$ filter aid usage as well as $\approx 4.5\%$ energy consumption. Nevertheless, if all impurities are separated by surface filtration, the benefit of optimal control is negligible. Herein, the efforts required to employ time-varying filter aid dosages in real processes are probably not justified.

We emphasize that the results are only valid to construct qualitative statements, as the models along with their parameters have been developed for cake filtration processes in general. We are confident that the results obtained in this study represent theoretically obtainable benefits for filter aid filtrations. However, especially when considering compressible filter aid materials such as fibers, the adapted models most likely require fine tuning of pressure relationships (Tien et al., 2001) as well as an additional parameter estimation with actual experimental data.

CRediT authorship contribution statement

Philip Pergam: Methodology, Software, Writing – original draft. **Michael Kuhn:** Conceptualization, Methodology, Writing – review & editing. **Heiko Briesen:** Conceptualization, Writing – review & editing, Supervision, Funding acquisition.

Data availability

Data will be made available on request.

Table A1
Parameter values used for model simulations.

		Parameter Set HC Material system with high compressibility	Parameter Set LC Material system with low compressibility
$\boldsymbol{k_0}$	$[m^2]$	10^{-12*}	10^{-11*}
$\boldsymbol{n_0}$	$[-]$	0.01	0.005
$\boldsymbol{p_a}$	$[Pa]$	1200	44000
$\boldsymbol{q_{lm}}$	$[\frac{m}{s}]$	$-2 \cdot 10^{-4}$	$-5 \cdot 10^{-4}$
$\boldsymbol{R_M}$	$[m^{-1}]$	10^{10**}	10^{10**}
$\boldsymbol{s}$	$[-]$	10^*	10^*
$\boldsymbol{T}$	$[s]$	1000	1000
$\boldsymbol{\beta}$	$[-]$	0.09	0.13
$\boldsymbol{\delta}$	$[-]$	0.49	0.57
$\boldsymbol{\varepsilon_{s0}}$	$[-]$	0.27	0.20
The following parameters are only used for the *Combined Model*:			
$\boldsymbol{n_{frac}}$	$[-]$	100^{**}	100^{**}
$\boldsymbol{\gamma}$	$[-]$	0/ 0.5 **	0/ 0.5 **
$\boldsymbol{\lambda_0}$	$[m^{-1}]$	100	100^{**}
$\boldsymbol{\lambda_c}$	$[-]$	5	5^{**}

Declaration of Competing Interest

The authors declare that they have no known competing financial interests or personal relationships that could have appeared to influence the work reported in this paper.

Acknowledgments

We thank Joaquín Steinhäuser, Master's student of our group (Chair of Process Systems Engineering, Technical University of Munich), for obtaining preliminary results that lead to the final success of this work. Moreover, we thank Diana Neuber and Prof. Urs Peuker (Institute of Mechanical Process Engineering and Mineral Processing, University of Freiberg), as well as Peter Michael Bandelt-Riess of our group for valuable input and beneficial discussions on the experimental side of filter aid filtration processes. This work was supported by the German Federal Ministry for Economic Affairs and Climate Action (via AiF and DECHEMA), IGF-Project No. 19947 BG.

Appendix A. Model parameters

The following parameters were used in this study (see Table A1). Simulation parameters are adapted from Ref. [Tien, 2006, p. 70; 87].

Parameters indicated with * do not correspond to the original value. These parameters are contained in Eq. (12), which is not part of the original models. We adjusted the parameter values with a focus on keeping the model simulations in realistic ranges of filtration pressure and solidosity. Parameters indicated with ** are based on assumptions. We emphasize that the parameter values do not correspond to real experimental set-ups and are only used to represent qualitative behavior of different degrees of filter cake compressibility.

Appendix B. Numerical transformations

The front fixing method (Crank, 1984) is used to define the height coordinates of time-dependent system boundaries in the ranges of $z = 0$ to $z = 1$ by applying the following relationship:

$$z = \frac{x}{L}. \tag{B-1}$$

Conversion of the governing partial differential equations is achieved by the transformations Eq. (B-2) and Eq. (B-3). Here, the $\wedge$-symbol denotes quantities in the fixed coordinate system.

$$\frac{\partial f}{\partial x} = \frac{1}{L}\frac{\partial \widehat{f}}{\partial z} \tag{B-2}$$

$$\frac{\partial f}{\partial t} = \frac{\partial \widehat{f}}{\partial t} - \frac{z}{L}\frac{dL}{dt}\frac{\partial \widehat{f}}{\partial z} \tag{B-3}$$

The following relationships were used to eliminate dimensions:

$$\widetilde{c} = \frac{c}{\varepsilon_{s0}} \tag{B-4}$$

$$\widetilde{k} = \frac{k}{k_0} \tag{B-5}$$

$$\widetilde{k}_{init} = \frac{k_{init}}{k_0} \tag{B-6}$$

$$\widetilde{L} = \frac{L}{L^*_{ref}} \tag{B-7}$$

$$\widetilde{n} = \frac{n}{\varepsilon_{s0}} \tag{B-8}$$

$$\widetilde{n}_0 = \frac{n_0}{\varepsilon_{s0}} \tag{B-9}$$

$$\widetilde{N} = \frac{NL^*_{ref}}{|q_{lm}|} \tag{B-10}$$

$$\widetilde{p}_a = \frac{p_a k_0}{|q_{lm}|\mu L^*_{ref}} \tag{B-11}$$

$$\widetilde{p}_l = \frac{p_l k_0}{|q_{lm}|\mu L^*_{ref}} \tag{B-12}$$

$$\widetilde{p}_s = \frac{p_s k_0}{|q_{lm}|\mu L^*_{ref}} \tag{B-13}$$

$$\widetilde{q}_l = \frac{q_l}{|q_{lm}|\varepsilon_{s0}} \tag{B-14}$$

$$\widetilde{q}_{lm} = \frac{q_{lm}}{|q_{lm}|\varepsilon_{s0}} = -\frac{1}{\varepsilon_{s0}} \tag{B-15}$$

$$\widetilde{q}_s = \frac{q_s}{|q_{lm}|\varepsilon_{s0}} \tag{B-16}$$

$$\widetilde{R}_m = \frac{R_M k_0}{L^*_{ref}} \tag{B-17}$$

$$\widetilde{t} = \frac{t|q_{lm}|}{L^*_{ref}} \tag{B-18}$$

$$\widetilde{u} = \frac{uL^*_{ref}}{\varepsilon_{s0} q_{lm}} \tag{B-19}$$

$$\widetilde{x} = \frac{x}{L^*_{ref}} \tag{B-20}$$

$$\widetilde{\varepsilon}_s = \frac{\varepsilon_s}{\varepsilon_{s0}} \tag{B-21}$$

$$\widetilde{\varepsilon}_{s2} = \frac{\varepsilon_{s2}}{\varepsilon_{s0}} \tag{B-22}$$

$$\widetilde{\lambda} = \frac{\lambda}{\lambda_0} \tag{B-23}$$

[3]

After minor rearrangements, the resulting system of equations for the *Surface Filtration Model* reads as follows. Note that all quantities are already transformed into the fixed coordinate system, but the $\wedge$-symbols are omitted for readability. The integral term in equation Eq. (2) from the main text can be approximated as the mean value $\overline{\widetilde{\varepsilon}}_s$ due to the equidistant mesh used to discretize the governing equations. Moreover, Eq. (3) from the main text was transformed into the form of Eq. (B-26), which describes the dynamic variation of the filter aid concentration as an ordinary differential equation. This transformation does not alter the model structure. Initially introduced linear functions can be represented by setting the right-hand side of Eq. (B-26) to a constant value and accordingly selecting an initial value $\widetilde{c}(t = 0)$ for said equation.

[3] $L^*_{ref} = L(t = 1s)$ according to Eq. 27 for the *Surface Filtration* Model $L^*_{ref} = L_{PC}$; for the *Combined Model*.

Constant filter aid dosages as required for the static optimization are obtained by setting $\tilde{u}\left(\tilde{t}\right) = 0$. Then, the initial value $\tilde{c}(t = 0)$ becomes the process-defining uniform filter aid dosage. Compared with the original form, the implementation of the transformed equation into the combined numerical optimization and integration procedure proved to be simpler, and we noticed a small improvement in the convergence properties.

$$\frac{\partial \tilde{\varepsilon}_s}{\partial \tilde{t}} = \frac{1}{\tilde{L}^2}\frac{\partial}{\partial z}\left(-\tilde{\varepsilon}_s \tilde{k}\frac{\partial \tilde{p}_s}{\partial z}\right) + \frac{1}{\tilde{L}}\left(1 + z\frac{d\tilde{L}}{d\tilde{t}}\right)\frac{\partial \tilde{\varepsilon}_s}{\partial z} \tag{B-24}$$

$$\frac{d\tilde{L}}{d\tilde{t}} = \frac{\tilde{c}}{\bar{\tilde{\varepsilon}}_s - \tilde{c}} \tag{B-25}$$

$$\frac{d\tilde{c}}{d\tilde{t}} = \tilde{u}\left(\tilde{t}\right) \tag{B-26}$$

$$\frac{d\tilde{\varepsilon}_{s2}}{d\tilde{t}} = \frac{1}{\tilde{L}}\frac{\partial \tilde{\varepsilon}_{s2}}{\partial z} \tag{B-27}$$

$$at\left(\tilde{t}, z = 0\right) : \frac{\tilde{k}}{\tilde{L}}\frac{\partial \tilde{p}_l}{\partial z} = 1 = \frac{\tilde{p}_l}{\tilde{R}_M} \tag{B-28}$$

$$at\left(\tilde{t}, z = 1\right) : \tilde{\varepsilon}_s = 1 \tag{B-29}$$

$$at\left(\tilde{t}, z = 1\right) : \tilde{\varepsilon}_{s2} = \frac{\tilde{\varepsilon}_s \tilde{n}_0}{\tilde{c}} \tag{B-30}$$

$$\tilde{p}_s = \tilde{p}_a\left(\tilde{\varepsilon}_s^{\frac{1}{\beta}} - 1\right) \tag{B-31}$$

$$\tilde{k}_{init} = e^{-s\cdot\tilde{\varepsilon}_{s2}} \tag{B-32}$$

$$\tilde{k} = \tilde{k}_{init}\cdot\tilde{\varepsilon}_s^{-\frac{\delta}{\beta}} \tag{B-33}$$

Similarly, for the *Combined Model*, we obtain the following:

$$\frac{\partial \tilde{\varepsilon}_s}{\partial \tilde{t}} = \frac{\partial \tilde{q}_l}{\partial z} + \frac{z}{\tilde{L}}\frac{d\tilde{L}}{d\tilde{t}}\frac{\partial \tilde{\varepsilon}_s}{\partial z} \tag{B-34}$$

$$\frac{\partial \tilde{\varepsilon}_{s2}}{\partial \tilde{t}} = -\frac{\partial \tilde{q}_s \tilde{\varepsilon}_{s2}}{\partial z} + \frac{\tilde{N}}{\varepsilon_{s0}} + \frac{z}{\tilde{L}}\frac{d\tilde{L}}{d\tilde{t}}\frac{\partial \tilde{\varepsilon}_{s2}}{\partial z} \tag{B-35}$$

$$\frac{\partial \tilde{n}}{\partial \tilde{t}} = \frac{1}{1 - \varepsilon_{s0}\tilde{\varepsilon}_s}\left(\epsilon_{s0}\left(\frac{\partial \tilde{\varepsilon}_s}{\partial \tilde{t}} - \frac{z}{\tilde{L}}\frac{d\tilde{L}}{d\tilde{t}}\frac{\partial \tilde{\varepsilon}_s}{\partial z}\right)\tilde{n} - \frac{1}{\tilde{L}}\varepsilon_{s0}\frac{\partial \tilde{q}_l \tilde{n}}{\partial z} - \frac{\tilde{N}}{\varepsilon_{s0}}\right) + \frac{z}{\tilde{L}}\frac{d\tilde{L}}{d\tilde{t}}\frac{\partial \tilde{n}}{\partial z} \tag{B-36}$$

$$\frac{d\tilde{L}}{d\tilde{t}} = \frac{\tilde{c}}{\bar{\tilde{\varepsilon}}_s - \tilde{c}} \tag{B-37}$$

$$\frac{d\tilde{c}}{d\tilde{t}} = \tilde{u}\left(\tilde{t}\right) \tag{B-38}$$

$$at\left(\tilde{t}, z = 0\right) : \frac{\tilde{k}}{\tilde{L}}\frac{\partial \tilde{p}_l}{\partial z} = 1 = \frac{\tilde{p}_l}{\tilde{R}_M} \tag{B-39}$$

$$at\left(\tilde{t}, z = 1\right) : \tilde{\varepsilon}_s = 1 \tag{B-40}$$

$$at\left(\tilde{t}, z = 1\right) : \tilde{\varepsilon}_{s2} = \frac{\tilde{\varepsilon}_s \gamma \tilde{n}_0}{\tilde{c}} \tag{B-41}$$

$$at\left(\tilde{t}, z = 1\right) : \tilde{n} = (1 - \gamma)\tilde{n}_0 \tag{B-42}$$

$$\tilde{q}_l = \frac{1}{\tilde{L}}\left(-\tilde{\varepsilon}_s \tilde{k}\frac{\partial \tilde{p}_l}{\partial z}\right) - \left(\frac{1}{\varepsilon_{s0}} - \tilde{\varepsilon}_s\right)\left(1 + \tilde{L}\int_0^z \tilde{N} dz\right) \tag{B-43}$$

$$\tilde{q}_s = \frac{1}{\tilde{L}}\left(\tilde{\varepsilon}_s \tilde{k}\frac{\partial \tilde{p}_l}{\partial z}\right) - \tilde{\varepsilon}_s\left(1 - \tilde{L}\int_0^z \tilde{N} dz\right) \tag{B-44}$$

$$\tilde{N} = \left(\tilde{q}_l - \tilde{q}_s\left(\frac{1 - \varepsilon_{s0}\tilde{\varepsilon}_s}{\varepsilon_{s0}\tilde{\varepsilon}_s}\right)\right)L^*_{ref}\lambda_0 \tilde{\lambda}\varepsilon_{s0}^2 \tilde{n} \tag{B-45}$$

$$\tilde{\lambda} = 1 + \left(\frac{\lambda_c \varepsilon_{s0}\tilde{\varepsilon}_{s2}}{1 - \varepsilon_s \tilde{\varepsilon}_{s2}}\right) \tag{B-46}$$

$$\tilde{p}_s = p_a\left(\tilde{\varepsilon}_s^{\frac{1}{\beta}} - 1\right) \tag{B-47}$$

$$\tilde{k}_{init} = e^{-s\cdot\tilde{\varepsilon}_{s2}} \tag{B-48}$$

$$\tilde{k} = \tilde{k}_{init}\cdot\tilde{\varepsilon}_s^{-\frac{\delta}{\beta}} \tag{B-49}$$

Note that the dynamic viscosity μ is eliminated from all governing equations by the shrewd selection of nondimensionalization relationships.

References

Alles, C.M., 2000. Prozeßstrategien für die Filtration mit kompressiblen Kuchen. Ph.D. thesis. Universität Fridericiana Karlsruhe (TH), Fakultät für Chemieingenieurwesen und Verfahrenstechnik.

Bennet, K., 2000. Precoat filtration, Filtration Separation 37 (3), 32–33, 4.

Berndt, R., 1981. Zur Prozessmodellierung der Filtration von Suspensionen unter besonderer Berücksichtigung der Anschwemmfiltration. Ph.D. thesis. Technische Universität Dresden.

Betts, J.T., 2010. Practical Methods for Optimal Control and Estimation Using Nonlinear Programming. Society for Industrial and Applied Mathematics, Philadelphia.

Blankert, B., Betlem, B.H.L., Roffel, B., 2006. Dynamic optimization of a dead-end filtration trajectory: Blocking filtration laws. J. Membr. Sci. 285 (1–2), 90–95.

Blankert, B., Kattenbelt, C., Betlem, B.H.L., Roffel, B., 2007. Dynamic optimization of a dead-end filtration trajectory: non-ideal cake filtration. J. Membr. Sci. 290 (1–2), 114–124.

Bluemelhuber, G., 2007. Kieselgurfilter-Schlämme? Entsorgungsprobleme? Brauwelt 147, 757–760.

Braun, F., Becker, T., Back, W., Krottenthaler, M., 2010. Investigation of beer filtration using cellulose fibers in a pilot-scale filter plant. J. Am. Soc. Brew. Chem. 68 (3), 139–147.

Braun, F.H., 2012. Auswirkungen des Einsatzes von Zellulose als Filterhilfsmittel in der Bierfiltration. Ph.D. thesis. Technische Universität München, Fakultät Wissenschaftszentrum Weihenstephan für Ernährung, Landnutzung und Umwelt, Lehrstuhl für Technologie der Brau und Getränkeindustrie.

Buttrick, P., 2007. Filtration – the facts. Brewer & Distiller Int. 3 (12), 12–19.

Carman, P.C., 1938. The action of filter aids. Ind. Eng. Chem. 30 (10), 1163–1167.

Coote, N., 1999. Turning the art of filter-aid filtration into a science. In: Höflinger, W. (Ed.), International Symposium: Filtration and Separation of Fine Particle Suspensions, Proceedings. Austrian Chemical Society, Vienna, pp. 315–328.

Crank, J., 1984. Free and Moving Boundary Problems. Oxford University Press, Oxford.

Gasper, H., Oechsle, D., Pongratz, E., 2000. Handbuch der industriellen Fest/Flüssig-Filtration. Wiley-VCH, Weinheim.

Haba, J., Koch, R., 1978b. Analyse des Filtrationsprozesses unter Einsatz von Filterhilfsmitteln. Chem. Tech. (Leipzig) 30 (2), 91–94.

Hebmüller, F., 2003. Einflussfaktoren auf die Kieselgurfiltration von Bier. Ph.D. thesis. Technische Universität Bergakademie Freiberg, Fakultät für Maschinenbau, Verfahrens- und Energietechnik.

Heertjes, P.M., Zuideveld, P.L., 1978a. Clarification of liquids using filter aids Part III. Cake Resistance in surface filtration. Powder Technol. 19 (1), 45–64.

Heertjes, P.M., Zuideveld, P.L., 1978b. Clarification of liquids using filter aids Part I. Mechanisms of filtration. Powder Technol. 19 (1), 17–30.

Heertjes, P.M., Zuideveld, P.L., 1978c. Clarification of liquids using filter aids Part II. Depth filtration. Powder Technol. 19 (1), 31–43.

Heidenreich, E., Tittel, R., Gorner, R., 1985. Rechnergestützte optimale Filterhilfsmitteldosierung für die Anschwemmfiltration. Chem. Tech. (Leipzig) 37 (2), 57–60.

Hunt, T., 2010. Filter aids. In: Flickinger, M.C. (Ed.), Encyclopedia of Industrial Biotechnology: Bioprocess, Bioseparation, and Cell Technology. John Wiley & Sons, Hoboken, pp. 1190–1197.

Husemann, K., Hebmüller, F., Esslinger, M., 2003. Importance of deep bed filtration during kieselguhr filtration (Part 2). Monatsschrift für Brauwissenschaft 56 (9–10), 152–160.
Iliev, O., Kirsch, R., Osterroth, S., 2018. Combined depth and cake filtration model coupled with flow simulation for flat and pleated filters. Chem. Eng. Technol. 41 (1), 70–78.
Kuhn, M., Briesen, H., 2015. Dosage of filter aids in the case of pure surface filtration – an optimal control approach. Comput. Aided Chem. Eng. 37, 1655–1660.
Kuhn, M., Briesen, H., 2016. Dynamic modeling of filter-aid filtration including surface- and depth-filtration effects. Chem. Eng. Technol. 39 (3), 425–434.
Kuhn, M., Briesen, H., 2021. Optimizing the axial resistance profile of submerged hollow fiber membranes. Processes 9 (1), 20.
Kuhn, M., Pietsch, W., Briesen, H., 2017. Clarifying thoughts about the clarification of liquids - filtration and the philosophy of science. Chem. Ing. Tech. 89 (9), 1126–1132.
Kuhn, M., Kirse, C., Briesen, H., 2017. Improving the design of depth filters: a model-based method using optimal control theory. AIChE J. 64 (1), 68–76.
Kuhn, M., 2018. New Paths in Filtration - Optimal Control Approaches Based on Continuum Models. Ph.D. thesis, Technische Universität München, Wissenschaftszentrum Weihenstephan für Ernährung, Landnutzung und Umwelt, Lehrstuhl für Systemverfahrenstechnik.
Lewis, F.L., Vrabie, D.L., Syrmos, V.L., 2012. Optimal Control. John Wiley & Sons, Hoboken.
Luckert, K., 2004. Handbuch der mechanischen Fest-Flüssig-Trennung. Vulkan Verlag, Essen.
Osterroth, S., 2018. Mathematical Models for the Simulation of Combined Depth and Cake Filtration Processes. Ph.D. thesis. Technische Universität Kaiserslautern, Fachbereich Mathematik, Fraunhofer-Institut für Techno- und Wirtschaftsmathematik ITWM.
Rettenmaier & Söhne, J. "Why Cellulose Filter Aids? 2022. [Online]. Available from: <https://www.jrs.eu/jrs_en/fiber-solutions/bu-filtration/why-organic-filter-aids/>. [Accessed 21 01 2022].
Rushton, A. (Ed.), 1985. Mathematical Models and Design Methods in Solid-Liquid Separation. Springer Netherlands, Dordrecht.
Schiesser, W.E., Griffiths, G.W., 2009. A Compendium of Partial Differential Equation Models: Method of Lines Analysis with Matlab. Cambridge University Press, Cambridge.
Sørensen, P.B., Moldrup, P., Hansen, J., 1996. Filtration and expression of compressible cakes. Chem. Eng. Sci. 51 (6), 967–979.
Stamatakis, K., Tien, C., 1991. Cake formation and growth in cake filtration. Chem. Eng. Sci. 46 (8), 1917–1933.
Sutherland, D.H., Hidi, P., 1966. An investigation of filter-aid behaviour. Trans. Inst. Chem. Eng. 44 (4), T122–T127.
The MathWorks, Inc., Floating-point relative accuracy. [Online]. Available from: <https://de.mathworks.com/help/matlab/ref/eps.html>. [Accessed 03 02 2022].
Tien, C., 2006. Introduction to Cake Filtration. Elsevier B. V, Amsterdam.
Tien, C., Bai, R.B., Ramarao, B.V., 1997. Analysis of cake growth in cake filtration: effect of fine particle retention. AIChE J. 43 (1), 33–44.
Tien, C., Teoh, S.K., Tan, R.B.H., 2001. Cake filtration analysis - the effect of the relationship between the pore liquid pressure and the cake compressive stress. Chem. Eng. Sci. 56, 5361–5369.
Tiller, F.M., Green, T.C., 1973. Role of porosity in filtration IX skin effect with highly compressible materials. AIChE J. 19 (6), 1266–1269.
Tittel, R., 1987. Die Anschwemmfiltration als ein Prozess zur Klärung von Flüssigkeiten. Ph.D. thesis, Technische Universität Dresden, Sektion Verarbeituns- und Verfahrenstechnik.
Wegner, K., 1985. Hydrodynamische Modellierung der Klärfiltration mit körnigen Stoffen unter besonderer Berücksichtigung der Anschwemmfiltration mit Schichtzunahme. Ph.D. thesis. Technische Universität Dresden, Fakultät für Maschinenwesen.
World Health Organization International Agency for Research on Cancer, 1997. IARC monographs on the evaluation of carcinogenic risks to humans, Vol. 68: Silica, Some Silicates, Coal Dustand para-Aramid Fibrils, Lyon: IARC..
Wouwer, A.V., Saucez, P., Vilas, C., 2014. Simulation of ODE/PDE Models with MATLAB®, OCTAVE and SCILAB. Springer, Cham.
Zamani, A., Maini, B., 2009. Flow of dispersed particles through porous media - deep bed filtration. J. Petrol. Sci. Eng. 69 (1–2), 71–88.

Glossary

Roman letters

c: filter aid concentration in suspension [-]
c_{η_i}: discretized filter aid concentration in suspension [-]
f: arbitrary function; Appendix only [-]
i: current iteration of mesh refinement [-]
e: area-specific energy consumption [J/m^{-2}]
k: permeability of filter cake; compressed [m^2]
k_0: permeability of pure filter aid; uncompressed [m^2]
k_{init}: permeability of filter cake; uncompressed [m^2]
L: filter cake height [m]
L_{PC}: filter cake height; precoat stage [m]
n: impurity concentration in suspension [-]
n_0: initial impurity concentration in suspension [-]
n_{frac}: maximum fraction of n_0 allowed in the filtrate [-]
N: rate of deposition for impurities [s^{-1}]
p_0: process pressure [Pa]
p_a: empirical compression parameter [Pa]
p_l: liquid pore pressure [Pa]
p_s: compressive stress acting on solid phase [Pa]
q_l: superficial flow rate of liquid phase [m/s]
q_{lm}: superficial flow rate of liquid phase at filter medium [m/s]
q_s: superficial flow rate of solid phase [m/s]
R_M: filter medium resistance [m^{-1}]
s: empirical Sutherland parameter [-]
t: Time [s]
T: simulation time span [s]
u: filter aid dosage control function [s^{-1}]
$\boldsymbol{u_p}$: vector of control parameters [*variable*]
$\boldsymbol{u_{\eta_i,p}}$: vector of control parameters associated to discretization set η_i [*variable*]
V_c: area-specific filter aid consumption [m]
V: area-specific filtrate volume [m]
x: height coordinate [m]
z: height coordinate treated by front fixing method [-]

Greek letters

β: empirical compression parameter [-]
δ: empirical compression parameter [-]
ε: porosity [-]
ε_s: solidosity [-]
ε_{s0}: solidosity; uncompressed [-]
ε_{s2}: impurity deposition [-]
γ: fraction of impurities separated by surface filtration [-]
λ: filter coefficient [m^{-1}]
λ_0: initial filter coefficient [m^{-1}]
λ_c: empirical filter coefficient parameter [-]
η_i: number of subintervals at iteration i [-]
μ: dynamic viscosity [Pa·s]

Accents

$\bar{\ }$: mean values; Appendix only
$\wedge$: quantities treated by front fixing method; Appendix only
$\sim$: nondimensional variables; Appendix only
$*$: adjusted parameter value; Appendix only

Full-Length Paper III

Reduced order modeling for compressible cake filtration processes using proper orthogonal decomposition

Pergam, Philip; Briesen, Heiko

Computers & Chemical Engineering, Volume 171, 2023, 108165

DOI: 10.1016/j.compchemeng.2023.108165

Copyright

© 2023 Computers & Chemical Engineering, published by Elsevier Ltd. All rights reserved.

Reprinted by permission of Elsevier for use in the author's dissertation. Individual licensing is not required.
https://www.elsevier.com/about/policies/copyright#Author-rights

CRediT

- Philip Pergam: Conceptualization, Methodology, Software, Writing - Original Draft
- Heiko Briesen: Conceptualization, Writing - Review & Editing, Supervision, Funding acquisition

Computers and Chemical Engineering 171 (2023) 108165

Contents lists available at ScienceDirect

Computers and Chemical Engineering

journal homepage: www.elsevier.com/locate/compchemeng

Reduced order modeling for compressible cake filtration processes using proper orthogonal decomposition

Philip Pergam, Heiko Briesen *

Process Systems Engineering, School of Life Sciences, Technical University of Munich, Gregor-Mendel-Str. 4, Freising 85354, Germany

ARTICLE INFO

Keywords:
Model order reduction
Proper orthogonal decomposition (POD)
Flow through porous media
Filtration
Simulation
Optimization

ABSTRACT

This work aims to increase the computational efficiency of a complex mathematical cake-filtration model with strong nonlinearities representing cake compression. To this end, we employ a hybrid data driven approach using the technique of proper orthogonal decomposition. Hereby, a few sample simulations from the initial system of partial differential equations are used as the foundation to find optimal, globally defined basis functions, which in return offer the possibility to build a reduced-order model. In summary, the dimension of the reduced order model is diminished by ≈98% compared to the full order model, which translates to a net decrease of ≈90 % computational time needed to solve a benchmark optimization problem. This significant numerical speed-up offers the possibility to use the reduced order model in further advanced process control and optimization methods.

1. Introduction

During recent decades, mathematical models have gained significant momentum as a tool in various engineering disciplines. More specifically, in the area of process systems engineering, the respective model simulations may serve as a basis for process design, process optimization, and process control (Kuhn and Briesen, 2019; Stephanopoulos, 2009). Especially for the latter two applications, the simulation algorithms are subject to computational time constraints since the models must be evaluated repeatedly. However, even though computational capabilities are increasing continuously, non-linear, high dimensional, and/or multi-scale models might still be demanding to solve in reasonable time spans (Geerling et al., 2019; Biegler et al., 2014), potentially rendering above applications infeasible for certain problems at the current time.

We in fact encountered such computational cost restrictions in a recent study, where we employed an optimal control algorithm for different compressible cake filtration models (Pergam et al., 2022). The calculation time took up to a day for some of the evaluated scenarios due to the complexity of the underlying non-linear partial differential equations. For our past work, this was merely an economic issue. Nonetheless, it is impossible to use the mathematical models as a basis for e.g., cyber-physical systems in process monitoring (Hoffmann et al., 2021) or closed-loop model predictive control approaches (Grüne and Pannek, 2011), since the simulations must fulfill real-time requirements here. This motivates our efforts in implementing numerical techniques to significantly reduce the computational cost of said mathematical problems.

In recent years, data-driven surrogate modeling approaches are more and more focused on by researchers in the area of process engineering to solve previously mentioned problem. Some of these techniques include the application of, e.g., sparse identification of nonlinear dynamics (SINDy) in combination with machine learning (Bhadriraju et al., 2019), physics-informed neural networks (Cai et al., 2021), combining mechanistic and data-based methods as hybrid modeling techniques (often referred to "grey box" models) (Zendehboudi et al., 2018), or linear modelling concepts from control theory, such as Koopman operators (Narasingam and Kwon, 2020). Another possible data-driven approach is projection-based model order reduction (MOR) (Baur et al., 2014). Several of such MOR approaches, such as Rational Interpolation and Balanced Truncation, have been described in the literature (see e.g., (Benner et al., 2015)). We will, however, focus on global dimensional reduction of the underlying compressive cake filtration model by the technique of proper orthogonal decomposition (POD) (Liang et al., 2002; Chatterjee, 2000) during the course of this work. So far, POD based reduced order models (ROM) have been applied widely in many engineering applications, e.g., in the analysis of turbulent fluid flows (Berkooz et al., 1993; Smith et al., 2005), aerodynamics (Bui-Thanh

* Corresponding author.
E-mail address: heiko.briesen@tum.de (H. Briesen).

https://doi.org/10.1016/j.compchemeng.2023.108165
Received 6 December 2022; Received in revised form 17 January 2023; Accepted 3 February 2023
Available online 5 February 2023
0098-1354/© 2023 Elsevier Ltd. All rights reserved.

et al., 2004; Bui-Thanh et al., 2003; Hall et al., 2000), mechanical systems (Lu et al., 2019; Kerschen et al., 2005), process engineering (Bremer et al., 2017; Marquardt, 2002; Ly and Tran, 2002; Nguyen et al., 2020), and population balance modeling (Feng et al., 2017; Khlopov and Mangold, 2016; Khlopov and Mangold, 2016; Khlopov and Mangold, 2015; Krasnyk et al., 2012) to name a few. Nevertheless, POD methods – as well as MOR in general – have merely found sparse recognition in the research area of solid-liquid separation. To the best of our knowledge, only Osterroth et al. (2017) made use of a ROM for a linear incompressible cake filtration process. Depending on the scenario, they managed to reduce the computational cost by up to 90-95 % enabling the model simulation to be viable for extensive parameter studies. In a broader context, however, filtration can also be interpreted as a problem of fluid flow through porous media for which POD had been introduced before (Ghasemi and Gildin, 2016; Ghasemi, 2015; Ghasemi and Gildin, 2015; Alotaibi et al., 2015; Gildin et al., 2013; Li and Hu, 2012). Therefore, more applications from related research areas, such as viscous fingering (Chaturantabut and Sorensen, 2011), reservoir engineering (Wang et al., 2018; Heijn et al., 2004), and groundwater flow (Dey and Dhar, 2020; Winton et al., 2011; Siade et al., 2010; Vermeulen et al., 2006) can be found. Moreover, the here to be investigated cake filtration models are categorized as mathematical moving- or free-boundary problems. In this context, some POD frameworks (Hinze et al., 2014; Utturkar et al., 2005; Sidhu et al., 2018), and applications for, e.g., phase-field problems (Redeker and Haasdonk, 2014; López-Quiroga, 2018; Volkwein, 2001) exist. When the previously mentioned studies included information on numerical efficiency, the respective elapsed simulation time was reduced significantly by up to 1–3 magnitudes, i.e., computational speed increases: ≈2.5 × in López-Quiroga (2018); ≈13 × in Li and Hu (2012); ≈45 × in Ghasemi and Gildin (2016); ≈230 × for Wang et al. (2018); ≈500 × for Dey and Dhar (2020); ≈700 × for Chaturantabut and Sorensen (2011); ≈1250 × for Volkwein (2001), while retaining sufficiently detailed solution features of the dynamic full order models (FOM).

Previously mentioned numbers support our hypothesis of POD based MOR being a suitable tool to enable our computationally expensive model for use in advanced process control methods with real-time requirements. This does not only expand the POD applications in the area of moving boundary problems, but also is the first application for compressible cake filtration processes. Hereby, the effect of compressibility induces exponential non-linearities to the governing model equations. It is therefore not clear *a priori* what benefits a derived ROM yields, especially compared to those of a linear cake filtration ROM. Moreover, in the context of solid-liquid separation processes, it is not clear how the proposed ROM of the underlying moving boundary problem performs in combination with an optimization framework. Hence, we will first review the complex non-linear mathematical model in the following sections. Subsequently, we will present a short overview of the POD method and how it can be used to obtain a ROM representing the dynamics of the FOM. Finally, we will solve an optimization problem as a benchmark for both, the FOM and the ROM, in order to examine the computational cost benefits.

2. Methods

Since this work is a numerical study, we will focus on mathematical methods for evaluating the process of dead-end cake filtration (Tien, 2006). Hereby, a pressure gradient causes the perpendicular flow of an impure suspension through a filter medium. While the liquid phase exits the apparatus as the filtrate, the solid phase is accumulated on top of said filter medium. The so-called filter cake increases in height during the course of the process, which further enhances the efficiency of fine-particle separation, but also increases the overall filter resistance over time. Ideally, the filter cake is approximatively incompressible, i.e., the characteristic quantities are independent of a growing filtration pressure that is needed to maintain a constant volumetric flow rate. However, in many applications, the aggregated solids are compressible due to particle deformation, breakage, rearrangement, or other morphological effects causing an inefficient exponential decrease in permeability (Alles and Anlauf, 2003; Alles, 2000). Further general information on the physical properties of cake filtration can be found in various textbooks, e.g., (Tien, 2006; Tarleton and Wakeman, 2007; Wakeman and Tarleton, 1999).

2.1. Full order cake filtration model

The model to be studied is based on a continuum-scale approach introduced by Stamatakis and Tien in 1991 (Stamatakis and Tien, 1991). Its foundation is the well-known continuity equation of liquid flow through porous media:

$$\frac{\partial \varepsilon_s}{\partial t} = \frac{\partial q_l}{\partial x} \tag{1}$$

Hereby, partial differential Eq. (1) describes the spatiotemporal development of solidosity[1] ε_s depending on the non-linear liquid phase's superficial velocity q_l, which offers further information about the system quantities on the time and space domain t and x. The original paper presents more like a framework for general compressible cake filtration processes and describes the mathematical derivation in detail. In the following, however, we will focus on compressible *filter aid* cake filtration processes. As the name suggests, filter aid materials, such as kieselguhr or cellulose, are added to the suspension in order to increase the process efficiency of hard-to-handle suspensions (Bennet, 2000; Gasper, 2000). This is a special case of cake filtration with two highly

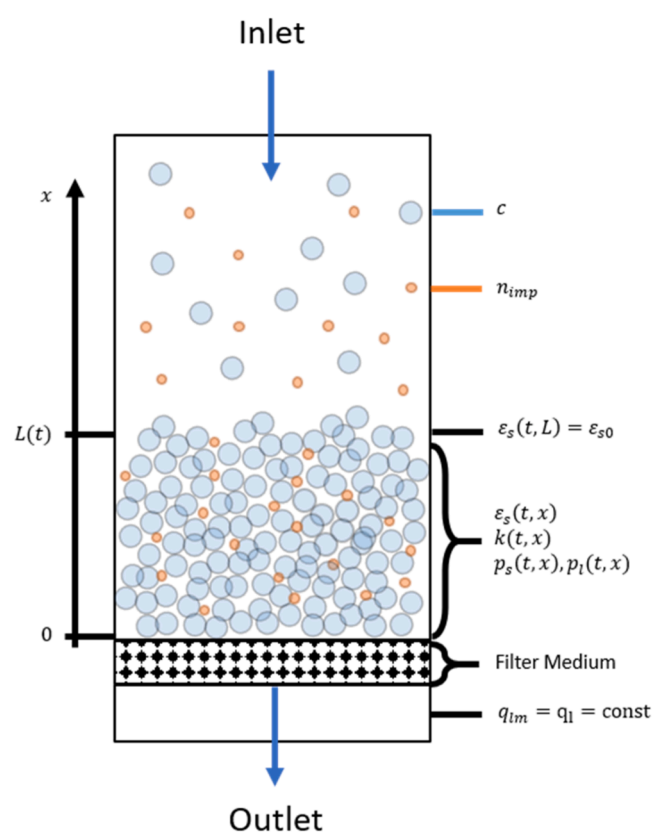

Fig. 1. Schematic representation of the filter aid Filtration Model. Adapted from (Pergam et al., 2022).

[1] The information content of the solidosity is equal to the more commonly used quantity porosity ε using the relationship $\varepsilon = 1 - \varepsilon_s$.

distinctive particle fractions offering the benchmark optimization problem of finding the ideal filter aid dosage (see Section 2.4 Optimization). Notably, all of our findings can be easily adapted to enable theoretical investigation of further case studies on general compressible filter cakes without filter aids.

With Eq. (1) being the mechanistic foundation, the final adapted system of partial differential equations can be obtained after a number of derivations and rearrangements found in (Pergam et al., 2022). To further facilitate the understanding of the cake filtration process, a schematic of the process is given in Fig. 1. All system states and the corresponding boundary conditions used by the mathematical model are marked in the graphic.

The resulting mathematical model to represent compressible filter aid cake filtration processes reads as follows:

$$\frac{\partial \varepsilon_s}{\partial t} = \frac{1}{L}\frac{\partial q_l}{\partial z} + \frac{z}{L}\frac{\mathrm{d}L}{\mathrm{d}t}\frac{\partial \varepsilon_s}{\partial z} \tag{2}$$

$$q_l = \frac{1}{L}\left(-\varepsilon_s k \frac{\partial p_s}{\partial z}\right) - \left(\frac{1}{\varepsilon_s^*} - \varepsilon_s\right) \tag{3}$$

$$\frac{dp_l}{dp_s} = -1 \tag{4}$$

$$p_s = p_a\left(\varepsilon_s^{\frac{1}{\beta}} - 1\right) \tag{5}$$

$$k = k_{init} \cdot \varepsilon_s^{-\frac{\delta}{\beta}} \tag{6}$$

$$k_{init} = \exp\left(-s\frac{\varepsilon_s^* n_{imp}}{c}\right) \tag{7}$$

The governing relationship (2) is defined by the superficial fluid velocity $q_l(t,z)$, which is calculated using the non-linear Eq. (3). Here, $k(t,z)$ denotes the permeability and $p_s(t,z)$ is the solid stress acting on the filter cake, which ultimately leads to an increasing solidosity $\varepsilon_s(t,z)$. Thereby, the compressive behavior for the material system is defined by the closing relationships Eqs. (5) and (6). Moreover, the solid stress is directly correlated to the liquid pore pressure $p_l(t,z)$ via Eq. (4). Since permeability is not only affected by compression but also by the volumetric concentration-ratio of filter aids c to impurities n_{im}, the additional constitutive relationship (7), often referred to as Sutherland law (Sutherland and Hidi, 1966), defines the initial permeability at an uncompressed state.

The second system state, i.e., filter cake height over time $L(t)$, is described by the following growth rate:

$$\frac{dL}{dt} = \frac{c}{\overline{\varepsilon_s} - c} \tag{8}$$

Hereby, Eq. (8), is dependent on the cake's time-dependent space-averaged solidosity $\overline{\varepsilon_s}$, as well as the supplied volumetric filter aid concentration c in the suspension. Notably, c is also the control parameter that may be adjusted by the optimization procedure.

All empirical model parameters, β, ε_s^*, δ, p_a and s must be determined from experimental data. Finally, using ε_{s0} as the uncompressed solidosity of the filter cake and setting q_{lm} as the constant superficial filtrate velocity at the filter outlet, the appropriate initial and boundary conditions read:

$$\text{for } (t=0,z): \ \varepsilon_s = \varepsilon_{s0} \quad L = 1 \tag{9}$$

$$\text{at } (t, z=0): \ q_l = q_{lm} \tag{10}$$

$$\text{at } (t, z=1): \ \varepsilon_s = \varepsilon_{s0} \tag{11}$$

Since we already introduced the FOM in detail in Pergam et al. (2022), we will omit a further analysis and discussion of the model equations here. We will only briefly explain some important numerical aspects in the following.

Note that the upper system boundary (height $L(t)$) is time dependent due to the cake growth rate defined by Eq. (8), which classifies the filtration model as a moving boundary problem. Therefore, the initial spatial dimension x has been treated by the front-fixing method[2] (Tayler, 1985). The resulting governing relationship in Eq. (2) is thus not defined on x, but depends on z. Hereby, z spans a new alternate coordinate system from 0 to 1 for each time step t.

Moreover, the complete mathematical model defined in Eq. (2) to (7) is given in a non-dimensionalized formulation. Mathematically, using non-dimensionalization offers two main advantages:

1. Since non-dimensionalization is based on process-inherent scaling of variables, highly different orders of magnitude in quantities may be reduced such that they are numerically easier to handle. We noticed that convergence properties significantly improved with the introduction of non-dimensionalization. The relationships used for non-dimensionalization can be found in Appendix B of (Pergam et al., 2022).
2. Non-dimensionalization may also yield a simplification of the model equations themselves. If the variables used for scaling are chosen carefully, some parameters can be eliminated completely. This is the reason why certain important, but constant process quantities, i.e., volumetric flow rate at the filter outlet and viscosity, do not appear any longer in the model Eq. (2) to Eq (7).

It is important to mention that non-dimensionalization does not alter the outcome of the qualitative solution features. Yet, similar to Kuhn's argumentation (Kuhn, 2018; Kuhn and Briesen, 2016), a non-dimensional model supports the process of drawing overall conclusions from numerical studies independent of operating conditions, and, ultimately, offers the possibility to apply the general results to more specific problems.

The non-dimensional parameter values used for the simulation can be found in Table 1. All parameters were obtained using the non-dimensionalization procedure described in Appendix B of (Pergam et al., 2022). Notably, some of the non-dimensionalized parameters depend on the varying filter aid concentration c. The stated parameters are valid for the reference control $c = 0.37$, as this was the initial value for the optimization algorithm in our previous study. Therefore, the numeric values of these parameters must be adjusted if the models are not evaluated at the reference control parameter, i.e., for each iteration during the benchmark optimization problem introduced in Section 2.4 Optimization.

All numerical procedures used in this work have been implemented in MATLAB 2022b (The MathWorks, Inc., Natick, Massachusetts, US). The system of partial differential equations was solved using the method of lines (MOL) (Wouwer et al., 2014; Schiesser and Griffiths, 2009).

Table 1
Non-dimensional parameter values used for all calculations

n	[−]	0.037
p_a	[−]	51
q_{lm}	[−]	-3.7
s	[−]	10
T	[−]	1700
β	[−]	0.09
$\varepsilon_s{}^*$	[−]	0.27
ε_{s0}	[−]	1
δ	[−]	0.49

[2] Sometimes also referred to as Landau Transformation in the literature (Wouwer et al., 2014; Landau, 1950)

Hereby, the partial spatial derivatives were approximated using a three-point centered finite differencing scheme, and the boundary conditions are implemented in vector form (see Eq. (17)).

The total number of discretization stencils for the fixed coordinate system z was 250. Notably, the qualitative solution features of the nonlinear model can be obtained using far fewer discretization points conducting simple forward simulations. However, the optimization and especially the optimal control procedure from (Pergam et al., 2022) require precisely calculated gradients. These are only obtainable if during the model evaluations a high-resolution discretization is used such that the approximation errors are as low as possible. Otherwise, the optimizations might become numerically unstable, and it is not guaranteed to find the unique global solution for varying parameter sets. Therefore, the previously mentioned discretization is chosen as our benchmark case. Hereby, the calculation time scales approximatively exponentially with an increased discretization, which further underlines the utility of a ROM framework.

For time integration, we used MATLAB's ode15s as an implicit ordinary differential equation solver (Shampine and Reichelt, 1997). All calculations were performed on a regular desktop computer (processor: Intel® Core™ i5-8400, performance: 2.80 GHz, memory: 16 GB RAM).

2.2. Reduced order model

The main idea of reduced order modeling lies in replacing the FOM with a proxy model that captures sufficient details of the initial model's dynamics, but at the same time is much more efficient to solve (Brunton and Kutz, 2019). As stated in the introduction, we focus on using a POD approach to reduce the model's dimensions. Hereby, the fundamental idea is similar to the Galerkin method as explained in detail in (Wouwer et al., 2014), which assumes that the unknown function $\mathrm{f}(\mathrm{x},\mathrm{t})$ solving a partial differential equation can also be expressed in the following form:

$$f(t,x) \approx \sum_{i=1}^{N} \Phi_i(x) m_i(t) \tag{12}$$

The right-hand side of Eq. (12) enables the initial unknown solution to be split into two parts, one of which depends either on time *or* space. Thus, the coefficients $m_i(t)$ can be interpreted as weighting factors of how the solution is reconstructed by the corresponding globally defined basis functions $\Phi_i(x)$ over time. To numerically solve an arbitrary problem using the Galerkin method, some general basis functions that are easy to integrate and differentiate, such as polynomials or Fourier modes, are usually introduced *a priori*. However, since the qualitative solution features for most problems are not known beforehand, a typically large number of previously mentioned basis functions must be chosen. This in return requires the costly computation of a high amount of the related parameters $m_i(t)$.

Instead, POD creates the possibility to find an $L2$-optimal set of basis functions, i.e., the minimal number of modes required to represent the original field $f(t,x)$ (Chatterjee, 2000). The complete set of POD modes thus effectively reduces the dimension of the model, since the optimal number of modes N is usually much smaller than the grid points used to solve the FOM with established discretization approaches. Moreover, the dynamics of the system can often also be captured with sufficient detail by truncating the total number of modes N, which further diminishes the dimension and ultimately enables a true ROM to be created.

Since the POD can only be performed using an available dataset, it is mandatory to collect experimental data, or, as in our case, create appropriate data snapshots using the FOM. Therefore, let $\boldsymbol{A} = [f(t_1,z), \cdots, f(t_n,z)] \in \mathbb{R}^{n\times n_t}$ be a matrix containing the discretized solution of the FOM in the spatial domain $\mathbf{z} \in \mathbb{R}^n$at various sampling times $\mathbf{t} \in \mathbb{R}^{n_t}$. Using the snapshot matrix $\boldsymbol{A}$, there are two separate approaches in finding the POD modes, commonly referred to as direct and indirect methods (Wouwer et al., 2014; Chatterjee, 2000). For the direct method, the POD can be obtained by employing the singular value decomposition (SVD):

$$\boldsymbol{A} = \boldsymbol{U}\boldsymbol{\Sigma}\boldsymbol{V}^{\mathrm{H}} \tag{13}$$

Following the derivation of Chatterjee (Chatterjee, 2000), the left singular vectors of $\boldsymbol{A}$ are then contained in the columns of $\boldsymbol{U} \in \mathbb{R}^{n\times n}$ and can be directly defined as the POD modes $\boldsymbol{\Phi}_i \in \mathbb{R}^n$. Notably, using this procedure yields discretized, i.e., point based functions. The basis functions $\boldsymbol{\Phi}_i = \mathrm{col}_i\boldsymbol{U}$ are not of analytical nature. The Hermitian transpose of the matrix $\boldsymbol{V}$ contains the right singular vectors of $\boldsymbol{A}$, which are of no further need at this point. Lastly, $\boldsymbol{\Sigma}$ is a corresponding diagonal matrix, comprising the unique, non-negative singular values $\boldsymbol{\Sigma} = \mathrm{diag}(\sigma_i) \in \mathbb{R}^{n\times n_t}$ linked to the equally ranked POD mode. Notably, the singular values σ_i are sorted according to size, beginning with the biggest element. Therefore, the relative proportion of the singular value σ_i compared to the sum of all singular values $\sum_{i=1}^{n}\sigma_i$ directly identifies the significance of the corresponding POD mode $\boldsymbol{\Phi}_i$:

$$E = \frac{\sigma_i}{\sum_{i=1}^{N}\sigma_i} \cdot 100\% \tag{14}$$

In POD literature, E is referred to as the energy capture, i.e., the detail level of solution features to be represented per basis function in percent. Using this definition, it becomes easy to identify the final number of required modes N to apply the Galerkin method in Eq. (12): the sum of E for the first N basis functions should exceed a previously defined energy capture of the ROM. Additional modes do not contribute any significant solution features and may be truncated. In this work, we set a desired energy capture of 99.99 %.

Remarkably, it might be more efficient to make use of the indirect POD method, in the literature commonly referred to method of snapshots, if the spatial dimension n is larger than the temporal dimension n_t as has been stated by various authors, e.g. (Wouwer et al., 2014; Chaturantabut and Sorensen, 2011; Chatterjee, 2000). Hereby, first computing the right-side matrix-multiplication $\boldsymbol{A}\boldsymbol{A}^{\mathrm{T}}$ yields a smaller dimensional problem. Readily available eigenvalue decomposition routines can then be used to obtain the POD modes (Weiss, 2019). However, numerical errors due to machine precision bounds may affect the accuracy of this alternative approach (Chaturantabut and Sorensen, 2011).

Consequently, we will employ the direct method in the following, since the snapshots from the FOM were of dimension $n_t = 500$ and $n = 250$. The SVD can then be easily calculated in MATLAB (or comparable scientific computing tools), i.e., [U,Sigma,~] = svd(A);. More information on the mathematical theory of the SVD can be found in, e.g., (Golub, 1996).

The method's name suggests that an important property of POD is the orthogonality of the obtained POD modes, i.e.,

$$\int_0^1 \Phi_i \Phi_j^* dz = \begin{cases} 0 \text{ for } i \neq j \\ 1 \text{ for } i = j \end{cases} \tag{15}$$

As derived in detail by e.g., (Brunton and Kutz, 2019), this mathematical property enables the final dimensional reduction of the FOM. Hereby, partial differential Eq. (2) is projected onto the obtained POD basis using the following procedure. First, the system's state ε_s is substituted by $\boldsymbol{\varepsilon}_{\mathbf{s}} = \boldsymbol{\Phi}(\mathrm{z})\boldsymbol{m}(t)$ as defined by the Galerkin method in Eq. (12):

$$\boldsymbol{\Phi}\frac{\partial \boldsymbol{m}}{\partial t} = \frac{1}{L}\frac{\partial \boldsymbol{q}_{\mathbf{l}}}{\partial z} + \frac{1}{L}\frac{\mathrm{d}L}{\mathrm{dt}}\frac{\partial \boldsymbol{\Phi}}{\partial z}\boldsymbol{m} \tag{16}$$

Now, the resulting left-hand side of the Galerkin discretized governing relationship in Eq. (16) may be elegantly simplified by applying the orthogonality condition from Eq. (15). This step is conducted via the left matrix multiplication with $\boldsymbol{\Phi}^{\mathrm{T}}$. After introducing the finite difference matrix $\mathbf{D}$ to approximate the remaining spatial derivatives and the corresponding vectors $\boldsymbol{b}_{\mathbf{q_l}}$ and $\boldsymbol{b}_{\boldsymbol{\varepsilon}_{\mathbf{s}}}$ representing the boundary conditions,

the fully discretized and dimensionally reduced model formulation reads:

$$\frac{\partial \boldsymbol{m}}{\partial t} = \boldsymbol{\Phi}^{\mathrm{T}}\left(\frac{1}{L}\mathbf{D}\left(\boldsymbol{q}_1 + \boldsymbol{b}_{\mathbf{q}_1}\right) + \frac{z}{L}\frac{\mathrm{d}L}{\mathrm{d}t}\mathbf{D}(\boldsymbol{\Phi}\boldsymbol{m} + \boldsymbol{b}_{\varepsilon_s})\right) \tag{17}$$

$$\boldsymbol{q}_1 = \frac{1}{L}((\boldsymbol{\Phi}\boldsymbol{m} + \boldsymbol{b}_{\varepsilon_s})\boldsymbol{k}\mathbf{D}\boldsymbol{p}_s) - \left(\frac{1}{\varepsilon_s^*} - (\boldsymbol{\Phi}\boldsymbol{m} + \boldsymbol{b}_{\varepsilon_s})\right) \tag{18}$$

$$\boldsymbol{p}_s = p_a\left((\boldsymbol{\Phi}\boldsymbol{m} + \boldsymbol{b}_{\varepsilon_s})^{\frac{1}{b}} - 1\right) \tag{19}$$

$$\boldsymbol{k} = k_{init}(\boldsymbol{\Phi}\boldsymbol{m} + \boldsymbol{b}_{\varepsilon_s})^{-\frac{\delta}{\beta}} \tag{20}$$

Subsequently inserting Eq. (18) – Eq. (20) into Eq. (17), as well as rearranging some terms, the final ROM reads as follows.

$$\frac{\partial \boldsymbol{m}}{\partial t} = \frac{1}{L^2}\boldsymbol{F}_1\left((\boldsymbol{NL})^{1-\frac{\delta}{\beta}}\,\mathbf{D}(\boldsymbol{NL})^{\frac{1}{\beta}}\right) + \frac{1}{L}(\boldsymbol{F}_2\boldsymbol{m} + \boldsymbol{F}_{345}) + \frac{1}{L}\frac{\mathrm{d}L}{\mathrm{d}t}(\boldsymbol{F}_6\boldsymbol{m} + \boldsymbol{F}_7) \tag{21}$$

$$\boldsymbol{NL} = \boldsymbol{\Phi}\boldsymbol{m} + \boldsymbol{b}_{\varepsilon_s} \tag{22}$$

$$\boldsymbol{F}_1 = k_{init}p_a\boldsymbol{\Phi}^{\mathrm{T}}\mathbf{D} \tag{23}$$

$$\boldsymbol{F}_2 = \boldsymbol{\Phi}^{\mathrm{T}}\mathbf{D}\frac{1}{\varepsilon_s^*} \tag{24}$$

$$\boldsymbol{F}_3 = \boldsymbol{\Phi}^{\mathrm{T}}\mathbf{D}\boldsymbol{\Phi} \tag{25}$$

$$\boldsymbol{F}_4 = \boldsymbol{\Phi}^{\mathrm{T}}\mathbf{D}\boldsymbol{b}_{\varepsilon_s} \tag{26}$$

$$\boldsymbol{F}_5 = \boldsymbol{\Phi}^{\mathrm{T}}\mathbf{D}\boldsymbol{b}_{\mathbf{q}_1} \tag{27}$$

$$\boldsymbol{F}_{345} = -\boldsymbol{F}_3 + \boldsymbol{F}_4 + \boldsymbol{F}_5 \tag{28}$$

$$\boldsymbol{F}_6 = \boldsymbol{\Phi}^{\mathrm{T}}z\mathbf{D}\boldsymbol{\Phi} \tag{29}$$

$$\boldsymbol{F}_7 = \boldsymbol{\Phi}^{\mathrm{T}}z\mathbf{D}\boldsymbol{b}_{\varepsilon_s} \tag{30}$$

Even without any numerical examples, it is easy to see that the reason for the increased computational efficiency is due to the smaller dimension $N \ll n$ of Eq. (21), which merely requires the numerical integration of the coefficients $\boldsymbol{m}$ on the time domain. Hereby, the above procedure is especially efficient on linear terms, i.e., for $\boldsymbol{F}_2 \cdots \boldsymbol{F}_7$. To obtain these coefficient matrices, high-dimensional matrix multiplications must be performed in Eq. (24) to Eq. (30). This procedure makes up the bulk of the computational load, but can be pre-calculated only once and stored in memory for reuse during numerical integration.

Notably, this is not the case for the non-linear term, i.e., $\boldsymbol{NL}$. Even though the required coefficient matrix $\boldsymbol{F}_1$ may be pre-calculated as well to save some computing efforts, matrix $\boldsymbol{NL}$ indeed needs to be reconstructed in the full-dimensional space for each iteration of the simulation procedure. For our application, however, this is not problematic, since by using the ROM, the nonlinearities could be reduced to merely one term, which yields only a minor performance sink. Further approaches for non-linear model reduction have been introduced that rely on sparse sampling of the underlying data matrix $\boldsymbol{A}$ (e.g. gappy POD, (discrete) empirical interpolation method, etc. (Brunton and Kutz, 2019; Chaturantabut and Sorensen, 2010; Chaturantabut and Sorensen, 2009)). Nevertheless, as can be seen in the next section, the proposed POD approach already yields a substantial increase of computational efficiency, even without additional treatment of the nonlinearities.

Since the cake height $L(t)$ resulting from the cake growth rate $\frac{\mathrm{d}L}{\mathrm{d}t}$ in Eq. (8) is a single ordinary differential equation, this system state cannot be reduced in dimensionality. It is however directly dependent on the mean value of the system state ε_s, the obtainment of which would require a costly computation using the reconstructed n-dimensional field of the FOM. Nevertheless, the computational efficiency can be significantly increased by pre-calculating the mean value of each basis function. The resulting averaged set of POD modes $\overline{\boldsymbol{\Phi}}$ may then be used to simplify Eq. (8) as follows.

$$\frac{\mathrm{d}L}{\mathrm{d}t} = \frac{c}{\overline{\boldsymbol{\Phi}}\boldsymbol{m} - c} \tag{31}$$

The calculation of Eq. (31) now only requires a vector multiplication of the size $N \ll n$.

2.3. Basis adaptation

The ROM may be built by populating the snapshot matrix $\boldsymbol{A}$ with the results of a FOM simulation using the initial parameter set corresponding to the reference control stated in Table 1. In the following, we will refer to this procedure as *local POD*. However, it is not guaranteed that the POD modes obtained from such a single dataset can also simulate the effects of a varying filter aid concentration yielding variable parameter sets accurately.

Arguably, the simplest method to find a POD basis that is approximatively valid for varying filter aid concentrations c is to enrich the snapshot matrix $\boldsymbol{A}$ used in the SVD (see Eq, (13)) with the data of several FOM simulations using different control values in the parameter range of interest. This approach is commonly referred to as *global POD*. In this work, the global POD basis was obtained using two different sample controls. However, a global basis might quickly yield a lower accuracy than a single representative basis for a given amount of POD modes used by the ROM. The computational cost is thus significantly increased, not only by the larger ROM dimension required to obtain a desired error tolerance, but especially by the higher amount of FOM simulations needed to acquire the initial data set (Osterroth et al., 2017; Amsallem and Farhat, 2008).

Another approach to enable the ROM to represent the FOM under parameter variations is called POD- or ROM-adaptation (Vetrano et al., 2012). Notably, many techniques exist that are often based on interpolation between POD modes or expanding Taylor series around a given POD basis (Osterroth, 2018; Osterroth et al., 2017). However, recall that an important property for model order reduction is the orthogonality of the POD base (see Eq. (15)). Now, for example, a simple interpolation between two POD bases from different parameter sets does not necessarily yield a new orthogonal base. Many of these techniques therefore require an additional expensive step of re-orthogonalization (Lieu and Lesoinne, 2004).

In the following, we will focus on the so-called sub-angle interpolation method (SAIM). For two available POD bases, the SAIM exploits the principal angles, i.e., the set of angles transforming one subset spanned by the POD basis into the other. An interpolation algorithm using these principal angles then enforces the orthogonality of the newly interpolated basis and thus automatically fulfils the MOR requirements. We follow the procedure as summarized by (Vetrano et al., 2012). For more theoretical information and a detailed derivation, we refer to (Bjorck and Golub, 1973). First, a SVD is performed for the product of the POD bases $\boldsymbol{\Phi}_1$ and $\boldsymbol{\Phi}_2$, which are associated with the manually set control parameters c_1 and c_2. In this work, the values for both concentrations are identical to those of the global POD approach in order to maintain comparability.

$$\boldsymbol{\Phi}_1^T\boldsymbol{\Phi}_2 = \boldsymbol{U}\boldsymbol{\Gamma}\boldsymbol{V}^{\boldsymbol{H}} \tag{32}$$

Hereby, the principal angles $\cos\boldsymbol{\theta}(c_1, c_2)$ are contained in the diagonal matrix $\boldsymbol{\Gamma} = \mathrm{diag}(\theta_i) \in \mathbb{R}^{N\times N}$. Performing a linear interpolation yields the principal angles from the reference point c_1 to the desired parameter c_i.

$$\boldsymbol{\theta}(c_1, c_i) = \left(\frac{c_i - c_1}{c_2 - c_1}\right)\boldsymbol{\theta}(c_1, c_2) \tag{33}$$

Next, the principal vectors for the first and second POD base can be

calculated.

$$\begin{aligned} \boldsymbol{Y} &= \boldsymbol{U}\boldsymbol{\Phi}_1 \\ \boldsymbol{Z} &= \boldsymbol{V}\boldsymbol{\Phi}_2 \end{aligned} \tag{34}$$

The sought-for POD basis $\boldsymbol{\Phi}_i$ may then be interpolated at an arbitrary filter aid concentration c_i using Eq. (35).

$$\boldsymbol{\Phi}_i(c_i) = \boldsymbol{U}\cos(c_1, c_2) + \frac{\boldsymbol{V} - (\boldsymbol{U}^{\mathrm{T}}\boldsymbol{V})\boldsymbol{U}}{||\boldsymbol{V} - (\boldsymbol{U}^{\mathrm{T}}\boldsymbol{V})\boldsymbol{U}||^2}\sin\boldsymbol{\theta}(c_1, c_i) \tag{35}$$

Notably, a limitation of the SAIM is that only a single parameter variation can be taken into account, which is suitable for our benchmark problem as will be seen below. However, Amsallam and Farhat also proved that the SAIM is a special case of the so-called Grassman-Manifold method (Amsallem and Farhat, 2008). This generalization of the SAIM allows a ROM adaptation for more than one varying parameter. Therefore, the SAIM can also be interpreted as a differential geometry procedure. Hereby, each of the initial POD bases form a subspace that compose a manifold. From here, the POD bases are mapped to a space that is tangential to the beforementioned manifold taking one of the single subspaces as reference. The interpolation is then performed in said tangential space. Finally, re-mapping the results to the initial manifold creates the adapted POD basis.

The sampling locations for both, the global POD and the SAIM, were set to the filter aid concentrations $c_1 = 0.1850$, and $c_2 = 0.4815$. It is important to mention that the sampling locations of the POD bases must enclose the control's optimum. Otherwise, the employed techniques yield no substantial accuracy benefits over the local POD approach. Therefore, the control values for sampling were chosen such that they may reflect a wide range of filter aid dosages that might occur in real processes. This requires an engineer's expert knowledge for the observed cake filtration process in order to achieve low relative errors. In this study, we presume this condition to be met due to our previous work in (Pergam et al., 2022). Nevertheless, desired error tolerances may also be preserved using automated adaptive POD methods. These approaches usually rely on automated selection of appropriate snapshots, basis sampling locations, reduction and online enrichment of the computed POD bases, and/or continuous adjustment of the employed reduced order dimension N such that a desired error tolerance is maintained. An introduction to POD adaption can be found in (Benner et al., 2021). These methods could, e.g., help to preserve the high precision reduced order model, if time-dependent controls should be considered in the presented filtration problem.

2.4. Optimization

In order to evaluate the numerical efficiency of our ROM approach, we chose the benchmark problem of energy minimization, i.e.,

$$\min_c \; e. \tag{36}$$

Hereby, the filter aid concentration c in the filter inlet is defined as the system's control parameter. The effect of c on the process energy consumption e can be calculated as the time integral of the superficial filtrate flow rate multiplied by the pressure drop (see (Pergam et al., 2022; Kuhn, 2018; Kuhn and Briesen, 2015)). However, since we assume a constant flow rate, this scaling factor can be discarded for numerical investigations. Therefore, the reduced cost function can be approximated taking only into account the constantly increasing filtration pressure p_0[3]:

$$e = \int_0^T p_0 \; dt \tag{37}$$

[3] p_0 can be obtained using constitutive relationship (4) and solving $p_l + p_s = p_0$

Since the filter aid concentration cannot be negative and must be smaller than the solidosity of the filter cake $\overline{\varepsilon_s}$, the control is bounded as $0 < c < \overline{\varepsilon_s}$. Mechanistically, this quantity causes two distinctive effects that ultimately increase the filtration pressure continuously over time for the case of constant flow filter aid filtration processes:

1. A high filter aid dosage increases the cake growth rate (see Eq. (8)) thus raising the overall filter resistance
2. A low filter aid dosage significantly decreases the permeability of the material system (see Eq. (7)).

Therefore, the existence of a single, global minimum, i.e., an ideal filter aid dosage acting as a trade-off between both effects, is guaranteed. This aspect is not only known from previous theoretical (Pergam et al., 2022; Kuhn, 2018; Heertjes and Zuideveld, 1978; Tittel, 1987) but also experimental (Haba and Koch, 1978; Sutherland and Hidi, 1966; Carman, 1938) works. Notably, the cost function Eq. (37) might not be the economically most feasible for real-life applications. However, any desired optimization problem with clearly defined minima may be applied without major adjustment to the MOR procedure presented in this work.

We used MATLAB's fmincon function with standard options for solving the optimization problem Eq. (36). Hereby, the gradient-based interior-point algorithm (The MathWorks, 2022) systematically iterates from a starting point for c towards the minimum of the cost function Eq. (37).

To examine the performance of the ROM solving the benchmark Eq. (36), we will analyze the achievable numerical accuracy. To this end, the relative error RE is calculated with the system quantities f_{FOM} from a FOM simulation and f_{ROM} for ROM results:

$$RE = \frac{||f_{FOM} - f_{ROM}||}{||f_{FOM}||} \cdot 100\%. \tag{38}$$

Notably, Eq. (38) will not only be evaluated for temporal dependencies as $RE(t)$, but also for parameter variations as $RE(c)$. Moreover, the time-averaged relative error $\overline{RE_t}$ may also be obtained from the results of the previous equation to acquire further conclusive information using the following integral.

$$\overline{RE_t} = \frac{1}{T}\int_0^T RE(t)\mathrm{d}t \tag{39}$$

Furthermore, the average relative error of the cost function e over the control parameter range $c_1 \cdots c_{n_c}$ may be calculated using Eq. (40), where n_c denotes the total number of discrete elements in said parameter range.

$$\overline{RE_e} = \frac{1}{n_c}\sum_{i=1}^{n_c} RE(c_i) \tag{40}$$

In spite of the achievable increase in computational efficiency of the ROM compared to the FOM, we will analyze:

1. The computational time needed to solve the FOM in order to populate the snapshot matrix $\boldsymbol{A}$ (see Eq. (13)) as well as the corresponding SVD to obtain the final POD basis (*stage 1*).
2. The elapsed time needed for the repeated time integration of the ROM to solve the benchmark problem Eq. (36) (*stage 2*).

3. Results

First, we will investigate the POD basis obtained by the snapshots of a single FOM simulation using the parameters stated in Table 1. After the SVD is performed, the singular values can be studied to evaluate energy capture of the corresponding POD modes. Fig. 2 shows how much influence each mode has on the representation of the dynamics of the FOM. Note that the numerical digits of the singular values are already

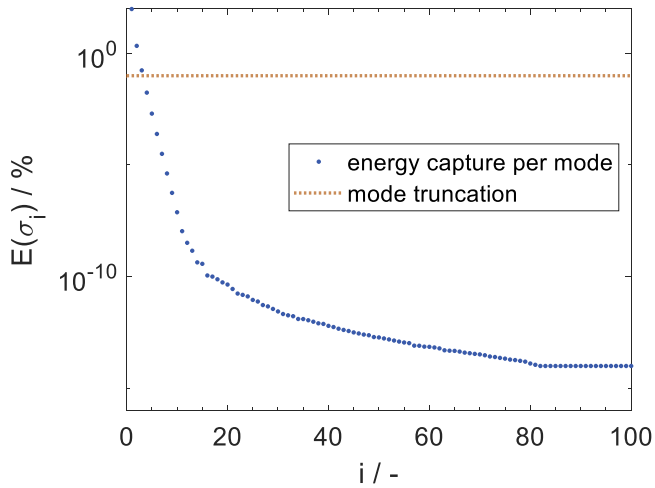

Fig. 2. Singular values σ_i describing the energy capture E, i.e., level of FOM dynamics represented per POD mode in percent (blue). The horizontal line represents the energy threshold for mode truncation (orange).

transformed into a relative percentual scale.

It can be observed that higher ranked basis functions quickly lose significance in the representation of the data. Moreover, starting from mode index $i = 82$, a plateau is reached. However, these latter modes do not contain any further information about the process dynamics but the respective singular values merely reflect numerical noise due to round-off errors occurring at $2.2{\cdot}10^{-16}$ using double precision variables (The MathWorks, 2022). Therefore, the whole dynamic spectrum of the FOM can be represented with a POD basis containing ≈80 modes in total. Furthermore, all POD modes > 3 may be truncated since the sum of these first three basis functions already capture an energy level of ≈99.9927 %, and thus exceed our set accuracy level of at least 99.99 % of the dynamics to be represented. This is also marked in Fig. 2 by the orange horizontal line. Accordingly, we yield a ROM with $N = 3$ degrees of freedom for the system state ε_s to represent the FOM.

The final POD basis for the initial parameter set is shown in Fig. 3(a). Lower ranked basis functions capture more of the model's dynamics, which can also be observed in the spatial variations of the respective mode. For instance, the first mode (blue) only shows minor changes over time. However, since higher mode indices capture faster and less significant solution features, the corresponding basis functions qualitatively contain more variational features. Since the ROM was built using the previously introduced POD basis, Fig. 3(b) shows how the parameters m_i describe the impact of the respective POD mode over time for a single simulation. While temporal dependencies can especially be observed for the first and second mode, the parameter m_3 corresponding to the third basis functions quickly approaches zero. Therefore, it can once again be observed that the latter mode only has a minor effect when the simulated results are transformed back into the full dimension using the linear combination of Eq. (12). Notably, this behavior is in accordance with POD theory (Wouwer et al., 2014).

Since the qualitative and quantitative behavior of filtration specific system quantities, most importantly solidosity ε_s, permeability k, time dependent filter cake height $L(t)$, and filtration pressure $p_0(t)$, are already analyzed in detail in (Pergam et al., 2022), we avoid plotting the FOM simulations as well as the results from the reconstructed ROM throughout the main text. Results of conducted forward simulations using the initial parameter set stated in Table 1 can be found in the Appendix A. Instead, we will investigate how the system states from a simulation of the ROM using the initial parameter set (see Table 1) perform in terms of the transient relative error $RE(t)$.

Fig. 4 displays the percentual accuracy of the system states ε_s and L. The highest temporal relative errors compared to the FOM simulation occur in the beginning of the simulated time span and subsequently decrease towards the end of the process. Taking into account all reconstructed states, the maximum transient error of $RE(t) \approx 1\%$ occurs in the beginning of the process for the solidosity at the cake height $z = 0.8$, normalized by the front-fixing method. In total, the time averaged relative error is $\overline{RE}_t \approx 0.09$ % for ε_s and $\overline{RE}_t \approx 0.07$ % for $L(t)$, which is quite low and represents the FOM fairly well.

However, the previously described achieved numerical accuracy is not completely representative, since the ROM calculations only reproduced a FOM simulation using the same set of reference parameters. Therefore, we will next analyze the benchmark problem Eq. (36), which uses the previously analyzed ROM to examine the model's behavior under parameter variation, in detail. The cost function Eq. (37), i.e., the reduced process energy consumption e depending on the control c, is plotted in Fig. 5 for both, the ROM, as well as the FOM.

Note that the values of the energy consumption e are scaled as $\tilde{e}$ to the global minimum as reference, such that the percentual increase of process energy can be directly read from the ordinate axis if the simulation is not conducted at the optimum. Same re-scaling applies to the abscissa; i.e., the transformed optimal filter aid concentration $\tilde{c}$ was set to 1 so that multiples of this dosage may be identified quickly. Notably, all re-scaled variables are denoted by a tilde (∼) accent. Since the ROM was built using only one data snapshot at the reference filter aid concentration $\tilde{c} = 1.265$, the reduced order model is especially accurate for this initial value. While the extremal point can still be found with reasonable accuracy, i.e., with a relative error of $RE(\tilde{c}) \approx 0.2\%$ (see also the dotted line in Fig. 6), error margins increase significantly the further the control parameter $\tilde{c}$ deviates from the initial data set. The mean error $\overline{RE}_e$ for the cost function displayed in Fig. 5 is ≈1.4 % compared to the FOM with a maximum $RE(\tilde{c}) \approx 5.7$ % at the right boundary of the parameter range.

In order to enable the ROM to perform better over wide ranges of parameter variations, we will next analyze the performance of the global ROM approach and the SAIM for ROM adaptation. We compare the results of the previously mentioned techniques to the local POD basis created by the snapshots of only one parameter set. Fig. 6 shows the control-dependent relative error performance in comparison to the local POD approach.

Using the first three POD modes again, the average error $\overline{RE}_e$ for the shown parameter range of the filter aid concentration $\tilde{c}$ is ≈1.7 % with a maximum relative error $RE(\tilde{c}) \approx 4.8$ % at $\tilde{c} = 2.5$. Thus, the global POD performs worse compared to the local POD as indicated by the blue function, especially considering that the minimal error from the local POD cannot be reached either. This is because the global ROM was built to represent a wide parameter range of $\tilde{c}$ instead of only one operation condition as was the case for the local POD. Therefore, the POD modes must now comprise a bigger information content on how to reflect these parameter variations. This ultimately leads to a loss of captured energy E per basis function. Consequently, the number of significant POD modes has to be increased to five in order to meet our chosen detail level. Rebuilding the ROM using these significant basis functions, it can be seen that the relative error depending on the control c is significantly decreased, now averaging at $\overline{RE}_e \approx 0.19$ %. Notably, the accuracy is most likely increased by one order of magnitude compared to the FOM since the energy capture exceeds the desired energy capture by far, i.e., 99.9994 %. Moreover, the global POD yields a more uniformly distributed relative error with two minima located near the initial sampling locations. In total, the accuracy of these minimal errors can also reach the magnitude of the local POD.

Next, the numerical performance of the SAIM is examined as a ROM adaptation method. The necessary data snapshots were obtained using the same sampling location as was the case in the global ROM, i.e., $\tilde{c}_1 = 0.633$, and $\tilde{c}_2 = 1.645$. Since the SAIM needs the same amount of FOM simulations as the global POD to populate the initial snapshot matrix $\boldsymbol{A}$, five modes were chosen in total in order to create an equal baseline for comparing the performance of both methods. Fig. 7 contains

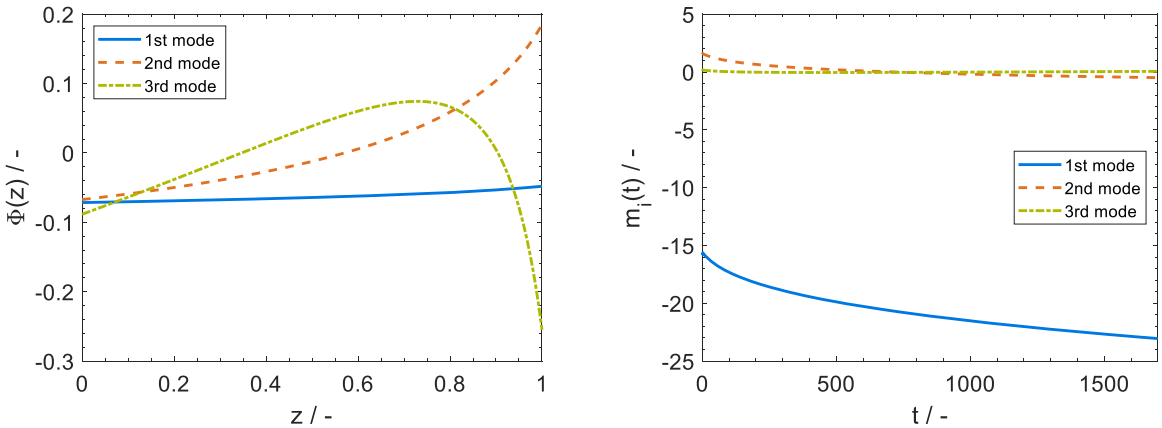

Fig. 3. (a) Final POD basis consisting of 3 modes defined for the whole spatial domain z. (b) Parameters $\boldsymbol{m}$ over time showing the impact of the respective POD modes in Eq. (12) to reconstruct the full-dimensional data field. This basis is valid to represent FOM simulations using the initial parameter set.

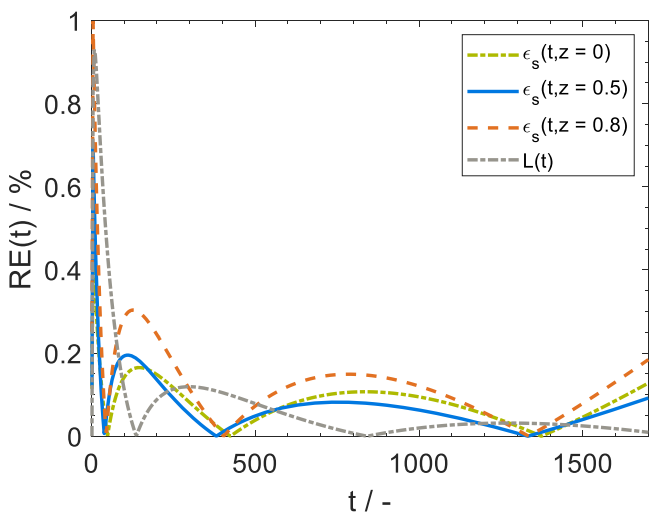

Fig. 4. Transient relative error $RE(t)$ for the system states ε_s, and L obtained by the ROM compared to the FOM simulations using the initial parameter set.

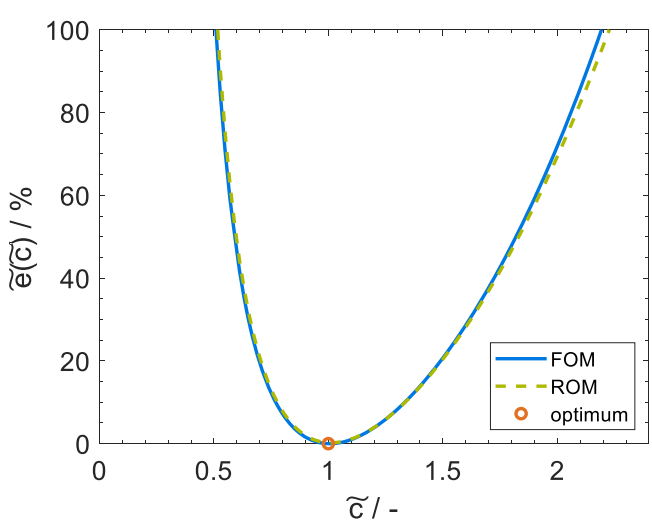

Fig. 5. Cost function Eq. (37) depending on filter aid concentration c. FOM (blue), local ROM (green), optimal filter aid dosage (orange).

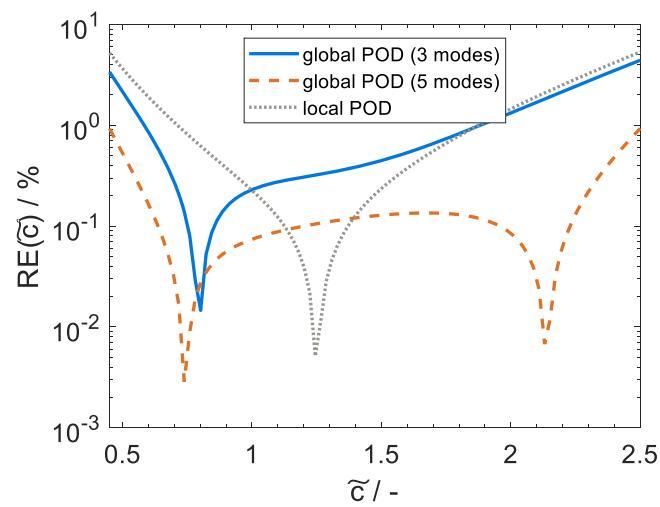

Fig. 6. Relative error $RE(\tilde{c})$ of the cost function Eq. (37) resulting from the ROM compared to the FOM. Local POD basis obtained with one sampling location (grey); global POD basis obtained with two sampling locations and three modes (blue) / five modes (orange).

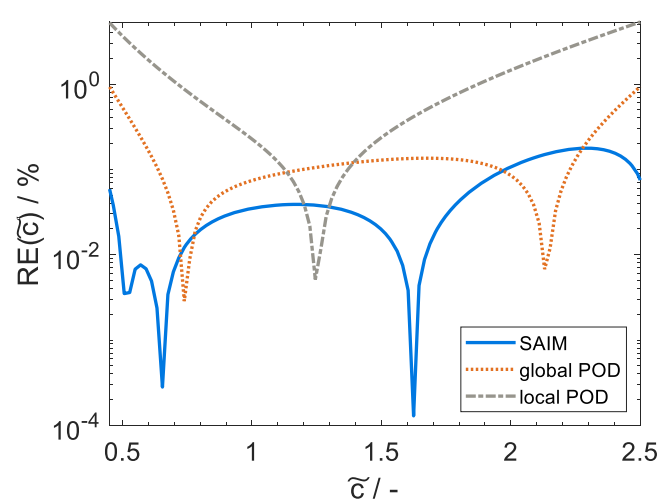

Fig. 7. Relative error $RE(\tilde{c})$ of the cost function Eq. (37) of the ROM compared to the FOM. SAIM basis (blue); global POD basis (orange); local POD basis (grey).

the relative error of the cost function depending on the filter aid concentration $RE(\widetilde{c})$ for the SAIM (blue) compared to the global ROM (orange), as well as the local ROM (grey).

Here, the relative error depending on the filter aid concentration $\widetilde{c}$ is uniformly distributed for the parameter range near the optimal dosage since the sampling locations enclose said point. Therefore, the SAIM qualitatively performs similar to the global POD. In direct comparison however, the SAIM-obtained minimal relative errors outperform the global POD by up to two orders of magnitude. This is also captured by the average error for the cost function, which results in $\overline{RE}_e \approx 0.06$ % performing one magnitude better over the whole parameter range. Upon closer inspection, one can also see that the global POD does not yield the minimal relative errors at the exact POD sampling locations, but only in a region near the sampling ordinates of the control $\widetilde{c}$. This is because the global POD basis must represent all data in an *L2*-optimal way. Contrary, this tradeoff must not be fulfilled by the SAIM – the minimal errors in the relative error graphs are indeed located at the exact snapshot ordinates. Here, both POD bases must only represent the local sampling locations, after which one set of optimal modes is interpolated into the other. Thus, the obtained bases maintain more of the original solution features of the FOM.

Considering the varying number of employed basis functions, and the varying preparation work needed for each method, a more meaningful comparison may be the computational time required to solve each ROM. Therefore, we will next analyze the computational cost caused by our optimization procedure to solve the benchmark problem Eq. (36). All results are collected in Table 2 for easier comparison. Notably, we normalized the calculation times to the procedure solving the benchmark problem using the FOM, where the global minimum was obtained after 41 separate model evaluations.

In total, the reduced computational times in *stage 2* are comparably small for all three introduced POD techniques. Independent of the method, the benchmark problem can be calculated approximatively 10 times faster using the different ROMs compared to the FOM. Remarkably, the ROM using three global POD modes does not necessarily perform faster than the counterpart using five modes. This is due to the overall higher relative errors that lead to a slower numerical convergence during the optimization procedure since the necessary gradients cannot be determined as precisely. Examining the numbers of necessary model evaluations to solve the benchmark problem reflects the same behavior: the higher the average relative error $\overline{RE}_e$, the more ROM evaluations have to be performed. In total, ≈40–60 runs must be simulated in order to find the global minimum using the presented ROMs, which is similar to the FOM benchmark.

When regarding the overall simulation time, it is clear that *stage 1* has the biggest impact on the calculations: two instead of one FOM simulations are necessary to obtain all required snapshots to employ the global POD and the SAIM. Moreover, the computational load in *stage 1* is slightly higher for the SAIM, since an additional SVD has to be performed (see Eq. (32)). Compared to the local ROM, the global POD approach needs ≈20 % (five modes) to ≈50 % (three modes) more time to solve the benchmark problem, while the SAIM has an additional ≈25 % impact on the computational cost. However, comparing the SAIM to global POD using five modes, these differences resulting from additional calculation steps are negligible, and most likely don't have a significant impact on real applications.

Also taking into consideration the achieved numerical accuracies shows how the SAIM is superior compared to the global POD in terms of representing parameter variations for our compressible cake filtration model. Far lower relative errors can be achieved since the basis does not comprise all global information but merely local details for two separate sample data sets. Choosing the same number of modes as in the global POD yields an interpolated basis that mostly maintains the accuracy level of the reference bases. Another advantage becomes clear considering that the SAIM needs exactly as many FOM simulations as the global POD to build the ROM. Therefore, for a given elapsed time span, the SAIM will outperform global POD. Furthermore, it is safe to say that due to the mathematical properties of the SAIM, this method is used preferably over naïve interpolation approaches. This is because a costly re-orthogonalization of the adapted POD base can be omitted, which in return offers additional benefits in acceleration of the computations.

Remarkably, even the local POD performs fairly well per an average error of $\overline{RE}_e \approx 1\%$ over the whole parameter range, which might be insignificant if the ROM simulations shall support real-life processes. However, note that the benchmark problem Eq. (36) is a simple version of the overall control problem since the unknown control is chosen to be constant. Transformed into a real time scale, the optimization problem only takes approximative 100 s to solve using the FOM. This time span does not pose significant expenses, and would not require a ROM approach to solve for a real application. Nevertheless, the optimization problem is merely intended to be a benchmark. Other problems, e.g., infinite-dimensional optimal control tasks, result in far more complex transient parameter variation computations. Therefore, the achieved 90% reduction of the computational cost is also to be expected in said applications, such that the initial day-long elapsed time spans we encountered in (Pergam et al., 2022) may be reduced by several hours. Moreover, our proposed ROM framework enables the model for online evaluations. Combining this with optimal time-dependent filter aid dosage strategies delivers all necessary components to develop a non-linear model predictive control approach, which will be addressed in future studies.

In conclusion, advanced model-based optimization, and control procedures need as high of an accuracy as possible in order to reliably calculate the gradients required for the underlying optimization algorithm. Especially in this regard, the SAIM might unlock further uses of MOR in solid liquid separation processes since it offers great potential for low computational cost as well as for the satisfaction of error margins for wide parameter ranges.

4. Conclusions

We showed how POD based MOR can serve as a powerful data-driven

Table 2
Dimension, i.e., number of states, number of model evaluations to solve the benchmark problem Eq. (36) using the FOM and the ROM, computational cost, and numerical accuracy of the ROM compared to the FOM using local POD, global POD, and the SAIM.

	Dimension[4]	Number of evaluations		Elapsed time			$\overline{RE}_e$
		FOM	ROM	stage 1	stage 2	total	
FOM (reference)	250	41	-	-	1	1	-
Local ROM	3	1	53	0.024	0.062	0.086	1.4487 %
Global ROM-3	3	2	57	0.049	0.081	0.130	1.7128 %
Global ROM-5	5	2	41	0.049	0.053	0.102	0.1845 %
SAIM ROM	5	2	40	0.051	0.057	0.108	0.0586 %

[4] Note, that each scenario has to solve for the additional state $L(t)$, yielding the final dimension $N+1$. However, since this state cannot be reduced in dimensionality, it was not accounted for in Table 2.

tool to increase the computational speed of a complex mechanistic compressible cake filtration model. Notably, this work does not only expand the ROM applications in the context of solid-liquid separation, but also embeds seamlessly into the class of moving boundary problems facing strong non-linearities due to the exponential constitutive relationships Eqs. (5)–(7). Hereby, we were able to reduce the high dimensional model of partial differential equations to a ROM comprising only three dimensions, which roughly translates into a 98% reduction in dimensionality. Moreover, we employed the SAIM as a ROM adaptation method in order to solve a benchmark optimization problem. To this end, the SAIM takes advantage of performing the interpolation of the respective POD modes in a tangential space. Due to special mathematical aspects of differential geometry, the necessity of an additional re-orthogonalization of the newly interpolated basis is eliminated. For our application, the SAIM-based ROM performs up to 2 magnitudes more accurately compared to a simple global POD approach while requiring similar computational costs. Using this procedure, the benchmark problem can be solved approximately 10 times faster compared to an optimization using the FOM. To the best of our knowledge, the initial mathematical model did not find any use in actual industrially scaled problems, which is most likely due to computational restrictions. The achieved significant speed-up therefore enables the ROM for potential use as a time-economic tool in process design, or in time-sensitive environments, such as model-based advanced process control methods. Moreover, we are confident that our findings can also be adapted to 2D or 3D problems to describe local effects of the filter cake in higher detail. Since single simulations for such model formulations usually take up to several hours to calculate, they are currently infeasible for applications requiring repeated evaluations (e.g., optimizations, or real-time applications). Therefore, MOR could serve as a tool to overcome this issue as well.

Glossary

Roman letters		
A	[–]	snapshot matrix
b_{ε_s}	[–]	boundary condition vector for ε_s
b_{q_l}	[–]	boundary condition vector for q_l
c	[–]	volumetric filter aid concentration in suspension
D	[–]	finite difference matrix
E	[%]	POD energy capture
e	[–]	reduced energy consumption
F	[–]	pre-calculated coefficient matrix for the ROM
f	[–]	arbitrary function(s)
I	[–]	identity matrix
i	[–]	index of m, Φ, σ, and for interpolated parameter c
j	[–]	index of σ
k	[–]	permeability of filter cake; compressed
k_0	[–]	permeability of pure filter aid; uncompressed
k_{init}	[–]	permeability of filter cake; uncompressed
L	[–]	filter cake height
m	[–]	time-dependent coefficient
N	[–]	total number of basis functions
NL	[–]	non-linear terms of the ROM requiring reconstruction
n	[–]	size of spatial discretization
n_c	[–]	number of discrete values in a given parameter range for c
n_{imp}	[–]	volumetric impurity concentration in suspension
n_t	[–]	size of temporal discretization
p_0	[–]	process pressure

(*continued on next column*)

(*continued*)

p_a	[–]	empirical compression parameter
p_l	[–]	liquid pore pressure
p_s	[–]	compressive stress acting on solid phase
q_l	[–]	superficial flow rate of liquid phase
q_{lm}	[–]	superficial flow rate of liquid phase at filter medium
RE	[%]	relative error
s	[–]	empirical Sutherland parameter
T	[–]	simulation time span
t	[–]	time
U	[–]	left singular orthonormal basis vectors from SVD
V	[–]	right singular orthonormal basis vectors from SVD
x	[–]	height coordinate
Y	[–]	principal vectors associated with Φ_1
z	[–]	height coordinate treated by front fixing method
Z	[–]	principal vectors associated with Φ_2
Greek letters		
β	[–]	empirical compression parameter
Γ	[–]	diagonal matrix comprising principal angles from SVD
δ	[–]	empirical compression parameter
ε	[–]	porosity
ε_s	[–]	solidosity
ε_{s0}	[–]	solidosity of uncompressed filter cake
Φ	[–]	global basis function
Σ	[–]	diagonal matrix comprising singular values from SVD
Accents		
$\bar{}$	mean values	
$\sim$	re-scaled variables	
$*$	scaling parameter resulting from non-dimensionalization	
bold	vectors or matrices	

Notably, most variables and parameters do not include units due to our non-dimensionalized mathematical model.

CRediT authorship contribution statement

Philip Pergam: Conceptualization, Methodology, Software, Writing – original draft. **Heiko Briesen:** Conceptualization, Writing – review & editing, Supervision, Funding acquisition.

Declaration of Competing Interest

The authors declare that they have no known competing financial interests or personal relationships that could have appeared to influence the work reported in this paper.

Data availability

Data will be made available on request.

Acknowledgments

We thank Verena Pannusch (Chair of Process Systems Engineering, Technical University of Munich) for valuable input and beneficial discussions regarding the theoretical aspects of reduced order modeling and proper orthogonal decomposition. This work was supported by the German Federal Ministry for Economic Affairs and Climate Action (via AiF and DECHEMA), IGF-Project No. 19947 BG.

Appendix A. Full order model simulations

This appendix includes sample simulations of the FOM for the most important system quantities. The following plots do not contain any new findings, and may be found similarly in previously conducted studies (compare, e.g., (Pergam et al., 2022; Tien, 2006; Stamatakis and Tien, 1991)). However, the figures are intended to help the understanding of the qualitative spatio-temporal development of the system states and corresponding

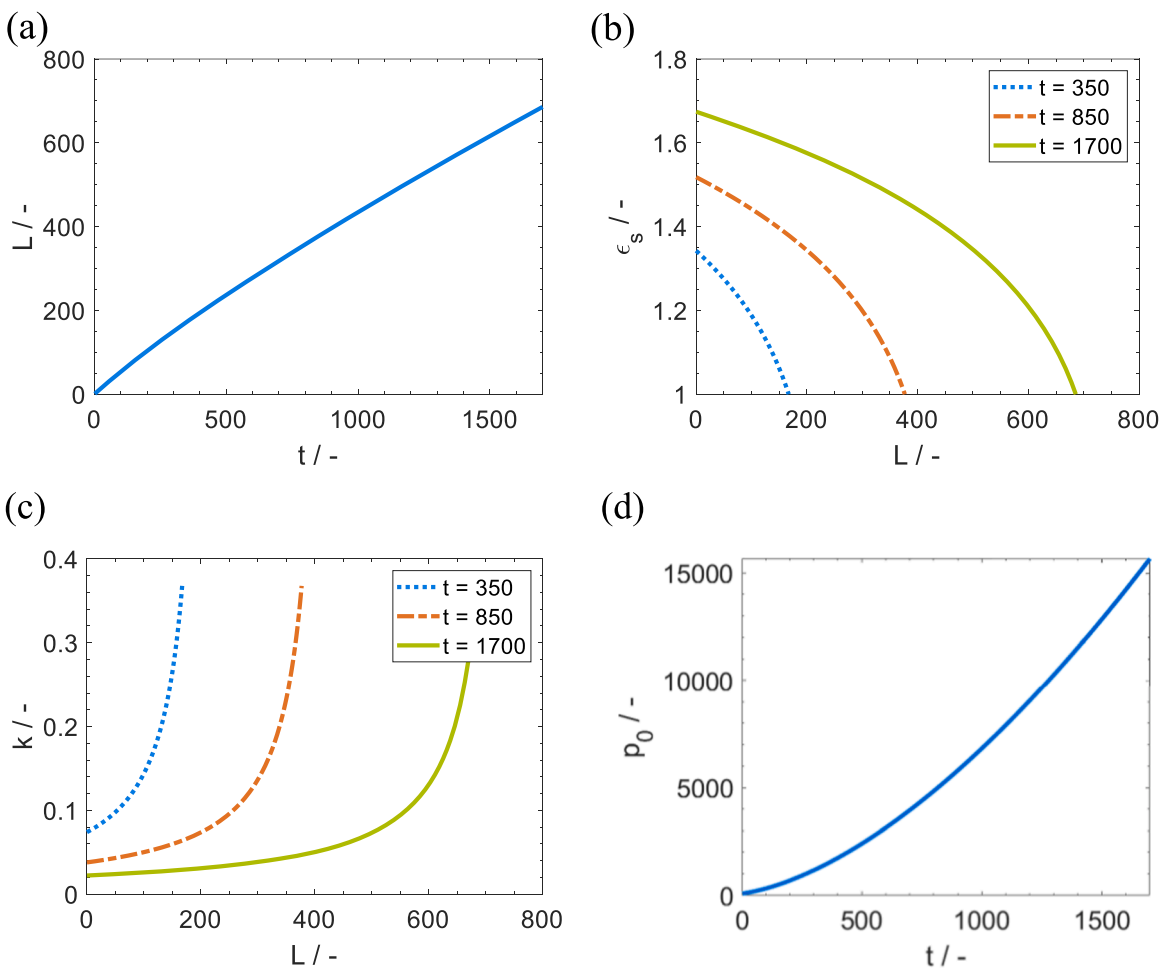

Fig. A-1. Non-dimensionalized model quantities; (a) filter cake height L over time t; (b) solidsoity ε_s over cake height L at process times $t = 350$, $t = 850$, and $t = 1700$; (c) permeability k over cake height L at process times $t = 350$, $t = 850$, and $t = 1700$; (d) filtration pressure p_0 over time t

constitutive relationships, especially regarding the interpretation of the examined relative errors in subsection 3.

Fig. A-1(a) displays the cake height L over time. As we examine the operation mode of a constant volumetric filtrate flow rate, the function should grow linearly in the ideal case of an incompressible process. However, due to cake compression affecting the filtration process, the cake growth rate $\frac{dL}{dt}$ slowly decays over time, since especially the lower cake layers are compacted. This can be observed in Fig. A-1(b) displaying the cake solidosity ε_s over cake height L for three representative process times. Since the filter cake becomes denser during the course of the process, naturally the characteristic quantity of permeability k, as described by the constitutive relationship Eq. (6), decreases over time. This can be observed in A-1(c). In return, the filtration pressure p_0 rises exponentially (Fig. A-1(d)), compared to the ideal case of a linear rise in process pressure of an incompressible cake filtration process. Notably, the pressure drop is processed in Eq. (37) by calculating the time integral over p_0 which equals the cost functional to be minimized.

References

Alles C.M., 2000. Prozeßstrategien für die Filtration mit kompressiblen Kuchen, Universität Fridericiana Karlsruhe (TH), Fakultät für Chemieingenieurwesen und Verfahrenstechnik: Ph.D. thesis.

Alles, C.M., Anlauf, H., 2003. Filtration mit kompressiblen Kuchen: effiziente konzeptefür eine anspruchsvolle trennaufgabe. Chem. Ing. Tech. 75, 1221–1230. September.

Alotaibi, M., et al., 2015. Global–local nonlinear model reduction for flows in heterogeneous porous media. Comput. Methods Appl. Mech. Eng. 292, 122–137. August.

Amsallem, D., Farhat, C., 2008. Interpolation method for adapting reduced-order models and application to aeroelasticity. AIAA J. 46, 1803–1813.

Baur, U., Benner, P., Feng, L., 2014. Model order reduction for linear and nonlinear systems: a system-theoretic perspective. Arch. Comput. Methods Eng. 21, 331–358. August.

Benner, P., et al., 2021. Model Order Reduction Volume 2: Snapshot-Based Methods and Algorithms. De Gruyter s.l.

Benner, P., Gugercin, S., Willcox, K., 2015. A survey of projection-based model reduction methods for parametric dynamical systems. SIAM Rev. 57, 483–531. January.

Bennet, K., 2000. Precoat filtration. Filtr. Sep. 37, 32–33. April.

Berkooz, G., Holmes, P., Lumley, J.L., 1993. The proper orthogonal decomposition in the analysis of turbulent flows. Annu. Rev. Fluid Mech. 25, 539–575. January.

Bhadriraju, B., Narasingam, A., Kwon, J.S.I., 2019. Machine learning-based adaptive model identification of systems: application to a chemical process. Chem. Eng. Res. Des. 152, 372–383. December.

Biegler, L.T., Lang, Y.D., Lin, W., 2014. Multi-scale optimization for process systems engineering. Comput. Chem. Eng. 60, 17–30. January.
Bjorck, A., Golub, G.H., 1973. Numerical methods for computing angles between linear subspaces. Math. Comput. 27, 579. July.
Bremer, J., et al., 2017. POD-DEIM for efficient reduction of a dynamic 2D catalytic reactor model. Comput. Chem. Eng. 106, 777–784. November.
Brunton, S.L., Kutz, J.N., 2019. Data-Driven Science and Engineering. Cambridge University Press, Cambrdige.
Bui-Thanh, T., Damodaran, M., Willcox, K., 2003. Proper Orthogonal Decomposition Extensions for Parametric Applications in Compressible Aerodynamics. American Institute of Aeronautics and Astronautics s.l.
Bui-Thanh, T., Damodaran, M., Willcox, K., 2004. Aerodynamic data reconstruction and inverse design using proper orthogonal decomposition. AIAA J. 42, 1505–1516. August.
Cai, S., et al., 2021. Physics-informed neural networks (PINNs) for fluid mechanics: a review. Acta Mech. Sin. 37, 1727–1738. DecemberBand.
Carman, P.C., 1938. The action of filter aids. Ind. Eng. Chem. 30, 1163–1167.
Chatterjee, A., 2000. An introduction to the proper orthogonal decomposition. Curr. Sci. 78 (7) pp. 808 - 817 April.
Chaturantabut, S., Sorensen, D.C., 2009. Discrete Empirical Interpolation for Nonlinear Model Reduction. IEEE s.l.
Chaturantabut, S., Sorensen, D.C., 2010. Nonlinear model reduction via discrete empirical interpolation. SIAM J. Sci. Comput. 32, 2737–2764. January.
Chaturantabut, S., Sorensen, D.C., 2011. Application of POD and DEIM on dimension reduction of non-linear miscible viscous fingering in porous media. Math. Comput. Model. Dyn. Syst. 17, 337–353. August.
Dey, S., Dhar, A., 2020. On proper orthogonal decomposition (POD) based reduced-order modeling of groundwater flow through heterogeneous porous media with point source singularity. Adv. Water Resour. 144, 103703. October.
Feng, L., Mangold, M., Benner, P., 2017. Adaptive POD–DEIM basis construction and its application to a nonlinear population balance system. AIChE J. 63, 3832–3844. April.
Gasper, H., 2000. Handbuch der Industriellen Fest/Flüssig-Filtration. Wiley-VCH, Weinheim.
Geerling, C., et al., 2019. Designing optimally-graded depth filter media using a novel multiscale method. AIChE J. 66. October.
Ghasemi, M., Gildin, E., 2015. Model order reduction in porous media flow simulation using quadratic bilinear formulation. Comput. Geosci. 20, 723–735. October.
Ghasemi, M., Gildin, E., 2016. Localized model order reduction in porous media flow simulation. J. Pet. Sci. Eng. 145, 689–703. September.
Ghasemi M.R., 2015. Model order reduction in porous media flow simulation and optimization. Texas A&M University: Ph.D. thesis.
Gildin, E., Ghasemi, M., Romanovskay, A., Efendiev, Y., 2013. Nonlinear Complexity Reduction for Fast Simulation of Flow in Heterogeneous Porous Media. SPE s.l.
Golub, G.H., 1996. Matrix Computations. Johns Hopkins University Press s.l.
Grüne, L., Pannek, J., 2011. Nonlinear Model Predictive Control. Springer, London s.l.
Haba, J., Koch, R., 1978. Analyse des filtrationsprozesses unter einsatz von filterhilfsmitteln. Chem. Tech. 30, 91–94.
Hall, K.C., Thomas, J.P., Dowell, E.H., 2000. Proper orthogonal decomposition technique for transonic unsteady aerodynamic flows. AIAA J. 38, 1853–1862. October.
Heertjes, P.M., Zuideveld, P.L., 1978. Clarification of liquids using filter aids part III. cake resistance in surface filtration. Powder Technol. 19, 45–64. January.
Heijn, T., Markovinovic, R., Jansen, J.D., 2004. Generation of low-order reservoir models using system-theoretical concepts. SPE J. (9), 202–218. June.
Hinze M., Krenciszek J. and Pinnau R., 2014. Proper orthogonal decomposition for free boundary value problems. Hamburger Beiträge zur Angewandten Mathematik. September 17, 2014.
Hoffmann, M., et al., 2021. Developing industrial CPS: a multi-disciplinary challenge. Sensors 21, 1991. March.
Kerschen, G., Golinval, J.C., Vakakis, A.F., Bergman, L.A., 2005. The method of proper orthogonal decomposition for dynamical characterization and order reduction of mechanical systems: an overview. Nonlinear Dyn. Band 41, 147–169. August.
Khlopov, D., Mangold, M., 2015. Automatic model reduction of linear population balance models by proper orthogonal decomposition. IFAC-PapersOnLine 48, 11–16.
Khlopov, D., Mangold, M., 2016. Automatic model reduction of population balance models by proper orthogonal decomposition. Computer Aided Chemical Engineering. Elsevier, pp. 163–168 s.l.
Krasnyk, M., Mangold, M., Ganesan, S., Tobiska, L., 2012. Numerical reduction of a crystallizer model with internal and external coordinates by proper orthogonal decomposition. Chem. Eng. Sci. 70, 77–86. March.
Kuhn M., 2018. New Paths in Filtration - Optimal Control Approaches Based on Continuum Models, Technical University of Munich: Ph.D. thesis.
Kuhn, M., Briesen, H., 2015. Dosage of filter aids in the case of pure surface filtration – an optimal control approach. Comput. Aided Chem. Eng. 37, 1655–1660.
Kuhn, M., Briesen, H., 2016. Dynamic modeling of filter-aid filtration including surface- and depth-filtration effects. Chem. Eng. Technol. 39, 425–434. January.
Kuhn, M., Briesen, H., 2019. Systemverfahrenstechnik – eine philosophische begriffsanalyse. Chem. Ing. Tech. 91, 1229–1237. July.
Landau, H.G., 1950. Heat conduction in a melting solid. Q. Appl. Math. 8, 81–94.
Liang, Y., et al., 2002. Proper orthogonal decomposition and its applications—part I: theory. J. Sound Vib. 252, 527–544. May.
Lieu, T., Lesoinne, M., 2004. Parameter Adaptation of Reduced Order Models for Three-Dimensional Flutter Analysis. American Institute of Aeronautics and Astronautics s.l.
Li, X., Hu, B.X., 2012. Proper orthogonal decomposition reduced model for mass transport in heterogenous media. Stoch. Environ. Res. Risk Assess. 27, 1181–1191. October.
López-Quiroga, E., 2018. Reduced order methods for the solution of solidification phase-field models. IFAC-PapersOnLine 51, 637–642.
Lu, K., et al., 2019. Review for order reduction based on proper orthogonal decomposition and outlooks of applications in mechanical systems. Mech. Syst. Signal Process. 123, 264–297. May.
Ly, H.V., Tran, H.T., 2002. Proper orthogonal decomposition for flow calculations and optimal control in a horizontal CVD reactor. Q. Appl. Math. 60, 631–656.
Marquardt, W., 2002. Nonlinear model reduction for optimization and control of transient chemical processes. AIChE Symposium Series 98, 12–42.
Narasingam, A., Kwon, J.S.I., 2020. Application of koopman operator for model-based control of fracture propagation and proppant transport in hydraulic fracturing operation. J. Process Control 91, 25–36. JulyBand.
Nguyen, V.B., et al., 2020. POD-DEIM model order reduction technique for model predictive control in continuous chemical processing. Comput. Chem. Eng. 133, 106638. February.
Osterroth, S., 2018. Mathematical Models for the Simulation of Combined Depth and Cake Filtration Processes. Fraunhofer Verlag s.l.
Osterroth, S., Iliev, O., Pinnau, R., 2017. On efficient approaches for solving a cake filtration model under parameter variation. Model Reduction of Parametrized Systems. Springer International Publishing, pp. 455–470 s.l.
Pergam, P., Kuhn, M., Briesen, H., 2022. Optimal dosage strategies for filter aid filtration processes with compressible cakes. Chem. Eng. Sci. 262, 117989. November.
Redeker, M., Haasdonk, B., 2014. A POD-EIM reduced two-scale model for crystal growth. Adv. Comput. Math. 41, 987–1013. July.
Schiesser, W.E., Griffiths, G.W., 2009. A Compendium of Partial Differential Equation Models: Method of Lines Analysis with Matlab. Cambridge University Press s.l.
Shampine, L.F., Reichelt, M.W., 1997. The MATLAB ODE Suite. SIAM J. Sci. Comput. 18, 1–22. January.
Siade, A.J., Putti, M., Yeh, W.W.G., 2010. Snapshot selection for groundwater model reduction using proper orthogonal decomposition. Water Resour. Res. 46. August.
Sidhu, H.S., Narasingam, A., Siddhamshetty, P., Kwon, J.S.I., 2018. Model order reduction of nonlinear parabolic PDE systems with moving boundaries using sparse proper orthogonal decomposition: application to hydraulic fracturing. Comput. Chem. Eng. 112, 92–100. April.
Smith, T., Moehlis, J., Holmes, P., 2005. Low-dimensional modelling of turbulence using the proper orthogonal decomposition: a tutorial. Nonlinear Dyn. 41, 275–307. August.
Stamatakis, K., Tien, C., 1991. Cake formation and growth in cake filtration. Chem. Eng. Sci. 46, 1917–1933.
Stephanopoulos, G., 2009. Process systems engineering: from solvay to the 21st century. a history of development, successes and prospects for the future. Computer Aided Chemical Engineering. Elsevier, pp. 149–155 s.l.
Sutherland, D.H., Hidi, P., 1966. An Investigation of Filter-Aid Behaviour. Trans. Inst. Chem. Eng. 44, T122–T127.
Tarleton, E.S., Wakeman, R.J., 2007. Solid/Liquid Separation - Equipment Selection and Process Design. Elsevier s.l.
Tayler, A.B., 1985. Free and moving boundary problems. by J. Crank. Clarendon, Oxford, 1984. 425 pp. \textsterling45.00 J. Fluid Mech. 158, 532–533. September.
The MathWorks, Inc., 2022. Constrained nonlinear optimization algorithms. [Online] Available at: https://de.mathworks.com/help/optim/ug/constrained-nonlinear-optimization-algorithms.html [Accessed November 16, 2022].
Tien, C., 2006. Introduction to Cake Filtration. Elsevier Science, Amsterdam.
The MathWorks, Inc., 2022. Floating-point relative accuracy. [Online] Available at: https://de.mathworks.com/help/matlab/ref/eps.html [Accessed November 16, 2022].
Tittel, R., 1987. Die Anschwemmfiltration als ein Prozess zur Klärung von Flüssigkeiten. Technische Universität Dresden, Sektion Verarbeituns- und Verfahrenstechnik: Ph.D. thesis.
Utturkar, Y., Zhang, B., Shyy, W., 2005. Reduced-order description of fluid flow with moving boundaries by proper orthogonal decomposition. Int. J. Heat Fluid Flow 26, 276–288. April.
Vermeulen, P.T.M.; Stroet, C.B.M.; Heemink, A.W.; 2006. Model inversion of transient nonlinear groundwater flow models using model reduction. Water Resour. Res. 42 (9), W09417 September.
Vetrano, F., Garrec, C.L., Mortchelewicz, G., 2012. Assessment of strategies for interpolating POD based reduced order model and application to aeroelasticity. J. Aeroelasticity Struct. Dyn. 2 (2), 85–104.
Volkwein, S., 2001. Optimal control of a phase-field model using proper orthogonal decomposition. ZAMM 81, 83–97. February.
Wakeman, R.J., Tarleton, E.S., 1999. Filtration - Equipment Selection, Modelling and Process Simulation. Elsevier, Oxford.
Wang, Y., Yu, B., Wang, Y., 2018. Acceleration of gas reservoir simulation using proper orthogonal decomposition. Geofluids 2018, 1–15.
Weiss, J., 2019. A Tutorial on the Proper Orthogonal Decomposition. American Institute of Aeronautics and Astronautics s.l.
Winton, C., et al., 2011. Application of proper orthogonal decomposition (POD) to inverse problems in saturated groundwater flow. Adv. Water Resour. 34, 1519–1526. December.
Wouwer, A.V., Saucez, P., Vilas, C., 2014. Simulation of ODE/PDE Models with MATLAB®, OCTAVE and SCILAB. Springer International Publishing s.l.
Zendehboudi, S., Rezaei, N., Lohi, A., 2018. Applications of hybrid models in chemical, petroleum, and energy systems: a systematic review. Appl. Energy 228, 2539–2566. OctoberBand.

List of Publications

Peer-Reviewed Full-Length Research Articles

- **Parameter Estimation for Incompressible Cake Filtration: Advantages of a Modified Fitting Method**
  - M. Kuhn, P. Pergam, H. Briesen
  - Chemical Engineering & Technology, Vol. 34 (3), March 2020, Pages 493-501
  - doi: 10.1002/ceat.201900511
- A novel method for assessing the coating uniformity of hot-melt coated particles using micro-computed tomography
  - B.M. Woerthmann, J.A. Lindner, T. Kovacevic, P. Pergam, F. Schmid, H. Briesen
  - Powder Technology, Vol. 378, Part A, January 2021, Pages 51-59
  - doi: 10.1016/j.powtec.2020.09.065
- **Optimal dosage strategies for filter aid filtration processes with compressible cakes**
  - P. Pergam, M. Kuhn, H. Briesen
  - Chemical Engineering Science, Vol. 262, November 2022, Page 117989
  - doi: 10.1016/j.ces.2022.117989
- **Reduced order modeling for compressible cake filtration processes using proper orthogonal decomposition**
  - P. Pergam, H. Briesen
  - Computers & Chemical Engineering, Vol. 171, March 2023, Page 108165
  - doi: 10.1016/j.compchemeng.2023.108165

Conference Proceedings and Presentations

- Warum man es der Filterzelle krummnehmen sollte: Vorteile nichtlinearer Parameterschätzung bei der inkompressiblen Kuchenfiltration
  - M. Kuhn, P. Pergam, H. Briesen
  - ProcessNet MFA, March 15/16, 2021, online conference due to pandemic
- Nutzung von µCT-Messdaten zur Validierung eines neuen Modells für Prozesse der Anschwemmfiltration
  - P. Pergam, M. Kuhn, H. Briesen
  - ProcessNet MFA, March 15/16, 2021, online conference due to pandemic
- An Optimal Control Method for Filter Aid Filtration Processes with Compressible Cakes
  - P. Pergam, J. Steinhäuser, M. Kuhn, H. Briesen
  - Filtech, February 23 – 25, 2021, Cologne, canceled due to pandemic

- Prozessverständnis und optimale Steuerung kompressibler Anschwemmfiltrationsprozesse (*Keynote*)
  - P. Pergam, D. Neuber, M. Kuhn, H. Briesen, U. A. Peuker
  - ProcessNet MFA, February 21/22, 2022, online conference due to pandemic

Posters

- Parameterschätzung für Anschwemmfiltrationsmodelle mittels µCT-Messungen
  - D. Neuber, P. Pergam, M. Kuhn, H. Briesen, U. A. Peuker
  - ProcessNet MFA, March 15/16, 2021, online conference due to pandemic

On the Advantages of Nonlinear Continuum Scale Filtration Models
cumulative doctoral thesis by Philip Schroeder, affiliated with:
Chair of Process Systems Engineering, TUM School of Life Sciences
Technical University of Munich, 2023.